Porous Polymer Scaffolds for the Maintenance of Stem Cell Pluripotency

Jessie Leigh Ratcliffe

A thesis presented for the degree of

Doctor of Philosophy

Materials Science & Engineering

November 2018

Abstract

Pluripotent stem cells (PSCs) have unique characteristics that make them the key resource in an enormous range of potential applications ranging from tissue engineering and cell therapy, to drug screening and disease modelling. PSCs can proliferate indefinitely and are able to differentiate into any somatic cell type, making them hugely flexible. However these cells are frequently cultured under conditions that limit their usefulness in research or clinical applications due to the use of undefined, xenogenic, and two-dimensional formats. A three-dimensional (3D), chemically-defined culture system is required to overcome the limitations of traditional culture and realise the potential of pluripotent stem cells. This thesis presents a 3D porous polymer scaffold that has suitable interconnected morphology for the culture of stem cells. This scaffold was composed of a UV-cured, thiol-acrylate, polymerised high internal phase emulsion (polyHIPE). Residual thiol groups within the material could be used as handles to add biofunctionality to the synthetic scaffold. In this thesis, triethylamine-catalysed Michael addition was optimised to allow the attachment of the adhesive peptide sequence cyclic-RGDfK (cRGD). This cRGD peptide has previously been shown to be highly effective in promoting cell adhesion, and to be capable of maintaining pluripotency of human embryonic stem cells under defined culture conditions. PolyHIPE scaffolds in this work were functionalised with both a commercial ECM-derived coating (Geltrex®) and the cRGD peptide. The Geltrex® coating required additional conjugation of a sulfo-SANPAH crosslinker, as protein adsorption alone was not sufficient to create a layer capable of supporting pluripotent stem cells in the material. Both the Geltrex® and cRGD functionalities were capable of supporting H9 human embryonic stem cells in the scaffold for up to 14 days. These stem cells expressed Oct4 and maintained the ability to form teratomas, indicating that they remained pluripotent. Thus a 3D, chemically-defined culture system for the maintenance of human pluripotent stem cells is presented herein.

Acknowledgements

I would like to thank my supervisors Neil Cameron & Andrew Laslett for the opportunity to undertake this project, and for their guidance over the years.

Thank you to the members of the Cameron lab group. Special thanks Caitlin for all the training, advice, and commiserations, and also to Ash for keeping my work ticking over in a crisis.

To the members of the Laslett lab, thank you for being so welcoming and open. Your training, expert advice, and willingness to change cell media on the occasional Sunday was integral to my success. To other helpful folk at CSIRO, I was very lucky to work around such kind and talented people.

Thank you to my international collaborators Ahmed Eissa, Marc Walker, Orvil Collart, and Oskar Radermecker for their contributions and insight.

Much appreciation to the technicians and experts at various technological platforms that provided training, equipment and professional services including Monash Centre for Electron Microscopy, Monash Histology Platform, Monash Medical Imaging, and the Ramaciotti Centre for Cryo-Electron Microscopy.

Finally I'd like to thank Mum for always encouraging curiosity and enthusiastically supporting all my endeavours, and Julian for the constant patience, love and positivity.

Declaration

I hereby declare that this thesis contains no material which has been accepted for the award of any other degree or diploma at any university or equivalent institution and that, to the best of my knowledge and belief, this thesis contains no material previously published or written by another person, except where due reference is made in the text of the thesis.

Student signature:

[redacted]

Date: November 2018

The undersigned hereby certify that the above declaration correctly reflects the nature and extent of the student's and co-authors' contributions to this work. In instances where I am not the responsible author I have consulted with the responsible author to agree on the respective contributions of the authors.

Main supervisor signature:

[redacted]

Date: November 2018

Statement of Copyright

I certify that I have made all reasonable efforts to secure copyright permissions for third-party content included in this thesis and have not knowingly added copyright content to my work without the owner's permission.

Publications Arising from this Work

All works were entitled " "Porous Polymer Scaffolds for Maintenance of Stem Cell Pluripotency"

28th Annual Conference of the European Society for Biomaterials, Athens Greece, 4th - 8th September 2018, poster.

25th Australasian Society for Biomaterials and Tissue Engineering Conference, Canberra Australia, 18th - 20th April 2017, oral presentation.

PolymersVic Meeting, Melbourne Australia, 4th - 5th July 2016, poster.

10th World Biomaterials Congress, Montreal Canada, 17th - 22nd May 2016, poster.

36th Australasian Polymer Symposium, Lorne Australia, 20th - 23rd November 2016, poster.

Contents

Abbreviations

2D	two-dimensional
3D	three-dimensional
ATR	attenuated total reflection
BET	Brunauer Emmett Teller
c-MYC	MYC proto-oncogene
cDNA	complementary DNA
cRAD-mal	cyclic-RADfK-maleimide
cRGD-mal	cyclic-RGDfK-maleimide
DAPI	4',6-diamidino-2-phenylindole
DCE	1,2-dichloroethane
DCM	1,2-dichloromethane
DIPEA	n,n-diisopropylethylamine
DMEM	Dulbecco's modified Eagle's medium
DMSO	dimethyl sulfoxide
DPEHA	dipentaerythritol penta/hexa-acrylate
E8	Essential8™
ECM	extracellular matrix
EDTA	ethylenediaminetetraacetic acid
Ellman's reagent	5,5' dithiobis (2-nitrobenzoic acid)
ESC	embryonic stem cell
FACS	fluorescence activated cell sorting
FBS	fetal bovine serum
H&E	haematoxylin & eosin

hESC	human embryonic stem cell
HIPE	high internal phase emulsion
iPSC	induced pluripotent stem cell
KLF4	Kruppel-like factor 4
LDEV	lactate dehydrogenase-elevating virus
MEF	mitotically inactivated mouse embryonic feeder cell
mESC	mouse embryonic stem cell
NEt_3	triethylamine
OCT	optimal cutting temperature compound
OCT4	octamer binding transcription factor 4
PBS	phosphate buffered saline
PEG	polyethylene glycol
PEGDA	polyethylene glycol diacrylate
PFA	paraformaldehyde
PLA	polylactic acid
polyHIPE	polymerised high internal phase emulsion
PS	polystyrene
PSC	pluripotent stem cell
PTFE	polytetrafluoroethylene
qPCR	quantitative polymerase chain reaction
RAD	arginine-alanine-apartate
RGD	arginine-glycine-apartate
RNA	ribonucleic acid
ROCK	Rho-associated coiled-coil containing protein kinase
ROCKi	ROCK inhibitor Y-27632
SEM	scanning electron microscopy

SOX2	sex determining region Y-box 2
sulfo-SANPAH	sulfosuccinimidyl 6-(4'-azido-2'-nitrophenylamino) hexanoate
TCPS	tissue culture polystyrene
THF	tetrahydrofuran
TMPTA	trimethylolpropane triacrylate
TMPTMP	trimethylolpropane tris (3-mercaptopropionate)
UV	ultraviolet
XPS	X-ray photoelectron spectroscopy

List of Figures

List of Tables

Chapter 1

Literature Review

1.1 Introduction

Pluripotent stem cells (PSCs) have an enormous range of potential applications in areas from tissue engineering and cell therapy, to drug screening and disease modelling [1, 2]. They have unique characteristics which make them the key resource in these technologies. PSCs can proliferate indefinitely where other cells, including adult stem cells, are limited [3, 4]. They are able to differentiate into any somatic cell type, making them hugely flexible [4, 5, 6]. They are also more permissive to genetic modification than adult stem cells [3].

There are two kinds of pluripotent stem cell. These are embryonic stem cells (ESCs) and induced pluripotent stem cells (iPSCs). Human embryonic stem cells (hESCs) are derived from the blastocyst stage of embryonic development and are considered the "gold standard" pluripotent cell type [7, 8]. Their amazing properties have attracted great interest since their isolation in 1998 [9]. However, research using these cells has been hampered by ethical concerns as they are derived from viable embryos [10, 11].

The main alternatives to embryo-derived stem cells are iPSCs, which are somatic cells that have been reprogrammed to have pluripotent characteristics. Reprogramming of cells into an embryonic state was first achieved by Takahashi and Yamanaka using overexpression of four key transcription factors (The Yamanaka factors) [6]. These factors are octamer

binding transcription factor 4 (OCT4), sex determining region Y-box 2 (SOX2), Kruppel-like factor 4 (KLF4) and MYC proto-oncogene (c-MYC) [6]. This process provides a way to produce highly flexible cells that do not have the immunogenic or ethical issues associated with ESCs [12, 13]. These induced cells are considered to be very similar to their inherently pluripotent counterparts [14, 15, 16].

Due to their ability to differentiate into any adult cell type, both ESCs and iPSCs are being investigated as solutions to a number of problems. Some of these applications are shown in Figure 1.1. Stem cells may be used to fill gaps in the supply of replacement organs [3, 17], to test new drugs more effectively [18, 19, 20, 21, 22, 23], as treatments for a range of diseases [24], and to study fundamental aspects of both healthy [25] and diseased [18, 26] cells *in vitro*. Induced pluripotent stem cells are being implemented in predictive cultures for disease modelling and drug testing as an alternative to the immortalised cell lines currently in use [27]. By deriving iPSCs from patients, a disease specific model can be created [17, 28, 29].

It has been suggested that the first disease likely to be successfully treated with hESC-based therapy is macular degeneration [26]. There are currently several clinical trials using hESC- or hiPSC-based cell transplants to treat this condition [30, 31, 32]. Stem cells are also being investigated as a treatment for type I diabetes [26, 33], cardiovascular diseases [34], Parkinson's disease [13, 35] and liver diseases [13, 36].

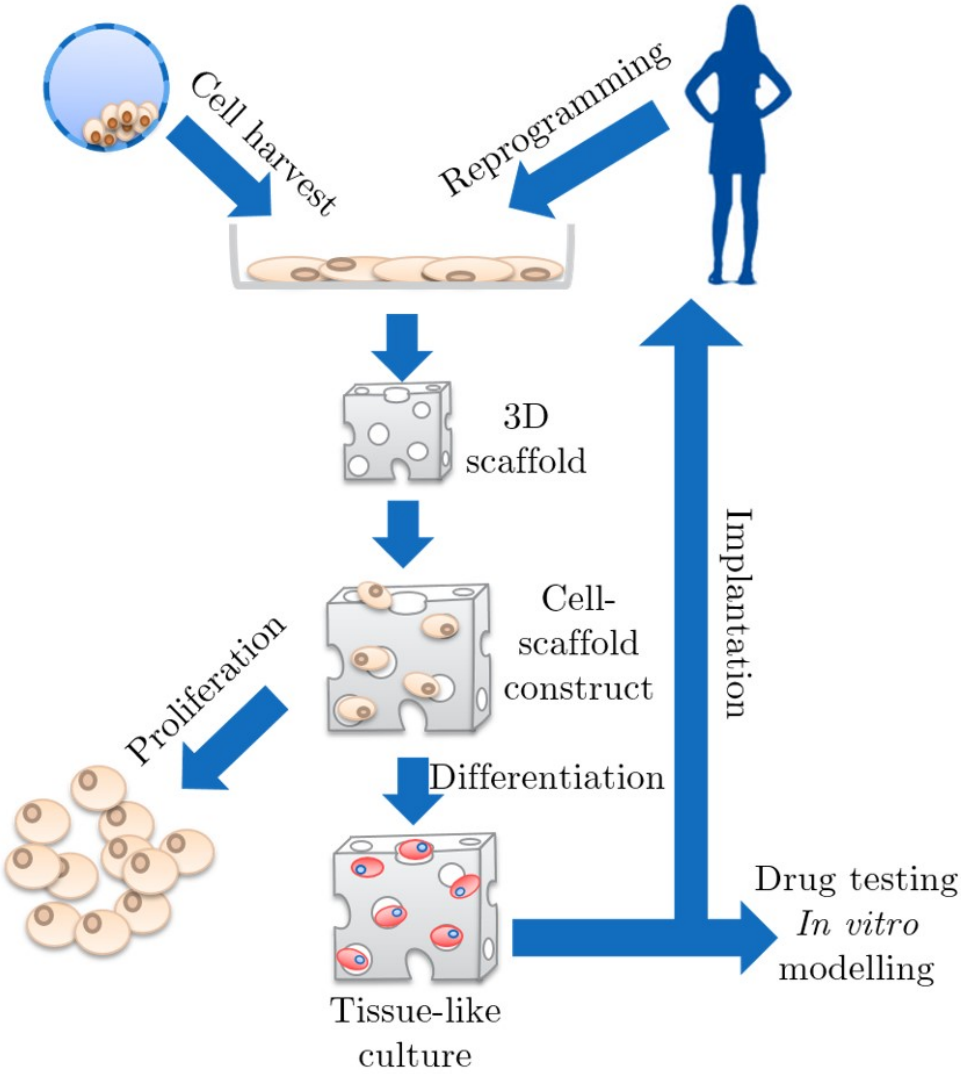

Figure 1.1: *Pluripotent stem cells may be derived from the inner mass of blastocysts or by reprogramming adult cells. They are then expanded in culture. One approach is to seed cells into a suitable 3D scaffold. Stem cell proliferation results in a cell-scaffold construct, which can be used in a wide range of applications. These include bulk production of pluripotent stem cells, or differentiation protocols to create cultures suitable for drug testing.*

Pluripotent stem cells are an area of intense research, with many groups achieving clinically promising results extremely rapidly. In fact, the first treatment of a patient with a hESC based therapy was just twelve years after the first reported isolation of an hESC line [26]. Despite the interest in stem cells and their many promising applications, the field still faces significant hurdles. Most cell therapies require huge numbers of cells [37], cells may be stressed during the repeated passaging required for expansion, many culture systems rely on the use of animal-derived compounds, and expanding cells is expensive using current approaches [4]. Complexity and interaction with animal derived components makes traditional culture systems for pluripotent cells unsuitable for clinical application [38]. *In vitro*, stem cells are prone to spontaneous differentiation as they do not have an appropriate environment for long-term self-renewal and maintenance of pluripotency [35]. Thus the creation of an effective *in vitro* culture system to expand stem cells is a major focus of current research [39].

Propagating pluripotent stem cells in a controlled manner is a major challenge impacting many downstream technologies. Several factors contribute to this, such as the heterogeneous nature of starting cell populations, the naturally transient nature of pluripotent stem cells, and the micro-environment experienced by the cells which can result in components interacting in unexpected ways [40]. Extracellular matrix (ECM) design specifically for maintaining ESCs or iPSCs in a pluripotent state is a relatively under-investigated area [4].

This review aims to summarise current knowledge regarding the maintenance, expansion, and manipulation of pluripotent stem cells in culture, with a focus on three-dimensional (3D), animal component free, and chemically defined approaches.

1.1.1 The Stem Cell Niche

The stem cell niche is the micro-environment directly surrounding a stem cell. It provides the cells with mechanical support, environmental control, and specific biological stimuli.

It is a multifaceted and dynamic system comprised of factors including cell-cell contact, cell-matrix interactions, oxygen concentration, matrix stiffness, and biochemical cues [3].

The niche provides an anchorage point for stem cells with specific adhesive molecules [41] and topography [35]. It is well known to regulate stemness and differentiation *in vivo* [35, 42, 43, 44]. The major component of the niche is the surrounding molecules collectively referred to as the extracellular matrix (ECM). Once believed to be a static support structure, the ECM is now known to be very important in the control of cell behaviour as it helps to regulate presentation of both soluble and insoluble factors [14, 45].

Some have argued that as embryonic stem cells only have a transitory native state, the niche concept does not apply [46]. However, understanding the native microenvironment is still critical for *in vitro* expansion and culture [46]. The *in vivo* stem cell environment is highly complex, and recreating it in its entirety would not likely give the robust, reliable, and cost effective culture format required to facilitate stem cell therapies. However, recreating one or more of the natural niche features is the typical approach used when designing new culture systems for pluripotent stem cells. For example, extracellular matrix proteins are an important part of the niche *in vitro* that can be translated to synthetic niche analogues [47]. Both traditional cultures and newer technologies take cues from the body to support and control cells *in vitro* [21].

1.1.2 Traditional Culture Systems

Current culture systems for stem cell maintenance typically include feeder cells or extracellular matrix coatings on 2D plastic cultureware [9, 48, 49]. Cells are frequently maintained in conditioned or serum-containing medium.

Feeder cells, such as murine (mouse) embryonic fibroblasts (MEFs), are mitotically inactivated somatic cells that provide the adhesion points and soluble factors required by pluripotent stem cells [41]. Soluble factors secreted depend on feeder cell origin and cell

line, and include TGFβ 1, activin A and FGF-2 [50]. The first human embryonic stem cells derived were supported by mouse feeder cells [9]. This method is labour intensive [51], culture components are undefined, and the mixed cell colonies can impede the analysis of morphogenesis [4]. Importantly, feeder cells are a potential source of transmitted pathogens and contamination. When using murine feeder cells, it is nearly impossible to isolate a pure supply of stem cells that do not also contain feeders [48]. In addition, pluripotent stem cells populations that have come in contact with foreign cells may have acquired viruses or other undesirable biomolecules from those cells [52]. Contamination with undesired cells complicates downstream applications such as modelling [48] and transplantation [53].

Conditioned or serum-containing medium is frequently used in conventional pluripotent stem cell culture [48]. Medium is conditioned by culturing cells, often feeder cells, which excrete soluble factors [1]. The factor-enriched media can then be used in other cultures. This supplementation can also be achieved by adding serum to the media. Conditioned media supports pluripotent cells, but introduces variability and the possibility of contamination even when used with a defined, feeder-free substrate.

These traditional methods have several issues that make them unsuitable for a number of emerging pluripotent stem cell applications. As a result of utilising undefined components such as feeders or serum, these methods are not precisely controlled. This means that the effect of each component is not easily quantifiable, and the potential for contamination and disease transmission is elevated. Cells are also grown in flat layers on the bottom of flasks or plates. There are a number of problems with this two-dimensional (2D) format, as discussed later in this review. Briefly, culturing in 2D demands significant effort, space, and therefore money while producing cells that lack some characteristics of those found *in vivo* [18].

Traditional culture formats have supported stem cell culture for decades. However, as more sophisticated technologies using these unique cells are developed, a new culture system is required to fit more stringent analytical and clinical requirements. Key features

of an ideal culture system for production of pluripotent stem cells would include: [2]

- Fully defined substrates and media
- Non-xenogenic components
- Scalability
- Good manufacturing practice (GMP) compatibility [54]
- Cost effectiveness

While traditional 2D culture on feeder cells does not satisfy these constraints, many groups are working towards systems that do. Such systems aim to fulfill the requirements listed above, but must also incorporate features that sufficiently recapitulate the *in vivo* stem cell niche in order to maintain stem cell pluripotency and growth.

1.2 Factors Required to Maintain Pluripotent Stem Cells

Pluripotent stem cell culture conditions need to promote stem cell growth, maintenance of pluripotency and self-renewal, and karyotypic stability [55]. *In vivo*, this is controlled by the stem cell niche. Due to its complexity, completely recreating this stem cell environment would be impractical. However, much research has been dedicated to understanding the impact of each aspect of the niche, and how they interact to direct stem cell fate. Several features of the stem cell niche have been successfully incorporated into simplified culture systems that support pluripotent cells. Some controlling factors are summarised in Figure 1.2, and discussed further herein.

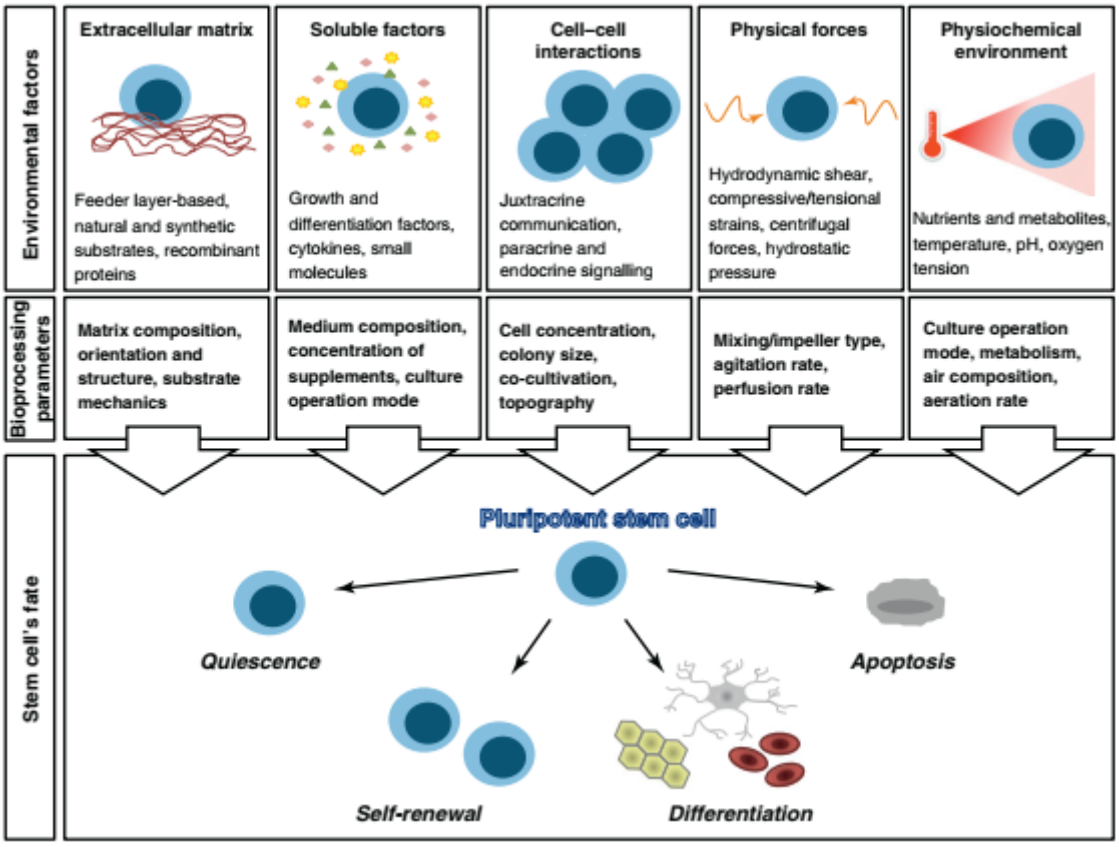

Figure 1.2: *Schematic representation of some of the factors that control cell fate in the stem cell niche, the bioprocessing parameters used to control these factors* in vitro, and the cell fates which result. While the extracellular matrix is the key factor of interest in this thesis, cell-cell interactions, physical factors, and physical environment are considered. Reproduced with permission from Trends in Biotechnology, *Serra* et al. *2012, copyright 2018 Elsevier [56].*

1.2.1 Oxygen

The oxygen level in culture affects pluripotent cell growth and metabolism [57] and so needs to be carefully regulated. It is particularly important to consider when culturing cells in 3D as maintaining homogeneous concentration may be more complex.

Cell culture is traditionally conducted at atmospheric oxygen concentrations of 21 % [58]. *In vivo* O_2 concentration typically ranges from 2-9 %, with hypoxic environments found in stem cell niches [57] and early embryogenesis [59, 60]. While hESCs can self-renew at atmospheric O_2 levels [61], studies suggest that low oxygen conditions favour a pluripotent state [57, 62, 63, 64]. Growing pluripotent cells in less than 5 % O_2 has been shown to result in up-regulation of pluripotency markers compared to 20 % oxygen [65, 64]. This effect has been shown in both 2D and 3D cultures [66].

While the exact mechanism behind this effect remains uncertain, it appears to be tied to pluripotent cell metabolism. Forristal *et al.* showed that the up-regulation of pluripotency factors was influenced by hypoxia inducible factors (HIFs) [64]. HIFs regulate approximately 200 genes, including many metabolic genes. HIF-2α was found to be of particular importance in hESCs. HIF-2α is an upstream regulator of GLUT1, which regulates glucose metabolism [64]. Interestingly, removing FGF2, a factor required for maintenance of pluripotency, had similar effects on glucose consumption as culturing calls at 20 % O_2 [64]. Thus, the metabolism rate and pathway adopted by cells is influenced by O_2 levels. Several other genes involved in glucose metabolism are also impacted by O_2 levels, indicating that the HIF-2α/GLUT1 pathway may not be the only mechanism of regulation.

Reprogramming cells to produce iPSCs is also enhanced under physiological (rather than atmospheric) O_2 conditions [67, 68, 69], and hypoxia alone has been shown to de-differentiate early lineage committed cells [59, 61]. Recent evidence suggests that stem cell fate, including maintenance of a pluripotent state, is a metabolism dependent process

[59]. This helps to explain why oxygen levels in culture are important when maintaining and expanding pluripotent stem cells.

However, under some conditions hypoxic environments can enhance the differentiation of mouse ESCs [57, 70] and iPSCs [71]. Other studies show that if hESCs are passaged weekly, there is no advantage to keeping oxygen at 5 % [72]. Thus, low oxygen tension is unlikely to be the only condition required to ensure the maintenance of pluripotency.

1.2.2 Proteins & Peptides

Human pluripotent stem cells are anchorage-dependent cells [14, 54] and so need to be adhered either to each other or to a scaffold in order to survive. In addition, cell-cell and cell-matrix interactions, along with soluble factors, are considered the most important effectors of stem cell fate [73]. In their native environment, pluripotent stem cells are supported within their niche, which contains supporting cells, soluble factors, and extracellular matrix (ECM). The natural ECM is composed of a mixture of hydrated fibres including collagen, laminins, fibronectin, vitronectin, and proteoglycans [4]. The ECM however is more than just an inert scaffold, it is a dynamic system that can act as a binding site for growth factors, and guide cell migration [17].

The interactions between stem cells and their surrounding matrix play a fundamental role in regulating several aspects of cell behaviour [4]. As cell-ECM interactions are considered essential for pluripotency and self-renewal of hESCs [55], 3D culture formats need to provide an analogue to these interactions. Incorporating one or more moieties from the *in vivo* niche is a popular approach when aiming to maintain pluripotent stem cells. Several ECM components have been shown to have roles in maintaining self-renewal ESCs and iPSCs. These include collagen I [41], laminin [3], vitronectin [55, 74], fibronectin [75, 76], and heparin [77].

However, the effect of each ECM component and their role in signalling has not been fully

elucidated [55]. This has led to a number of investigations that give inconsistent guidelines as to which molecules best support stem cell growth, pluripotency, and karyotypic stability. Several examples are summarised in Table 1.1.

1.2.2.1 ECM-Derived Protein Coatings

Such coatings are also suitable for culture in defined medium such as E8 or mTeSR1. Early attempts to replace feeder cells used Matrigel and MEF-conditioned medium [78]. This combination supported pluripotent cells for over 180 days, where gelatin substrates or other conditioned media resulted in differentiation. Later, Braam *et al.* found that Matrigel could support growth of hESCs in defined mTeSR1 media for seven passages [55]. Matrigel has also been used in conjunction with 3D scaffolds in the transition to 3D culture. Cytodex 3 microcarriers are commercially available cell culture beads that have been used with a Matrigel coating to expand hESCs in a 3D system. This system had the added advantage of allowing direct cryopreservation of cells on the coated microcarriers, and improved cell recovery compared to typical preservation in suspension [79].

While ECM-derived coatings are commercially produced and widely used, they have similar issues to feeder cells in that they are of xenogenic origin and carry the risk of contamination [80]. There is concern Matrigel may contain the non-human sialic acid Neu5Gc [81]. This immunogenic molecule can be transferred to human stem cells and has been detected on the surface of hESCs [55, 81]. Viral and microbial contamination is also a risk. Matrigel and other animal-derived coatings such as Geltrex are therefore not preferred for clinical applications. As they are naturally derived products, ECM coatings such as Matrigel and Geltrex also have some inherent variability. The specific amounts of proteins are batch variable and not fully defined, thus selection of growth factors for self-renewal can be difficult [55].

Table 1.1: *ECM components used as culture substrates for human pluripotent stem cells and their effectiveness in supporting cell maintenance*

Substrate	**Cell Type**	**Defined Medium**	**Culture Period**	**Pluripotency Maintenance**	**Notes**
Laminin	hESCs (HES-3 and H7)	Yes	20+ passages	Yes [80]	Murine LN 2D & 3D.
	hESCs (HUES1, HES2, HESC-NL3)	Yes (mTeSR1)	N/A	No [55]	Growth not supported
	hESCs (HUES1, HES2, HESC-NL3)	No (MEF Conditioned)	5 passages (1 month)	Yes [55]	
	hESCs (HS207, HS420, HS401) & iPSCs (BJ12, LDS1.4)	No (Human albumin)	20 passages (4 months)	Yes [47]	LN-511 2D.
	hESCs (KhES-1,KhES-2,KhES-3)	No (Conditioned + FGF-2)	10 passages	Yes & No [85]	Maintenance is isoform dependant.
	hESCs (H1, H7, H9, H14)	No (Conditioned + FGF2)	42 days	Yes [78]	

continues on next page

	iPSCs (reprogrammed new line)	Yes (E8)	10 passages	Yes [35]	LN521
Fibronectin	hESCs (HUES1, HES2, HESC-NL3)	Yes (mTeSR1)	N/A	No [55]	Growth not supported
	hESCs (HUES1, HES2, HESC-NL3)	No (MEF Conditioned)	5 passages (1 month)	Yes [55]	
	(H1, H7, H9, H14)	No (Conditioned + FGF2)	6 passages	No [78]	
	hiPSCs (UTA1)	No (hESF9a)	27 passages	Yes [76]	Uses bovine insulin
	hESCs (H9)	Yes (NutriStem XF/FF)	5 passages	Yes [86]	
Vitronectin	hESCs (HES-3, H7)	Yes	20+ passages	Yes [80]	TCPS + PS microcarriers
	hESCs (HUES1, HES2, HESC-NL3)	Yes (mTeSR1)	Up to 12 weeks	Yes [55]	
	iPSCs, ESCs (H9, H14)	Yes (mTeSR1)	9 passages	Yes [38]	2D
	hPSCs (HES-3)	No (Conditioned)	7 weeks (7 passages)	Yes [74]	2D. Analyses effect of concentration.

continues on next page

	hESCs (HES-3, H1)	No (mTeSR1 + animal derived BSA)	<20 passages	Yes [87]	2D. Analyses effect of concentration
	hESC (MEL1, MEL2)	Yes (StemPro without ascorbate)	10+ passages	Yes [88]	Recombinant vitronectin segments
	iPSCs	Yes (E8)	4 passages	Yes [89]	2D & 3D (microcarriers, static & stirred)
Matrigel	hESCs (HUES1, HES2, HESC-NL3)	Yes (mTeSR1)	7 passages	Yes [55]	
	hESCs (H1, H7, H9, H14)	No (Conditioned + FGF2)	180 days	Yes [78]	
	iPSCs, ESCs (H9, H14)	Yes (mTeSR1)	9 passages	Yes [38]	2D
	hESCs (H9)	Yes (mTeSR1)	5 passages	Yes [90]	Coated on porous membrane
Collagen IV	hESCs (H1, H7, H9, H14)	No (Conditioned + FGF2)	6 passages	No [78]	
	hESCs (HUES1, HES2, HESC-NL3)	Yes (mTeSR1)	N/A	No [55]	Growth not supported

continues on next page

	hESCs (HUES1, HES2, HESC-NL3)	No (MEF Conditioned)	5 passages (1 month)	Yes [55]	
Combined	hESCs (HS181)	Yes (TeSR2 + recombinant human albumin)	20 passages	Yes [83]	Combined Laminin-511 E8 frag + E-Cadherin
	Mouse iPSCs (iPS-MEF-Ng-178B-5)	No (bovine serum)	up to 17 passages	Yes [48]	Genetically Engineered (RGD + Cadherins + elastin-like)
	hESCs (H9) hIPCs (clone 2a)	Yes (mTeSR1)	20 - 37 passages	Yes [91]	E-cadherin + IG Fc domain

1.2.2.2 Laminin

Laminin is a glycoprotein found in the ECM that is known to mediate cell adhesion through interactions with polysaccharides and integrin receptor proteins [80]. It is the first glycoprotein found in the ECM of developing embryos [47, 82], making it a logical substrate for maintaining a naive cell state. As such, laminin and laminin fragments are now frequently used to promote adhesion and maintenance of human pluripotent stem cells [2, 80]. There are at least sixteen different laminin isoforms identified in mammalian tissues [83, 84]. It has been shown that not all of forms of laminin are suitable for promoting self-renewal in stem cells [3]. Rodin *et al.* used recombinant laminin-511 to culture both hESCs and iPSCs without any animal products or feeder cells. They further clarified that $\alpha 6\beta 1$ are the most important integrins for laminin-511 binding. Laminin-511 is practically ubiquitous throughout the body. Other isoforms have specific locations. For example, laminin-211 is only located in the early embryo and certain epithelial cells [47]. Interestingly, despite its early embryo association laminin-211 does not necessarily promote the adhesion or proliferation of embryonic stem cells [85].

Derda *et al.* used surface arrays to analyse 18 laminin-derived peptides for hESC renewal, five of which could promote proliferation of undifferentiated hESCs [92]. However, this study used serum coated surfaces which may limit relevance due to serum's high fibronectin content [55]. One study concluded that laminin was unable to support pluripotency of mouse ESCs in serum-free media [93]. However, mouse results are difficult to translate to human cells [55] as the expression of cell cycle mechanisms is slightly different between the species [47]. It is clear that under many culture conditions, laminins assist with maintaining pluripotent stem cells. Care should be taken when selecting the isoform to use.

1.2.2.3 Vitronectin & Fibronectin

Vitronectin is a protein found in the blood at a concentration of approximately 300 µg/mL [94]. Unlike most of the bioactive sequences being investigated as pluripotent cell substrates, it is not found in Matrigel [55]. Induced pluripotent stem cells were found to retain pluripotency and normal karyotype on vitronectin for nine passages, suggesting this may be a suitable ligand to replace undefined ECM-derived coatings [38].

Fibronectin is an ECM glycoprotein that binds to other ECM components including collagen and fibrin [95]. It has been reported as a suitable substrate to support pluripotency in both ESCs [96, 55] and iPSCs [76]. Fibronectin may lead to differentiation of mouse ESCs [41].

1.2.2.4 The RGD Peptide Sequence

Full proteins are often not needed to elicit the appropriate response from cells, allowing short peptide sequences to be used in their place. These short sequences can be synthesised more easily than the full protein, which is a significant advantage when developing defined culture systems. Peptides may also reduce complexity and cost, and are often more stable than the full protein. Arginine-glycine-apartate (RGD) was originally identified as the key adhesion sequence in vitronectin. It is now a commonly used attachment sequence when designing biomaterials which can bind to several integrins [97]. The RGD sequence can also be found in fibronectin, fibrogenin, osteopontin and bone sialoprotein [38, 48].

RGD is used in both its standard linear form, and as a cyclised molecule. Cyclic-RGD (cRGD) is a more potent adhesive motif than its linear counterpart [98]. This is due to the conformational restriction achieved by cyclisation [98]. Cyclic peptides are even more stable than linear short peptides [99], making them a good choice for routine *in vitro* stem cell culture. In a screen of over 30 peptide sequences, cRGD was by far the

best peptide for the growth of pluripotent stem cells [100]. This sequence gave similar colony numbers to commercial coatings Geltrex, Synthemax and Stemadhere. The cRGD peptide has also successfully supported embryonic stem cells in defined mTeSR1 media [98].

1.2.2.5 Cadherins

E-cadherin mediated cell-cell interactions are thought to be essential for stem cell morphogenesis and the organisation of solid tissue [4]. E-cadherin coated substrates can mimic cell-cell interactions required for maintenance of pluripotency, and thus maintain cells for several passages without feeder cells [91, 101]. Undifferentiated ESCs have been found to express E-cadherin but not N- and VE-cadherins [102, 103]. This is supported by Haque *et al.*, who found that undifferentiated ESCs and iPSCs have a low affinity for N-cadherin, so N-cadherin coated substrates could be used to purge these cells and produce homogeneous differentiation [104]. Modulating the expression of E-cadherin can also regulate the differentiation of ESCs [105].

The re-establishment of E-cadherin mediated cell-cell contacts after cell dissociation is required to maintain hESC clonogenic capacity and survival [106]. This is an important factor to consider when passaging pluripotent stem cells.

1.2.2.6 Hybrid Surfaces & Custom Synthesised Peptides

Many protein-based culture surfaces rely on a single sequence in conjunction with components in the cell culture media to support cells. This provides simplicity and may lower cost, but is a major diversion from the complexity found in the ECM or in traditional cell culture supports like Matrigel. Maintenance of stem cell pluripotency *in vitro* may be better supported by a combination of different bioactive sequences. Thus, some studies have used a combination of biofunctional sequences. A mixed E-cadherin and laminin-521 surface was used to promote long term maintenance of human embryonic cells under a

defined, xeno-free environment [83]. This study concluded that individual peptides were unable to ensure survival of hESCs, and the synergistic effects of the two sequences were required.

In addition to using sequences already found in the native ECM, researchers have access to synthesis technologies which allow the production of tailor-made proteins and peptide sequences. Custom recombinant proteins have been used to allow self-renewal of both ESCs and iPSCs. A sequence containing a combination of E-cadherin and the E8 laminin-511 fragment has been found to be an efficient system for human pluripotent stem cell culture [47]. Production of recombinant proteins *via* an eukaryotic system makes them high cost. Adnan *et al.* used a prokaryotic system to reduce both cost and time of peptide production [48]. Their recombinant protein combined attachment motifs, including RGD, to promote the long term maintenance of mouse iPSCs. Artificial ECM with immobilised recombinant growth factors has been shown to influence signal transduction pathways in a different manner from the soluble form [4]. This suggests that investigating the use of soluble bioactive molecules as immobilised components could also be a promising method to increase our control of pluripotent stem cells.

Specifically designed protein sequences provide the opportunity to combine the strengths of several different ECM components to effectively direct pluripotent stem cells. As more is discovered about the factors required for pluripotency and the role of different supporting factors, engineering peptides may provide an effective route to synthesising culture scaffolds that are clinically applicable.

1.2.3 Biophysical Factors

Biochemical cues such as bound proteins are an effective method to control cell behaviour. However, they can be expensive to scale up. They can also be difficult to control long term as the functional half-life of biological molecules is fairly short, and is variable across different types [14]. Manipulating the mechanical properties or microstructure of

3D scaffolds can offer a more easily defined, scalable method for pluripotency maintenance or direction of cell lineage. Using biomechanical direction is also free from immunogenic compounds, and may be less expensive than other defined substrates such as recombinant sequences [107]. Several physical properties of materials are known to affect cell behaviour [14]. These include substrate stiffness [108], topography [107], and hydrophobicity [109]. Whether the substrate presents a 2D or 3D environment to cells modifies the roles of other factors [110] and may influence cell behaviour in its own right.

However, many studies in areas such as scaffold mechanics have been conducted on multipotent stem cells and not yet been extended to pluripotent cells. Other studies focus on the differentiation of stem cells rather than maintenance of pluripotency. In addition, it can be difficult to precisely determine the effect of each physical cue as biochemical factors from media can influence results. For example, it can be difficult to determine whether topography directly affects cell behaviour, or whether it changes protein adsorption from the media and so has an indirect effect [111]. The next section aims to outline how substrate properties can be manipulated when designing a stem cell scaffold, with focus on those with have been shown to promote pluripotency.

1.2.3.1 Substrate Stiffness & Elasticity

Cell culture was first performed on glass petri dishes, and is now typically conducted on tissue culture polystyrene (TCPS) cultureware. While much attention has been paid to the biological components in cell culture, it is only more recently that the mechanical properties of these underlying substrates have been considered. Mechanical properties of the supporting matrix or substrate have increasingly proven important in controlling cell behaviour particularly in cell signalling [112], migration [107], proliferation, and determination of cell fate [107, 113]. These effects have been extensively investigated in relation to mesenchymal stem cells (MSCs) [108, 113]. MSCs appear to respond reliably to substrate stiffness. However, caution must be exercised when attempting to generalise conclusions achieved using multipotent lineages to pluripotent cells. For example, Poh

et al. found that mouse embryonic stem cells did not undergo the typical stiffening and spreading process when presented with stiffer substrates [114]. Manipulation of matrix stiffness is frequently applied as a method to direct differentiation of stem cells, rather than to maintain their pluripotency. This is reviewed elsewhere [115, 116].

Much less is known about the effect of substrate stiffness on stemmness when compared to evidence on how this factor affects differentiation [107], but pluripotent stem cells do appear to be directed by biophysical factors. It has been suggested that mechanical forces are an important regulator of transcription [117]. This occurs due to altering cell traction forces [107]. The embryonic stem cells 'feel' the physical cues provided by the ECM and respond accordingly [118]. During embryogenesis, mechanical cues such as forces (compression, shear, tension) and changes in cell shape are transmitted to the nucleus [117].

There are several studies to suggest that a soft substrate is preferable for maintaining mouse embryonic stem cell (mESC) stemness [107, 119]. Sthanam *et al.* investigated the stiffness and soluble factors presented by MEFs, which are used to maintain pluripotent mESCs. They found that softer matrices produced by the MEFs resulted in higher pluripotency and self-renewal [41]. Previous experiments on polacrylamide (PA) and polydimethylsiloxane (PDMS) gels have also demonstrated higher self-renewal on soft substrates. It was found that the soft substrates produced lower cell-matrix tractions [119, 120]. Human pluripotent stem cells preferred soft RGDSP-functionalised PEG gels (G' = 300Pa) in a study by Caiazzo *et al.* [121]. Very soft matrices have also been shown to enhance reprogramming of fibroblasts into human iPSCs [122]. Together these studies suggest that softer matrices encourage pluripotent phenotypes in culture. This correlates with the softness of native hESCs as reported by Chowdhury *et al.* [119]. Lu *et al.* used micro-fabricated polyacrylamide (PA) hydrogel with two elastic moduli to test the effect of mechanical properties on mouse ESCs [107]. Expression of pluripotency markers were higher on the softer PA gel. On PA hydrogels, mESCs better retained their pluripotency on soft (6.1kPA) substrates when compared to stiffer (46.7kPa) gels [107]. However, in

this case substrate stiffness alone was not sufficient to regulate mESC proliferation and morphology, though it did regulate stemness.

In contrast, hESCs preferred stiffer gels (10kPa) over soft (0.7kPa) when grown in mTeSR1 media [123], and Lee *et al.* found no difference in metabolic activity of ESCs with changing elastic modulus of their PEG hydrogel scaffold [124]. This suggests that the influence of stiffness on stem cell behaviour works in conjunction with many other factors including scaffold composition, cell line, and culture protocol.

Mechanical influence on cell culture is not limited to the manipulation of static scaffold properties. Dynamic strains have also been demonstrated to affect pluripotent cell behaviour. Human ESCs cultured on polymeric membranes were exposed to cyclic strains by Saha *et al.* resulting in inhibited differentiation [125]. However, applying cyclic strain on a different scale by magnetically twisting 4 μm beads on the cells resulted in reduced Oct4 expression [119, 126]. It can be difficult to isolate the effects of mechanical properties as the same stiffness may not generate the same cell response on different materials [107]. Therefore the effect of stiffness and elasticity should be taken into consideration when designing novel substrates.

1.2.3.2 Topography

Scanning electron microscopy (SEM) shows that the natural ECM has a variety of topographical features, including pores and structures created by intertwined protein fibres [127, 128]. Numerous studies have investigated the effect of natural and synthetic surface topography on a range of cell types [111, 129, 130]. Topography affects the distribution of cell focal adhesions and modulates cell traction [107, 131]. Cells interact with nano-topographical features, resulting in changes to cell spreading, polarity, and the actin skeleton [127, 129]. These topography-induced changes influence downstream behaviours including cell fate. Topography plays an important role in stem cell function [107, 127, 132], with many studies investigating the effects of surface texture on differen-

tiation [133, 134]. Topographical cues required to maintain proliferation or differentiation capacity of pluripotent cells is a less thoroughly investigated area [127]. However, there is evidence that the structure of supporting substrates can help maintain pluripotent stem cells.

Appropriate surface topographies may be formed during initial synthesis of the material, for example the fibre structures of hydrogels and electrospun scaffolds [135], or the interconnected pores in emulsion templated polymer foams [136, 137]. Alternatively, topography may be changed post-synthesis using methods such as lithography [138] and ion beam milling [139, 140].

Effects of surface texture vary depending on cell phenotype, topography selected (e.g. groove, pit, or pillar), feature size, and order [14]. Dense, rounded ESCs have been shown to have higher expression of pluripotent markers than flattened cells when cultured *in vitro* [117]. Micro-sized topographical features can influence cell shape and therefore fate. Nano-scale patterns are also physiologically relevant. A recent study investigated the effects of feature size, shape, and distribution on human iPSCs. Over one thousand topographies were produced by lithography and hot embossing. Cells were grown on these surfaces in defined E8 medium supplemented with Rho-associated kinase (ROCK) inhibitor. A surface with a high density of small (typically 10 μm) features promoted proliferation and pluripotency most effectively [141].

Mouse embryonic stem cells (mESCs) are also highly sensitive to topographical structure [107]. Lu *et al.* investigated the effect of both stiffness and topography on mouse embryonic stem cells using polyacrylamide (PA) substrates with planar, hexagonal or square pillar structures. They found that micropatterned PA hydrogels were a reasonable substitute for MEF cell layers [107, 142]. Hexagonal and grooved patterns complemented the soft gels to improve maintenance of stemness. Stiffness and topography combined to affect 2D and 3D maintenance, with topography being the secondary characteristic [107]. The effect of topography was more apparent on stiff substrates, where hexagonal patterns were able to regulate Oct4 expression independent of the mechanical properties. The un-

derlying mechanisms causing the differences in cell behaviours on different topographies was not clear and required further investigation [107]. Another study conducted on stiff polystyrene substrates suggested that the regularity of the pattern, rather than pattern shape, was important in maintaining human iPSCs [127]. A gradient of polystyrene pillars was used to investigate the response of hESCs in feeder-free conditions [143]. This investigation found an increase in Oct4 expression on structured materials compared to smooth substrates. It further illustrated the effect of feature size, and showed that stemness was best maintained on 120 - 170 nm pillars [143].

The ability to control pluripotency or differentiation of stem cells using topography of synthetic surfaces may allow the replacement of protein coating and peptide surface functionalisation, assisting in the shift towards chemically defined surfaces for cell culture. This approach is also likely to be cheaper and more reproducible than ECM-derived substrates [141]. However, there are still gaps in our understanding of the mechanisms underlying the effect of topography on stem cell fate [144]. This is a fairly recent area of investigation, as the development of feeder-free stem cell culture was required before topography could be clearly examined [143]. It is currently difficult to make generalisations regarding the effect of topography, due to the multifaceted nature of cell culture and the enormous variety of topographies available [145]. Other substrate properties such as elastic modulus and surface chemistry also affect cell behaviour. The addition of media with soluble factors and variations in culture protocols further impedes derivation of general trends. For example, random nanostructured features have been shown to both increase and inhibit cell adhesion [146]. Micro- and nano-scale topographies are an aspect of the stem cell niche that can be incorporated when developing new scaffolds for pluripotent stem cell culture.

1.2.3.3 Translation of 2D Research to 3D Results

Cells have been cultured on 2D culture surfaces since the early 20th century [147]. Routine cell culture is still conducted in 2D due to a range of factors including relative simplicity,

accessibility of suitable systems, low cost, and well-developed protocols. This means that the majority of our knowledge regarding the behaviour and requirements of cultured cells is drawn from 2D experiments. Several factors which influence the pluripotency of stem cells outlined in this section have been tested in 2D.

Culturing cells in 3D has many advantages. It is being used more frequently as researchers strive for *in vivo*-like properties and bulk expansion. However, 3D systems can have many issues with cell monitoring, homogeneity, and complexity. For example, cells cultured in 2D can be examined visually to monitor morphological changes that may indicate differentiation. This is not possible in many 3D formats.

Knowledge of 2D cell culture parameters is used as a starting point when developing 3D culture systems. The fundamental requirements of cells, from media to temperature, can be applied directly to new 3D systems. Further modifications unique to the 3D system may also be applied. These too are often based on 2D results, for example the use of peptides on surfaces. Others are specific to 3D systems, such as modified passaging techniques. There is still much to that we do not know about pluripotent stem cells. It is up to each researcher to select the most suitable culture system for their particular area of investigation, while considering the limitations of each method when interpreting results.

1.3 3D, Defined, & Animal-Free Culture of Pluripotent Stem Cells

1.3.1 Advantages of 3D Cell Culture

Another biophysical factor that appears to have a strong effect on cell behaviour is dimensionality. There are many advantages of 3D culture systems over their 2D counterparts. These include improved physiological relevance of stem cells, scalability of production,

potential to be more cost effective, space and labour savings, and the ability to be good manufacturing practice (GMP) compatible. It is widely acknowledged that designing 3D culture models which more closely represent living tissues is a promising approach to basic health research [148].

Traditional culture uses 2D culture surfaces, typically tissue culture polystyrene (TCPS). Routine stem cell culture is conducted on Matrigel or feeder cell layers, which are spread thinly on this flat surface. Most of the experiments used to determine the conditions for maintaining pluripotent stem cells have also been conducted in this 2D system. However, the native stem cell niche is not two-dimensional. Cultures in a flat dish can not effectively recreate the structure and functionality of real body systems [17, 21]. In adapting to 2D, cells become artificially polarised and concentrate their focal adhesions on their basal surface. This alters the shape of cells, flattening them [21]. This flat morphology changes the internal cytoskeleton of the cell and the shape of the nucleus. Such changes have been shown to influence gene expression [149].

Cell-cell and cell-matrix interactions also differ between 2D and 3D cultures [150], with flattened cells grown in 2D lacking the cell-cell and cell-matrix interactions that appear to be essential for mimicking the *in vivo* environment. Altered adhesions can lead to differences in regulatory pathways and therefore in cell behaviour [150]. Cells that lose these interactions may lose their specified phenotype, and may have altered response to applied stimuli [17]. In addition, cell-cell contacts are thought to be required for pluripotency [151, 119].

The native niche is 3D and allows complex cell-cell interactions [21]. Three-dimensional culture environments can better recapitulate the connections found in tissues [27]. A 3D support also allows a more natural cell morphology as cells can spread in all directions instead of being artificially flattened [152]. Cells that are adapted to a 3D environment have demonstrated improved post-implantation survival, reducing issues with cell death when transplanting cells from culture to a patient [153].

The usefulness of a cell model is proportional to its ability to recreate the relevant *in vivo* physiology [27]. The changes in cell shape, adhesion, and gene expression of cells grown in traditional flat culture leads to concerns that experiments using 2D culture may give misleading results [57]. Studies regarding the effects of cancer drugs show this situation clearly. Drugs that appear to kill malignant cells in a culture dish have been found to fail in 3D culture, and also in *in vivo* experiments [154]. There is substantial evidence that 3D cancer models are superior to 2D cultures [155]. Drug sensitivity for both single drugs and combinations, has been found to change between 2D and 3D cultures [155]. For example, in murine breast cancer models high drug resistance was found in 2D cultures that was not present *in vivo*. The resistance under 3D conditions was similar to that of the live tissue situation [150]. An appropriately engineered culture environment could improve the precision of the drug discovery process [149]. Such differences are likely to carry over to pluripotent stem cell-derived models. Two-dimensional cultures, while commonly used, are not truly adequate to screen drugs [21]. With 2D cultures rapidly proving inadequate, the other alternative is animal models. However, the use of animals is limited due to ethical reasons [17]. Therefore, a system that combines some of the advantages of 2D culture, such as ready availability and low ethical constraint, with the increased relevance of an animal model is being sought. Three dimensional tissue culture seems to fill these requirements.

Cells grown in 3D are currently part-way between 2D culture and a tissue in terms of their modelling capability. They are more physiologically relevant than 2D adapted cells [121], but more amenable to high throughput techniques than xenografts [17, 150, 152]. Three-dimensional systems are therefore a promising bridge between *in vitro* cultures and living tissue [150].

Investigations of fundamental biology questions will be benefited by a suitable 3D culture format. Very little is known about the effect of the third dimension on somatic cell reprogramming, for example [119]. Caiazzo *et al.* systematically assessed the effects of microenvironmental stiffness, degradability and biochemical composition of PEG-based

hydrogels to investigate the role these factors play in the promotion of iPSC reprogramming. They concluded that 3D micro-environmental signals aided transcription factors to increase somatic plasticity [121]. Zujur *et al.* found that a 3D environment promoted increased proliferation in mESCs over the 2D control. These 3D cells maintained pluripotency marker expression without leukaemia inhibitory factor (LIF), which is typically required to maintain mouse-derived pluripotent stem cells. Their experiments confirmed that it was the 3D format, and not their atelocollagen material, that was maintaining pluripotency [150]. It was suggested that the 3D culture allows cells to interact in a more biologically relevant manner, resulting in self-organisation that recapitulates *in vivo* conditions. These results were analogous to another study which encapsulated mESCs in PEG-based hydrogels and found that the cells remained pluripotent after LIF removal [121, 150]. Long term maintenance on PEG hydrogels with adhesion peptides was also achieved [150]. The results found by Zujur *et al.* suggest that the differences observed between 2D and 3D cultures are more likely to be due to spatial conformation rather than ECM composition. Nava *et al.* engineered a nano-patterned substrate that also made use of the effect of spatial constraint on mESCs [156]. In this study, photo-polymerised 'nichoid' scaffolds were able to maintain Oct4 expression in spatially confined embryoid bodies, while 2D cultures lost pluripotency marker expression [156].

Three-dimensional culture systems are also likely to be more practical for large scale applications. Two dimensional cultures are not an efficient use of space and resources [157]. They are labour-intensive, expensive, and difficult to scale up, and it is difficult to produce uniform pluripotent stem cells in 2D culture [21]. Therefore it is not feasible to produce the predicted number of stem cells required for therapies, drug testing, and studies with this method. Static, flat plate culture systems cannot be scaled to bridge the gap between research laboratory and industrial scale [18]. It is expected that most therapeutic applications will require up to 10^{12} cells for allogenic transplant. For example, treating a single case of myocardial infarction is estimated to require 1-2 billion cells [15], for which 5,000 - 10,000 cm^2 of 2D culture surface would be needed to supply each patient [1]. This is due to low transplanted cell survival and low target differentiation

efficiency, meaning excess cells are required to get the minimum therapeutic dose [2]. 3D cultures allow an efficient use of space and high cell density that would make this therapy possible with a much more reasonable area. Several reviews discuss the issues with 2D plate-based expansion of cells [18, 40, 158]. 3D scaffold technologies will be instrumental in producing the billions of anchorage dependent cells needed to apply stem cells as therapeutics [18, 80].

1.3.2 Importance of Chemically-Defined & Animal Component-Free Stem Cell Culture

In order to produce pluripotent stem cells for a range of potential uses, culture systems need to provide surfaces and media that suit cell growth and pluripotency. Additionally, these new culture systems need to maintain cells in an environment that ensures they are safe to use in future clinical applications. The cell environment should also be conducive to accurate modelling, drug testing, and other studies. This means that while animal-derived components such as Matrigel and feeder cells are able to support pluripotent stem cells, they are not ideal.

Using animal products results in a range of issues including variability, the potential for pathogen transfer, and immune rejection [47, 55]. MEFs can contain viral particles that are able to infect humans [13, 159]. Thus feeder cells must be screened for multiple diseases such as LDEV (Lactate Dehydrogenase Elevating Virus), a single strand RNA virus, prior to use [160]. Some batches of Matrigel have also been contaminated with LDEV [91]. While not a pathogen, the non-human sialic acid Neu5Gc found in mouse feeder cells can be incorporated into hESCs [13]. Most healthy people have antibodies against Neu5Gc, meaning increased immune response to stem cells that incorporate it [53]. The routine use of foetal calf serum in culture media potentially exposes the cells to bovine diseases including prions [13]. Issues with pathogen transmission may still be present even after cells are transferred to a feeder-free, synthetic system, rendering entire

cell lines permanently unsuitable as they have an increased risk of transmitted infections or immune rejection [13]. Most currently available hESC lines have been exposed to animal products during derivation or culture [13, 86].

Human feeder cells remove the issue of contamination with animal pathogens or immunogenic particles. These feeder cells are able to support stem cell pluripotentcy in culture. Human ESCs grown on commercially available human foreskin fibroblasts (HFFs) have been shown to remain undifferentiated in xeno-free culture media for over 80 passages [13, 161]. Some risk of pathogen transfer still exists with human feeders. One way around this is to create feeders from the cell line being cultured [13]. These cells do not remove issues with variability associated with natural products, and they still provide an undefined surface. Commercially available laminin has been shown to contain a variety of fragmented proteins, isoform mixtures, and fibronectin contamination [162], indicating that even purified extracts are not completely safe from contamination and batch variation.

Ideally, culture should be synthetic and fully chemically defined [55]. Greater control over cell response should be possible with artificial ECM [163]. Many hESC applications will require defined growth conditions, and both clinical applications and fundamental research would benefit from fully defined substrates [55]. Defined culture conditions would facilitate studies into the molecular basis for pluripotency, and allow us to greatly increase our understanding of the control systems behind cell fate [54].

1.4 3D Substrates for Pluripotent Stem Cell Culture

There are a range of approaches to creating a 3D environment for pluripotent stem cells, each with its own strengths. Cells may be cultured in 3D with or without a supporting scaffold material [149]. There is currently no single method that has proven suitable for

all pluripotent cell expansion and maintenance [149]. This section summarises some of the current approaches.

An early method for 3D stem cell culture is embryoid body (EB) formation. These embryo-like structures are tight colonies of cells which differentiate spontaneously. This method is intended to recreate embryonic development as found *in vivo* [164]. It allows 3D cellular interactions without the need for a supporting scaffold [21]. Embryoid bodies can be formed *via* several techniques including hanging drop [149], low attachment plate, and rotating cultures. Human embryonic stem cells have been cultured as cell spheroids in spinner flasks, yielding a 1 x 10^{13} fold expansion [18]. An advantage of this method is the ability to use defined media, making the process chemically defined as no further surface or scaffold is required. However, the diameter of cell spheroids and embryoid bodies tends to be variable. This leads to issues such as necrosis in the centre of larger spheres as there is limited diffusion of nutrients and oxygen into the centre of the body [165]. Thus the cell environment is heterogeneous throughout the culture [166]. Due to this heterogeneity, EB culture methods have been used most effectively for studying differentiation and cancer [21, 149, 167, 168]. They are not typically used for expansion of pluripotent cells.

Culture systems that incorporate biomaterial scaffolds offer better control over cultured cells. Biomaterials are materials which have either an innate or engineered ability to control interactions with living systems [169]. These materials may be naturally derived, fully synthetic, or hybrid materials.

1.4.1 Naturally Derived Materials

1.4.1.1 Decellularised Tissues

Decellularised tissues offer a ready-made 3D scaffold with the ideal structure for creating specific cell types [170]. They come 'prefabricated' with specific molecular composition,

topography and stiffness which is thought to direct cell behaviour and which can be difficult to recreate when designing synthetic scaffolds [5, 41]. Promising results have been achieved with a number of tissues including whole organs [171]. Examples include heart [172], lung [173], kidney [174], and blood vessels [175].

The decellurisation process typically involves perfusing the tissue with decellularising agents including surfactants [5], enzymes, acids, and bases [176]. There are several methods, with immersion being the most widely accepted and perfusion being more modern [171]. Successful decellularisation results in an extracellular matrix that should not be immunogenic and can subsequently be re-cellularised [177]. An example of this process is shown in Figure **??**. Pluripotent stem cells have been highlighted as a suitable source of cells for the re-cellularisation process [171]. The use of hPSCs to bioengineer organs is predicted to be key in therapeutics [5]. While decellularised scaffolds have been seeded with different stem cell lines [176], the end goal is generally to differentiate the cells and repopulate the original organ rather than to keep an ongoing pluripotent cell culture.

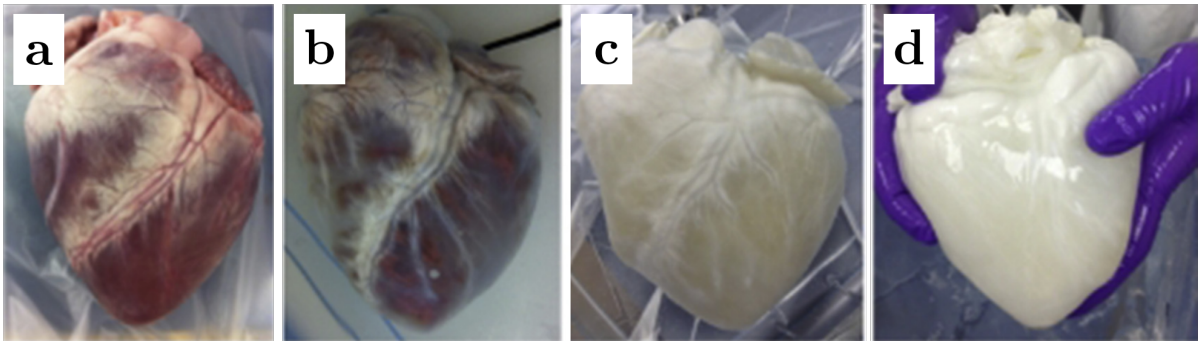

Figure 1.3: *Decellularisation of a porcine heart via perfusion. a) Porcine heart prior to decellularisation b) Porcine heart after 8 hours of perfusion c) Porcine heart after 48 hours of perfusion d) Fully decellularised heart after perfusion process has been completed. The native extracellular structure is preserved. Reproduced under Creative Commons license from* Surgery, *Seetapun & Ross 2016 [171].*

Decellularisation has been used to produce a supporting ECM from feeder cells for the growth of pluripotent cells [41]. This method effectively maintained pluripotency of mouse embryonic stem cells, but it does not result in a scalable 3D culture system. In addition,

processing typically reduces material integrity of tissue [177]. The use of decellularised tissues still requires the use of animal or human derived components, leading to issues with sourcing original tissues, variability, and disease transfer.

1.4.1.2 Natural Polymers

Naturally derived polymers are widely used due their inherent biocompatibility, biofunctionality, and biodegradability [172, 178]. Like decellularised tissues, natural polymers present appropriate recognition sites and structures to cells without further modification. Advantages of natural polymers over feeder cells or decellularised scaffolds include ease of chemical modification, and the ability to synthesise them in a range of formats such as coatings or beads. This makes them applicable to a wider range of culture formats and cell outcomes. They are also more scalable. The native extracellular matrix contains several natural polymers which can be purified for use as cell culture substrates. These include collagen [179], laminin, hyaluronic acid, fibronectin, and gelatin [172, 180, 181]. Non-ECM natural polymers such as agarose [182], alginate [169, 183], chitosan [178], and silk [184, 185], have also been investigated as cell substrates [21, 172]. Natural polymers may be applied as coatings on 2D substrates, or prepared as 3D culture scaffolds. Three-dimensional scaffold formats include monolith [150], electrospun mesh [186], microcarrier [187], microcapsule [188], and hydrogel [140].

Porous atelocollagen scaffolds are commercially available for 3D cell culture under the brand name AteloCell®. AteloCell® MIGHTY scaffolds have been found to support mouse ESCs without exogenous factors [150]. This experiment highlighted the importance of the 3D structure by comparing the scaffold to both a standard gelatin-coated culture plate, and to a 2D atelocollagen layer. The 2D atelocollegen showed the same differentiation behaviours as a 2D gelatin control. Both 2D formats were less able to maintain pluripotency in LIF-negative, defined, serum-free media compared to the 3D scaffold [150]. This suggested that the 3D structure could substitute for exogenous signalling when maintaining pluripotency of mESCs on atelocollagen.

Another monolithic structure comprised of porous chitosan-alginate formed by lyophilisation (Figure 1.4) could be used to support pluripotency of human embryonic stem cells for 21 days without passaging [178]. In contrast, cells maintained on feeder cells required passaging every 6 days as the supporting cell layers deteriorated. Thus the 3D culture system not only provided a 3D environment that could support human pluripotent cells, it also required less frequent handling than the more traditional culture approach.

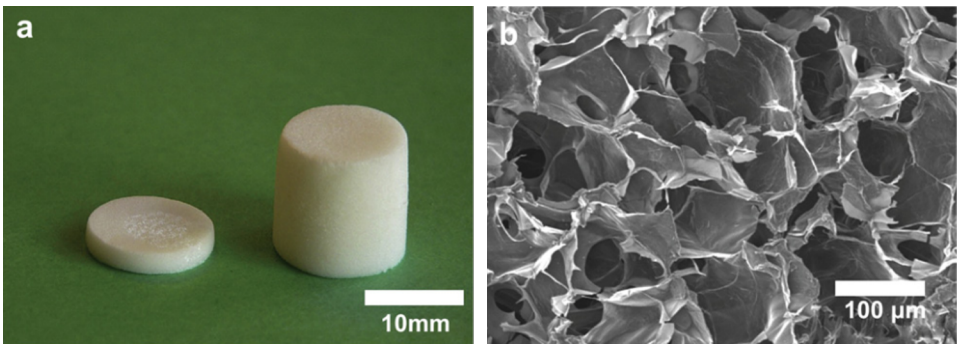

Figure 1.4: *Porous chitosan-alginate scaffolds synthesised by Li et al. provide a 3D environment for effective stem cell expansion. Reproduced with permission from* Biomaterials, *Li* et al. *2010, copyright 2018 Elsevier [178].*

Natural polymers are frequently formed into hydrogels. Hydrogels are 90 - 95 % water making them biocompatible [172]. This water content also mimics the soft, hydrated structure of the natural ECM [21, 189], making hydrogels a key cell support due to their structural biomimicry. Hydrogels may be physically cross-linked or chemically cross-linked. Physically cross-linked gels are also called reversible gels, as their bonds are formed by a reversible change in conditions such as pH or temperature. They are usually mechanically weak [21]. Chemically cross-linked hydrogels are held together with covalent bonds, and are typically stronger than physical hydrogels [21]. Hydrogels may be coated onto a structural substrate such as TCPS and microcarriers, or used as a 3D culture environment. Hyluaronic acid (HA) is found in both developing embryos and undifferentiated cells [190]. In light of this observation, soft HA based hydrogels have been developed in an attempt to to mimic the microenvironment inside a blastocyst [117]. Soft HA gels can be utilised to support pluripotent cells for over 20 days without passaging [191]. Gerecht *et al.* reported a hyaluronic acid-based hydrogel that supported pluripotent hESCs [191].

Downsides of this hydrogel include the use of UV photoinitation which may induce point mutations in the cells, and difficulty of analysis during culture [55].

Natural polymers can be modified to enhance their biofunctionality. RGD-functionalised alginate hydrogels were used to investigate the 3D culture of a range of stem cells, including an embryonic line [183]. By changing the RGD concentration, cell spreading could be manipulated. Interestingly, the effect of the RGD peptide was found to outweigh the effect of varied stiffness on stem cell behaviour [183]. Deng *et al.* presented a chitosan hydrogel with functional peptides and vitronectin. Chitosan is a glycosaminoglycan with inherent biocompatibility and antibacterial properties [192]. The gel could be coated on TCPS plates, and supported human iPSCs for 10 passages using defined media [192]. This type of coating could be a replacement for more complicated ECM mixtures like Matrigel.

Hydrogels have many desirable properties for pluripotent stem cell culture. However, they are restricted by practical issues including gel preparation, storage, and viability [148]. Another issue is restricted scale-up potential due to the limited diffusion of nutrients through hydrogels in static culture [21]. Combining hydrogels with other materials creates composites which may overcome mechanical limitations [193].

Microcapsules can be used to provide engineered cell niches. Alginate is a common encapsulation material, and has been shown to support both iPSCs [188] and ESCs [194]. Human ESCs encapsulated by alginate fibres have been maintained in mTeSR1 media in static culture for 5 passages [194]. These capsules can be multi-phase, allowing further engineering of the microenvironment presented. An alginate-chitosan hydrogel 'shell' around a liquid alginate core was synthesised and used to support mESCs [195]. The encapsulation examples here were applied to static culture. Microcapsules are particularly useful in agitated culture due to their ability to protect cells from excessive shear. Agitated culture is discussed further in Section 1.4.3.2.

Many issues with natural polymers relate to the inherent variability in products that

come from living organisms. They may have inconsistencies in structure, composition and mechanical properties, which can lead to uncertainty [196]. Low mechanical strength can lead to issues with handling, making culture more labour intensive and limiting their practicality. Naturally derived polymers also share some of the issues with contamination found in feeder cells [21, 181]. Recombinant proteins resolve this issue but are expensive, and not all natural polymers are simple to recreate synthetically.

1.4.2 Synthetic Polymers

Using natural products has the advantage of presenting ready-made recognition sites and appropriate physical structures, as well as proven long-term biocompatibility [172]. However, it also introduces several potential issues. Natural materials have a complex structure, are difficult to fully purify, and can be immunogenic or variable [4, 196, 197]. These issues have prompted a shift towards defined, animal component-free cell culture on synthetic substrates and scaffolds [4]. Synthetic polymers are the key material in this strategy as they are highly versatile and controllable, with defined chemistries, surface functionalisation, and geometries. Sheets, porous sponges, fibres, meshes, gels and composites may all be formed from polymers for use as 3D cell scaffolds [198]. Polymers have architecture which can be modified to mimic natural features [172, 196], they can be very cost effective, and are in ample supply.

This flexibility allows them to have a wide range of stiffnesses, for example, while remaining non-fouling and biochemically consistent [126]. Mechanical properties are known to impact cell outcomes such as proliferation, viability, and cell fate [199, 200], so the ability to control the stiffness of synthetic polymers is advantageous. Synthetic polymers do not typically elicit an immune response due to their lack of biologically active groups [196]. They are a 'blank slate' to which specific functionality can be added, allowing investigation into the effects of specific properties and stimuli on stem cells. They also avoid the contamination risks associated with growing cells on animal or human derived substrates.

Polymer stem cell scaffolds can be formed using several techniques. These include electrospinning, self-assembly, emulsion templating, 3D-printing, casting, and foaming [201, 202]. The most commonly used synthetic polymers in cell scaffolds are poly-lactic acid (PLA), poly-glycolic acid (PGA), poly-lactic acid-co-glycolic acid (PLGA) [196] and polyethylene glycol (PEG) [21]. Poly-caprolactone (PCL) and poly-L-lysine (PLL) are also commonly used. PCL has FDA approval for clinical applications [196]. These polymers can be functionalised with a range of moieties to enhance crosslinking or bioactivity [181]. Scaffolds aim to mimic the cell niche, effectively supporting cells and reducing cell aggregation [203]. However it is not always necessary to replicate the full complexity of the native environment to achieve a functional result [177], allowing synthetic culture systems to be simpler than their naturally-derived counterparts. Many synthetic polymers have tunable degradation properties. Tissue engineering applications typically require a material that will degrade in the body, making natural polymers attractive. However, in culture this adds another variable that may not be required long term [149]. For *in vitro* culture, non-degradable synthetic scaffolds are an attractive option. As they do not need to integrate into body, their inertness is an advantage because it provides a consistent and reproducible culture environment [152].

Synthemax® is a chemically defined, xeno-free, RGD peptide modified acrylate surface available from Corning. Human iPSCs could be maintained for more the ten passages on cultureware coated with Synthemax [90]. Combined with mTeSR1 media, this provided a synthetic, animal-free surface for pluripotent stem cell expansion. Melkoumian *et al.* also utilised peptide-functionalised acrylate to culture pluripotent cells. Human embryonic stem cells were cultured on acrylate coatings functionalised with the active domains from one of five different ECM proteins (bone sialoprotein, vitronectin, long- and short-fibronectin, and laminin). Both cell lines could be maintained on the sialoprotein and vitronectin decorated surfaces in four different commercially available defined media for more than ten passages.

Another synthetic coating was developed using poly[2-(methacryloyloxy)ethyl dimethyl-

(3-sulfopropyl)ammonium hydroxide] (PMEDSAH) [204]. This material supported human ESCs for over 25 passages in conditioned media and 10 passages in defined StemPro media. The authors noted that due to its chemically defined nature, the PEDMESAH surface could be reproducibly synthesised, stored long-term, and handled easily [204]. These coatings do not provide 3D environments, but they do demonstrate the utility of synthetic polymer materials in stem cell maintenance. Knowledge gathered from these 2D analysis can then be applied when designing 3D systems.

Synthetic polymers can also used to form hydrogels, taking advantage of the bio-mimicry associated with high water content and low modulus, while maintaining a chemically defined environment. Mouse ESCs encapsulated in degradable, vitronectin-derived RGDSP sequence functionalised PEG hydrogels remained pluripotent without LIF, while their 2D counterparts differentiated [121]. This again highlights the importance of 3D culture environments. It is also suggested that spatial confinement plays a role in maintaining pluripotency [121] and indeed in controlling differentiated fate. Pluripotent stem cells have been maintained for over 50 passages on a thermoresponsive copolymer hydrogel under defined conditions [205]. This poly(N-isopropylacrylamide)-co-poly(ethylene glycol) (PNIPAAm-PEG) hydrogel allowed passaging by simply cooling the culture from 37 °C to 4 °C. The long term maintenance of embryonic stem cells produced an approximately 20-fold expansion per five day passage, with high purity of Oct4 positive cells. Another thermoreversible hydrogel was synthesied using PNIPAAm and hyaluronic acid (HA). This hybrid natural-synthetic copolymer hydrogel supported long term expansion of human embryonic and induced pluripotent cells in defined E8 media [206].

Electrospun scaffolds emulate the fibrous structure of the ECM [172] and can enhance stem cell survival, direct stem cell fate, or act as a drug delivery substrate [207]. This method uses either a polymer solution or melt that is drawn into fibres by a high voltage electric field [151]. The fibres are then collected as a non-woven mesh. The fibres can be made from a wide variety of natural or synthetic materials [207]. Electrospun polystyrene has been shown to support iPSC aggregates under xeno-free conditions [21].

Zonca *et al.* used a poly(ether sufone) (PES) electrospun matrix with a grafted N-[3-(dimethylamino)propyl] methacrylamide (DMAPMA) polymer previously shown to support strong attachment and self renewal of mouse embryonic stem cells [207]. Synthetic electrospun scaffolds for stem cell culture have also been synthesised using polyamide [208], polyurethane [209, 210], PCL, PLA, and PLGA. An interesting approach to 3D culture by Leong *et al.* veers away from making the scaffold bioactive and adhesive to cells and instead tries to recreate a cell aggregate culture in a bulk 3D system. Porous electrospun polystyrene scaffolds were constructed with minimal cell interactions [151]. These meshes could trap hiPSCs as aggregates, resulting in pluripotent clusters that could be cultured for 10 passages. The fibres prevented excessively large clumps from forming by creating "compartments" between the fibres. A major downside of electrospun scaffolds is the difficulty in creating thick constructs. The thin fibres produced result in sheets of scaffold, which some consider a pseudo-3D environment.

Bulk 3D scaffolds can be produced simply using porous polymers. Salt leaching [211, 212], freeze-drying [213, 214], block copolymer-templating [215, 216], gas foaming [202], and emulsion-templating [217, 218] can all be used to create polymer monoliths with suitable morphology for cell culture. Emulsion templating results in interconnected foams that have been used to culture a range of cell types in 3D [219, 220, 221]. These polymerised high internal phase emulsions, known as polyHIPEs, have porosities of at least 74 % and up to 99 % [222, 223]. They have potential as scaffolds for cell culture due to their highly interconnected structure allowing perfusion of nutrients and wastes within the cell culture [224]. Alvetex® is a commercially available polystyrene-based polyHIPE scaffold that is suitable for a range of 3D cell culture applications [225, 226, 227, 228, 229]. Emulsion templated polymers have been shown to support adipose derived stem cells [230], muscle stem cells [231], and stem cell differentiation to neural progenitors [136]. Advantages of porous solid polymers include highly flexible porosity and pore diameter, stable interconnected porosity, and tailorable macro-architecture. Using light-cured polyHIPEs, Sherborne *et al.* applied lithography to polyHIPE emulsions, forming a multi-scale porous structure for cell culture [232].

As understanding of the factors that influence stem cell pluripotency increases, synthetic polymer culture systems can be modified accordingly. An interesting study by Ying *et al.* suggests suggests that embryonic stem cells are a basal state that will intrinsically self-maintain if effectively shielded from certain stimuli, such as those found in undefined culture conditions [233]. Synthetic polymers are the ideal material to present a range of inert of functional environments to test such hypotheses.

1.4.3 Scalable 3D Culture Formats

1.4.3.1 Microcarriers & Microcapsules

One way to overcome the problems associated with monolithic biomaterials is to form them into smaller particles, known as microcarriers. These small supports are typically 100-300 μm in diameter, and can be used in static [80] or agitated [157] culture. Microcarriers can be synthesised from a range of natural and synthetic polymers including collagen, dextran, and polystyrene [66]. These structures can be further modified with coatings such as ECM proteins [21]. Microcarriers provide a high surface area to which cells can adhere, as well helping to prevent aggregation and the associated necrosis [79]. This aids control of cell fate, as the cells in the centre of aggregates tend to differentiate.

Microcarriers are regularly used to grow cells in biopharmaceutical applications. They have also been used as the basis for stem cell expansion [18]. Commercially available microcarriers such as the dextran-based Cytodex and polystyrene Solo-Hill have been used for a range of stem cell expansions [234, 235]. Expansion and maintenance of pluripotent stem cells has been achieved on Matrigel-coated cellulose [21], dextran, and polystyrene. Coating the microcarriers provides further options for maintaining pluripotent cells [21]. Xeno-free cultures are favoured for clinical applications, and have been used in conjunction with dextran microcarriers to achieve a 12-fold increase in hESC growth [236]. Human pluripotent stem cells have also been successfully expanded on microcarriers and subsequently differentiated into a range of cell types [157].

Chen *et al.* investigated 10 different commercially available microcarriers for their capacity to allow hESC attachment, growth, and pluripotency [187]. These carriers were comprised of cellulose, dextran, gelatin, or hydroxylated methacrylate and interestingly included both spherical and cylindrical geometries. This analysis concluded that a coating was required to maintain stem cell pluripotentcy on all of the microcarriers investigated, and that Matrigel was the most widely applicable coating. However a laminin coating was also able to support cells. Solid carriers provide less surface area for cell expansion than porous microcarriers. However, the removal of cells after expansion is simpler which can lead to higher yields [237]. Biosilon and RapidCell are examples of commercially available solid borosilicate carriers [237].

Some of the issues with solid carriers are overcome by using porous carriers. Porous carriers increase cell density, and protect the cells from shear forces. CultiSpher, Cytopore and Cytoline are commercially available porous systems [18]. The highly porous structure of these scaffolds allows for nutrients and wastes to diffuse thorough the material, and provides a high surface area on which the cells can grow. This allows high cell densities and efficient use of culture space [18]. Incorporating these 3D structures into bioreactors provides a boost to yield per litre [18].

Microcapsules are gel spheres that are formed with the cells already contained, rather relying on the cells to attach to the outside of the structure. Microcapsules trap cells in semi-permeable materials that protects them from agglomeration and shear, while allowing diffusion to and from the cells [21, 203]. There is also evidence that such encapsulation prevents immune response when cells are transplanted. Alginate and agarose are commonly used to encapsulate cells. The microenvironment inside the microcapsules can be tailored for maintenance of pluripotency [21]. A 20-fold expansion of hESCs in alginate microspheres has been achieved [18, 238]. Defined media conditions were used with an alginate encapsulation system, providing a defined platform for maintaining undifferentiated cells for up to 260 days without passaging [239]. A similar result has been achieved using thermo-reversible hydrogels to expand hPSCs under fully defined condi-

tions [18, 240]. The advantage of this second system are twofold. Firstly, defined systems fit with good manufacturing practices, and secondly the thermo-reversible gels allow removal of the cells without exposure to proteolytic enzymes that can adversely affect the cell's downstream viability. Microcarriers for stem cell culture are reviewed in more detail elsewhere [89, 157].

1.4.3.2 Bioreactors

Even with the use of 3D cell scaffolds, expanding pluripotent stem cells in typical flasks or well plates is not conducive to large scale applications. Two-dimensional cell factories have been reported, which enable "scale-out" of culture by multiplying the number of flasks used and introducing a degree of automation [241]. However these systems still typically use static culture, potentially introducing unfavourable gradients in oxygen, nutrients, growth factors, and pH. Bioreactors offer the opportunity to drastically increase scale-up of pluripotent stem cell culture. They can provide a more homogenous, easily monitored environment than static culture while taking advantage of the scalability of 3D cell cultures [79]. Cells can often be sampled non-destructively as dissociation is not required to take a cell sample, meaning monitoring and control systems can be incorporated more easily into bioreactors. This would allow quantitation of culture parameters and development of GMP-compliant processes. As with static culture formats, bioreactors require control of parameters such as temperature, O_2, nutrients, pH and wastes [21, 242]. Cell seeding density, feeding method [243] and the incorporation of scaffolds can also impact cell fate. They have the additional challenge of balancing dynamic mechanical forces.

Spinner flasks are a simple and inexpensive bioreactor setup. An internal impeller or stirrer bar is used to stir the culture media. The shear applied by mixing ensures a more homogenous distribution of nutrients and oxygen, but excessive shear can lead to cell death [21]. Rotating wall vessels reduce the shear experienced by cells as they do not use an internal stirrer. Other bioreactor systems include flow perfusion systems,

which operate in a continuous fashion rather than as a batch process, mechanical force bioreactors, which aim to mimic the tension and compression found in natural tissues, and wave bioreactors [241]. Microfluidic devices also offer the opportunity to study cells under dynamic conditions [56]. However these are smaller scale and not suitable for bulk cell expansion. Several bioreactor formats are illustrated in Figure 1.5.

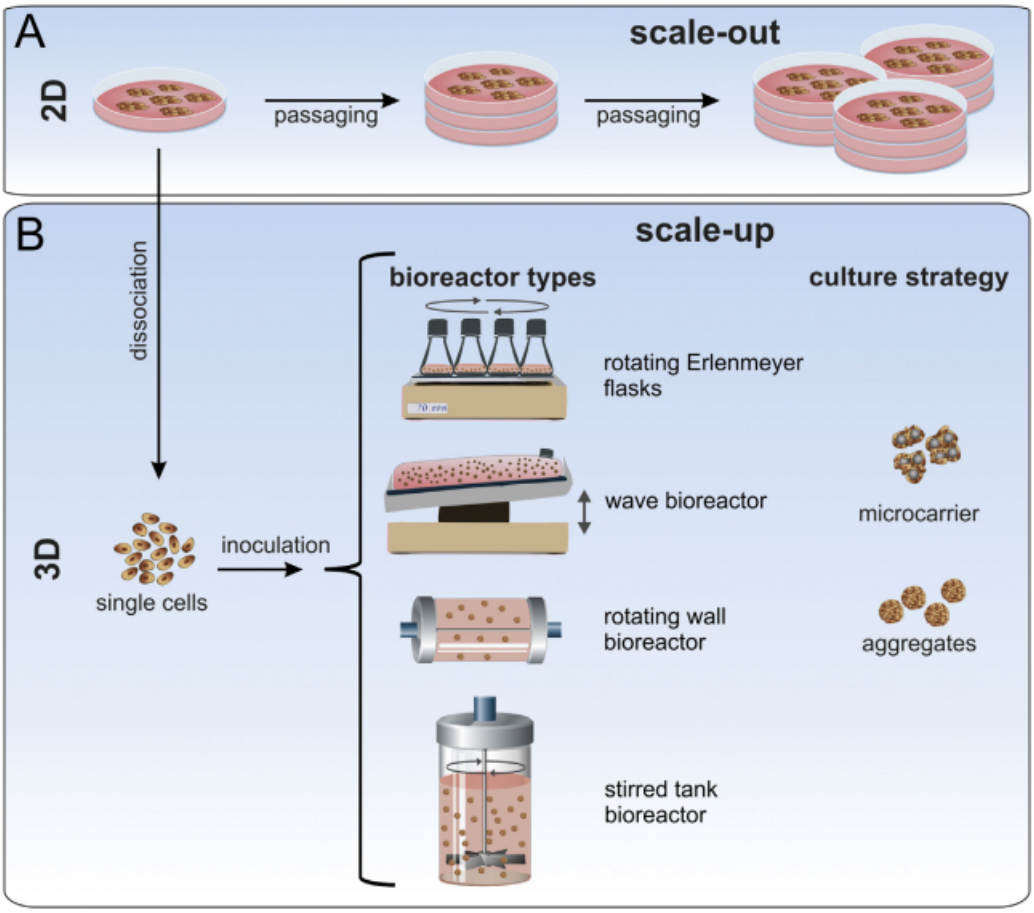

Figure 1.5: *Summary of expansion strategies in bioreactors. a) 2D "scale-out" b) 3D scale-up. Cells may be grown as aggregates, supported by microcarriers, or encapsulated. Reproduced under Creative Commons license from* Process Biochemistry, *Kropp* et al. *2017, [241].*

In a bioreactor, stem cells may be cultured in scaffold-free aggregates, on microcarriers, or after encapsulation [244]. Aggregate strategies are typically associated with stem cell differentiation [56]. However, the combination of a suspension culture environment with multicellular aggregates appears to adequately support the maintenance of embryonic

stem cells under the correct conditions [56, 241]. Shafa *et al.* maintained human iPSCs as aggregates in a xeno-free, stirred suspension bioreactor environment. They achieved 58-fold expansion over 4 days, while maintaining differentiation capacity [245]. Stirred suspension bioreactors paired with serum-free mTeSR media containing ROCK inhibitor and rapamycin have been reported to allow the batch-wise expansion of hESCs [246]. Abecasis *et al.* used perfused, stirred-tank bioreactors to culture human iPSC aggregates. They were able to achieve continuous expansion of pluripotent, genomically stable stem cells in this system, with a 1,100× expansion factor over the 11 day culture [247]. Control of dissolved oxygen was found to be an important parameter in this system, with maximum cell concentration achieved using 4 % oxygen. This method maintains natural cell-cell contact, is capable of high production yields, and does not include the added complexity of supporting matrices or scaffolds [56]. The dynamics of the pluripotent stem cell aggregate microenvironment is reviewed in [248]. A major disadvantage of cell aggregate culture is the difficulty in controlling aggregate size, which leads to cell gradients across the aggregate. This can result in necrosis in the centre if aggregates become too large (over 0.5-1 mm), or cell differentiation [80]. This method therefore requires frequent dissociation, which can stress pluripotent cells. Cells may also be damaged due to physical forces in this format [56].

Design of 3D culture systems typically tries to mimic the stem cell niche. However, the effects of mechanical stress in the developing embryo are still unclear [14, 249]. While it is clear that high shear stress reduces stem cell viability, a low, constantly applied shear stress may help maintain stem cell pluripotency [14]. Guess and Suggs concluded that shear of under 8 dyn/cm^2 likely helped to maintain pluripotency in human iPSCs and ESCs [250]. Tight regulation of shear by the control of stir speed is essential to maintaining pluripotent stem cells in bioreactors. A combination of commercially available Cytodex 3 microcarriers and a spinner flask setup allowed the long term survival of mouse iPSCs at 25 rpm [235]. Higher rates caused cell detachment, while low rates did not achieve proper microcarrier suspension.

Providing a scaffold for stem cells in a bioreactor may provide better control over culture parameters and cell fate. A microcarrier or encapsulating hydrogel allows for specific design of the microenvironment to provide an appropriate niche and direct cell fate. Thus bioreactors are frequently used in conjunction with microcarriers or encapulation [157]. Microcarriers can help overcome the issues of aggregation and shear damage found in aggregates. Another advantage of microcarriers is their ability to tailor the available surface area for expansion. Several microcarriers are available for the culture of pluripotent stem cells as discussed in the previous section [187]. Issues with microcarriers may arise if visual monitoring of cells is required, as porous scaffolds may make this difficult. Microcarriers also add cost to the culture system compared to a scaffold-less system, though this would be offset by improved culture outcomes. Microcarriers may also have issues with clumping [56]. Encapsulation drastically reduces the effect of shear stress on stem cells while reducing aggregation [56]. Capsules are typically comprised of alginate-based materials [169, 238]. Serra *et al.* compared single, clumped and microcarrier-immobilised cells encased in crosslinked alginate microcapsules and cultured in spinner flasks. The combination of microcarrier and alginate capsule provided the most robust maintenance of pluripotency.

Stirred-suspension bioreactors for hPSCs are reviewed in [244], and stem cell culture in bioreactors in [40], [198], and [251]. As novel 3D culture scaffolds are produced, these systems are likely to be considered as the next step in scaling human pluripotent stem cells to industrial quantities.

1.5 Challenges & Outlook

Large scale stem cell expansion is one of the key hurdles facing modern tissue engineering [196]. While 3D culture has been highlighted as a promising approach to culture scale-up, standardised methods for 3D culture have not yet been agreed upon by the scientific community [21]. To progress from laboratory bench to clinical application, cultures must

be designed to be reproducible, predictable, effective, GMP-compliant, and affordable [56]. Major challenges include not only producing a suitable quantity of cells, but also control of cell fate including ensuring population purity, quality of cells, as well as logistic factors such as storage, transport and implementation [56].

Ensuring sufficient nutrient supply to the cells is a crucial hurdle to effective 3D culture. The delivery of oxygen and nutrients is a challenge in thick bioengineered constructs [171]. Where small or short-term cultures are needed, for example in drug screening, this is not as critical. However, as cells are expanded for downstream applications nutrient availability becomes restricted. The oxygen diffusion across engineered tissue is typically limited to 200 µm [5], meaning that innovative solutions such as bioreactors or 3D printing will need to used in conjunction with suitably bioengineered materials to achieve homogeneous stem cell maintenance.

The complexity of the *in vivo* cell environment and our limited understanding of the biological pathways that control stem cell behaviour makes designing appropriate biomaterials for pluripotent stem cell culture challenging [73, 196]. 3D culture for stem cell expansion is still an area of intense research [21]. Future studies will need to focus on clarifying the individual and synergistic effects of biochemical and biophysical factors on stem cell phenotype [14]. To complicate matters, individual cell lines may have different responses to specific culture environments [65]. Understanding the minimal effective factors for controlling stem cell fate will allow more directed design of culture systems that mimic the niche in a way that is amenable to cells, while still fulfilling clinical needs.

It is clear that a fully defined, 3D culture system will be required to realise the potential of pluripotent stem cells in research and clinical applications. A synthetic polymer construct will likely be the most appropriate scaffold for developing this defined, xeno-free system for industrial scale stem cell expansion. Complying with the stringent requirements of those utilising stem cell technologies will likely require the cooperation of a number of groups, including fundamental researchers in biology, process engineers, automation experts and regulatory bodies.

This thesis presents the development of a 3D culture system that uses aspects of the cell niche to maintain pluripotent stem cells, while also fulfilling the growing requirements for 3D, animal component-free, and chemically-defined culture. An emulsion templated polymer scaffold was selected as the basis for this system due to the advantageous properties of these materials, particularly their rapid bulk synthesis, fully interconnected 3D morphology, and ability to be surface-functionalised. Surface functionalisation focused on a commercially available ECM coating, and the highly potent cyclic-RGD adhesive peptide. Both of these have previously been shown to promote stem cell pluripotency under a range of conditions.

1.6 Aims & Objectives

This thesis aims to show the development and optimisation of a chemically-defined, animal component-free, 3D culture system for maintaining human pluripotent stem cells *in vitro*. To achieve this aim, the first focus will be the production of a 3D scaffold with suitable properties for pluripotent stem cell culture. A polyHIPE polymer scaffold material is investigated due to its interconnected morphology. In order to improve the scaffold's ability to maintain stem cells, a major objective of this section is to develop a versatile functionalisation protocol that can be used to tailor the surface chemistry of the polyHIPE scaffold under benign, biocompatible conditions. The ability of the polyHIPE material to support 3D embryonic stem cell culture will then investigated using human embryonic stem cells. This will involve altering the culture surface to support cells, and assessing their proliferation *via* cell staining. The void and interconnect diameter of the scaffold are key characteristics that will be assessed and optimised. Finally this work will establish whether human pluripotent stem cells can maintain their differentiation capacity when cultured in a functionalised 3D polyHIPE scaffold in defined media.

References

[1] Lambshead, J. W.; Meagher, L.; O'Brien, C.; Laslett, A. L. *Cell Regen.* **2013**, *2*, 7.

[2] Adil, M. M.; Schaffer, D. V. *Curr. Opin. Chem. Eng* **2017**, *15*, 24–35.

[3] Perez, R. A.; Choi, S.-j.; Han, C.-m.; Kim, J.-J.; Shim, H.; Leong, K. W.; Kim, H.-W. *Prog. Mater. Sci.* **2016**, *82*, 234–293.

[4] Haque, M. A.; Nagaoka, M.; Hexig, B.; Akaike, T. *Sci. Technol. Adv. Mater.* **2010**, *11*, 014106.

[5] Garreta, E.; Oria, R.; Tarantino, C.; Pla-Roca, M.; Prado, P.; Fernández-Avilés, F.; Campistol, J. M.; Samitier, J.; Montserrat, N. *Mater. Today* **2017**, *20*, 166–178.

[6] Takahashi, K.; Tanabe, K.; Ohnuki, M.; Narita, M.; Ichisaka, T.; Tomoda, K.; Yamanaka, S. *Cell* **2007**, *131*, 861–872.

[7] Kobold, S.; Guhr, A.; Kurtz, A.; Löser, P. *Stem Cell Reports* **2015**, *4*, 914–925.

[8] Sproul, A. A. *Mol. Aspects Med.* **2015**, *43-44*, 54–65.

[9] Thomson, J. A.; Itskovitz-Eldor, J.; Shapiro, S. S.; Waknitz, M. A.; Swiergiel, J. J.; Marshall, V. S.; Jones, J. M. *Science* **1998**, *282*, 1145–1147.

[10] de Miguel-Beriain, I. *Adv. Drug Deliv. Rev.* **2015**, *82*, 176–180.

[11] King, N. M.; Perrin, J. *Stem Cell Res. Ther.* **2014**, *5*, 85.

[12] Hazeltine, L. B.; Selekman, J. A.; Palecek, S. P. *Biotechnol. Adv.* **2013**, *31*, 1002–1019.

[13] Desai, N.; Rambhia, P.; Gishto, A. *Reprod. Biol. Endocrinol.* **2015**, *13*, 9.

[14] Ding, S.; Kingshott, P.; Thissen, H.; Pera, M.; Wang, P.-y. *Biotechnol. Bioeng.* **2017**, *114*, 260–280.

[15] Wang, Y.; Cheng, L.; Gerecht, S. *Ann. Biomed. Eng.* **2014**, *42*, 1357–1372.

[16] Kingham, E.; Oreffo, R. O. *ACS Nano* **2013**, *7*, 1867–1881.

[17] Akkerman, N.; Defize, L. H. *BioEssays* **2017**, *39*, 1600244.

[18] Kumar, A.; Starly, B. *Biofabrication* **2015**, *7*, 044103.

[19] Polini, A.; Prodanov, L.; Bhise, N. S.; Manoharan, V.; Dokmeci, M. R.; Khademhosseini, A. *Expert Opin. Drug Discov.* **2014**, *9*, 335–352.

[20] Gómez-Lechón, M. J.; Tolosa, L.; Conde, I.; Donato, M. T. *Expert Opin. Drug Metab. Toxicol.* **2014**, *10*, 1553–1568.

[21] McKee, C.; Chaudhry, G. R. *Colloids. Surf. B Biointerfaces* **2017**, *159*, 62–77.

[22] Centeno, E. G. Z.; Cimarosti, H.; Bithell, A. *Mol. Neurodegener.* **2018**, *13*, 27.

[23] Soo, J. Y.-C.; Jansen, J.; Masereeuw, R.; Little, M. H. *Nat. Rev. Nephrol.* **2018**, *14*, 378–393.

[24] Stadtfeld, M.; Hochedlinger, K. *Genes Dev.* **2010**, 2239–2263.

[25] Purpura, K. A.; Bratt-Leal, A. M.; Hammersmith, K. A.; McDevitt, T. C.; Zandstra, P. W. *Biomaterials* **2012**, *33*, 1271–1280.

[26] Ilic, D.; Ogilvie, C. *Stem Cells* **2017**, *35*, 17–25.

[27] Fraietta, I.; Gasparri, F. *Expert Opin. Drug Discov.* **2016**, *11*, 501–514.

[28] Lancaster, M. A.; Knoblich, J. A. *Nat. Protoc.* **2014**, *9*, 2329–2340.

[29] Brafman, D. A.; Chang, C. W.; Fernandez, A.; Willert, K.; Varghese, S.; Chien, S. *Biomaterials* **2010**, *31*, 9135–9144.

[30] Schwartz, S. D. et al. *Lancet* **2015**, *385*, 509–516.

[31] Qi, Z. *Treatment of Dry Age Related Macular Degeneration Disease With Retinal Pigment Epithelium Derived From Human Embryonic Stem Cells* **2017**, Clinical Trial NCT03046407.

[32] Belfort, R. *Stem Cell Therapy for Outer Retinal Degenerations* **2017**, Clinical Trial NCT02903576.

[33] Kushner, J. A.; MacDonald, P. E.; Atkinson, M. A. *Cell Stem Cell* **2014**, *15*, 535–536.

[34] Lemcke, H.; Voronina, N.; Steinhoff, G.; David, R. *Stem Cells Int.* **2018**, *2018*.

[35] Lu, H. F.; Chai, C.; Lim, T. C.; Leong, M. F.; Lim, J. K.; Gao, S.; Lim, K. L.; Wan, A. C. *Biomaterials* **2014**, *35*, 2816–2826.

[36] Tolosa, L.; Pareja, E.; Gómez-Lechón, M. J. *Transplantation* **2016**, *100*, 2548–2557.

[37] Fan, Y.; Wu, J.; Ashok, P.; Hsiung, M.; Tzanakakis, E. S. *Stem Cell Rev.* **2015**, *11*, 96–109.

[38] Rowland, T. J.; Miller, L. M.; Blaschke, A. J.; Doss, E. L.; Bonham, A. J.; Hikita, S. T.; Johnson, L. V.; Clegg, D. O. *Stem Cells Dev.* **2010**, *19*, 1231–1240.

[39] Khalil, S.; El-Badri, N.; El-Mokhtaar, M.; Al-Mofty, S.; Farghaly, M.; Ayman, R.; Habib, D.; Mousa, N. *PLoS One* **2016**, *11*, e0167116.

[40] Rodrigues, C. A.; Fernandes, T. G.; Diogo, M. M.; da Silva, C. L.; Cabral, J. M. *Biotechnol. Adv.* **2011**, *29*, 815–829.

[41] Sthanam, L. K.; Barai, A.; Rastogi, A.; Mistari, V. K.; Maria, A.; Kauthale, R.; Gatne, M.; Sen, S. *Biomaterials* **2017**, *119*, 9–22.

[42] Scadden, D. T. *Nature* **2006**, *441*, 1075–1079.

[43] Burdick, J. A.; Vunjak-Novakovic, G. *Tissue Eng. Part A* **2009**, *15*, 205–19.

[44] Freyman, T. M.; Yannas, I. V.; Gibson, L. J. *Prog. Mater. Sci.* **2001**, *46*, 273–282.

[45] Gattazzo, F.; Urciuolo, A.; Bonaldo, P. *Biochim. Biophys. Acta. Gen. Subj.* **2014**, *1840*, 2506–2519.

[46] Sharma, S.; Raju, R.; Sui, S.; Hu, W.-S. *Biotechnol J.* **2011**, *6*, 1317–1329.

[47] Rodin, S.; Domogatskaya, A.; Ström, S.; Hansson, E. M.; Chien, K. R.; Inzunza, J.; Hovatta, O.; Tryggvason, K. *Nat. Biotechnol.* **2010**, *28*, 611–615.

[48] Adnan, N.; Mie, M.; Haque, A.; Hossain, S.; Mashimo, Y.; Akaike, T.; Kobatake, E. *Bioconjug. Chem.* **2016**, *27*, 1599–1605.

[49] Ren, Y.; Ma, Z.; Yu, T.; Ling, M.; Wang, H. *Sci. Rep.* **2018**, 1–11.

[50] Eiselleova, L.; Peterkova, I.; Neradil, J.; Slaninova, I.; Hampl, A.; Dvorak, P. *Int. J. Dev. Biol.* **2008**, *52*, 353–363.

[51] Baek, J. A.; Seol, H. W.; Jung, J.; Kim, H. S.; Oh, S. K.; Choi, Y. M. *Tissue Eng. Regen. Med.* **2017**, *14*, 453–464.

[52] Cobo, F.; Talavera, P.; Concha, Á. *Virology* **2006**, *347*, 1–10.

[53] Martin, M. J.; Muotri, A.; Gage, F.; Varki, A. *Nat. Med.* **2005**, *11*, 228–232.

[54] Villa-Diaz, L.; Ross, A.; Lahann, J.; Krebsbach, P. *Stem Cells* **2013**, *31*, 1–7.

[55] Braam, S. R.; Zeinstra, L.; Litjens, S.; Ward-van Oostwaard, D.; van den Brink, S.; van Laake, L.; Lebrin, F.; Kats, P.; Hochstenbach, R.; Passier, R.; Sonnenberg, A.; Mummery, C. L. *Stem Cells* **2008**, *26*, 2257–2265.

[56] Serra, M.; Brito, C.; Correia, C.; Alves, P. M. *Trends Biotechnol.* **2012**, *30*, 350–359.

[57] Weingarten, M.; Akhavan, N.; Hanau, J.; Peter, Y. *AIMS Bioeng.* **2015**, *2*, 15–28.

[58] Jagannathan, L.; Cuddapah, S.; Costa, M. *Curr. Pharmacol. Rep.* **2016**, *2*, 64–72.

[59] Folmes, C. D.; Terzic, A. *Semin. Cell Dev. Biol.* **2016**, *52*, 68–75.

[60] De Miguel, M. P.; Alcaina, Y.; de la Maza, D. S.; Lopez-Iglesias, P. *Curr. Mol. Med.* **2015**, *15*, 343–59.

[61] Mathieu, J.; Zhang, Z.; Nelson, A.; Lamba, D. A.; Reh, T. A.; Ware, C.; Ruohola-Baker, H. *Stem Cells* **2013**, *31*, 1737–1748.

[62] Mohyeldin, A.; Garzón-Muvdi, T.; Quiñones-Hinojosa, A. *Cell Stem Cell* **2010**, *7*, 150–161.

[63] Forristal, C. E.; Wright, K. L.; Hanley, N. A.; Oreffo, R. O. C.; Houghton, F. D. *Reproduction* **2010**, *139*, 85–97.

[64] Forristal, C. E.; Christensen, D. R.; Chinnery, F. E.; Petruzzelli, R.; Parry, K. L.; Sanchez-Elsner, T.; Houghton, F. D. *PLoS One* **2013**, *8*, 1–9.

[65] Prasad, S. M.; Czepiel, M.; Cetinkaya, C.; Smigielska, K.; Weli, S. C.; Lysdahl, H.; Gabrielsen, A.; Petersen, K.; Ehlers, N.; Fink, T.; Minger, S. L.; Zachar, V. *Cell Prolif.* **2009**, *42*, 63–74.

[66] Silva, M. M.; Rodrigues, A. F.; Correia, C.; Sousa, M. F.; Brito, C.; Coroadinha, A. S.; Serra, M.; Alves, P. M. *Stem Cells Transl. Med.* **2015**, *4*, 731–742.

[67] Harvey, A. J.; O'Brien, C.; Lambshead, J.; Sheedy, J. R.; Rathjen, J.; Laslett, A. L.; Gardner, D. K. *PLoS One* **2018**, *13*, 1–19.

[68] Shimada, H.; Hashimoto, Y.; Nakada, A.; Shigeno, K.; Nakamura, T. *Biochem. Biophys. Res. Commun.* **2012**, *417*, 659–664.

[69] Yoshida, Y.; Takahashi, K.; Okita, K.; Ichisaka, T.; Yamanaka, S. *Cell Stem Cell* **2009**, *5*, 237–241.

[70] Pimton, P.; Lecht, S.; Stabler, C. T.; Johannes, G.; Schulman, E. S.; Lelkes, P. I. *Stem Cells Dev.* **2015**, *24*, 663–676.

[71] Yang, Y.; Lu, Y.; Chen, T.; Zhang, S.; Chu, B.; Gong, Y.; Zhao, W.; Zhu, J.; Liu, Y. *Int. J. Dev. Biol.* **2016**, *60*, 85–93.

[72] Chen, H. F.; Kuo, H. C.; Chen, W.; Wu, F. C.; Yang, Y. S.; Ho, H. N. *Hum. Reprod.* **2009**, *24*, 71–80.

[73] Dennis E. Discher,; David J. Mooney,; Peter W. Zandstra, *Science* **2009**, *324*, 1673–1677.

[74] Li, J.; Bardy, J.; Yap, L. Y. W.; Chen, A.; Victor, N.; Cool, S. M.; Oh, S. K. W.; Birch, W. R. *Biointerphases* **2010**, *5*, 132–142.

[75] Amit, M.; Shariki, C.; Margulets, V.; Itskovitz-Eldor, J. *Biol. Reprod.* **2004**, *70*, 837–845.

[76] Hayashi, Y.; Chan, T.; Warashina, M.; Fukuda, M.; Ariizumi, T.; Okabayashi, K.; Takayama, N.; Otsu, M.; Eto, K.; Furue, M. K.; Michiue, T.; Ohnuma, K.; Nakauchi, H.; Asashima, M. *PLoS One* **2010**, *5*.

[77] Furue, M. K.; Na, J.; Jackson, J. P.; Okamoto, T.; Jones, M.; Baker, D.; Hata, R.-I.; Moore, H. D.; Sato, J. D.; Andrews, P. W. *Proc. Natl. Acad. Sci. U.S.A.* **2008**, *105*, 13409–14.

[78] Xu, C.; Inokuma, M. S.; Denham, J.; Golds, K.; Kundu, P.; Gold, J. D.; Carpenter, M. K. *Nat. Biotechnol.* **2001**, *19*, 971–974.

[79] Nie, Y.; Bergendahl, V.; Hei, D. J.; Jones, J. M.; Palecek, S. P. *Biotechnol. Prog.* **2009**, *25*, 20–31.

[80] Heng, B. C.; Li, J.; Chen, A. K.-l.; Reuveny, S.; Cool, S. M.; Birch, W. R.; Oh, S. K.-w. *Stem Cells Dev.* **2012**, *21*, 1701–1715.

[81] Lanctot, P. M.; Gage, F. H.; Varki, A. P. *Curr. Opin. Chem. Biol.* **2007**, *11*, 373–380.

[82] Zagris, N. *Micron* **2001**, *32*, 427–438.

[83] Rodin, S. et al. *Nat. Commun.* **2014**, *5*, 3195.

[84] Klecker, C.; Nair, L. S. *Biol. Eng. Stem Cell Niches*; Elsevier Inc., 2017; Chapter 13, pp 195–213.

[85] Miyazaki, T.; Futaki, S.; Hasegawa, K.; Kawasaki, M.; Sanzen, N.; Hayashi, M.; Kawase, E.; Sekiguchi, K.; Nakatsuji, N.; Suemori, H. *Biochem. Biophys. Res. Commun.* **2008**, *375*, 27–32.

[86] Meng, G.; Liu, S.; Rancourt, D. E. *Stem Cells Dev.* **2012**, *21*, 2036–2048.

[87] Yap, L. Y.; Li, J.; Phang, I. Y.; Ong, L. T.; Ow, J. Z.-E.; Goh, J. C.; Nurcombe, V.; Hobley, J.; Choo, A. B.; Oh, S. K.; Cool, S. M.; Birch, W. R. *Tissue Eng. Part C Methods* **2011**, *17*, 193–207.

[88] Prowse, A. B. J.; Chong, F.; Gray, P. P.; Munro, T. P. *Stem Cell Res.* **2011**, *6*, 1–12.

[89] Badenes, S. M.; Fernandes, T. G.; Rodrigues, C. A.; Diogo, M. M.; Cabral, J. M. *J. Biotechnol.* **2016**, *234*, 71–82.

[90] Jin, S.; Yao, H.; Krisanarungson, P.; Haukas, A.; Ye, K. *Tissue Eng. Part A* **2012**, *18*, 1419–1430.

[91] Nagaoka, M.; Si-Tayeb, K.; Akaike, T.; Duncan, S. A. *BMC Dev. Biol.* **2010**, *10*, 60.

[92] Derda, R.; Li, L.; Orner, B. P.; Lewis, R. L.; Thomson, J. A.; Kiessling, L. L. *ACS Chem. Biol.* **2007**, *2*, 347–355.

[93] Hayashi, Y.; Furue, M. K.; Okamoto, T.; Ohnuma, K.; Myoishi, Y.; Fukuhara, Y.; Abe, T.; Sato, J. D.; Hata, R.-I.; Asashima, M. *Stem Cells* **2007**, *25*, 3005–3015.

[94] Prowse, A. B.; Doran, M. R.; Cooper-White, J. J.; Chong, F.; Munro, T. P.; Fitzpatrick, J.; Chung, T.-l.; Haylock, D. N.; Gray, P. P.; Wolvetang, E. J. *Biomaterials* **2010**, *31*, 8281–8288.

[95] Higuchi, A.; Ling, Q.-d.; Kumar, S. S.; Chang, Y.; Kao, T.-C.; Munusamy, M. A.; Alarfaj, A. A.; Hsu, S.-t.; Umezawa, A. *Prog. Polym. Sci.* **2014**, *39*, 1585–1613.

[96] Tsutsui, H.; Valamehr, B.; Hindoyan, A.; Qiao, R.; Ding, X.; Guo, S.; Witte, O. N.; Liu, X.; Ho, C.-m.; Wu, H. *Nat. Commun.* **2011**, *2*, 167.

[97] de Mel, A.; Jell, G.; Stevens, M. M.; Seifalian, A. M. *Biomacromolecules* **2008**, *9*, 2969–2979.

[98] Kolhar, P.; Kotamraju, V. R.; Hikita, S. T.; Clegg, D. O.; Ruoslahti, E.; Ramana, V.; Hikita, S. T.; Clegg, D. O.; Ruoslahti, E. *J. Biotechnol.* **2010**, *146*, 143–146.

[99] Hersel, U.; Dahmen, C.; Kessler, H. *Biomaterials* **2003**, *24*, 4385–4415.

[100] Lambshead, J. W.; Meagher, L.; Goodwin, J.; Labonne, T.; Ng, E.; Elefanty, A.; Stanley, E.; O'Brien, C. M.; Laslett, A. L. *Sci. Rep.* **2018**, *8*, 701.

[101] Nagaoka, M.; Koshimizu, U.; Yuasa, S.; Hattori, F.; Chen, H.; Tanaka, T.; Okabe, M.; Fukuda, K.; Akaike, T. *PLoS One* **2006**, *1*, e15.

[102] D'Amour, K. A.; Agulnick, A. D.; Eliazer, S.; Kelly, O. G.; Kroon, E.; Baetge, E. E. *Nat. Biotechnol.* **2005**, *23*, 1534–1541.

[103] Eastham, A. M.; Spencer, H.; Soncin, F.; Ritson, S.; Merry, C. L. R.; Stern, P. L.; Ward, C. M. *Cancer Res.* **2007**, *67*, 11254–11262.

[104] Haque, A.; Adnan, N.; Motazedian, A.; Akter, F.; Hossain, S.; Kutsuzawa, K.; Nag, K.; Kobatake, E.; Akaike, T. *PLoS One* **2015**, *10*, e0135170.

[105] Chou, Y.-F.; Chen, H.-H.; Eijpe, M.; Yabuuchi, A.; Chenoweth, J. G.; Tesar, P.; Lu, J.; McKay, R. D.; Geijsen, N. *Cell* **2008**, *135*, 449–461.

[106] Li, L.; Wang, S.; Jezierski, A.; Moalim-Nour, L.; Mohib, K.; Parks, R. J.; Francesco Retta, S.; Wang, L. *Stem Cells* **2010**, *28*, 247–257.

[107] Lü, D.; Luo, C.; Zhang, C.; Li, Z.; Long, M. *Biomaterials* **2014**, *35*, 3945–3955.

[108] Hao, J.; Zhang, Y.; Jing, D.; Shen, Y.; Tang, G.; Huang, S.; Zhao, Z. *Acta Biomater.* **2015**, *20*, 1–9.

[109] Ayala, R.; Zhang, C.; Yang, D.; Hwang, Y.; Aung, A.; Shroff, S. S.; Arce, F. T.; Lal, R.; Arya, G.; Varghese, S. *Biomaterials* **2011**, *32*, 3700–3711.

[110] Walters, N. J.; Gentleman, E. *Acta Biomater.* **2015**, *11*, 3–16.

[111] Koegler, P.; Clayton, A.; Thissen, H.; Santos, G. N. C.; Kingshott, P. *Adv. Drug Deliv. Rev.* **2012**, *64*, 1820–1839.

[112] Fu, J.; Wang, Y.-K.; Yang, M. T.; Desai, R. A.; Yu, X.; Liu, Z.; Chen, C. S. *Nat. Methods* **2010**, *7*, 733–736.

[113] Tse, J. R.; Engler, A. J. *PLoS One* **2011**, *6*, e15978.

[114] Poh, Y. c.; Chowdhury, F.; Tanaka, T. S.; Wang, N. *Biophys. J.* **2010**, *99*, L19–L21.

[115] Lv, H.; Li, L.; Sun, M.; Zhang, Y.; Chen, L.; Rong, Y.; Li, Y. *Stem Cell Res. Ther.* **2015**, *6*, 103.

[116] Murphy, W. L.; McDevitt, T. C.; Engler, A. J. *Nat. Mater.* **2014**, *13*, 547–557.

[117] Mammoto, A.; Mammoto, T.; Ingber, D. E. *J. Cell Sci.* **2012**, *125*, 3061–3073.

[118] Sun, Y.; Villa-Diaz, L. G.; Lam, R. H. W.; Chen, W.; Krebsbach, P. H.; Fu, J. *PLoS One* **2012**, *7*, e37178.

[119] Chowdhury, F.; Li, Y.; Poh, Y. c.; Yokohama-Tamaki, T.; Wang, N.; Tanaka, T. S. *PLoS One* **2010**, *5*, e15655.

[120] Evans, N. D.; Minelli, C.; Gentleman, E.; LaPointe, V.; Patankar, S. N.; Kallivretaki, M.; Chen, X.; Roberts, C. J.; Stevens, M. M. *Eur. Cell. Mater.* **2009**, *18*, 1–14.

[121] Caiazzo, M.; Okawa, Y.; Ranga, A.; Piersigilli, A.; Tabata, Y.; Lutolf, M. P. *Nat. Mater.* **2016**, *15*, 344–352.

[122] Higuchi, S.; Watanabe, T. M.; Kawauchi, K.; Ichimura, T.; Fujita, H. *J. Biosci. Bioeng.* **2014**, *117*, 749–755.

[123] Musah, S.; Morin, S. A.; Wrighton, P. J.; Zwick, D. B.; Jin, S.; Kiessling, L. L. *ACS Nano* **2012**, *6*, 10168–10177.

[124] Lee, S. T.; Yun, J. I.; Jo, Y. S.; Mochizuki, M.; van der Vlies, A. J.; Kontos, S.; Ihm, J. E.; Lim, J. M.; Hubbell, J. A. *Biomaterials* **2010**, *31*, 1219–1226.

[125] Saha, S.; Ji, L.; de Pablo, J. J.; Palecek, S. P. *Biophys. J.* **2008**, *94*, 4123–4133.

[126] Ashton, R. S.; Keung, A. J.; Peltier, J.; Schaffer, D. V. *Annu. Rev. Chem. Biomol. Eng.* **2011**, *2*, 479–502.

[127] Ko, J.-Y.; Oh, H.-J.; Lee, J.; Im, G.-I. *Tissue Eng. Part A* **2018**, *24*, 595–606.

[128] Mestres, P.; Gomez, L. L.; Lopez, T. N.; del Rosario, G.; Lukas, S. W.; Hartmann, U. *Ann. Anat.* **2014**, *196*, 108–118.

[129] Hulshof, F. F.; Zhao, Y.; Vasilevich, A.; Beijer, N. R.; de Boer, M.; Papenburg, B. J.; van Blitterswijk, C.; Stamatialis, D.; de Boer, J. *Acta Biomater.* **2017**, *62*, 188–198.

[130] Abagnale, G.; Sechi, A.; Steger, M.; Zhou, Q.; Kuo, C.-C.; Aydin, G.; Schalla, C.; Müller-Newen, G.; Zenke, M.; Costa, I. G.; van Rijn, P.; Gillner, A.; Wagner, W. *Stem Cell Reports* **2017**, *9*, 654–666.

[131] Kilian, K. A.; Bugarija, B.; Lahn, B. T.; Mrksich, M. *Proc. Natl. Acad. Sci. U.S.A.* **2010**, *107*, 4872–4877.

[132] Li, Z.; Gong, Y.; Sun, S.; Du, Y.; Lü, D.; Liu, X.; Long, M. *Biomaterials* **2013**, *34*, 7616–7625.

[133] Ankam, S.; Suryana, M.; Chan, L. Y.; Moe, A. A. K.; Teo, B. K. K.; Law, J. B. K.; Sheetz, M. P.; Low, H. Y.; Yim, E. K. F. *Acta Biomater.* **2013**, *9*, 4535–4545.

[134] Park, S.; Im, G.-i. *J. Biomed. Mater. Res. A* **2015**, *103*, 1238–1245.

[135] Hall, M. E.; Mohtaram, N. K.; Willerth, S. M.; Edwards, R. *J. Biol. Eng.* **2017**, *11*, 38.

[136] Murphy, A. R.; Laslett, A.; O'Brien, C. M.; Cameron, N. R. *Acta Biomater.* **2017**, *54*, 1–20.

[137] Carnachan, R. J.; Bokhari, M.; Przyborski, S. A.; Cameron, N. R. *Soft Matter* **2006**, *2*, 608.

[138] Wang, P.-Y.; Ding, S.; Sumer, H.; Wong, R. C.-B.; Kingshott, P. *J. Mater. Chem. B* **2017**, *5*, 7927–7938.

[139] Griffin, M. F. *World J. Stem Cells* **2015**, *7*, 37.

[140] Kim, Y.; Abuelfilat, A. Y.; Hoo, S. P.; Al-Abboodi, A.; Liu, B.; Ng, T.; Chan, P.; Fu, J. *Soft Matter* **2014**, *10*, 8448–8456.

[141] Reimer, A.; Vasilevich, A.; Hulshof, F.; Viswanathan, P.; van Blitterswijk, C. A.; de Boer, J.; Watt, F. M. *Sci. Rep.* **2016**, *6*, 18948.

[142] Franzin, C.; Piccoli, M.; Serena, E.; Bertin, E.; Urbani, L.; Luni, C.; Pasqualetto, V.; Eaton, S.; Elvassore, N.; De Coppi, P.; Pozzobon, M. *Biol. Cell* **2013**, *105*, 549–560.

[143] Bae, D.; Moon, S.-h.; Park, B. G.; Park, S.-j.; Jung, T.; Kim, J. S.; Lee, K. B.; Chung, H.-m. *Biomaterials* **2014**, *35*, 916–928.

[144] Hulsman, M.; Hulshof, F.; Unadkat, H.; Papenburg, B. J.; Stamatialis, D. F.; Truckenmüller, R.; van Blitterswijk, C.; de Boer, J.; Reinders, M. J. *Acta Biomater.* **2015**, *15*, 29–38.

[145] Cheng, D.; Hou, J.; Hao, L.; Cao, X.; Gao, H.; Fu, X.; Wang, Y. *J. Biomed. Mater. Res. B Appl. Biomater.* **2016**, *104*, 1056–1063.

[146] Dalby, M. J.; Gadegaard, N.; Oreffo, R. O. *Nat. Mater.* **2014**, *13*, 558–569.

[147] Jedrzejczak-Silicka, M. *New Insights into Cell Culture Technology*; IntechOpen, 2017.

[148] Bokhari, M.; Carnachan, R. J.; Cameron, N. R.; Przyborski, S. A. *J. Anat.* **2007**, *44*, 567–576.

[149] Knight, E.; Przyborski, S. *J. Anat.* **2015**, *227*, 746–756.

[150] Zujur, D.; Kanke, K.; Lichtler, A. C.; Hojo, H.; Chung, U.-i.; Ohba, S. *Sci. Adv.* **2017**, *3*, e1602875.

[151] Leong, M. F.; Lu, H. F.; Lim, T. C.; Du, C.; Ma, N. K.; Wan, A. C. *Acta Biomater.* **2016**, *46*, 266–277.

[152] Hayward, A. S.; Eissa, A. M.; Maltman, D. J.; Sano, N.; Przyborski, S. A.; Cameron, N. R. *Biomacromolecules* **2013**, *14*, 4271–4277.

[153] Shao, Y.; Sang, J.; Fu, J. *Biomaterials* **2015**, *52*, 26–43.

[154] Carvalho, M. P.; Costa, E. C.; Miguel, S. P.; Correia, I. J. *Carbohydr. Polym.* **2016**, *150*, 139–148.

[155] Kimlin, L. C.; Casagrande, G.; Virador, V. M. *Mol. Carcinog.* **2013**, *52*, 167–182.

[156] Nava, M. M.; Piuma, A.; Figliuzzi, M.; Cattaneo, I.; Bonandrini, B.; Zandrini, T.; Cerullo, G.; Osellame, R.; Remuzzi, A.; Raimondi, M. T. *Stem Cell Res. Ther.* **2016**, *7*, 132.

[157] Lam, A. T.-l. L.; Chen, A. K.-l. L.; Ting, S. Q.-p. P.; Reuveny, S.; Oh, S. K.-w. W. *Biochem. Biophys. Res. Commun.* **2016**, *473*, 764–768.

[158] Liu, N.; Zang, R.; Yang, S.-T.; Li, Y. *Eng. Life Sci. 14*, 4–15.

[159] Cobo, F.; Navarro, J. M.; Herrera, M. I.; Vivo, A.; Porcel, D.; Hernández, C.; Jurado, M.; García-Castro, J.; Menendez, P. *Cloning Stem Cells* **2008**, *10*, 65–74.

[160] Amsbio, *Ready-To-Use Feeder Cells FAQ* http://www.amsbio.com/human–and–mouse–feeder–cells.aspx, Accessed 17–08–2018.

[161] Rajala, K.; Hakala, H.; Panula, S.; Aivio, S.; Pihlajamäki, H.; Suuronen, R.; Hovatta, O.; Skottman, H. *Hum. Reprod.* **2007**, *22*, 1231–1238.

[162] Wondimu, Z.; Gorfu, G.; Kawataki, T.; Smirnov, S.; Yurchenco, P.; Tryggvason, K.; Patarroyo, M. *Matrix Biol.* **2006**, *25*, 89–93.

[163] Nagaoka, M.; Hagiwara, Y.; Takemura, K.; Murakami, Y.; Li, J.; Duncan, S. A.; Akaike, T. *J. Biol. Chem.* **2008**, *283*, 26468–26476.

[164] Xu, F.; Sridharan, B.; Wang, S.; Gurkan, U. A.; Syverud, B.; Demirci, U. *Biomicrofluidics* **2011**, *5*, 022207.

[165] Valamehr, B.; Jonas, S. J.; Polleux, J.; Qiao, R.; Guo, S.; Gschweng, E. H.; Stiles, B.; Kam, K.; Luo, T.-J. M.; Witte, O. N.; Liu, X.; Dunn, B.; Wu, H. *Proc. Natl. Acad. Sci. U.S.A.* **2008**, *105*, 14459–14464.

[166] Rigamonti, A.; Repetti, G. G.; Sun, C.; Price, F. D.; Reny, D. C.; Rapino, F.; Weisinger, K.; Benkler, C.; Peterson, Q. P.; Davidow, L. S.; Hansson, E. M.; Rubin, L. L. *Stem Cell Reports* **2016**, *6*, 993–1008.

[167] Abbott, A. *Nature* **2003**, *424*, 870–872.

[168] Han, X.; Chen, H.; Huang, D.; Chen, H.; Fei, L.; Cheng, C.; Huang, H.; Yuan, G. C.; Guo, G. *Genome Biol.* **2018**, *19*, 1–19.

[169] Chen, Y.-W.; Kuo, C. W.; Chueh, D.-y.; Chen, P. *Surf. Sci.* **2016**, *648*, 47–52.

[170] Agmon, G.; Christman, K. L. *Curr. Opin. Solid State Mater. Sci.* **2016**, *20*, 193–201.

[171] Seetapun, D.; Ross, J. J. *Surgery* **2016**, *161*, 1474–1478.

[172] Edalat, F.; Sheu, I.; Manoucheri, S.; Khademhosseini, A. *Curr. Opin. Biotechnol.* **2012**, *23*, 820–825.

[173] Ghaedi, M.; Le, A. V.; Hatachi, G.; Beloiartsev, A.; Rocco, K.; Sivarapatna, A.; Mendez, J. J.; Baevova, P.; Dyal, R. N.; Leiby, K. L.; White, E. S.; Niklason, L. E. *J. Tissue Eng. Regen. Med.* **2018**, *12*, e1623–e1635.

[174] Ott, H. C. *Transplantation* **2015**, *99*, 1753.

[175] Quint, C.; Kondo, Y.; Manson, R. J.; Lawson, J. H.; Dardik, A.; Niklason, L. E. *Proc. Natl. Acad. Sci. U.S.A.* **2011**, *108*, 9214–9219.

[176] Peloso, A.; Dhal, A.; Zambon, J. P.; Li, P.; Orlando, G.; Atala, A.; Soker, S. *Stem Cell Res. Ther.* **2015**, *6*, 107.

[177] Harrison, R. H.; St-Pierre, J.-P.; Stevens, M. M. *Tissue Eng. Part B Rev.* **2014**, *20*, 1–16.

[178] Li, Z.; Leung, M.; Hopper, R.; Ellenbogen, R.; Zhang, M. *Biomaterials* **2010**, *31*, 404–412.

[179] Lee, M.; Kim, Y.; Ryu, J. H.; Kim, K.; Han, Y. M.; Lee, H. *Acta Biomater.* **2016**, *32*, 138–148.

[180] Jung, J.-H.; Kim, B. S. *J. Vis. Exp.* **2015**, 1–7.

[181] Kraehenbuehl, T. P.; Langer, R.; Ferreira, L. S. *Nat. Methods* **2011**, *8*, 731–736.

[182] Stenberg, J.; Elovsson, M.; Strehl, R.; Kilmare, E.; Hyllner, J.; Lindahl, A. *Cytotechnology* **2011**, *63*, 227–237.

[183] Dumbleton, J.; Agarwal, P.; Huang, H.; Hogrebe, N.; Han, R.; Gooch, K. J.; He, X. *Cell. Mol. Bioeng.* **2016**, *9*, 277–288.

[184] Wu, S.; Johansson, J.; Damdimopoulou, P.; Shahsavani, M.; Falk, A.; Hovatta, O.; Rising, A. *Biomaterials* **2014**, *35*, 8496–8502.

[185] Garcia-Fuentes, M.; Meinel, A. J.; Hilbe, M.; Meinel, L.; Merkle, H. P. *Biomaterials* **2009**, *30*, 5068–5076.

[186] Yi, B.; Zhang, H.; Yu, Z.; Yuan, H.; Wang, X.; Zhang, Y. *J. Mater. Chem. B* **2018**, *6*, 3934–3945.

[187] Chen, A. K.-L.; Chen, X.; Choo, A. B. H.; Reuveny, S.; Oh, S. K. W. *Stem Cell Res.* **2011**, *7*, 97–111.

[188] Ashida, T.; Sakai, S.; Taya, M. *Artif. Cells Nanomed. Biotechnol.* **2016**, *44*, 1–4.

[189] Fisher, O. Z.; Khademhosseini, A.; Langer, R.; Peppas, N. A. *Acc. Chem. Res.* **2010**, *43*, 419–428.

[190] Toole, B. P. *Semin. Cell Dev. Biol.* **2001**, *12*, 79–87.

[191] Gerecht, S.; Burdick, J. A.; Ferreira, L. S.; Townsend, S. A.; Langer, R.; Vunjak-Novakovic, G. *Proc. Natl. Acad. Sci. U.S.A.* **2007**, *104*, 11298–303.

[192] Deng, Y.; Wei, S.; Yang, L.; Yang, W.; Dargusch, M. S.; Chen, Z. G. *Adv. Funct. Mater.* **2018**, *28*, 1–17.

[193] Shin, S. R.; Bae, H.; Cha, J. M.; Mun, J. Y.; Chen, Y.-C.; Tekin, H.; Shin, H.; Farshchi, S.; Dokmeci, M. R.; Tang, S.; Khademhosseini, A. *ACS Nano* **2012**, *6*, 362–372.

[194] Leong, M. F.; Lu, H. F.; Lim, T. C.; Narayanan, K.; Gao, S.; Wang, L. Y.; Toh, R. P.; Funke, H.; Abdul Samad, M. H.; Wan, A. C.; Ying, J. Y. *Tissue Eng. Part C Methods* **2016**, *22*, 884–894.

[195] Zhang, W.; Zhao, S.; Rao, W.; Snyder, J.; Choi, J. K.; Wang, J.; Khan, I. A.; Saleh, N. B.; Mohler, P. J.; Yu, J.; Hund, T. J.; Tang, C.; He, X. *J. Mater. Chem. B* **2013**, *1*, 1002–1009.

[196] Chen, F. M.; Liu, X. *Prog. Polym. Sci.* **2016**, *53*, 86–168.

[197] Atala, A.; Kasper, F. K.; Mikos, A. G. *Sci. Transl. Med.* **2012**, *4*, 160rv12–160rv12.

[198] Tandon, N.; Marolt, D.; Cimetta, E.; Vunjak-Novakovic, G. *Biotechnol. Adv.* **2013**, *31*, 1020–1031.

[199] Allen, A. B.; Priddy, L. B.; Li, M.-T. A.; Guldberg, R. E. *Ann. Biomed. Eng.* **2015**, *43*, 555–567.

[200] Krishna, L.; Dhamodaran, K.; Jayadev, C.; Chatterjee, K.; Shetty, R.; Khora, S. S.; Das, D. *Stem Cell Res. Ther.* **2016**, *7*, 1–12.

[201] Rossi, E.; Gerges, I.; Tocchio, A.; Tamplenizza, M.; Aprile, P.; Recordati, C.; Martello, F.; Martin, I.; Milani, P.; Lenardi, C. *Biomaterials* **2016**, *104*, 65–77.

[202] Jing, X.; Mi, H.-Y.; Turng, L.-S. *Mater. Sci. Eng. C* **2017**, *72*, 53–61.

[203] Dellatore, S. M.; Garcia, A. S.; Miller, W. M. *Curr. Opin. Biotechnol.* **2008**, *19*, 534–540.

[204] Villa-Diaz, L. G.; Nandivada, H.; Ding, J.; Nogueira-de Souza, N. C.; Krebsbach, P. H.; O'Shea, K. S.; Lahann, J.; Smith, G. D. *Nat. Biotechnol.* **2010**, *28*, 581–583.

[205] Lei, Y.; Schaffer, D. V. *Proc. Natl. Acad. Sci. U.S.A.* **2013**, *110*, 5039–5048.

[206] Ekerdt, B. L.; Fuentes, C. M.; Lei, Y.; Adil, M. M.; Ramasubramanian, A.; Segalman, R. A.; Schaffer, D. V. *Adv. Healthc. Mater.* **2018**, *7*, 1800225.

[207] Zonca, M. R.; Yune, P. S.; Williams, J. K.; Gu, M.; Unser, A. M.; Imbrogno, J.; Belfort, G.; Xie, Y. *Macromol. Biosci.* **2014**, *14*, 215–224.

[208] Nur-E-Kamal, A.; Ahmed, I.; Kamal, J.; Schindler, M.; Meiners, S. *Stem Cells* **2006**, *24*, 426–433.

[209] Carlberg, B.; Axell, M. Z.; Nannmark, U.; Liu, J.; Kuhn, H. G. *Biomed. Mater.* **2009**, *4*, 045004.

[210] Zandén, C.; Hellström Erkenstam, N.; Padel, T.; Wittgenstein, J.; Liu, J.; Kuhn, H. G. *Nanomedicine* **2014**, *10*, e949–e958.

[211] Levenberg, S.; Huang, N. F.; Lavik, E.; Rogers, A. B.; Itskovitz-Eldor, J.; Langer, R. *Proc. Natl. Acad. Sci. U.S.A.* **2003**, *100*, 12741–12746.

[212] Nazarov, R.; Jin, H.-J.; Kaplan, D. L. *Biomacromolecules* **2004**, *5*, 718–726.

[213] Mozafari, M.; Kargozar, S.; de Santiago, G. T.; Mohammadi, M. R.; Milan, P. B.; Foroutan Koudehi, M.; Aghabarari, B.; Nourani, M. R. *Mater. Technol.* **2018**, *33*, 29–37.

[214] Kanimozhi, K.; Khaleel Basha, S.; Sugantha Kumari, V. *Mater. Sci. Eng. C* **2016**, *61*, 484–491.

[215] Beattie, D.; Wong, K. H.; Williams, C.; Poole-Warren, L. A.; Davis, T. P.; Barner-Kowollik, C.; Stenzel, M. H. *Biomacromolecules* **2006**, *7*, 1072–1082.

[216] Liu, Q.; Tang, Z.; Ou, B.; Liu, L.; Zhou, Z.; Shen, S.; Duan, Y. *Mater. Chem. Phys.* **2014**, *144*, 213–225.

[217] Lovelady, E.; Kimmins, S. D.; Wu, J.; Cameron, N. R. *Polym. Chem.* **2011**, *2*, 559–562.

[218] Cameron, N. R. *Polymer* **2005**, *46*, 1439–1449.

[219] Naranda, J.; Sušec, M.; Maver, U.; Gradišnik, L.; Gorenjak, M.; Vukasović, A.; Ivković, A.; Rupnik, M. S.; Vogrin, M.; Krajnc, P. *Sci. Rep.* **2016**, *6*.

[220] Johnson, D. W.; Langford, C. R.; Didsbury, M. P.; Lipp, B.; Przyborski, S. A.; Cameron, N. R. *Polym. Chem.* **2015**, *6*, 7256–7263.

[221] Lee, A.; Langford, C. R.; Rodriguez-Lorenzo, L. M.; Thissen, H.; Cameron, N. R. *Biomater. Sci.* **2017**, *5*, 2035–2047.

[222] Richez, A.; Deleuze, H.; Vedrenne, P.; Collier, R. *J. Appl. Polym. Sci.* **2005**, *96*, 2053–2063.

[223] Cameron, N. R.; Sherrington, D. C.; Ando, I.; Kurosu, H. *J. Mater. Chem.* **1996**, *6*, 719–726.

[224] Bokhari, M.; Carnachan, R. J.; Przyborski, S. A.; Cameron, N. R. *J. Mater. Chem.* **2007**, *17*, 4088.

[225] Luckert, C.; Schulz, C.; Lehmann, N.; Thomas, M.; Hofmann, U.; Hammad, S.; Hengstler, J. G.; Braeuning, A.; Lampen, A.; Hessel, S. *Arch. Toxicol.* **2017**, *91*, 393–406.

[226] Knight, E.; Murray, B.; Carnachan, R.; Przyborski, S. In *3D Cell Culture: Methods and Protocols*; Haycock, J., Ed.; Methods Mol. Biol.; Humana Press Inc, 2011; Vol. 695; pp 323–340.

[227] MacDonald, C.; Finlay, D. B.; Jabed, A.; Glass, M.; Graham, E. S. *J. Neurosci. Methods.* **2014**, *238*, 70–77.

[228] Hayman, M.; Smith, K.; Cameron, N.; Przyborski, S. *J. Biochem. Biophys. Methods* **2005**, *62*, 231–240.

[229] Martín-Saavedra, F.; Crespo, L.; Escudero-Duch, C.; Saldaña, L.; Gómez-Barrena, E.; Vilaboa, N. *Sci. Rep.* **2017**, *7*, 15182.

[230] Neofytou, E. A.; Chang, E.; Patlola, B.; Joubert, L.-m.; Rajadas, J.; Gambhir, S. S.; Cheng, Z.; Robbins, R. C.; Beygui, R. E. *J. Biomed. Mater. Res. A* **2011**, *98A*, 383–393.

[231] Lumelsky, Y.; Lalush-Michael, I.; Levenberg, S.; Silverstein, M. S. *J. Polym. Sci. A Polym. Chem.* **2009**, *47*, 7043–7053.

[232] Sherborne, C.; Owen, R.; Reilly, G. C.; Claeyssens, F. *Mater. Des.* **2018**, *156*, 494–503.

[233] Ying, Q.-l.; Wray, J.; Nichols, J.; Batlle-Morera, L.; Doble, B.; Woodgett, J.; Cohen, P.; Smith, A. *Nature* **2008**, *453*, 519–523.

[234] Storm, M. P.; Orchard, C. B.; Bone, H. K.; Chaudhuri, J. B.; Welham, M. J. *Biotechnol. Bioeng.* **2010**, *107*, 683–695.

[235] Gupta, P.; Ismadi, M. Z.; Verma, P. J.; Fouras, A.; Jadhav, S.; Bellare, J.; Hourigan, K. *Cytotechnology* **2016**, *68*, 45–59.

[236] Serra, M.; Brito, C.; Sousa, M. F.; Jensen, J.; Tostões, R.; Clemente, J.; Strehl, R.; Hyllner, J.; Carrondo, M. J.; Alves, P. M. *J. Biotechnol.* **2010**, *148*, 208–215.

[237] Freimark, D.; Pino-Grace, P.; Pohl, S.; Weber, C.; Wallrapp, C.; Geigle, P.; Pörtner, R.; Czermak, P. *Transfus. Med. Hemother.* **2010**, *37*, 3–3.

[238] Serra, M.; Correia, C.; Malpique, R.; Brito, C.; Jensen, J.; Bjorquist, P.; Carrondo, M. J. T.; Alves, P. M. *PLoS One* **2011**, *6*, e23212.

[239] Siti-Ismail, N.; Bishop, A. E.; Polak, J. M.; Mantalaris, A. *Biomaterials* **2008**, *29*, 3946–3952.

[240] Lei, Y.; Jeong, D.; Xiao, J.; Schaffer, D. V. *Cell. Mol. Bioeng.* **2014**, *7*, 172–183.

[241] Kropp, C.; Massai, D.; Zweigerdt, R. *Process Biochem.* **2017**, *59*, 244–254.

[242] Haycock, J. W. *Methods Mol. Biol.*; 2011; Vol. 695; pp 1–15.

[243] Kropp, C.; Kempf, H.; Halloin, C.; Robles-Diaz, D.; Franke, A.; Scheper, T.; Kinast, K.; Knorpp, T.; Joos, T. O.; Haverich, A.; Martin, U.; Zweigerdt, R.; Olmer, R. *Stem Cells Transl. Med.* **2016**, *5*, 1289–1301.

[244] Kehoe, D. E.; Jing, D.; Lock, L. T.; Tzanakakis, E. S. *Tissue Eng. Part A* **2010**, *16*, 405–21.

[245] Shafa, M.; Sjonnesen, K.; Yamashita, A.; Liu, S.; Michalak, M.; Kallos, M. S.; Rancourt, D. E. *J. Tissue Eng. Regen. Med.* **2012**, *6*, 462–472.

[246] Krawetz, R.; Taiani, J. T.; Liu, S.; Meng, G.; Li, X.; Kallos, M. S.; Rancourt, D. E. *Tissue Eng. Part C Methods* **2010**, *16*, 573–582.

[247] Abecasis, B.; Aguiar, T.; Arnault, É.; Costa, R.; Gomes-Alves, P.; Aspegren, A.; Serra, M.; Alves, P. M. *J. Biotechnol.* **2017**, *246*, 81–93.

[248] Sart, S.; Bejoy, J.; Li, Y. *Process Biochem.* **2017**, *59*, 276–288.

[249] Ahsan, T.; Nerem, R. M. *Tissue Eng. Part A* **2010**, *16*, 3547–3553.

[250] Geuss, L. R.; Suggs, L. J. *Biotechnol. Prog.* **2013**, *29*, 1089–1096.

[251] Azarin, S. M.; Palecek, S. P. *Biochem. Eng. J.* **2010**, *48*, 378–384.

Chapter 2

Materials & Methods

2.1 Scaffold Synthesis & Functionalisation

All reagents for polymer synthesis and functionalisation were purchased from Sigma Aldrich and used without further purification, unless otherwise stated. The surfactant Hypermer B246SF-LQ-(AP), a copolymer consisting of polyhydroxystearic acid and polyethylene glycol, was obtained from Croda. The photo-initiator was a diphenyl (2,4,6-trimethylbenzoyl)phosphine oxide/2-hydroxy-2-methyl-propiophenone blend.

2.1.1 TMPTA PolyHIPE Synthesis

TMPTA polyHIPEs with 80 % porosity were synthesised according to a method that has been described previously [1]. The oil phase of the emulsion consisted of trimethylolpropane tris (3-mercaptopropionate) (TMPTMP) (3.98 g), trimethylolpropane triacrylate (TMPTA) (2.96 g), surfactant Hypermer B246SF (5 wt% of organic phase, 0.78 g) and photoinitiator (7 wt % of monomer content, 0.7 ml) in 1,2-dichloroethane (DCE) (7 ml). All oil phase components except for the photoinitiator were combined and added to a foil-covered 250 ml flask with a Teflon D-shaped paddle stirring at 350 rpm. Photoinitiator was then added to complete the oil phase. MilliQ ultrapure water (56 ml) was added dropwise to produce a homogeneous emulsion that was then poured into a polytetrafluoroethylene (PTFE) mould enclosed by glass plates.

The emulsion was cured using a Fusion UV Systems Inc. Light Hammer 6 variable power UV curing system. The ultraviolet (UV) light power per pass under the lamp was 5.74 mW cm^{-2} as measured with an International Light Technologies ILT400 belt radiometer. The sample was passed under the UV lamp four times at a speed of approximately 3.5 m min^{-1}, turning the sample over after each pass to ensure even curing. Cured polymers were then soaked in acetone (Merck) overnight before being washed *via* soxhlet extraction with 1,2-dichloromethane (DCM) or ethanol and dried in a vacuum oven.

Routine polymerised high internal phase emulsion (polyHIPE) synthesis was modified as needed for specific applications, as described below:

- Void size was increased to promote better cell infiltration in H9 stem cell culture by changing the stirrer speed from 350 rpm to 250 rpm or 300 rpm during emulsion preparation.
- Porosity was altered by increasing the added water phase from 56 ml (80 %) to 125.5 ml (90 %) to aid in stem cell infiltration into the scaffold.
- PolyHIPE monoliths were subject to air drying, covered, and on filter paper in a fume hood when required. This helped to reduce potential contamination of X-ray photoelectron spectroscopy (XPS) samples.

2.1.2 Analysis of Scaffold Structure

2.1.2.1 Mercury Intrusion Porosimetry

The diameter of interconnects between voids was measured using mercury porosimetry at the Department of Chemical Engineering, Monash University. Prior to analysis, polyHIPE monoliths were cut to size with a razor blade, dried in a vacuum oven for 1 week, and degassed for 3 days using a VacPrep Degasser 061 (Micromeritics). Analysis was conducted using a Mercury Autopore IV Porosimeter 9520 (Micromeritics). Penetrome-

ter and stem volumes were 4.23 ml and 1.19 ml respectively. Mercury contact angle was taken as 130° for both intrusion and extrusion. Applied pressure ranged from 0 to 1600 psi.

2.1.2.2 Scanning Electron Microscopy

Scanning electron microscopy (SEM) was used to analyse the morphology of polyHIPE scaffolds. Samples were either sliced into pieces approximately 2 mm × 2 mm × 5 mm with a razor blade, or sectioned into 200 μm thick disks using a VT1000 S vibrating blade microtome (Leica). PolyHIPE pieces were attached to an aluminium stub with carbon tape, with additional strips of carbon tape securing the ends where necessary. Samples were then typically coated in an approximately 2 nm thick layer of iridium (Ir) with a Sputter Coater 208HR (Cressington). Alternately, a 10 nm layer of carbon was applied using a Polaron E3700 evaporative carbon coater (Quorum Technologies).

Images were taken at spot size 2, aperture 6 (30 μm), 5 kV, at a range of magnifications using an FEI Nova NanoSEM 450 FEGSEM. Typical magnifications were 200×, 500×, 1,000×, and 1,500×.

2.1.2.3 Determining Void Diameter

SEM images were analysed using ImageJ [2] and Fiji [3] image analysis software (NIH Image). At least 100 void diameters were measured per image, and there were typically three or more images for each synthesis condition. Measured diameters were corrected using a statistical correction factor of $\frac{2}{\sqrt{3}}$ as described by Barbetta and Cameron [4]. This correction factor accounts for the fact that voids are cut at a random distance from the void centre, and is routinely applied to these measurements [1, 5, 6].

2.1.2.4 Helium Pycnometry

Skeletal density was determined using an AccuPyc II 1340 Gas Pycnometer (Micromeritics). Helium gas pressure was 150 kPa, and measurement chamber size was 10 cm^3. Density was measured 10 times for each sample. The skeletal density ($\rho_{skeletal}$) was used in conjunction with bulk density (ρ_{bulk}) measurements to calculate porosity (ϕ) as per equation 2.1. Bulk density was calculated by cutting cubes of dry material, measuring dimensions with calipers, and weighing accurately.

$$\phi = 1 - \frac{\rho_{bulk}}{\rho_{skeletal}} \tag{2.1}$$

2.1.2.5 Gas Adsorption

Gas adsorption was used to assess the specific surface area and porosity of the TMPTA polyHIPE material. Gas adsorption isotherms for pressures in the range of 0 - 1.2 bar were measured by a volumetric method using an ASAP 2420 Surface Area and Porosimetry System (Micromeritics). Freshly prepared sample was transferred to a pre-dried and weighed analysis tube, which was stoppered with a Transeal cap. Samples were evacuated and activated under dynamic vacuum (10 - 6 Torr) at 100 °C for 24 hours. Accurate sample masses were calculated using degassed samples. Gas adsorption measurements were performed using ultra-high purity He and N_2 gases. Adsorption isotherms were collected at 77 K and the surface area was calculated using the Brunauer Emmett Teller (BET) theory.

2.1.3 Functionalising PolyHIPE Materials with Maleimide *via* Michael Addition

Dry TMPTA polyHIPEs were either cut into sheets approximately 1 cm × 1 cm in size with a razor blade, or were sectioned into 200 μm thick disks using a Leica VT1000 S vibrating blade microtome. Samples were hydrated by submersion in a 50:50 solution of absolute ethanol (Merck) and 0.01 M phosphate buffered saline (PBS) (Gibco), then rinsed twice in 0.01 M PBS. Maleimide was weighed to give the appropriate molar ratio with respect to surface thiols on the polyHIPE sample, and then dissolved in either PBS or a 50:50 ethanol:PBS solution. PolyHIPE samples were added to the maleimide solution and placed on an orbital shaker at room temperature for up to 120 hours. After functionalisation, the polyHIPE samples were removed from the maleimide solution and washed *via* soxhlet extraction with ethanol for 24 hours. Samples were then rinsed with reverse osmosis water and allowed to air-dry under the cover of filter paper. Further details of conditions trialled during optimisation are listed in Table 2.1.

2.1.4 Functionalising PolyHIPE Materials with Cyclic-RGD-Maleimide and Cyclic-RAD-Maleimide *via* Michael Addition

200 μm thick disks of dry TMPTA polyHIPE were hydrated by two × 10 minute submersions in 100 % ethanol (Merck), followed by two × 10 minute submersions in 70 % ethanol diluted with 0.01 M PBS. Cyclic-RGDfK-maleimide (cRGD-mal) (Peptides International) was weighed and then dissolved in 50:50 ethanol:PBS solution. Sonication was used to break peptide clumps when manual shaking was insufficient. PolyHIPE samples were added to the peptide solution and placed on an orbital shaker. 2.82 μl of a 72 mM stock catalyst solution containing triethylamine (NEt_3) in PBS was added per scaffold. The reaction was left for 48 hours at room temperature. After functionalisation,

Table 2.1: *Functionalisation conditions trialled during optimisation of maleimide attachment via Michael addition. 'NEt$_3$' refers to triethylamine. 'Mixed' refers to a mixed solvent containing 50 % PBS and 50 % ethanol.*

PolyHIPE shape	**Maleimide:Thiol Ratio**	**Reaction Time**	**Catalyst**	**Solvent**	**Drying Method**
1cm^2 sheet	0.5:1, 1:1, 2:1	5 days	None	PBS	Vacuum
1cm^2 sheet	0.5:1, 1:1, 2:1, 5:1, 10:1	5 days	None	PBS	Vacuum
1cm^2 sheet	0.5:1, 1:1, 2:1, 5:1, 10:1	5 days	NEt$_3$	PBS	Vacuum
1cm^2 sheet	0.5:1, 1:1, 2:1, 5:1, 10:1	5 days	None	Mixed	Vacuum
1cm^2 sheet	0.5:1, 1:1, 2:1, 5:1, 10:1	5 days	NEt$_3$	Mixed	Vacuum
200 μm thick disk	0.5:1, 1:1, 2:1, 5:1, 10:1	5 days	NEt$_3$	Mixed	Air
1cm^2 sheet	0.5:1, 1:1, 2:1, 5:1, 10:1	5 days	NEt$_3$	Mixed	Air
1cm^2 sheet	1:1	1h, 2h, 4h, 8h, 24h, 32h, 38.5h, 48h, 72h, 96h	NEt$_3$	Mixed	Air

the polyHIPE samples were removed from the cRGD-mal solution, washed with excess reverse osmosis water, and air-dried under the cover of filter paper.

The same protocol was used to attach cyclic-RADfK-maleimide (cRAD-mal). The cRAD-mal peptide was custom-synthesised by Mimotopes, and used without further purification. As the molecular weight of arginine-alanine-apartate (RAD) is different from RGD, 0.225 mg was used per scaffold.

2.1.5 Functionalising PolyHIPE Materials with Sulfo-SANPAH *via* Photoinitiated Addition

Dry TMPTA polyHIPE monoliths were sectioned into 200 μm thick disks using a Leica VT1000 S vibrating blade microtome. Samples were hydrated by submersion in 100 % ethanol (Merck) twice, followed by 70 % ethanol in 0.01 M PBS. Hydrated scaffold disks were placed in a 12 well cell culture plate. Sulfosuccinimidyl 6-(4'-azido-2'-nitrophenylamino) hexanoate (sulfo-SANPAH) (ThermoFisher) 2.5 mg was dissolved in 10 μl dimethyl sulfoxide (DMSO) (Sigma Aldrich). This solution was made up to 5 ml with ultra-pure water (MilliQ), and 0.5 ml added to each well.

The plate was passed under a Light Hammer 6 variable power UV curing system (Fusion UV Systems Inc.). The UV light power per pass under the lamp was 5.74 mW cm^{-2} as measured with an ILT400 belt radiometer (International Light Technologies). The sample was passed under the UV lamp three times at a speed of approximately 3.5 m min^{-1}. Scaffolds were then washed in excess ultra pure water. This method was adapted from a protocol supplied by Dr. Ahmed Eissa, University of Warwick, Coventry, UK [7].

2.1.6 Analysis of Functionalised PolyHIPE Materials

2.1.6.1 Raman Spectroscopy

Raman spectroscopy was used to detect the presence of thiol groups in as-synthesised and functionalised polyHIPE materials, and thus to qualitatively assess functionalisation. Thiol peaks were detected by a NXR Fourier transform Raman spectrometer (Thermo Scientific) with attenuated total reflection (ATR) configuration. Each sample spectrum consisted of 50 scans with a sweep range of 400 to 4000 cm^{-1}.

2.1.6.2 Determination of Residual Maleimide Content using Ellman's Colourimetric Assay

Thiol loading was determined *via* a colourimetric assay as described previously [1]. TMPTA PolyHIPE was frozen in liquid nitrogen and ground with a mortar and pestle. The powdered polyHIPE (5 - 10 mg) was then measured into volumetric flasks and the weight recorded. Tetrahydrofuran (THF) (1ml, Merck) was added to each flask and left for 10 minutes to swell the polyHIPE powder. A 5 μM solution of 5,5' dithiobis (2-nitrobenzoic acid) (Ellman's reagent) in ethanol was prepared while the polyHIPE powder soaked in THF. After swelling, 1 ml of the Ellman's regent solution and 5 μl of n,n-diisopropylethylamine (DIPEA) (Auspep) was added to each polyHIPE flask. This mixture was left on an orbital shaker at room temperature for 30 minutes before being diluted to 5 ml with ethanol. After mixing, 0.5 ml was taken from each flask, filtered using a 0.2 μm or 1 μm Teflon syringe filter, and diluted to several concentrations between 5 μmol and 5 mmol with ethanol. After dilution, 340 μl was taken from each vial and placed into a 96 well plate. This plate was then analysed with a UV-Visible spectrometer (Multiscan Spectrum, Thermofisher) at 412 nm. The wavelength used was found by running a sweeping absorbance scan on a concentrated solution and selecting the wavelength with peak absorbance.

2.1.6.3 X-Ray Photoelectron Spectroscopy

XPS was used to analyse the atomic composition of TMPTA polyHIPE surfaces before and after functionalisation. XPS analysis was performed using an AXIS Nova spectrometer (Kratos Analytical Inc., Manchester, UK) with a monochromated Al Kα source at a power of 150 W (15 kV $\times$ 10 mA) and a hemispherical analyser operating in the fixed analyser transmission mode. Survey spectra were acquired at a pass energy of 160 eV. To obtain more detailed information, high resolution spectra were recorded from individual peaks at 40 eV pass energy.

Each specimen was analysed at an emission angle of 0° as measured from the surface normal. Assuming typical values for the electron attenuation length of relevant photoelectrons the XPS analysis depth (from which 95 % of the detected signal originates) ranges between 5 and 10 nm for a flat surface. As the actual emission angle is ill-defined for rough surfaces (ranging from 0° to 90°), the sampling depth may range from 0 nm to approximately 10 nm.

Data processing was performed using CasaXPS processing software version 2.3.15 (Casa Software Ltd., Teignmouth, UK). Core level spectra were analysed using mixed Gaussian-Lorentzian (Voigt) lineshapes and Shirley backgrounds. Lorentzian was set to 30 %, higher ratios and asymmetry were not needed. Total elemental compositions were determined via the use of the transmission function and relative sensitivity factors supplied by the manufacturer of the two instruments used in this investigation (Kratos Analytical, Manchester, UK), leading to a compositional accuracy of better than 5 %. The electrically-insulating nature of the samples necessitated charge referencing during the data analysis, with the C-C/C-H bond at 284.8 eV used as the reference for the binding energy scale. Binding energies were allowed to float within a small range, typically 0.2 - 0.4 eV. Full-width half-maximum (FWHM) was also allowed to vary within reason (up to 1.6 for C 1s and 1.8 for O 1s). High-resolution spectra were normalised to peak area. The accuracy associated with quantitative XPS is 10 % - 15 %.

XPS was conducted by Chris Easton, CSIRO, Victoria, Australia and Marc Walker & Ahmed Eissa, University of Warwick, Coventry, U.K.

2.2 Preparing PolyHIPE Materials as Cell Scaffolds

PolyHIPE scaffolds prepared for cell culture were washed with ethanol or DCM by soxhlet extraction. Monoliths were sectioned to 200 μm thick disks using a Leica VT1000 S vibrating blade microtome before being functionalised with the appropriate peptide or crosslinker. Functionalised scaffolds were stored in petri dishes lined with filter paper or in PBS until use. The commercially available polystyrene polyHIPE cell culture scaffold Alvetex® (ReproCELL) was used as supplied.

2.2.1 Sterilisation and Culture Setup

Porous polyHIPE scaffolds were supported in solid plastic frames during cell culture. Alvetex® is supplied in a polystyrene frame, and was used as supplied when a comparison to the commercial product was required. Alternately, the Alvetex® scaffold was removed from the supplied frame and replaced with the materials synthesised in this project. Scaffold exchange was conducted under aseptic conditions in a Aura 2000 M.A.C. Class II Biosafety cabinet (LAF technologies) to maintain sterility of the Alvetex® frame. If used, the included Alvetex® scaffold required hydration. To hydrate, Alvetex® scaffolds were placed in 70 % ethanol for at least 15 minutes before being washed twice with sterile PBS, in accordance with manufacturer's guidelines. These materials were then used without further coating, or coated with Geltrex® by adapting the Matrigel coating protocol prescribed by ReproCELL [8]. Briefly, Geltrex® was diluted to 1:400 with cold, sterile Dulbecco's modified Eagle's medium (DMEM)/F-12, and 3.5 ml added to Alvetex® scaffolds in a 12 well plate to cover culture surface. The coating was then incubated for 1 hour at 37 °C and 5 % CO_2 before use or storage at 4 °C.

Custom 3D-printed scaffold frames, shown in Figure 2.1, were designed as an alternative to the commercial product. This allowed rapid modification of the clipping mechanism and frame shape to better suit the requirements of this project. Solidworks 2016 (Dassault Systèmes) was used to render frame designs, which were prepared for printing using Simplify 3D software. Models produced using this software are shown in Figure 2.2. Frames were printed using a Creator PRO 2016 Dual Head 3D Printer (Flashforge) with polylactic acid (PLA) filament. Typical printing parameters were infill 80 %, speed 2000 mm/min, platform temperature 60 °C, and nozzle temperature 230 °C.

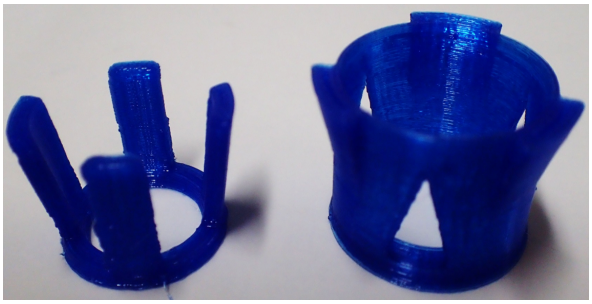

Figure 2.1: *The 3D printed frame is comprised of two components. The inner section (left) is pressed into the outer (right), securing the polyHIPE scaffold in place while allowing media access. The outer is shaped so that it holds the scaffold suspended above the bottom of a 12-well tissue culture plate.*

TMPTA polyHIPE scaffolds and 3D printed frames required hydration and sterilisation prior to use in cell culture. To sterilise, 3D printed frames were separated into their components and submerged in 70 % ethanol for 15 minutes prior to insertion of TMPTA polyHIPE scaffolds. Scaffolds were then placed in frames, submerged in ethanol in a 12 well plate, and placed under the UV sterilisation lamps of an Aura 2000 M.A.C. Class II Biosafety cabinet (LAF technologies) for 30 minutes. Ethanol was then aspirated and the scaffolds washed twice with sterile PBS.

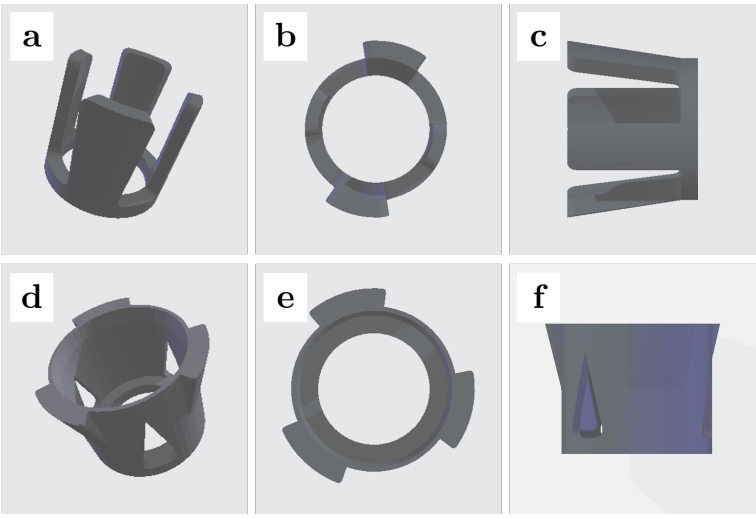

Figure 2.2: *The 3D printed parts were first modelled in 3D using SolidWorks. a) Isometric projection of the frame inner. b) Top-down view of frame inner. c) Side view of frame inner. d) Isometric projection of frame outer. e) Top-down view of frame outer. f) Side view of frame outer.*

After sterilisation peptide functionalised materials were considered ready to use. Sulfo-SANPAH functionalised 3D scaffolds were additionally coated with Geltrex®. Scaffolds were coated in their frames to reduce handling post-sterilisation. Coatings were applied as described for Alvetex® scaffolds, except that DMEM/F-12 was replaced with PBS++ (PBS containing Calcium and Magnesium) (Gibco). Coated scaffolds were transferred to clean 12 well plates before cell seeding.

2.2.1.1 Optimising Geltrex® Coating

Geltrex® was coated on Alvetex® scaffolds according to the the protocol outlined in Section 2.2.1. The same protocol was also trialled on TMPTA materials. To optimise the coating, the application of 1:800, 1:400, 1:300, and 1:200 dilutions of Geltrex® was investigated. The protein concentration in as-supplied Geltrex® ranges from 12 – 18 mg/mL. Subsequently, a sulfo-SANPAH crosslinker was added to the TMPTA scaffold prior to Geltrex® coating. Immunohistochemistry and H9 stem cell culture was used to investigate the Geltrex® coating on TMPTA scaffolds.

2.3 Culture of H9 Human Embryonic Stem Cells

2.3.1 Maintenance & Passaging of H9 Stem Cells

The human embryonic stem cell line hESC-WA09 (H9) (WiCell) was cultured in Essential8™ (E8) medium (Life Technologies). Cultures were grown on tissue culture polystyrene (TCPS) (Corning) coated with Geltrex® basement membrane matrix (ThermoFisher). Geltrex® was coated according to the manufacturer's instructions for thin coating. Briefly, Geltrex® was diluted to 1:400 with cold, sterile DMEM/F-12 and added to flasks to coat culture surface. The coating was then incubated for 1 hour before use or storage at 4 °C. Cultures were kept in a humidified incubator at 37 °C and 5 % CO_2. Cells were passaged in small clusters with 0.5 mM ethylenediaminetetraacetic acid (EDTA) (Gibco) applied for 5 - 7 minutes once they reached 80 % confluency. Splits of 1:4 - 1:8 were used depending on desired cell expansion time. Routine monitoring was *via* brightfield microscopy conducted with a Olympus IX71 inverted microscope.

The use of human embryonic stem cells in this project was approved by the Monash Human Research Ethics Committee in accordance with the NHMRC guidelines. Project ID 2963.

2.3.2 Culturing H9 Stem Cells in 3D

H9 stem cells were cultured on both commercially available and novel porous polymer scaffolds. Prior to seeding on porous 3D scaffolds, 80 % confluent cells were removed from flasks by applying 0.5 mM EDTA for 5 - 7 minutes (for clumped cells) or Accutase® (Stemcell Technologies) for 5 minutes (for single cells) and centrifuged in E8 media for 2 minutes at 2000 rpm (805 g). Supernatant was aspirated and cells re-suspended in a small amount of E8 media before being seeded at 1 million cells / scaffold. Seeding rates of 0.5, 1.5, and 2 million cells / scaffold were also trialled.

Seeded cells were incubated for 1 hour before 3.5 ml of E8 media with 0.1 μl/ml penicillin / streptomycin (Life Technologies) was added to each well. A 3 hour initial incubation time was also trialled. Media was changed 48 hours after seeding, and subsequently every day. Culture was maintained for up to 14 days.

2.3.3 Histological Processing & Embedding of 3D Cultures

Scaffolds containing cells were preserved in 4 % paraformaldehyde (PFA) (Electron Microscopy Sciences) for 30 minutes at room temperature, or overnight at 4 °C. Fixed samples were then permeabilised and dehydrated through a series of ethanols to prevent cell shrinkage. Ethanol concentrations used were 30 %, 50 %, 70 %, 80 %, 90 %, 95 % and finally 100 %. Samples were cleared in Histoclear, and embedded in paraffin as previously described by Johnson *et al.* [9].

Sectioning was completed using a Cut4060 Microtome (microTec) prior to floating on a 40 °C histology water bath and mounting onto coated poly-L-lysine slides.

2.3.3.1 OCT Embedding & Cryosectioning of 3D Cultures

Optimal cutting temperature compound (OCT) embedding was used as an alternative to paraffin embedding when optimising processing for better scaffold adhesion during immunostaining. Poly-l-lysine slides were purchased from Thermo Scientific and epoxy slides were made as required. To make epoxy slides, solution of approximately 0.5 ml of epoxy glue (Selleys) in 5 ml acetone (Emsure) was applied to slides immediately prior to placing a section. Slides were allowed to dry at room temperature overnight.

Isopropanol (Emsure) was chilled to -20 °C in a freezer, and kept cold in a liquid nitrogen bath during use. Cryomold® disposable specimen molds (Tissue-Tek) were trimmed to size and a small amount of OCT (Tissue-Tek) added. The mould was placed at -20 °C briefly to thicken OCT. Scaffolds were cut to size, positioned in cryo-moulds, and

covered in OCT. Blocks were frozen by submerging in the chilled isopropanol. Blocks were sectioned to 5 or 20 μm on a Leica cryo-microtome and placed on poly-l-lysine slides or epoxy slides. Slides were stored frozen until staining.

2.3.3.2 Haematoxylin & Eosin Staining

Haematoxylin & eosin (H&E) staining was used to visualise cells cultured in polyHIPE scaffolds. Prior to staining, slides are baked at 60 °C for 25 minutes. H&E staining was conducted using an Autostainer XL (Leica). The program involves a series of washes as described in Table 2.2. After staining slides are mounted using ProLong Gold Antifade Mountant (Invitrogen). Brightfield images were taken using a Nikon DS-Ri2 upright microscope.

Table 2.2: *Process for haematoxylin & eosin autostaining of slides.*

Xylene x 3	2 minutes	Running tap water	30 seconds
Absolute alcohol	2 minutes	Scott's tap water	3 - 10 seconds
Running tap water	30 seconds	Eosin	5 minutes
Harris's haematoxylin	5 minutes	Absolute alcohol x3	2 minutes
Running tap water	30 seconds	Xylene x3	2 minutes
Acid alcohol	1 second		

2.3.3.3 Immunohistochemistry

Fixed, paraffin embedded, and sectioned scaffolds were de-waxed and rehydrated as for H&E staining. Before staining, OCT embedded sections were defrosted and allowed to equilibrate at room temperature for up to 12 hours. Slides were then dipped into 1× dilution Dako Wash Buffer (Agilent) before being placed in a Dako PT Link antigen retrieval machine. Retrieval was conducted in 1× dilution Dako Target Retrieval Solution (Agilent) for 30 minutes at 98 °C. Slides were then placed in 1× dilution Dako Wash Buffer for 10 minutes.

Samples were permeabilised with 0.01 % Triton X-100 (Sigma Aldrich) in PBS for 5 minutes. Sections were washed with PBS before being blocked with blocking buffer comprising 10 % goat serum (Gibco) in PBS for 30 minutes at room temperature. Primary antibodies were diluted in blocking buffer and applied to slides for a further 30 minutes at room temperature. Additional blocking buffer was applied to control slides not receiving primary antibody treatment. Sections were washed with PBS. Secondary antibodies were diluted and applied as for primary antibodies. After a further PBS wash, 4',6-diamidino-2-phenylindole (DAPI) was diluted in blocking buffer and applied to slides for 5 minutes. Antibody dilutions are shown in Table 2.3. Immunostaining was conducted manually or with a Dako Autostainer Link 48 (Agilent).

Stained scaffolds were washed 3 times with PBS, mounted, and coverslipped. Scaffolds were mounted using Vectashield mounting media (Vector Labs) or Dako mounting media (Agilent) and coverslipped using nail polish (Revlon) to secure. Stained scaffolds were routinely imaged using a Nuance FX fluorescent microscope or a Nikon DS-Ri2 microscope. Confocal microscopy was conducted on a SP5 5-Channel confocal microscope (Leica).

2.3.3.4 Analysis of Oct4 Expression

Fiji image processing software was used to analyse images of immunostained sections and calculate the ratio of Oct4 positive cells present. Figure 2.3 shows the main steps in this process. Single channel images were imported in Fiji and adjusted to achieve appropriate brightness and contrast. It was important to minimise autofluorescence of the scaffold. This was completed by the imaging software, or using Fiji. As there was autofluorescence from the material present in both the green and blue channels, and the green does not contain any biologically relevant staining, erasing the scaffold post-imaging could be achieved by subtracting the green channel image from the channel of interest.

Once the contrast between cells and scaffold was sufficient (Figure 2.3a), morphological

Table 2.3: *Stains used for immunostaining*

Visualisation Target	**Reagent**	**Antibody**	**Supplier**	**Dilution**
Geltrex	Primary	Anti-Laminin L9393	Sigma	1:250
Geltrex	Secondary	Alexa fluor 488 goat anti-rabbit IgG1(γ1)	Invitrogen	1:500
Oct4	Primary	Anti-Oct4 Monoclonal MAB4401	Merck	1:250
Oct4	Secondary	Alexa fluor 568 goat anti-mouse IgG1(γ1)	Invitrogen	1:500
Oct4	Isotype	Anti-mouse IgG1 κ	BD Biosciences	1:250
Cell Nucleus	DAPI	N/A	Invitrogen	1:500

segmentation was conducted with the MorphoLibJ plugin [10]. Appropriate watershed tolerance settings were set for each sample. From this segmentation, a watershed lines image was produced (Figure 2.3b). By dilating the watershed lines as shown in Figure 2.3c, the cells could be counted using the particle analyser feature.

If this automated process was unable to accurately select cells, then cell counts were conducted manually. The number of OCT4 positive cells could then be compared to the total cell number as shown by DAPI staining.

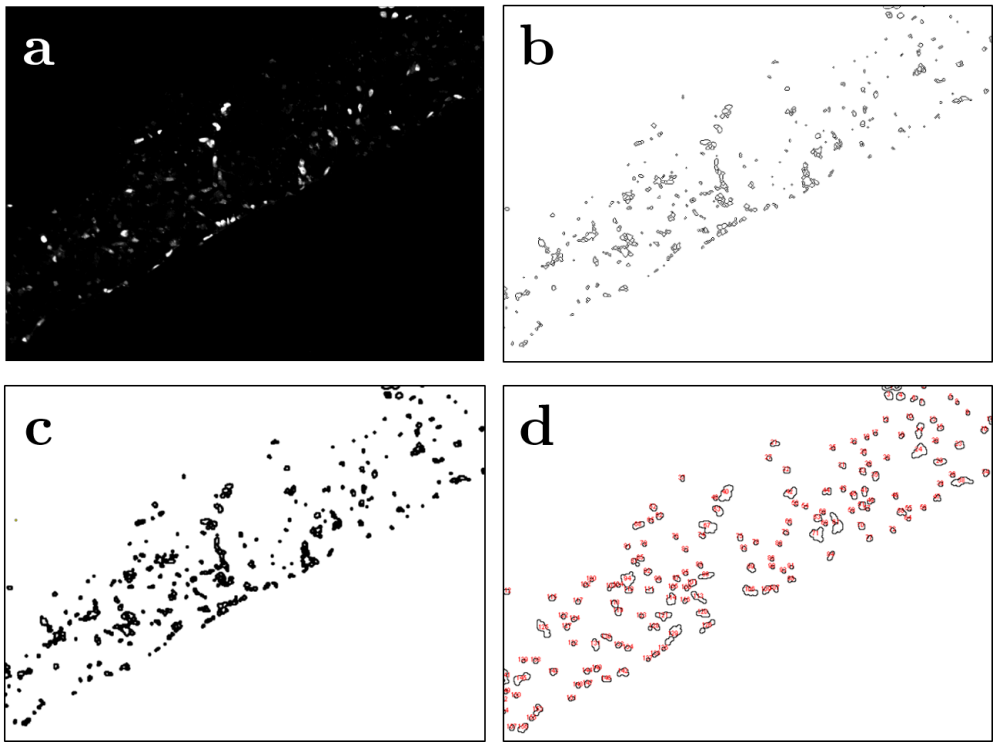

Figure 2.3: *Watershed process for measuring cell number in immunostained images. a) Original image after brightness / contrast adjustment. b) Watershed lines around cells. c) Dilated watershed lines. d) Counted cells were numbered in red, allowing the process to be checked easily.*

2.3.4 Other Culture Analyses

2.3.4.1 Stem Cell Metabolic Activity Measurement

Stem cell metabolism was compared across cultures using the commercially available cell viability reagent PrestoBlue® (Invitrogen). This assay is resazurin-based.

PrestoBlue® reagent was diluted 1:10 with E8 media in accordance with the manufacturer's protocol. Scaffolds were removed from their supporting frames, washed gently with PBS, and placed in a clean 12 well plate. 1 ml PrestoBlue® was added to each well before incubation at 37 °C and 5 % CO_2 for 90 minutes. After incubation, 100 μl of media was transferred to a Nunclon Delta Surface microwell plate (Thermo Scientific). Fluorescence was measured at an excitation wavelength of 560 nm using Enspire 2300 Multilabel Reader (Perkin Elmer).

The PrestoBlue® metabolic assay was also conducted on scaffolds remaining in their frames to reduce disruption to the cells. This resulted in a different rate of reagent consumption inside the frame compared to outside, despite the channels allowing media diffusion. To avoid this discrepancy, all media was removed after incubation and combined to obtain an average result across the culture.

2.3.4.2 Infiltration Depth Analysis

Fiji image processing software was used to analyse H&E stained sections and measure the depth of cell infiltration within 3D scaffolds. A line was drawn to mark the surface of the polymer. Measurements were then taken at 90° to this line at three evenly spaced points, with the furthest cell that touched the line being counted. At least 25 images were analysed per infiltration condition.

2.3.4.3 pH measurement

Cell culture pH was measured by placing a small drop of media on a H38 Minilab pH meter (Hach). Measurements were recorded inside and outside of the scaffold frame. The meter was washed with distilled water and dried between measurements.

2.3.5 Analysis of Gene Expression by Quantitative Polymerase Chain Reaction

2.3.5.1 Cell Lysis in 3D Scaffolds

Prior to cell lysis, 1 % β-mercaptoethanol (Sigma Aldrich) was added to RLT lysis buffer (Qiagen). Scaffolds were removed from their frames and rinsed by submerging in PBS. Rinsed scaffolds were placed in a fresh 12 well plate and 600 μl of RLT buffer added per well. The scaffolds were placed on a shaker platform for 10 minutes at approximately 100 rpm at ambient temperature. Lysate was transferred to an Eppendorf tube and stored at -80 °C.

2.3.5.2 RNA Isolation

Ribonucleic acid (RNA) isolation was conducted using an RNeasy Mini Kit (Qaigen) according to the manufacturer's protocols. The kit contains 'shredder' columns, 'spin' columns, buffers RW1 and RPE, and collection tubes. Lysates were defrosted on ice before being transferred to an RNeasy shredder column. The columns were centrifuged at 13,200 rpm (16,168 g) for 5 minutes. One volume of 70 % ethanol was added to the flow-through lysate and mixed by pipetting. The sample was added to an RNeasy spin column and centrifuged at 12,000 rpm (13,362 g) for 15 seconds. Buffer RW1 (700 μl) was added to the spin column and centrifuged at 12,000 rpm for 15 seconds. Flow through was discarded and 500 μl buffer RPE added. The column was centrifuged, and

the buffer RPE rinse repeated. Extracted RNA was eluted from the column by adding RNAse-free water to the spin column and centrifuging for 2 minutes at 12,000 rpm in a clean collection tube.

RNA concentration and purity was measured using a ND-1000 NanoDrop Spectrophotometer (Thermo Fisher). Isolated RNA was subsequently used to synthesise complementary DNA (cDNA), or stored at -80 °C.

2.3.5.3 RNA Conversion to cDNA

Isolated RNA was converted to cDNA using a High-Capacity RNA-to-cDNA Kit (Applied Biosystems) with TaqMan Gene Expression Master Mix (Thermo Fisher). Kit components were thawed on ice, and combined to produce a 2× concentration reverse transcription Master Mix in accordance with kit protocol. The Master Mix contained 2 μl 10× RT Buffer, 0.8 μl 25× dNTP Mix, 2 μl 10× RT random primers, 1 μl MultiScribe™ reverse transcriptase, 1 μl RNase inhibitor, and 3.2 μl nuclease-free H_2O per reaction. After mixing gently on ice, 10 μl/reaction Master Mix was added to individual Eppendorf tubes containing 1 μg RNA diluted to 10 μl with water. The diluted RNA and Master Mix were mixed by vortexing. Reverse transcription was conducted using a T100 Thermal Cycler (Bio-Rad). The thermal cycler conditions are shown in Table 2.4. The resulting cDNA was then used directly for quantitative polymerase chain reaction (qPCR) or stored at -20 °C.

Table 2.4: *Thermal cycler conditions used for transcription to cDNA.*

	Step 1	**Step 2**	**Step 3**	**Step 4**
Temperature (°C)	25	37	85	4
Time (minutes)	10	120	5	∞

2.3.5.4 qPCR

TaqMan™ probes were defrosted, vortexed, and centrifuged. Reaction mixtures containing 10 μl TaqMan Universal PCR Master Mix and 1 μl of the relevant TaqMan probe for each reaction were added to fresh Eppendorf tubes, vortexed, and centrifuged. Probes are detailed in Table 2.6. The mixtures were transferred to a MicroAmp® 96-well optical reaction plate at a rate of 11 μl per well. 9 μl cDNA in water was added to each microplate well to produce a final reaction mixture of 20 μl. The plate was sealed, centrifuged briefly to remove bubbles, and placed in a 7500 Real Time PCR System (Applied Biosystems). The thermal profile for the cycles is shown in Table 2.5.

Table 2.5: *Thermal cycle conditions used for qPCR.*

	Stage 1	**Stage 2**	**Stage 3**	**Stage 4**
Repetition	1	1	40	1
Temperature (°C)	50	95	95	60
Time (minutes)	2	10	0.25	1

2.3.6 Karyotype Analysis

Cells were tested for genetic abnormality by G-banding analysis. G-banding is a common assay for detecting gross karyotypic abnormalities [11]. Flasks containing 40 - 50 % confluent H9 cells were submitted to the Cytogenetics Laboratory, Monash Pathology, Monash Medical Centre, Victoria, Australia for analysis.

2.3.7 Statistical Analysis

To determine statistical significance of observed trends, cell data were analysed using 2-way ANOVA. GraphPad Prism (GraphPad Software) was used to conduct this analysis.

Table 2.6: *Probes used for qPCR.*

Marker	**Origin**	**Probe ID**	**Marker**	**Origin**	**Probe ID**
GAPDH	All cells (control)	Hs02786624_g1	Runx1	Mesoderm	Hs00231079_m1
Oct4	Pluripotent Cells	Hs00742896_s1	Gata-4	Endoderm	Hs00171403_m1
Nanog	Pluripotent Cells	Hs02387400_g1	Pax6	Ectoderm	Hs00240871_m1
T	Mesoderm	Hs00610080_m1	Sox1	Ectoderm	Hs00534426_s1

2.4 Optimising Cell Retrieval Protocols

2.4.1 Cell Culture

H9 pluripotent stem cells were seeded on polyHIPE scaffolds with either 80 or 90 % porosity. These scaffolds were functionalised with either cRGD-mal or sulfo-SANPAH. Sulfo-SANPAH scaffolds were additionally coated with Geltrex®. Cells were cultured as for standard 3D culture for 7 days (see Section 2.3.2). Selected cultures were treated with ROCK inhibitor Y-27632 (ROCKi) for 2 or 23 hours before proceeding with cell retrieval. See Chapter 5, Table 5.1 for a summary of culture and retrieval conditions.

2.4.2 Cell Retrieval *via* Dissociation Agent

Stem cells were retrieved from 3D thiol-acrylate scaffolds using a modified version of the protocol developed for the Alvetex® scaffold. Several conditions were trialled with varied dissociation agent, time, and temperature. The general approach was to rinse scaffolds gently, either by exchanging media for PBS in culture wells, or by removing scaffolds from their frames and dipping into a tube of PBS. Scaffold disks were then optionally cut into quarters or halves with a sterile scalpel blade. Next, scaffolds were transferred to a sterile 15 ml centrifuge tube containing dissociation agent (Accutase® or TrypLE™ Express).

The tube was incubated at 37 °C 5 % CO_2 or on ice, on its side, on a shaking platform set to approximately 100 rpm for 5 - 20 minutes. After incubation the tube was shaken briefly by hand. The resulting cell suspension was transferred to a 50 ml centrifuge tube containing E8 medium. Collected cells were centrifuged at 2000 rpm for 2 - 5 minutes. The supernatant was removed gently, and the cells resuspended in E8. Detached cells were reserved at 37 °C, 5 % CO_2. A new aliquot of dissociation agent was added to the tube containing the scaffold, and the incubation and cell collection repeated. Cell

count was conducted using Trypan Blue and a Countess II Automated Cell Counter (ThermoFisher). PrestoBlue® assay was as standard (1:10 reagent in complete E8 media, 90 minute incubation). This process is summarised in Figure 2.4.

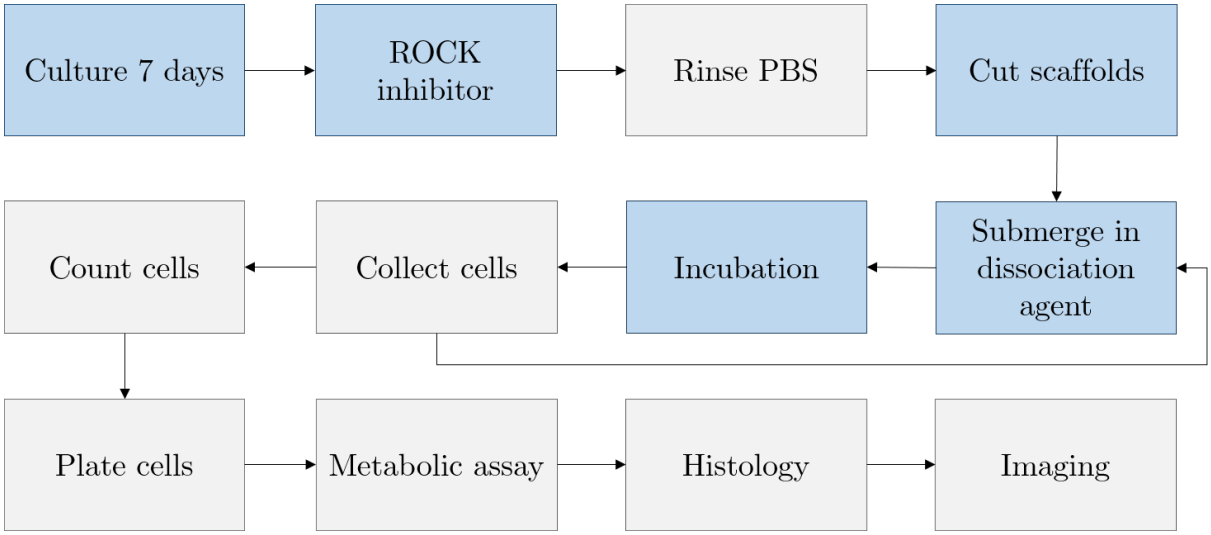

Figure 2.4: *Process for stem cell retrieval via dissociation agent. Grey boxes indicate processes that are consistent across experiments. Blue boxes indicate variable steps. These variables are listed in Table 5.1.*

2.4.3 Cell Retrieval *via* Explant-Inspired Approach

Stem cell retrieval was also conducted using a 'synthetic explant' approach. Scaffold cultures were removed from their supporting frames and placed top-down on Geltrex®-coated tissue culture polystyrene (TCPS). Cell egress was monitored *via* brightfield microscopy as for routine culture in 2D (see section 2.3.1). Once H9 stem cell colonies were established on the TCPS, the scaffold cultures were removed. The extracted cultures were passaged carefully with EDTA and allowed to expand for 3 - 4 days.

2.4.4 Teratoma Assay

Protocols and use of animals in this project were undertaken with approval of the Monash University Animal Welfare Committee, following the 2004 Australian Code of Practice for the Care and Use of Animals for Scientific Purposes, and the Victorian Prevention of Cruelty to Animals Act and Regulations legislation.

H9 human embryonic cells were harvested when suitably confluent (approximately 80 %) using EDTA to obtain small clumps of cells as described previously in Section 2.3.1. Cell pellets were re-suspended in DMEM/F-12 with 33 % v/v Matrigel at a concentration of approximately 2x10^4 cells/μl. Cell suspensions were kept on ice prior to injection into mice. Cell culture for teratoma assays was conducted in part by Ashley Murphy, Monash University, Victoria, Australia. Preparation of cells for injection was conducted by Bei Wang, Manufacturing CSIRO, Victoria, Australia.

Approximately 1 million cells were injected under the skin of each flank of anesthetised, NODSCID IL2R$\gamma^{-/-}$ mice using a 26-gauge needle. Mice were monitored daily post-transplantation to track health and tumour size. Animals were euthanized at 12 weeks, or earlier if growing tumors approached the maximum teratoma size of 1 cm^3, or if they were unwell. The teratomas were removed and prepared for histological analysis. Animal experiments and handling were completed by Jessica Hatwell-Humble, Manufacturing CSIRO, Victoria, Australia.

After extraction, teratomas were placed in 4 % PFA. Fixative volume was approximately 5$\times$ tissue volume. Teratomas were then placed under vacuum for 72 hours before fixative was replaced with Sorensen's Buffer containing 5 % sucrose. Samples were subsequently processed to paraffin wax by the Monash Histology Platform. Paraffinized samples were embedded in a paraffin wax block and sectioned with a Leica 2040 microtome. Sections were cut 3 μm thickness and collected at intermittent intervals of around 30 - 60 μm. Teratoma processing, sectioning and staining was completed by Chad Heazlewood,

Maufacturing CSIRO, Victoria, Australia.

Stained sections were imaged in brightfield using an Olympus IX71 microscope for assessment of the human tissue types generated.

References

[1] Langford, C. R.; Johnson, D. W.; Cameron, N. R. *Polym. Chem.* **2014**, *5*, 6200–6206.

[2] Rueden, C. T.; Schindelin, J.; Hiner, M. C.; DeZonia, B. E.; Walter, A. E.; Arena, E. T.; Eliceiri, K. W. *BMC Bioinformatics* **2017**, *18*, 529.

[3] Schindelin, J. et al. *Nat. Methods* **2012**, *9*, 676.

[4] Barbetta, A.; Dentini, M.; De Vecchis, M. S.; Filippini, P.; Formisano, G.; Caiazza, S. *Adv. Funct. Mater.* **2004**, *15*, 118–124.

[5] Pulko, I.; Krajnc, P. *Macromol. Rapid. Commun.* **2012**, *33*, 1731–46.

[6] Carnachan, R. J.; Bokhari, M.; Przyborski, S. A.; Cameron, N. R. *Soft Matter* **2006**, *2*, 608.

[7] Eissa, A. M. *Personal Communication* **2016**,

[8] ReproCELL, *Matrigel® Coating of Alvetex® Scaffold* **2018**, http://reinnervate.com/alvetex/alvetex–documentation/protocols/.

[9] Johnson, D. W.; Langford, C. R.; Didsbury, M. P.; Lipp, B.; Przyborski, S. A.; Cameron, N. R. *Polym. Chem.* **2015**, *6*, 7256–7263.

[10] Legland, D.; Arganda-Carreras, I.; Andrey, P. *Bioinformatics* **2016**, *32*, btw413.

[11] Rebuzzini, P.; Zuccotti, M.; Redi, C. A.; Garagna, S. *Cytogenet. Genome Res.* **2015**, *147*, 1–9.

Chapter 3

Optimising Conditions for Peptide Functionalisation of Thiol-Acrylate Poly-HIPEs

3.1 Introduction

Porous polymers are attractive materials for biomedical applications due to their flexibility, the variety of chemistries by which they can be produced, and their ease of processing. Much research has focused on using porous polymers as animal-free, chemically-defined scaffold materials for tissue engineering [1, 2]. Such scaffolds can easily comply with good manufacturing processes and could be suitable for clinical use. Porous scaffolds provide a support for cells and developing tissue while also allowing efficient nutrient and waste product diffusion. Porosity can be introduced by a variety of methods including salt-leaching [3], freeze-drying [4, 5], block copolymer-templating [6, 7], gas foaming [8], electrospinning [9, 10] and emulsion-templating [11, 12]. This thesis focuses on emulsion-templated porous polymers, specifically polymerised high internal phase emulsions (poly-HIPEs).

The droplet phase content of a high internal phase emulsion (HIPE) is 74 % or greater [13]. When the continuous phase of a HIPE contains reactive monomers, it can be cured and the droplet phase subsequently removed, creating a polymerised HIPE or

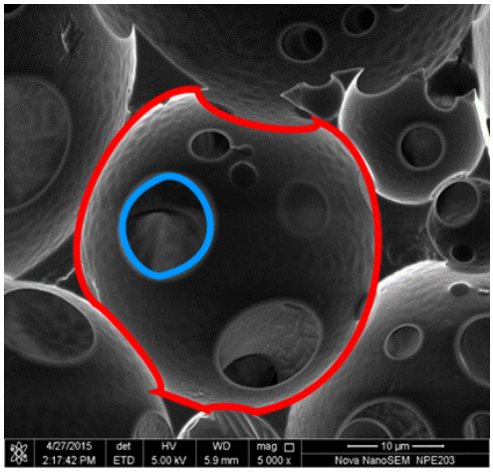

Figure 3.1: *SEM micrograph of typical polyHIPE morphology. An example of a void, formed by an internal phase droplet, is outlined in red. A smaller interconnect is shown in blue.*

polyHIPE [14]. These materials are highly porous polymer foams (porosity up to 95 %) with a fully interconnected network of voids [15, 16]. The typical structure of these materials is shown in Figure 3.1, with a large void highlighted in red and the smaller interconnect in blue. They have a range of applications including as catalyst supports [17, 18], filtration media [19, 20], materials for gas capture [21, 22], and tissue engineering scaffolds [23, 24]. A polystyrene-based polyHIPE scaffold is commercially available for use in three-dimensional cell culture under the name Alvetex® [25, 26, 27, 28, 29]. A range of other polyHIPE compositions are being investigated as scaffolds for specific cell and tissue types, including chondrocytes [24], neurons [30], muscle stem cells [31], fibroblasts [32] and osteoblasts [33].

An advantage of synthetic polymers as tissue scaffolds is their ease of functionalisation. Specific functionality may be incorporated into the polyHIPE material by adding functional monomers to the initial emulsion [34]. However, such additions may destabilise the emulsion, changing the droplet diameter or even leading to emulsion collapse [35]. Alternately, chemistries which introduce reactive chemical groups into the polymer monolith allow attachment of desired molecules post-curing. Functionalisation *via* this method allows for better control over the morphology and void diameter of the polyHIPE. In

the case of thiol-acrylate polyHIPEs, homopolymerisation of acrylate monomers leads to materials bearing residual thiol groups [36, 37] since acrylate groups are consumed more rapidly (Figure 3.2). These thiols are convenient 'handles' for subsequent chemical functionalisation. Several methods for functionalising polyHIPEs have been described in the literature, including some to functionalise thiol-acrylate materials. These methods are conducted in organic solvents to swell the polymer matrix [37, 38].

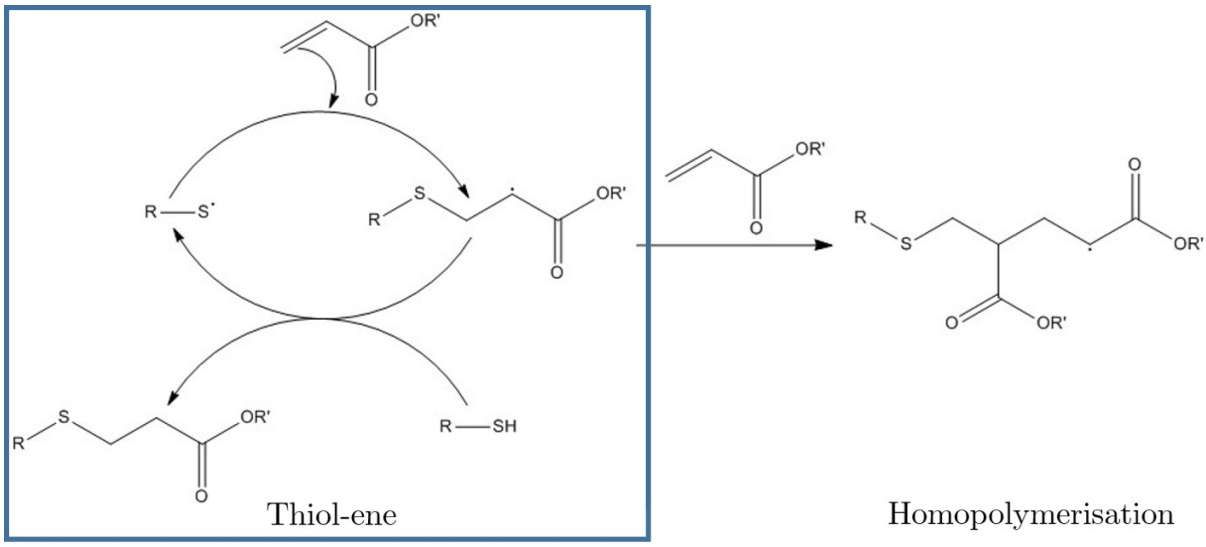

Figure 3.2: *Thiol-acrylate polyHIPEs are formed by two competing reactions, the thiol-ene reaction (left) and acrylate homopolymerisation (right).*

Adding bioactive species to the surface of synthetic biomaterials is an efficient way to control cell-material interactions [39, 40]. Processing methods used in the production of biomaterials should consider their final interaction with cells or tissues. Therefore, benign reaction conditions are preferred to reduce the risk of residual toxic components in the final product. In addition, many molecules that are suitable for bio-functionalisation such as peptides and sugars are not compatible with harsh reaction conditions or organic solvents. PolyHIPEs have shown much potential as scaffolds for cell culture and tissue engineering as their highly interconnected structure allows the perfusion of nutrients and wastes within the cell culture [41]. However, as-synthesised thiol-acrylate polyHIPEs do not possess any bioactive functionality to promote cell attachment and growth. Functionalisation with peptide sequences and other biomolecules would allow the material to

better mimic the *in vivo* cell environment. To the best of the author's knowledge, the only example of this in the literature is the functionalisation of polystyrene-based polyHIPEs with galactose residues to enhance hepatocyte attachment and growth [42].

This chapter explores the functionalisation of thiol-acrylate polyHIPE materials with a cyclised arginine-glycine-aspartate (RGD) peptide, which has been shown to lead to the expansion of human pluripotent stem cells in 2D culture [43]. In this manner, this chapter demonstrates the production of enhanced materials for *in vitro* pluripotent stem cell culture and expansion in 3D. Residual thiols in the polyHIPE materials are able to react with maleimide or maleimide-functionalised biomolecules, *via* a Michael addition. Maleimide itself was employed as a model for the peptide as it is a small, water-soluble, and relatively inexpensive molecule. Maleimide was used to functionalise hydrophobic thiol-acrylate polyHIPEs under a range of mild, aqueous-based conditions, including the use of NEt_3 as a catalyst and ethanol as a water-miscible co-solvent. As the reaction proceeds under mild conditions [44] that are suitable for the attachment of bioactive species, including peptides, this enabled the optimisation of conditions for the attachment of cyclic-RGDfK-maleimide. For clarity, commonly used single letter amino acid abbreviations in this thesis are listed in Table 3.1.

Table 3.1: *List of amino acid abbreviations used frequently in this thesis*

A	alanine	G	glycine
R	arginine	K	lysine
D	aspartate	f	D-phenylalanine

3.2 Chapter Aims

The first aim of this chapter was to synthesise a thiol-acrylate polyHIPE scaffold with suitable morphology for 3D stem cell culture. The polyHIPE composition presented herein is known to have residual thiol groups after curing. Therefore, the next aim was to functionalise these residual groups with maleimide. It was hypothesised that by optimising the reaction parameters for the addition of maleimide to residual thiol, a procedure could be developed with would be suitable for the addition of biofunctional groups.

To test this hypothesis, this chapter aimed to functionalise the material with a maleimide-functionalised peptide, cRGD-mal. It was anticipated that this peptide could be added to residual thiols using the same mechanism as maleimide, demonstrating the utility of the optimised Michael addition as a route to biofunctionalisation of 3D polymer scaffolds.

3.3 Results & Discussion

3.3.1 Preparation of Thiol-Acrylate Polymers

Equal molar equivalents of trimethylolpropane tris(3-mercaptopropionate) (TMPTMP) (Figure 3.3a) and trimethylolpropane triacrylate (TMPTA) (Figure 3.3b) create a stable emulsion with water, allowing them to be photopolymerised in a range of mould shapes without risking emulsion collapse [37, 45]. This produces a highly porous, interconnected polyHIPE structure. Using SEM imaging and ImageJ, the void diameter was found to be consistent at 38 ± 22 μm. The nominal porosity, as determined by the HIPE aqueous phase volume fraction, was 80 %.

During curing of the thiol-acrylate polyHIPEs, the thiol-ene "click" reaction forms the bulk of the polymer network. This reaction is accompanied by a secondary acrylate

homopolymerisation reaction, which consumes only acrylate groups (see Figure 3.2) [37]. This side reaction results in the presence of unreacted residual thiol groups in the as-synthesised polyHIPE material, which can be quantified *via* an Ellman's colourimetric assay [38]. Residual thiol groups are useful for post-polymerisation functionalisation of the thiol-acrylate polymers [37].

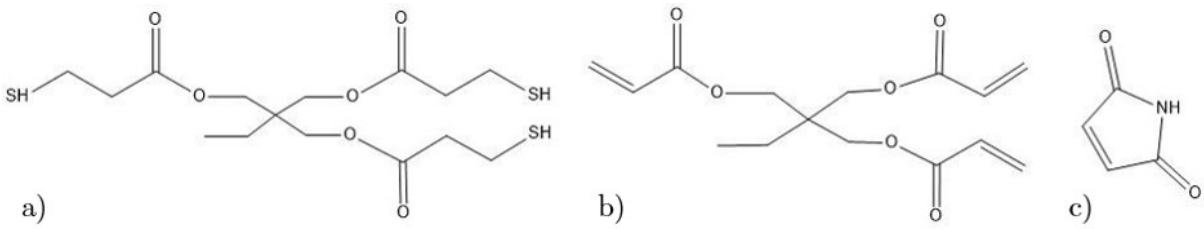

Figure 3.3: *Chemical structures of the monomers used to prepare and functionalise thiol-acrylate polyHIPEs. a) trimethylolpropane tris(3-mercaptopropionate) (TMPTMP) b) trimethylolpropane triacrylate (TMPTA) c) maleimide.*

3.3.2 Characterisation of Thiol-Acrylate Materials

The morphology of polyHIPEs is critical to any of their potential applications, including their use as a scaffold for stem cell culture. The precise diameter of voids and interconnects must be maintained before and after functionalisation to meet requirements for support of cells and nutrient flow. One of the intended outcomes of post-synthesis functionalisation was to maintain the designed polyHIPE structure. SEM was therefore used to confirm morphology before and after functionalisation, and void diameter was calculated. The polyHIPEs have an open cell structure with a continuous network of interconnects between the voids. This structure is maintained after functionalisation, as shown in Figure 3.4, and the average void size remains consistent at 30 - 40 μm.

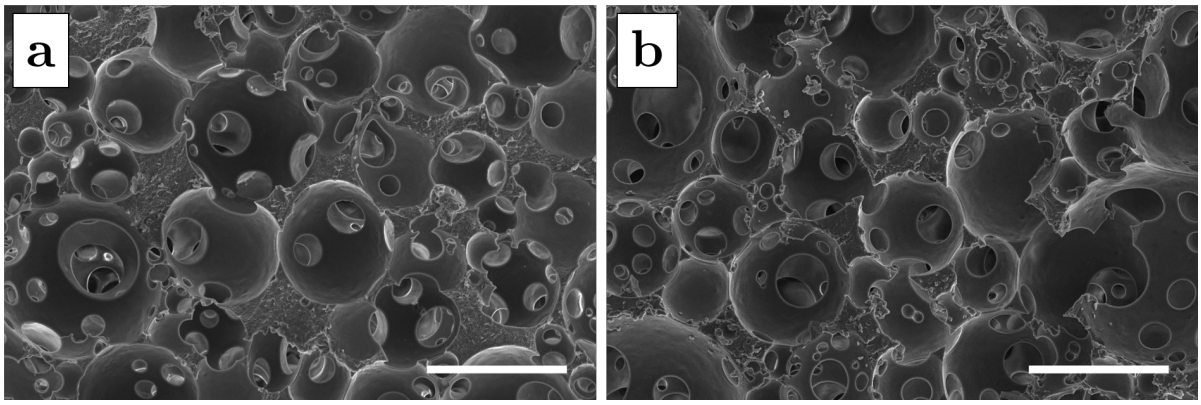

Figure 3.4: *Morphology of TMPTA polyHIPE with 80 % porosity, functionalised post-polymerisation as obtained by SEM. a) As-synthesised, before functionalisation and b) after functionalisation with maleimide via Michael addition. Scale bar = 30 μm.*

Porosity and interconnect size are important traits of the 3D scaffold as they influence how cells, nutrients, and wastes move through the material. Nominal porosity is determined by the internal (water) fraction added to the templating HIPE. The porosity can be measured post-curing using mercury intrusion porosimetry and gas pycnometry. Mercury porosimetry is a well-established method for determining the porosity, void size and interconnect diameter of porous materials, and is accepted as the most reliable method for determining interconnect diameter of polyHIPE materials. Table 3.2 shows the measured values for the thiol-acrylate polyHIPE scaffold. Figure 3.5 shows the mercury intrusion plot for this material.

Table 3.2: *The average diameter of interconnects between voids was measured via mercury porosimetry. The expression 4 × (total intrusion volume)/surface area was used to determine interconnect diameter. Porosity was measured using both mercury porosimetry and helium pycnometry*

Average Interconnect Diameter	7.98 μm
Nominal Porosity	80 %
Measured Porosity (Porosimetry)	81.25 %
Measured Porosity (Pycnometry)	84.4 ± 0.03 %

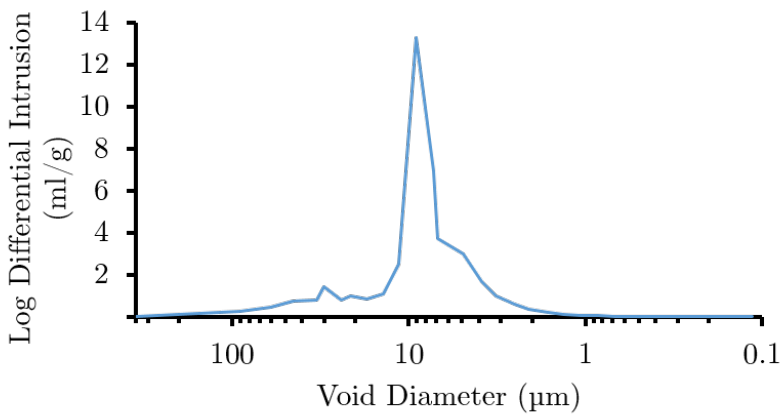

Figure 3.5: *Log differential intrusion plot for as-synthesised polyHIPE monolith as analysed by mercury porosimetry.*

SEM was not used to determine interconnect diameter as it is not a suitable method for this analysis. To measure voids, the SEM is focused on the surface of the polymer cross section. This allows the measurements to all be taken across one plane, at a known angle and working distance. A correction factor can then be uniformly applied to account for the voids being sectioned at different points (i.e. not through the centre). Attempting to measure interconnect diameters *via* SEM would be problematic as the interconnecting windows are located in the curved walls of the voids. Therefore, each measurement would be taken at an unknown working distance, and at unknown angles from the normal. No uniform correction factor would be able to account for these parameters. Qualitative assessment suggests that the interconnect diameter of 7.98 μm is in agreement with SEM images such as Figure 3.4.

3.3.3 Post-Polymerisation Functionalisation of Residual Thiols In Aqueous Solvent

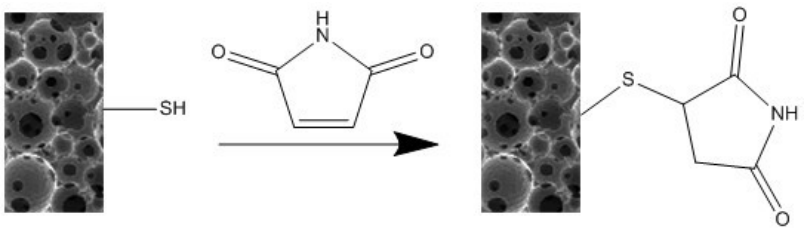

Figure 3.6: *Functionalisation of residual thiols with maleimide via Michael addition.*

Thiol groups can be used as reactive 'handles' to attach a range of moieties including methacrylates, acrylonitriles, and maleimides [44]. This chapter explores the attachment of a maleimide group *via* a Michael addition reaction as shown in Figure 3.6. Maleimide (Figure 3.3c) was selected as a suitable model for more biologically-relevant species such as maleimide-functionalised peptides. The quantity of maleimide used was calculated relative to the expected amount of residual thiols in the as-synthesised polyHIPE [38].

The concentration of residual thiols in the polyHIPE materials was quantified pre- and post-polymerisation using an Ellman's assay. Figure 3.7 shows the relative efficiency of maleimide functionalisation at different maleimide concentrations. Ellman's assay detects a decreasing thiol content as thiol groups are progressively bound to maleimide. When reactions are carried out in phosphate buffered saline, the concentration of remaining thiols decreases with increasing maleimide content (red plot, Figure 3.7). However, the reaction appears to saturate with almost half (43 ± 10 %) of the original thiols remaining. Increasing the maleimide content in the reaction solution past two molar equivalents does not improve functionalisation significantly.

Triethylamine (NEt_3) is a weak base which can be used in catalytic amounts to improve the yield of Michael addition reactions at room temperature. As it is readily water soluble, it is simple to remove from the final product. This is important for downstream applications, particularly those where biocompatibility is required. In catalysed reactions, triethylamine was added to the reaction vessel at the start of functionalisation. This resulted in an increased level of maleimide attachment, with just 20 % of the residual thiols remaining when 1 molar equivalent of maleimide was used (Figure 3.7).

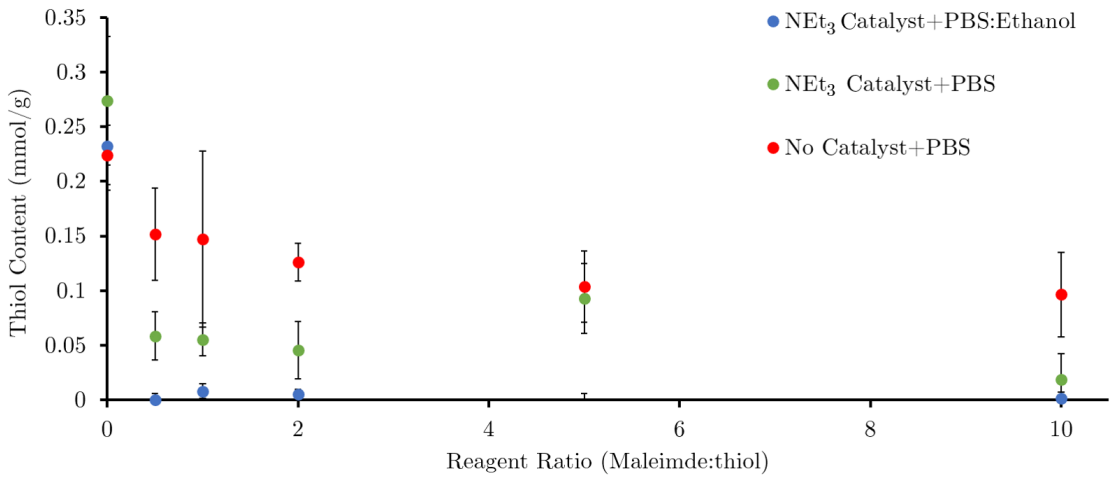

Figure 3.7: *Thiol content of TMPTA polyHIPE after functionalisation with maleimide for 120h, as determined by Ellman's colourimetric assays. It is clear that functionalisation is more efficient when a 50:50 solution of PBS and ethanol is used as the solvent, and triethylamine (NEt_3) is added as a catalyst. Error bars indicate standard deviation, n=3.*

Figures 3.8 & 3.11 shows the Raman spectra of thiol-acrylate polyHIPE materials prior to functionalisation, and after functionalisation with maleimide. The thiol peak appears at 2580 cm^{-1}. This peak is too weak to discern any significant trend in thiol concentration with variation of maleimide concentration. However, it can be used to give a qualitative assessment of functionalisation. Table 3.3 summarises characteristic peaks found in these materials *via* Raman spectroscopy. These surfaces were also analysed by XPS. The high resolution carbon 1s show a shift to lower binding energy at around 288 eV. This energy is due to the imide functionality [46], and correlates with the addition of maleimide. Together these data indicate that residual thiols were reacting with maleimide as anticipated.

Table 3.3: *Characteristic peaks found in thiol-acrylate polyHIPEs* via *Raman spectroscopy.*

Raman Shift (cm^{-1})	679	1420-1470	1737	2535	2580
Group	C-S	CH_3	C=O	C-H	S-H

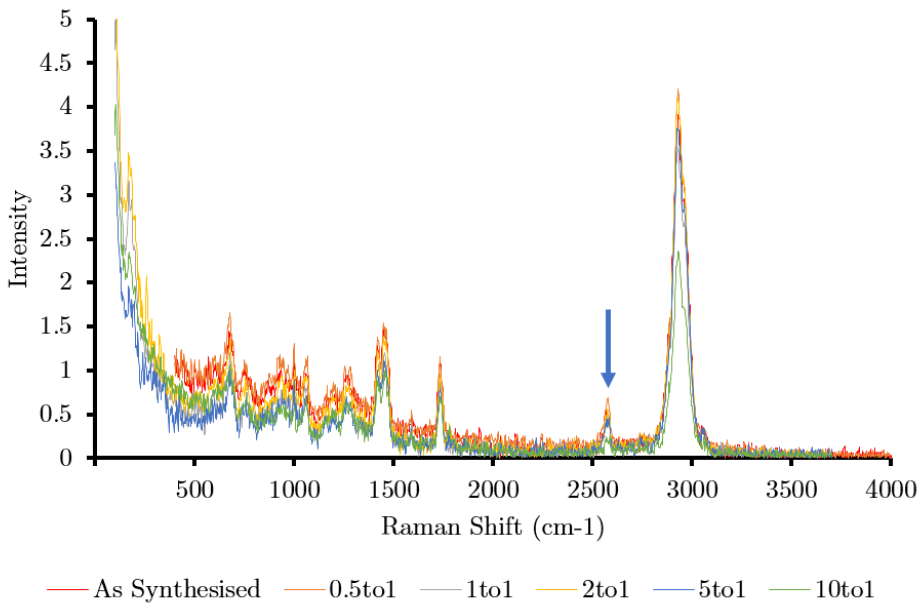

Figure 3.8: *Raman analysis of polyHIPE materials as-synthesised and after un-catalysed maleimide functionalisation. The arrow highlights the S-H peak at 2580 cm^{-1}.*

To achieve complete functionalisation, it was hypothesised that the polymer needed to be swollen in order to improve accessibility to surface reactive sites. The importance of swelling polyHIPE monoliths is discussed in a previous report [47]. Michael addition was repeated with a 50:50 solution of PBS and ethanol as a relatively benign, water-miscible solvent. This resulted in highly efficient polyHIPE functionalisation at all maleimide concentrations, as shown in Figure 3.7. Thus this method is suitable for functionalising thiol-acrylate polyHIPEs in benign solvents, and may be utilised for attaching sensitive biomolecules to the polymer post-synthesis.

The extent of functionalisation was also evaluated by XPS, which detects the increasing ratio of nitrogen to carbon as maleimide is attached. The XPS data shown in Figure 3.10 confirms the trend of increasing level of maleimide attachment with increasing maleimide:thiol content, and also demonstrates the increased efficiency obtained in the presence of ethanol co-solvent. High resolution C1s spectra (Figures 3.9 & 3.12) confirms maleimide as the nitrogen source.

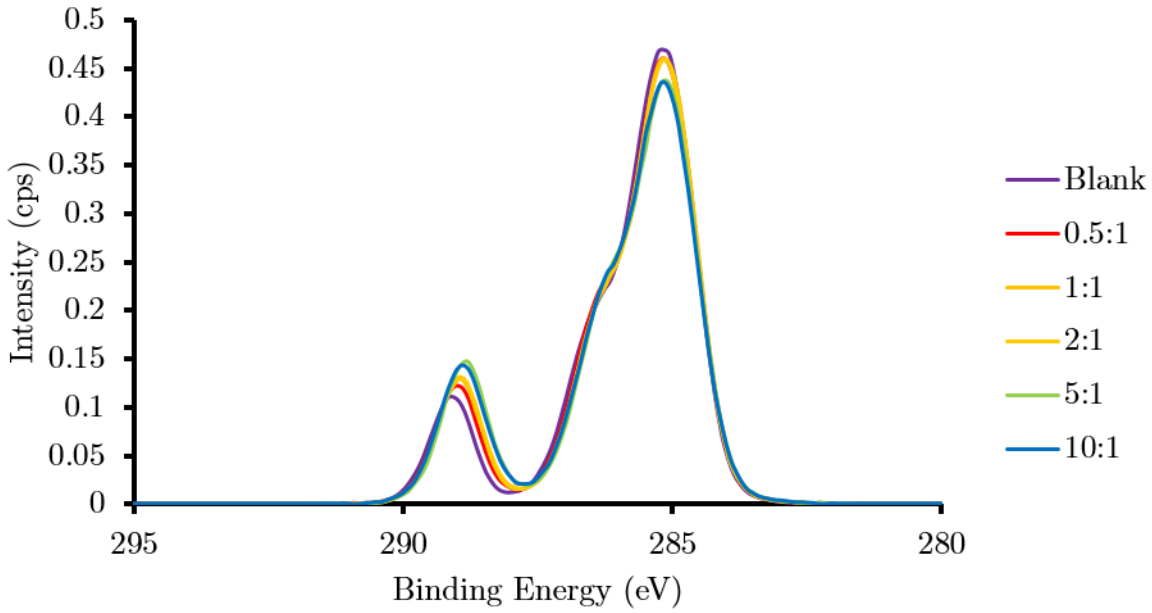

Figure 3.9: *High resolution C1s spectra confirm the presence of maleimide after uncatalysed Michael addition in PBS. The legend indicates the amount of maleimide added to the reaction solution as a ratio of the residual thiol content. Blank (purple) data was taken from a sample which underwent the same functionalisation process, but which had no maleimide added. The peak shift at 288 eV indicates that maleimide is binding to the surface.*

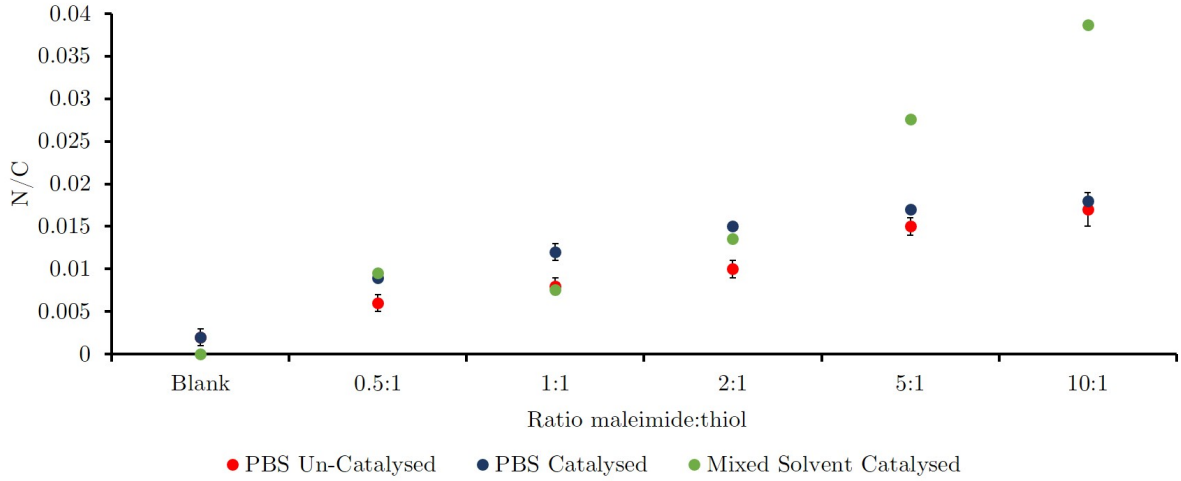

Figure 3.10: *Relative nitrogen content of polyHIPEs after functionalisation with maleimide for 120 hours, as determined by XPS. Addition of triethylamine catalyst increases the total nitrogen content of the material compared to the uncatalysed reaction, particularly at low molar equivalents of maleimide. Using a mixed solvent greatly improves functionalisation. Error bars indicate standard deviation (n=3).*

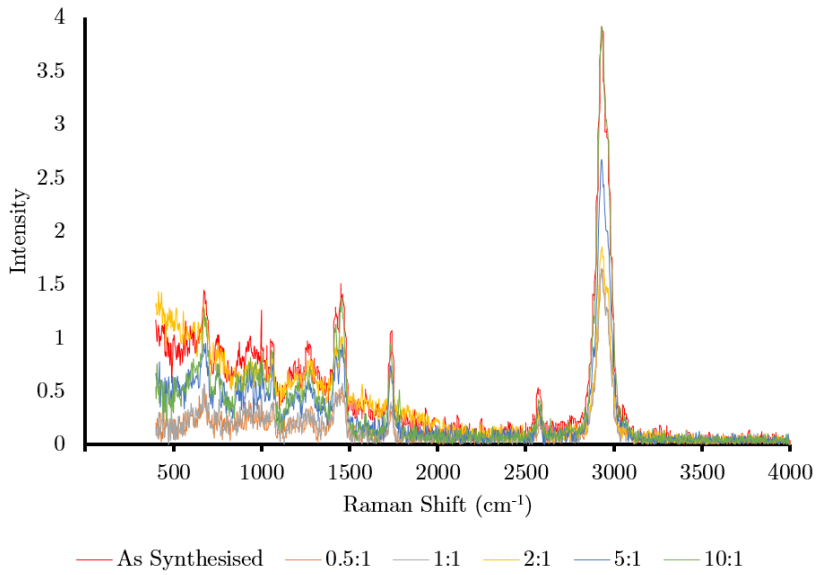

Figure 3.11: *Raman analysis of polyHIPE materials as-synthesised and after NEt_3 catalysed maleimide functionalisation. The ratio of maleimide to residual thiol is shown by the legend. As for the analysis of un-catalysed samples, the thiol peak at 2580 cm^{-1} is too weak to discern any trends.*

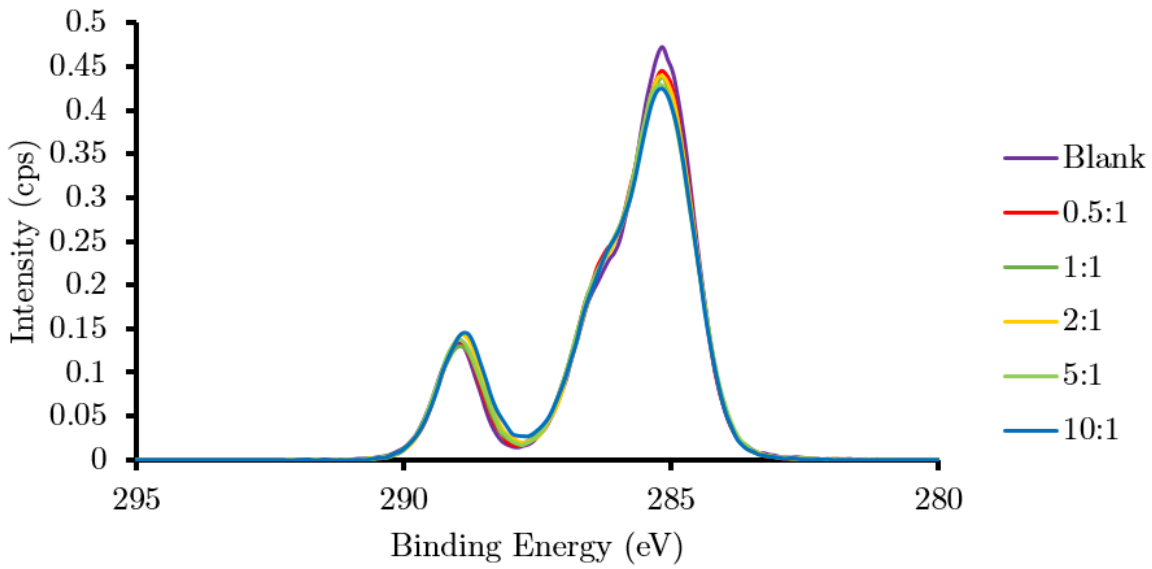

Figure 3.12: *High resolution C1s spectra confirm the presence of maleimide after catalysed Michael addition in PBS. The legend indicates the amount of maleimide added to the reaction solution as a ratio of the residual thiol content. Blank (purple) data was taken from a sample which underwent the same functionalisation process, but which had no maleimide added. As for the analysis of un-catalysed samples, the imide shift at 288 eV indicates that maleimide is binding to the surface.*

3.3.4 Optimising Reaction Time for Efficient Maleimide Attachment

The functionalisation reactions described in Section 3.3.3 were conducted for 120 hours at room temperature, to ensure that the maximum level of functionalisation was reached. This method was able to achieve a high degree of functionalisation, however a more time-efficient process is desirable. The reaction was therefore repeated with 1 molar equivalent of maleimide in PBS:ethanol with triethylamine, and analysed *via* Ellman's assay and XPS at several time points to determine the minimum time required to reach maximum functionalisation. These results are shown in Figure 3.13.

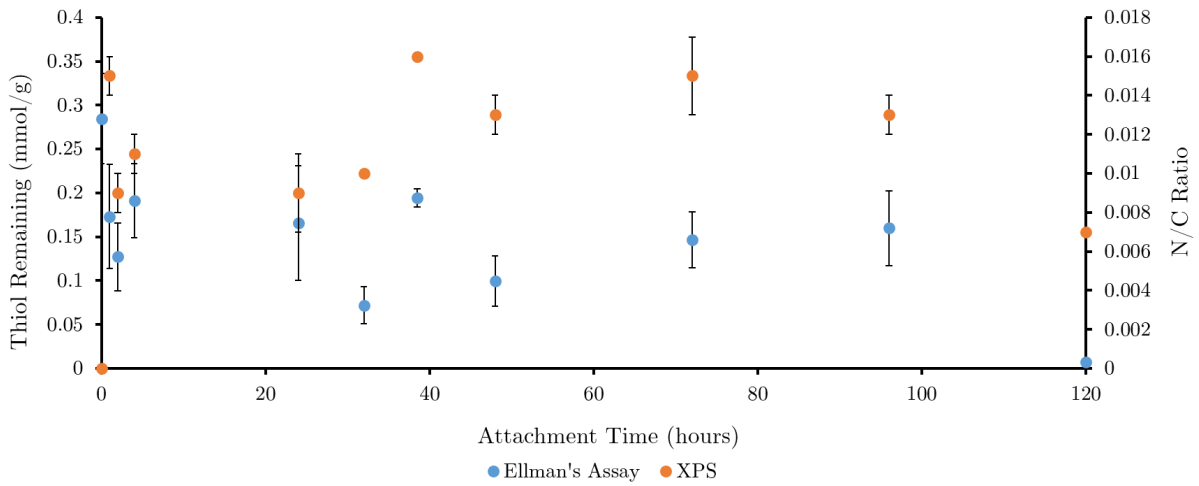

Figure 3.13: *Extent of polyHIPE functionalisation with maleimide as evaluated by Ellman's assays and XPS. The graph shows a decrease in residual thiol content with reaction time as detected by Ellman's assay, and increasing nitrogen content detected by XPS. Errors bars indicate standard deviation (n=3).*

Ellman's assays shown in Figure 3.13 indicate that the Michael reaction requires the full 120 hours to reach completion. XPS results however suggested that the reaction was complete after just two hours. This difference may be explained by the nature of the analysis techniques used. Ellman's assays were conducted on ground samples in tetrahydrofuran (THF), which is a good swelling solvent for the polyHIPE used, meaning that it quantifies all thiols throughout the bulk of the sample. XPS on the other hand

is a surface analysis method. The photoelectrons generated by the interaction between the incident X-ray radiation and the material have short mean free paths, meaning only those from the top few nanometres of the material are detected. It is possible that the surface is functionalised within two hours, as illustrated by the XPS data in Figure 3.13, but significantly longer is required to fully exhaust the total amount of residual thiols within the polyHIPE. Reaction of residual thiols in a 50 wt% acrylate polymer with 80 % porosity, while not complete, was considered to be satisfactory after 48 hours. This method was therefore adopted for subsequent functionalisations.

3.3.5 Functionalisation with Cyclic-RGD-Maleimide

The optimised maleimide Michael addition conditions were then employed using a maleimide-functionalised peptide sequence, cyclic-RGDfK-maleimide (cRGD-mal), to promote cell adhesion to the polyHIPE material. XPS analysis indicates successful surface functionalisation, with higher levels of attachment indicated as the peptide concentration is increased, as expected (Figure 3.14a). High resolution C 1s spectra indicate increasing levels of components indicative of peptide functionalisation (C-N and O=C-N) as the concentration of cRGD-mal is increased. These results indicate that the maleimide-to-residual-thiol attachment method is suitable for functionalising hydrophobic porous polyHIPE scaffolds post-synthesis with water-soluble, bioactive molecules.

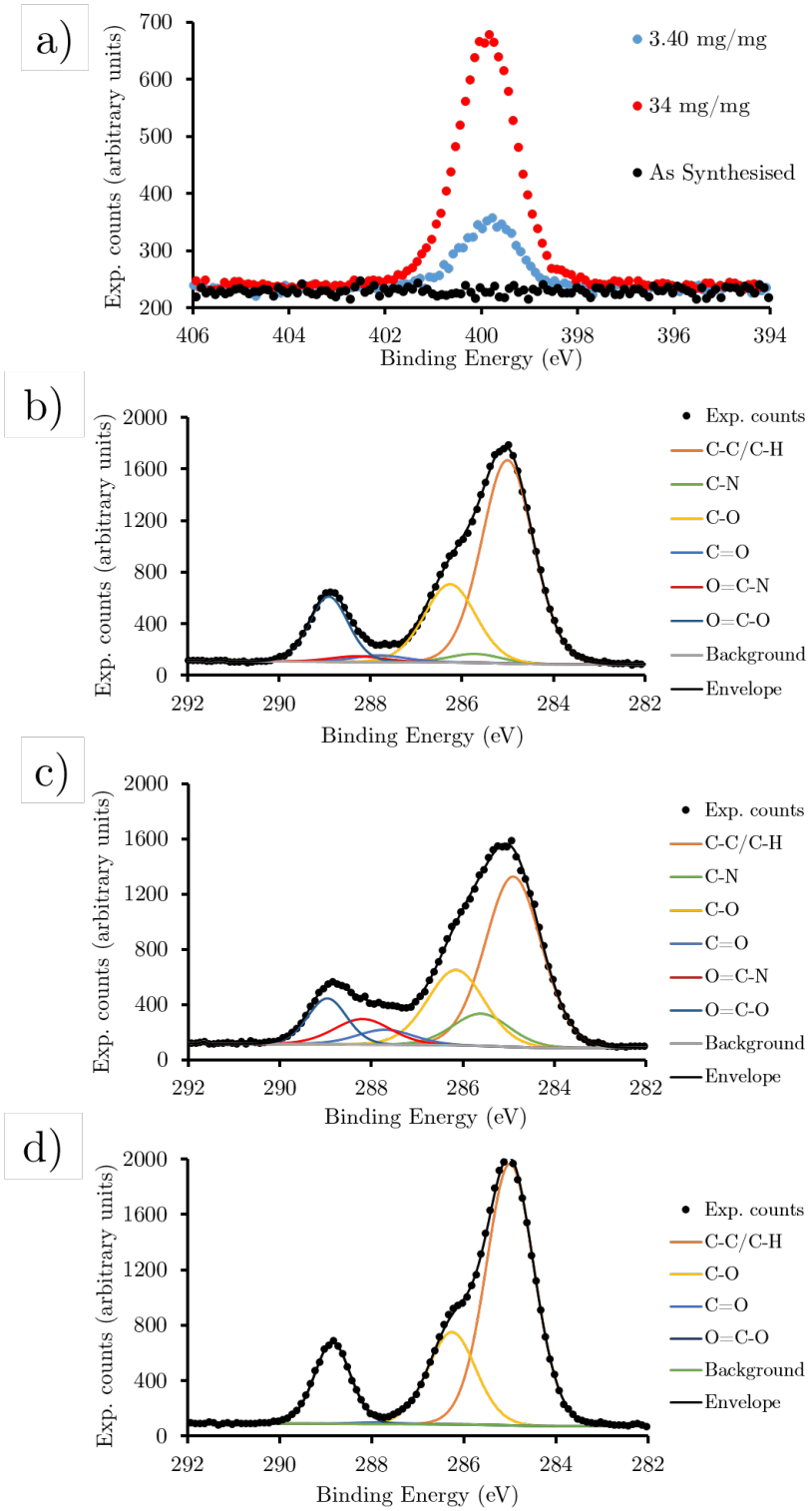

Figure 3.14: *a) XPS spectra showing nitrogen content of polyHIPE surfaces after functionalisation with cRGD-mal at two different concentrations (3.4 and 34.0 mg/mg of polyHIPE). b) High resolution C 1s spectra of cRGD-mal functionalised samples (3.40 mg cRGD-mal / mg polyHIPE). c) High resolution C 1s of cRGD-mal functionalised samples (34.0 mg cRGD-mal / mg polyHIPE). d) High resolution C 1s of blank polyHIPE.*

3.4 Conclusions

Hydrophobic thiol-acrylate polyHIPE materials were produced and functionalised with maleimide *via* base-catalysed Michael addition under biocompatible conditions. This small molecule acts as a model for water-soluble biomolecules such as amino acids and peptides. Ellman's colourimetric assays and XPS were used to monitor the extent of functionalisation. This process was optimised to achieve maximum functionalisation under aqueous conditions, showing a potential method for the functionalisation of hydrophobic polymer monoliths with water-soluble molecules. The use of very mild conditions means that the polyHIPEs could be functionalised without negative impact on their interconnected porous structure or on the attached biomolecules. This method can be used as a route for bio-functionalisation of polyHIPE materials for use as cell culture scaffolds and other applications, as demonstrated by the attachment of the adhesive peptide cyclic-RGDfK-maleimide (cRGD-mal). Further investigation *via* cell culture is required to confirm the functional state of the peptide.

References

[1] Caiazzo, M.; Okawa, Y.; Ranga, A.; Piersigilli, A.; Tabata, Y.; Lutolf, M. P. *Nat. Mater.* **2016**, *15*, 344–352.

[2] Leong, M. F.; Lu, H. F.; Lim, T. C.; Du, C.; Ma, N. K.; Wan, A. C. *Acta Biomater.* **2016**, *46*, 266–277.

[3] Nazarov, R.; Jin, H.-J.; Kaplan, D. L. *Biomacromolecules* **2004**, *5*, 718–726.

[4] Mozafari, M.; Kargozar, S.; de Santiago, G. T.; Mohammadi, M. R.; Milan, P. B.; Foroutan Koudehi, M.; Aghabarari, B.; Nourani, M. R. *Mater. Technol.* **2018**, *33*, 29–37.

[5] Kanimozhi, K.; Khaleel Basha, S.; Sugantha Kumari, V. *Mater. Sci. Eng. C* **2016**, *61*, 484–491.

[6] Beattie, D.; Wong, K. H.; Williams, C.; Poole-Warren, L. A.; Davis, T. P.; Barner-Kowollik, C.; Stenzel, M. H. *Biomacromolecules* **2006**, *7*, 1072–1082.

[7] Liu, Q.; Tang, Z.; Ou, B.; Liu, L.; Zhou, Z.; Shen, S.; Duan, Y. *Mater. Chem. Phys.* **2014**, *144*, 213–225.

[8] Jing, X.; Mi, H.-Y.; Turng, L.-S. *Mater. Sci. Eng. C* **2017**, *72*, 53–61.

[9] Vieira, T.; Silva, J. C.; Borges, J. P.; Henriques, C. *Eur. Polym. J.* **2018**, *103*, 271–281.

[10] Sadeghi, A.; Pezeshki-Modaress, M.; Zandi, M. *Int. J. Biol. Macromol.* **2018**, *114*, 1248–1256.

[11] Lovelady, E.; Kimmins, S. D.; Wu, J.; Cameron, N. R. *Polym. Chem.* **2011**, *2*, 559–562.

[12] Cameron, N. R. *Polymer* **2005**, *46*, 1439–1449.

[13] Silverstein, M. S. *Polymer* **2017**, *126*, 261–282.

[14] Silverstein, M. S. *Polymer* **2014**, *55*, 304–320.

[15] Silverstein, M. S. *Prog. Polym. Sci.* **2014**, *39*, 199–234.

[16] Carnachan, R. J.; Bokhari, M.; Przyborski, S. A.; Cameron, N. R. *Soft Matter* **2006**, *2*, 608.

[17] Yuan, W.; Chen, X.; Xu, Y.; Yan, C.; Liu, Y.; Lian, W.; Zhou, Y.; Li, Z. *RSC Adv.* **2018**, *8*, 5912–5919.

[18] Kimmins, S. D.; Wyman, P.; Cameron, N. R. *Polymer* **2014**, *55*, 416–425.

[19] McGann, C. L.; Daniels, G. C.; Giles, S. L.; Balow, R. B.; Miranda-Zayas, J. L.; Lundin, J. G.; Wynne, J. H. *Macromol. Rapid. Commun.* **2018**, *39*, 1800194.

[20] Tebboth, M.; Menner, A.; Kogelbauer, A.; Bismarck, A. *Curr. Opin. Chem. Eng* **2014**, *4*, 114–120.

[21] Duan, C.; Du, Z.; Zou, W.; Li, H.; Zhang, C. *Ind. Eng. Chem. Res.* **2018**, *57*, 5291–5300.

[22] He, H.; Li, W.; Lamson, M.; Zhong, M.; Konkolewicz, D.; Hui, C. M.; Yaccato, K.; Rappold, T.; Sugar, G.; David, N. E.; Damodaran, K.; Natesakhawat, S.; Nulwala, H.; Matyjaszewski, K. *Polymer* **2014**, *55*, 385–394.

[23] Eissa, A. M.; Barros, F. S. V.; Vrljicak, P.; Brosens, J. J.; Cameron, N. R. *Biomacromolecules* **2018**, 3343–3350.

[24] Naranda, J.; Sušec, M.; Maver, U.; Gradišnik, L.; Gorenjak, M.; Vukasović, A.; Ivković, A.; Rupnik, M. S.; Vogrin, M.; Krajnc, P. *Sci. Rep.* **2016**, *6*.

[25] Luckert, C.; Schulz, C.; Lehmann, N.; Thomas, M.; Hofmann, U.; Hammad, S.; Hengstler, J. G.; Braeuning, A.; Lampen, A.; Hessel, S. *Arch. Toxicol.* **2017**, *91*, 393–406.

[26] Knight, E.; Murray, B.; Carnachan, R.; Przyborski, S. In *3D Cell Culture: Methods and Protocols*; Haycock, J., Ed.; Methods Mol. Biol.; Humana Press Inc, 2011; Vol. 695; pp 323–340.

[27] MacDonald, C.; Finlay, D. B.; Jabed, A.; Glass, M.; Graham, E. S. *J. Neurosci. Methods.* **2014**, *238*, 70–77.

[28] Hayman, M.; Smith, K.; Cameron, N.; Przyborski, S. *J. Biochem. Biophys. Methods* **2005**, *62*, 231–240.

[29] Martín-Saavedra, F.; Crespo, L.; Escudero-Duch, C.; Saldaña, L.; Gómez-Barrena, E.; Vilaboa, N. *Sci. Rep.* **2017**, *7*, 15182.

[30] Murphy, A. R.; Laslett, A.; O'Brien, C. M.; Cameron, N. R. *Acta Biomater.* **2017**, *54*, 1–20.

[31] Lumelsky, Y.; Lalush-Michael, I.; Levenberg, S.; Silverstein, M. S. *J. Polym. Sci. A Polym. Chem.* **2009**, *47*, 7043–7053.

[32] Johnson, D. W.; Langford, C. R.; Didsbury, M. P.; Lipp, B.; Przyborski, S. A.; Cameron, N. R. *Polym. Chem.* **2015**, *6*, 7256–7263.

[33] Lee, A.; Langford, C. R.; Rodriguez-Lorenzo, L. M.; Thissen, H.; Cameron, N. R. *Biomater. Sci.* **2017**, *5*, 2035–2047.

[34] Caldwell, S.; Johnson, D. W.; Didsbury, M. P.; Murray, B. A.; Wu, J. J.; Przyborski, S. A.; Cameron, N. R. *Soft Matter* **2012**, *8*, 10344.

[35] Kircher, L.; Theato, P.; Cameron, N. R. *Polymer* **2013**, *54*, 1755–1761.

[36] Chen, C.; Eissa, A. M.; Schiller, T. L.; Cameron, N. R. *Polymer* **2017**, *126*, 395–401.

[37] Langford, C. R.; Johnson, D. W.; Cameron, N. R. *Polym. Chem.* **2014**, *5*, 6200–6206.

[38] Badyal, J. P.; Cameron, A. M.; Cameron, N. R.; Coe, D. M.; Cox, R.; Davis, B. G.; Oates, L. J.; Oye, G.; Steel, P. G. *Tetrahedron Lett.* **2001**, *42*, 8531–8533.

[39] Chen, F. M.; Liu, X. *Prog. Polym. Sci.* **2016**, *53*, 86–168.

[40] Re'em, T.; Tsur-Gang, O.; Cohen, S. *Biomaterials* **2010**, *31*, 6746–6755.

[41] Bokhari, M.; Carnachan, R. J.; Przyborski, S. A.; Cameron, N. R. *J. Mater. Chem.* **2007**, *17*, 4088.

[42] Hayward, A. S.; Eissa, A. M.; Maltman, D. J.; Sano, N.; Przyborski, S. A.; Cameron, N. R. *Biomacromolecules* **2013**, *14*, 4271–4277.

[43] Lambshead, J. W.; Meagher, L.; Goodwin, J.; Labonne, T.; Ng, E.; Elefanty, A.; Stanley, E.; O'Brien, C. M.; Laslett, A. L. *Sci. Rep.* **2018**, *8*, 701.

[44] Nair, D. P.; Podgórski, M.; Chatani, S.; Gong, T.; Xi, W.; Fenoli, C. R.; Bowman, C. N. *Chem. Mater.* **2014**, *26*, 724–744.

[45] Langford, C. R.; Johnson, D. W.; Cameron, N. R. *Macromol. Rapid. Commun.* **2015**, *36*, 834–839.

[46] Mittal, K. L. *Polyimides and Other High Temperature Polymers: Synthesis, Characterisation & Applications*; CRC Press, 2007; Vol. 4; p 247.

[47] Cameron, N. R.; Sherrington, D. C.; Ando, I.; Kurosu, H. *J. Mater. Chem.* **1996**, *6*, 719–726.

Chapter 4

Optimisation of PolyHIPE Scaffolds for 3D Pluripotent Stem Cell Culture

4.1 Introduction

There are a range of features that affect the proliferation and stemness of embryonic stem cells in culture. The porous polymer scaffold synthesised in Chapter 3 possesses several suitable characteristics for 3D cell culture, including high porosity, interconnected morphology, and appropriate void diameter. To tailor this material to specifically support human pluripotent stem cells, several other aspects of the material can also be manipulated. Surface functionalisation, mechanical properties, interconnect diameter, and macro-scale scaffold presentation may all contribute to the effectiveness of the 3D culture system. Surface functionalisation is a key parameter in promoting cell adhesion, proliferation, and pluripotency. A wide range of surface functionalisations have been employed to improve cell adhesion, from plasma treatment and oxidisation, to protein coatings and conjugation of specific bioactive species. This chapter's main focus is the surface functionalisation of the thiol-acrylate polyHIPE scaffold with protein and peptide components, and the subsequent effects on pluripotent stem cells in culture. Other material modifications and investigation of culture protocol parameters are also discussed.

4.1.1 2D Culture Conditions

Mitotically inactivated mouse embryonic feeder cells (MEFs) were used to support derivation of the first embryonic stem cell cultures. The are still employed today in pluripotent stem cell culture as they provide both suitable binding sites and growth factors to the cells. Use of MEFs requires simultaneous growth of the feeder layers and the stem cells of interest. Contamination, either with cells, viruses, or immunogenic particles, is a major risk when culturing on MEF layers. Commercially available MEFs need to be screened for a wide variety of pathogens before use including Sendai virus, mouse hepatitis virus, and lactate dehydrogenase-elevating virus (LDEV) [1] to reduce this risk. Passaging cells on these layers is labour intensive. Significant development of feeder-free culture methods for pluripotent cells has allowed a shift away from the use of MEFs and other supporting cell layers.

Established methods for feeder-free culture of human pluripotent stem cells frequently use an ECM coating such as Matrigel® or Geltrex® in place of feeder cells. These products are murine sarcoma-derived basement membrane coatings containing an undefined mixture of proteins. ECM derived coatings provide similar anchorage points to feeder layers, but do not include whole cells. Cells cultured on these coatings are easier to distinguish from the supporting layer, making passaging simpler. Feeder-free coatings can be used with chemically defined media to reduce the number of undefined components in the culture system.

4.1.2 Adapting 2D Conditions to 3D Culture

Human pluripotent stem cells can be routinely cultured in E8 media on Geltrex®-coated TCPS, and passaged using EDTA. While such 2D culture has a number of drawbacks, which were discussed previously in Chapter 1, these methods have been thoroughly tested and optimised in many labs over decades. The cultureware, media, and supporting sub-

strates are all commercially available which improves reproducibility. Using Geltrex® and E8 media, the H9 human embryonic stem cell line used to assess the materials presented in this thesis can be maintained in a feeder-free environment for several passages. It is therefore beneficial to use aspects of these successful 2D cultures when attempting to progress to 3D formats.

Porous polyHIPE materials have been successfully used to culture a range of cell lines in 3D [2, 3, 4, 5]. Their fully interconnected morphology presents a 3D environment to the cells, while allowing nutrients and wastes to diffuse through the culture. This chapter explores the optimisation of the thiol-acrylate polyHIPE presented in Chapter 3 for 3D culture of human embryonic stem cells. Two approaches for modifying the surface of the scaffold are presented. The first approach incorporates the Geltrex® coating used in 2D culture and a crosslinker known as sulfo-SANPAH to form a 3D, feeder-free culture scaffold. Sulfo-SANPAH is a hetero bi-functional, water soluble crosslinker regularly used for binding primary amines to polymers [6, 7]. It contains an azide which can be activated with ultraviolet light, and an amine reactive ester group. The azide anchors sulfo-SANPAH to polymers, while the ester group can bind to proteins such as those found in Geltrex®. The crosslinking process is shown in Figure 4.1.

4.1.3 Cyclic-RGD as a Biofunctional Ligand for 3D Cell Culture

While the use of ECM coatings allows the maintenance of pluripotent stem cells without the need for feeder cells, these coatings are not ideal as they are not chemically defined. This lack of definition means that cells cultured on Geltrex® are not clinically applicable. There is a need for a culture substrate that is both 3D and chemically defined, which also has the ability to promote stem cell pluripotency. Functionalisation with peptides is an approach that allows culture scaffolds to mimic the stem cell niche and provide the required cues for cell maintenance. Chapter 3 outlines the optimisation of a method for

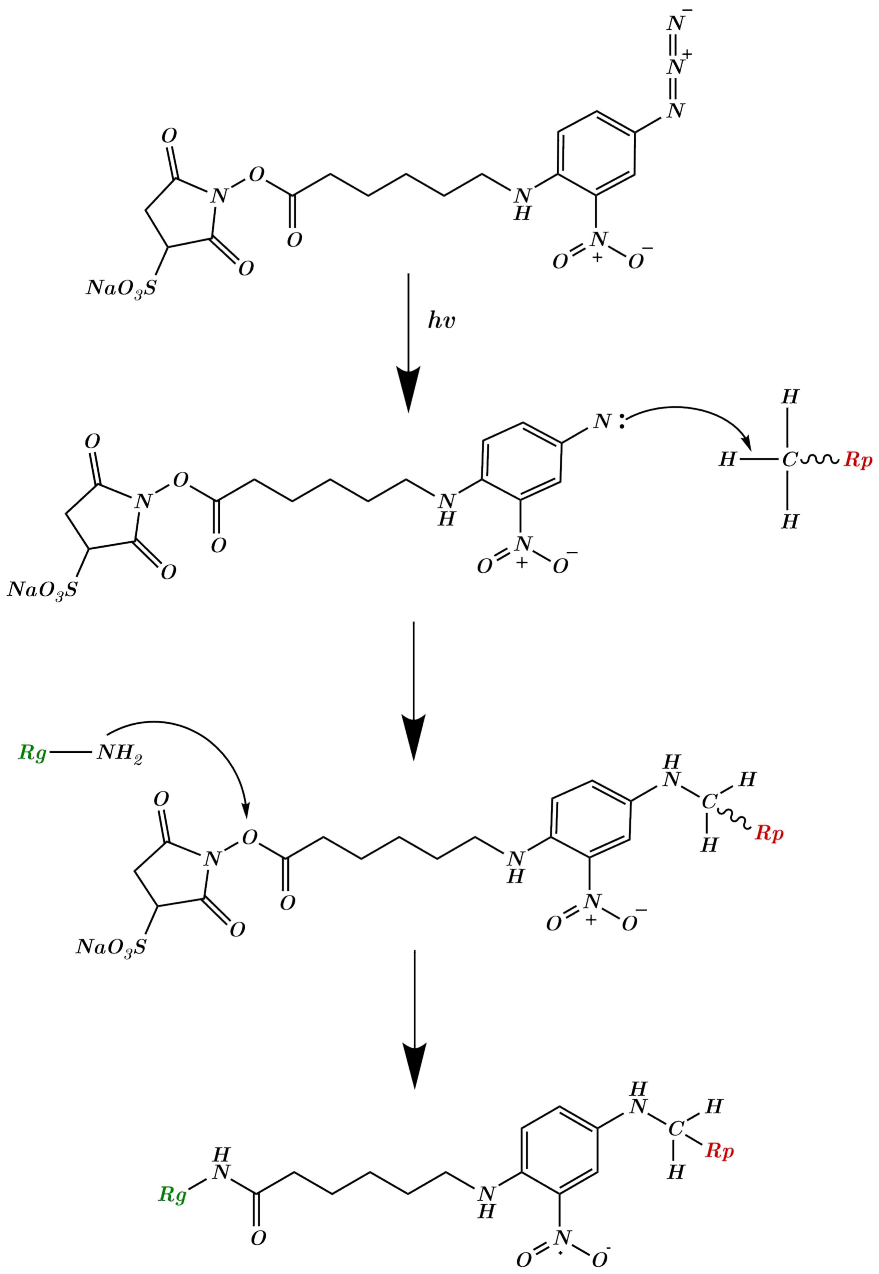

Figure 4.1: *Sulfo-SANPAH crosslinking reaction scheme. Rp denotes the thiol-acrylate polyHIPE scaffold, Rg denotes amine-containing Geltrex® proteins.*

modifying thiol-acrylate polyHIPE scaffolds *via* functionalisation of residual thiol groups. This protocol proceeds under mild conditions, allowing the polymer to be functionalised with bioactive molecules such as proteins and peptides.

A wide range of peptides have been incorporated into materials to support and direct stem cells in culture. RGD is a peptide sequence found in fibronectin, laminin and other ECM proteins that promotes cell adhesion [8]. The RGD peptide is effective and commonly used, and has perhaps featured in the largest number of biomaterials studies [9]. Cyclic-RGD has higher potency than the linear RGD sequence [10], and has been previously shown to support human embryonic stem cells in 2D culture [11]. Therefore the second polyHIPE modification approach presented in this chapter involves the addition of a cRGD peptide to the scaffold in place of the crosslinked Geltrex® coating.

4.2 Chapter Aims

The overarching aim of this chapter was to optimise a polymer scaffold-based culture system to allow maintenance of H9 pluripotent stem cells in a chemically defined, 3D environment.

In Chapter 3, a porous scaffold was produced, characterised, and functionalised. In this chapter, the first aim was to adapt the established culture protocol used in 2D to 3D culture on the thiol-acrylate polyHIPE material. It was hypothesised that this could be achieved by adding the same protein coating used routinely in 2D to polyHIPE scaffolds.

The next aim was to use the functionalisation route developed in Chapter 3 to add a bioactive peptide group to the 3D scaffold. It was predicted that the peptide would be successfully incorporated into the material, and could be used as a substitute for the protein coating resulting in a chemically defined, 3D scaffold that could support pluripotent stem cell culture.

Finally, this chapter aimed to optimise other material properties and culture parameters

to increase cell proliferation and pluripotency within the 3D polyHIPE scaffold.

4.3 Results & Discussion

4.3.1 Two-Dimensional H9 Stem Cell Culture

H9 human pluripotent stem cells were cultured on a 2D substrate before seeding onto 3D scaffolds. Figure 4.2 shows typical H9 embryonic stem cell morphology in 2D. The colonies were compact with defined edges, as is typical of embryonic stem cells [12]. These cells typically appear small and round, with a high cytoplasm to nucleus ratio. Cells were routinely monitored for changes in morphology which may indicate differentiation. Additionally, behaviour during passaging was noted as changes may also indicate an undesired phenotype. For example, cells requiring longer than typical EDTA exposure to loosen from the TCPS substrate were watched closely and considered for karyotype analysis.

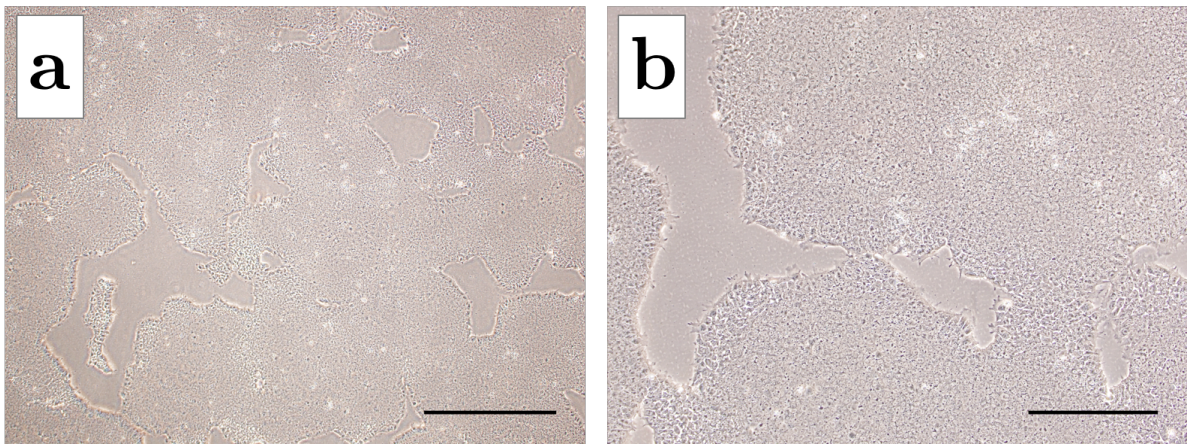

Figure 4.2: *Micrographs showing typical H9 stem cell morphology during 2D culture on Geltrex®-coated TCPS at a) 4× magnification, scale bar = 1 mm, and b) 20× magnification, scale bar = 200 μm.*

4.3.2 Culture on As-Synthesised Thiol-Acrylate PolyHIPE Scaffolds

Thiol-acrylate polyHIPEs were first assessed as culture substrates in their as-synthesised form. This was necessary to clarify the effect of subsequent functionalisation on cell attachment and proliferation. This was compared to the same polymer coated with Geltrex®. Geltrex® is a basement membrane protein mixture routinely used to support H9 embryonic stem cells cultured on TCPS.

H9 pluripotent stem cells were seeded at a rate of 1 million cells per scaffold onto hydrated and sterilised thiol-acrylate scaffolds. Scaffolds were either left as-synthesised, or coated with an adsorbed layer of Geltrex®. The Geltrex® coating was applied as per routine 2D culture, with a larger volume of coating solution added to account for the greater surface area of the 3D culture format. Culture was conducted for three days. Micrographs of H&E stained sections in Figure 4.3 show that cell attachment was minimal to null on both as-synthesised scaffolds and on materials that had undergone the Geltrex® coating process. Some cells were evident on the Geltrex®-coated scaffold, as indicated by arrows in Figure 4.3b. Culture was not extended further as it was apparent that cells had not sufficiently adhered to the material.

This result was not necessarily expected as a range of polyHIPE scaffolds have been used in cell culture previously. However, these previous cultures involved different cell lines [3, 13] and polyHIPE chemistries [5, 14]. As-synthesised thiol-acrylate polyHIPE materials do not have any specific bioactive motifs, leading to a lack of stem cell attachment. However, the Geltrex® coating was expected to provide adhesion sites on the 3D scaffold as is does on 2D TCPS. The lack of cell attachment shown in Figure 4.3b may have been due to the coating failing to efficiently adhere to the thiol-acrylate substrate.

Another possibility is inconsistent cell seeding. As a very small volume of media containing a concentrated cell suspension was applied to each scaffold, it was crucial that

the suspension was thoroughly mixed to achieve even distribution. Care was taken to agitate cells regularly. In addition, multiple samples of each scaffold type were analysed and showed consistent results. This type of error is therefore less likely to be the sole cause of low cell numbers.

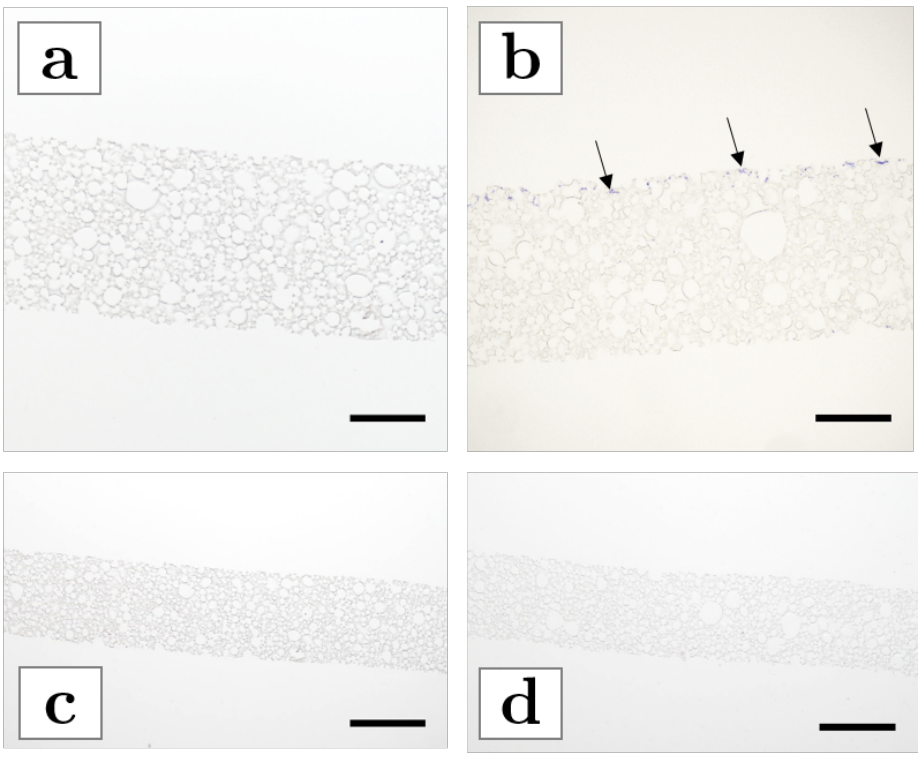

Figure 4.3: *Micrographs of H&E stained H9 stem cell cultures after 3 days in thiol-acrylate polyHIPE scaffolds a) as-synthesised, 20× magnification, scale bar = 100 μm b) with Geltrex® coating, 20× magnification, scale bar = 100 μm c) as-synthesised, 10×, scale bar = 200 μm, and d) with Geltrex® coating, 10× magnification, scale bar = 200 μm. Arrows indicate H&E staining suggesting some cell adhesion.*

4.3.3 Adapting 2D Culture Protocols to 3D Pluripotent Stem Cell Culture

4.3.3.1 Addition of Geltrex® Coating *via* Physical Adsorption

A Geltrex® coating was applied to a commercially available polystyrene polyHIPE scaffold (Alvetex®) and to the thiol-acrylate polyHIPE scaffold synthesised in Chapter 3. The combination of polystyrene polyHIPE and Geltrex® produces a 3D scaffold with equivalent surface chemistry to the routine 2D culture surface. This material served as a positive control scaffold and allowed initial assessment of the new thiol-acrylate system.

The Geltrex®-coated polystyrene and thiol-acrylate materials were intended to provide a series of adaptation steps between routine culture and novel defined 3D culture. Cell culture was conducted on these scaffolds for 5 days. Figure 4.4 shows the response of H9 pluripotent stem cells to these scaffolds. Geltrex®-coated Alvetex® supports robust cell proliferation and infiltration into the scaffold (Figure 4.4 a&b). This commercially available material has previously been used for a range of cell types [4, 15, 16] including H9 stem cells [17]. Matrigel®, an ECM derived protein coating which is very similar to Geltrex®, is known to adhere to Alvetex®. Therefore, it was expected that Geltrex®-coated Alvetex® would support cell growth. Figure 4.4 c&d demonstrates a lack of cell adhesion to as-synthesised thiol-acrylate polyHIPEs, reiterating the result shown in Figure 4.3. Coating the thiol-acrylate material with Geltrex® does not promote cell adhesion on this material, as shown by Figure 4.4 e&f.

Figure 4.5 a-c shows thiol-acrylate polyHIPE scaffolds that have been coated with Geltrex® and immunostained with an anti-laminin antibody to visualise the coating. There is a concentration of staining around the edges of the sections. The edges correlate with the outer surfaces of the scaffold during coating. This suggests that the low cell number on these scaffolds may have been due to the coatings being restricted to the outer surface. Staining suggested that the coating was inconsistent on thiol-acrylate materials, with

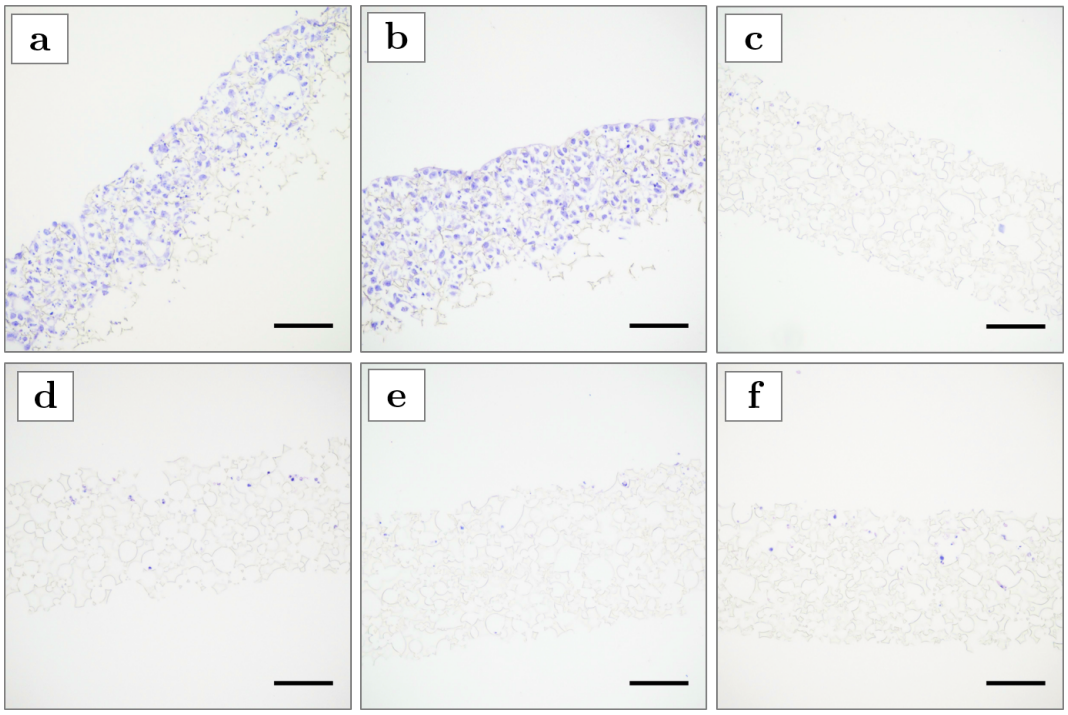

Figure 4.4: *Micrographs of H&E stained H9 stem cells cultured on as-synthesised thiol-acrylate polyHIPE, Geltrex®-coated thiol-acrylate polyHIPE, and Geltrex®-coated Alvetex® for up to 5 days. a) Geltrex®-coated Alvetex®, 2 days, b) Geltrex®-coated Alvetex®, 5 days, c) as-synthesised thiol-acrylate polyHIPE, 2 days d) as-synthesised thiol-acrylate polyHIPE, 5 days e) Geltrex®-coated thiol-acrylate polyHIPE, 2 days f) Geltrex®-coated thiol-acrylate polyHIPE, 5 days. Scale bar = 100 μm.*

some stained sections showing low overall laminin staining. This potentially indicates that Geltrex® does not adhere reliably to the thiol-acrylate scaffold.

Figure 4.5 d&e shows sections of Alvetex® scaffold coated with Geltrex® and immunostained with an anti-laminin antibody. These scaffolds typically had a more consistent coating. This outcome is expected due the proven ability of Geltrex® to adhere to polystyrene substrates, as demonstrated in 2D culture. In conjunction with cell culture results, it appears that coating Geltrex® on the thiol-acrylate scaffold using the same method as for polystyrene does not achieve a sufficiently high Geltrex® surface concentration.

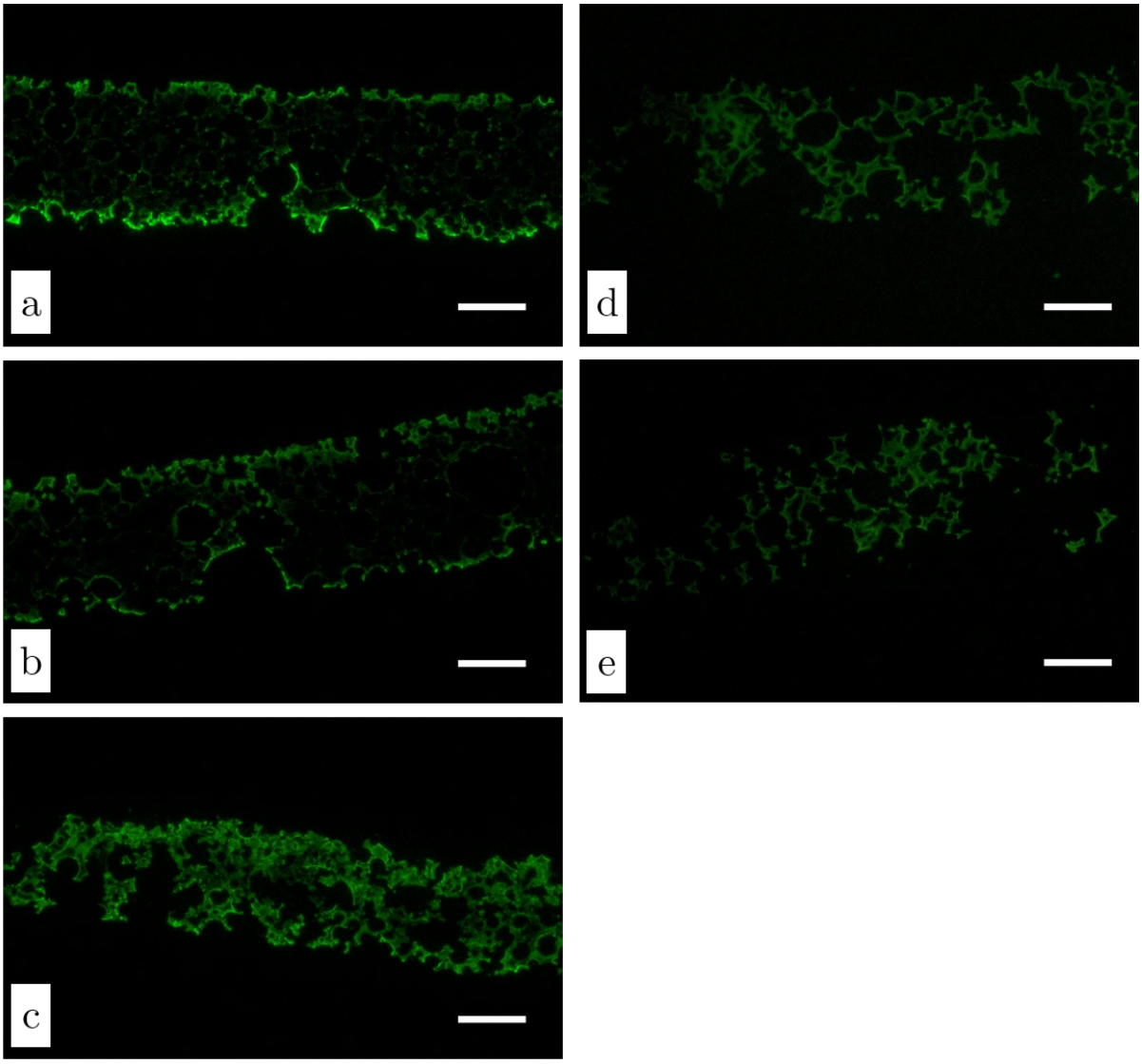

Figure 4.5: *Anti-laminin immunostained polyHIPE sections coated in Geltrex® using the physical adsorption method. Thiol-acrylate (a-c) and Alvetex® (d-e) materials are shown. Geltrex® was diluted to a) 0.125 % b) 0.25 % c) 0.5 % d) 0.125 % and e) 0.25 % solutions. Scale bar = 100μm. Images taken at equal exposure and gain.*

The protocol used to coat the scaffolds in Figures 4.3 - 4.5 relies on the physical adsorption of ECM components in Geltrex® to the polymer scaffolds. Alvetex® is composed of polystyrene (PS), which is a hydrophobic polymer which contains an aromatic ring structure. PS is known to effectively adsorb a range of proteins [18, 19]. Hydrophobic interactions are believed to be the main mechanism of protein adsorption onto polystyrene [18]. These interactions result in enough Geltrex® adsorption onto the Alvetex® to form a coating sufficient for cell growth. Physical adsorption of Geltrex® onto the thiol-acrylate polyHIPEs was possibly less effective due to the different chemical structure of these materials. The thiol-acrylate polymer is also hydrophobic, so hydrophobic interactions are still a possible mechanism for protein adsorption. However this polymer lacks the aromatic ring found in PS. Surface energy characteristics are also known to impact the extent and rate of protein adsorption [20]. Thus the difference in surface free energies may contribute to the difference in protein adsorption between the polymers.

4.3.3.2 Addition of Geltrex® Coating *via* Covalent Crosslinker

Thiol-acrylate polyHIPEs were functionalised with sulfo-SANPAH using UV activated azide addition. Sulfo-SANPAH crosslinking is a commonly used method for functionalising polymer surfaces with peptides [21, 22, 23]. Therefore, this crosslinker was expected to anchor the Geltrex® coating to the polyHIPE scaffold and create a layer sufficient to support pluripotent stem cell culture. Peptides such as the adhesive motif RGD are also available pre-functionalised with a SANPAH group to allow simple attachment to a range of surfaces [24, 25].

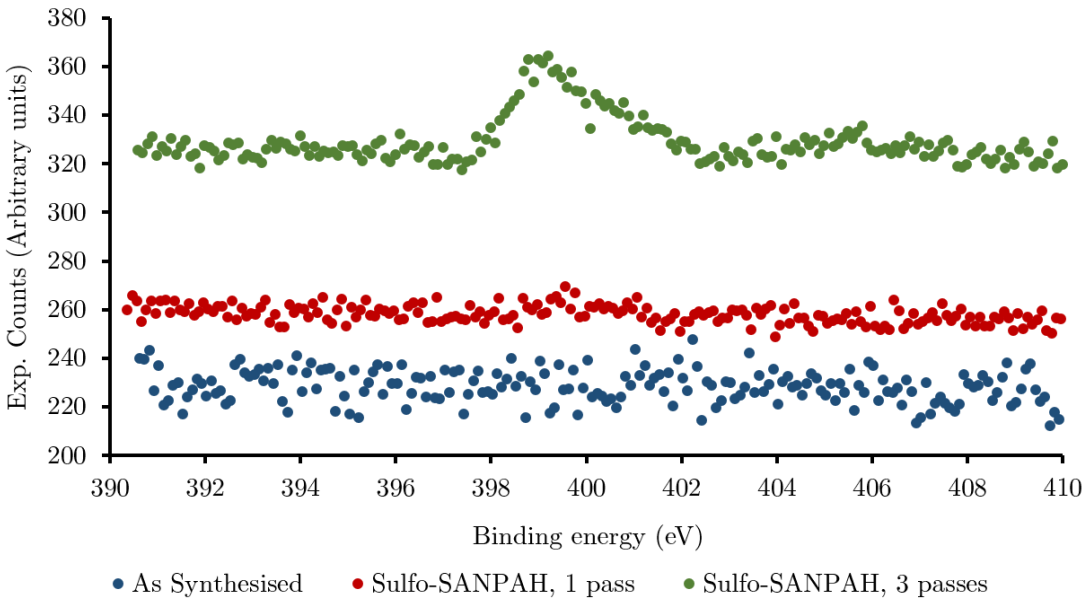

Figure 4.6: *Comparison of nitrogen peaks from XPS survey scans of as-synthesised thiol-acrylate polyHIPEs, and thiol-acrylate polyHIPEs functionalised with sulfo-SANPAH. Functionalisation was conducted using 1 (red points) or 3 (green points) separate exposures to UV irradiation using a Light Hammer UV irradiation conveyor belt system.*

XPS analysis in Figure 4.6 shows the addition of nitrogen to the surface of the thiol-acrylate scaffold when sulfo-SANPAH was conjugated. This indicated that sulfo-SANPAH was bound to the polyHIPE scaffold. This analysis also confirmed that three passes under UV light were required to achieve a measurable nitrogen signal. A single pass did not result in a defined nitrogen peak (Figure 4.6, red), suggesting that sulfo-SANPAH did not bond to the polymer surface in sufficiently high concentration. After three passes, a distinct nitrogen peak was evident (Figure 4.6, green).

After addition of sulfo-SANPAH, scaffolds were coated with Geltrex®. Immunostaining the Geltrex® coating with an anti-laminin antibody showed more intense staining on sulfo-SANPAH functionalised thiol-acrylate polyHIPEs (Figure 4.7 d&e) than on as-synthesised, coated materials (Figure 4.7 a&b). This suggests a more consistent coating was possible when the crosslinker was utilised. Two concentrations of Geltrex® were investigated. Figure 4.7 shows that strong protein adhesion could be achieved at both

concentrations. Due to the known utility of sulfo-SANPAH as a polymer to peptide crosslinker, the increased surface concentration and homogeneity of the Geltrex® coating after crosslinking was expected.

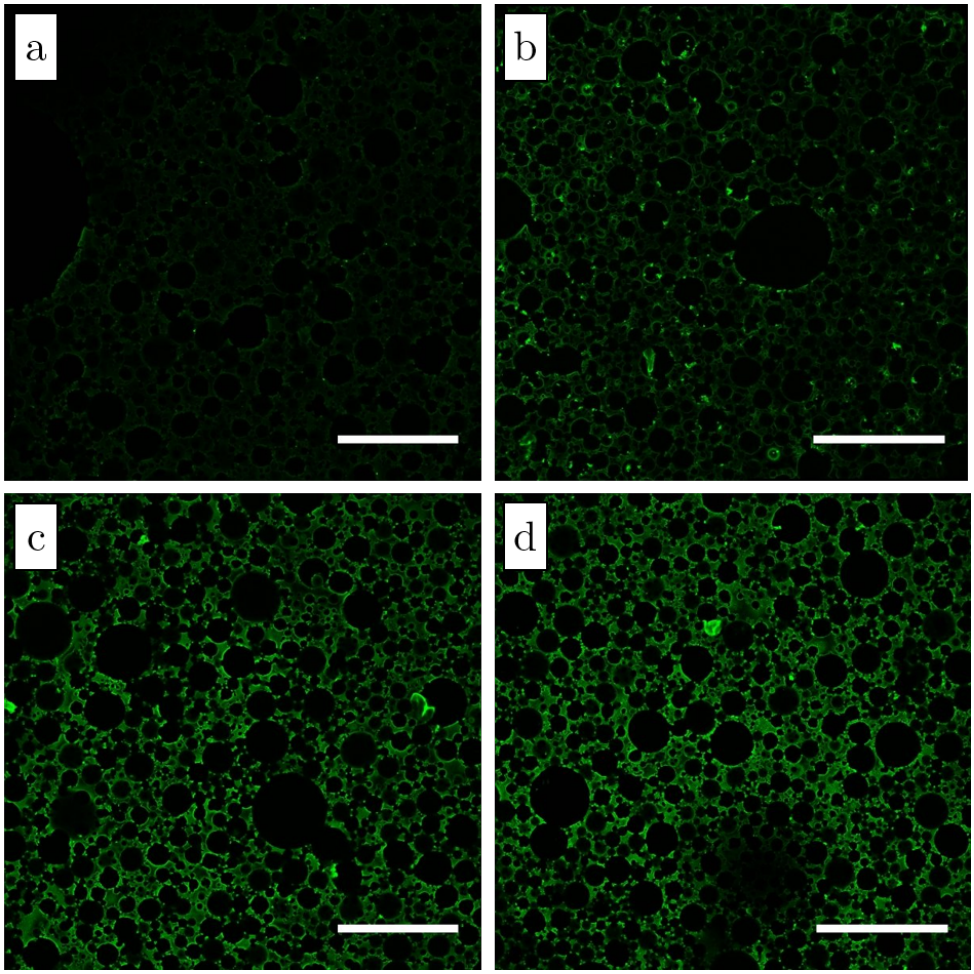

Figure 4.7: *Immunostained scaffold discs showing attachment of Geltrex® coating to the surface of thiol-acrylate polyHIPEs with or without sulfo-SANPAH functionalisation. Geltrex® coating was diluted to 0.125 % or 0.25 % solutions. a) As synthesised thiol-acrylate polyHIPE, 0.125 % b) as synthesised thiol-acrylate polyHIPE, 0.25 % c) sulfo-SANPAH functionalised thiol-acrylate polyHIPE, 0.125 % and d) sulfo-SANPAH functionalised thiol-acrylate polyHIPE, 0.25 %. Stain is anti-laminin, shown in green. Scale bar = 200 μm.*

Cell culture in the sulfo-SANPAH functionalised materials confirmed the increased adhesion of the Geltrex® coating. Figure 4.8 shows the typical cell density in thiol-acrylate materials with sulfo-SANPAH functionalisation and Geltrex® coating after up to 14 days

in culture. It can be seen that when the crosslinker was used to anchor the protein coating, cells could adhere and proliferate rapidly through the scaffold. The cell infiltration was comparable to Geltrex®-coated Alvetex® scaffolds. These results indicated that the underlying thiol-acrylate polyHIPE scaffold had a suitable morphology for cell growth. They also suggest that the as-synthesised material was unable to support cell growth due to a lack of biofunctionality, rather than toxicity or other adverse material properties.

Further analysis of H9 stem cell cultures on sulfo-SANPAH functionalised polyHIPEs with Geltrex® coating showed that cells grown in these scaffolds retained OCT4 expression for up to seven days. As OCT4 expression is a pluripotency marker, this suggested that the H9 cells were able to maintain their stemness. These results are shown in Figure 4.9.

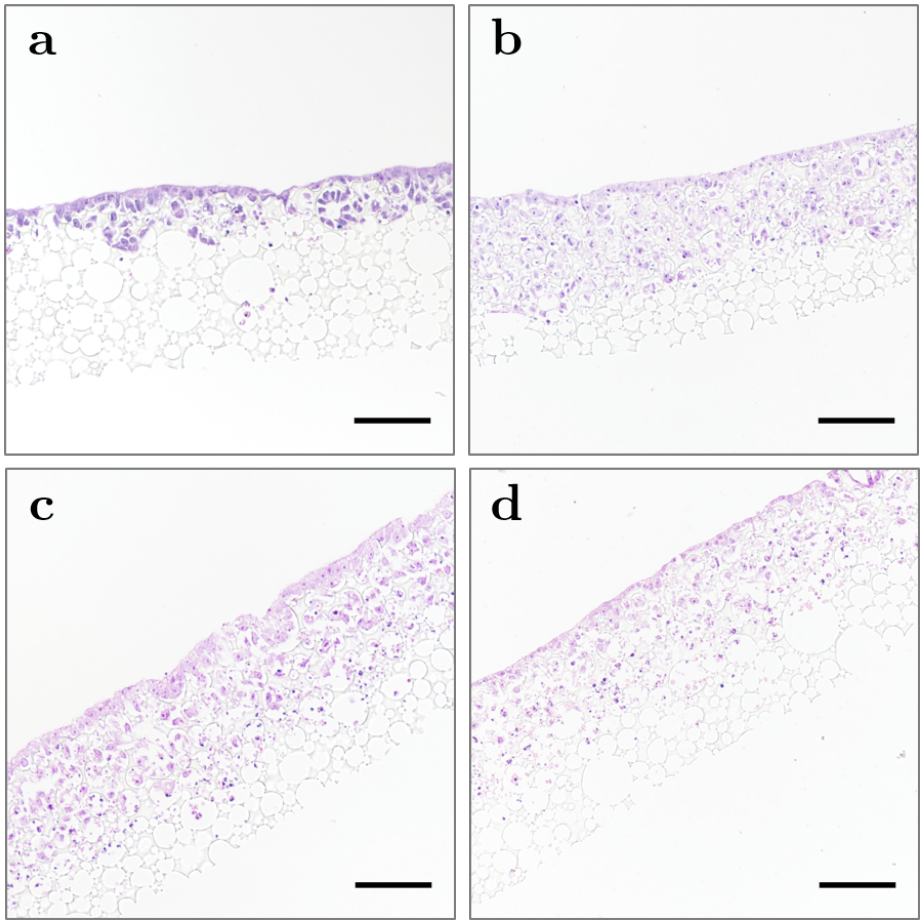

Figure 4.8: *H9 stem cell culture on sulfo-SANPAH functionalised thiol-acrylate polyHIPE scaffolds with Geltrex® coating after a) 3 b) 7 c) 10 and d) 14 days. H&E stain, scale bar = 100 μm.*

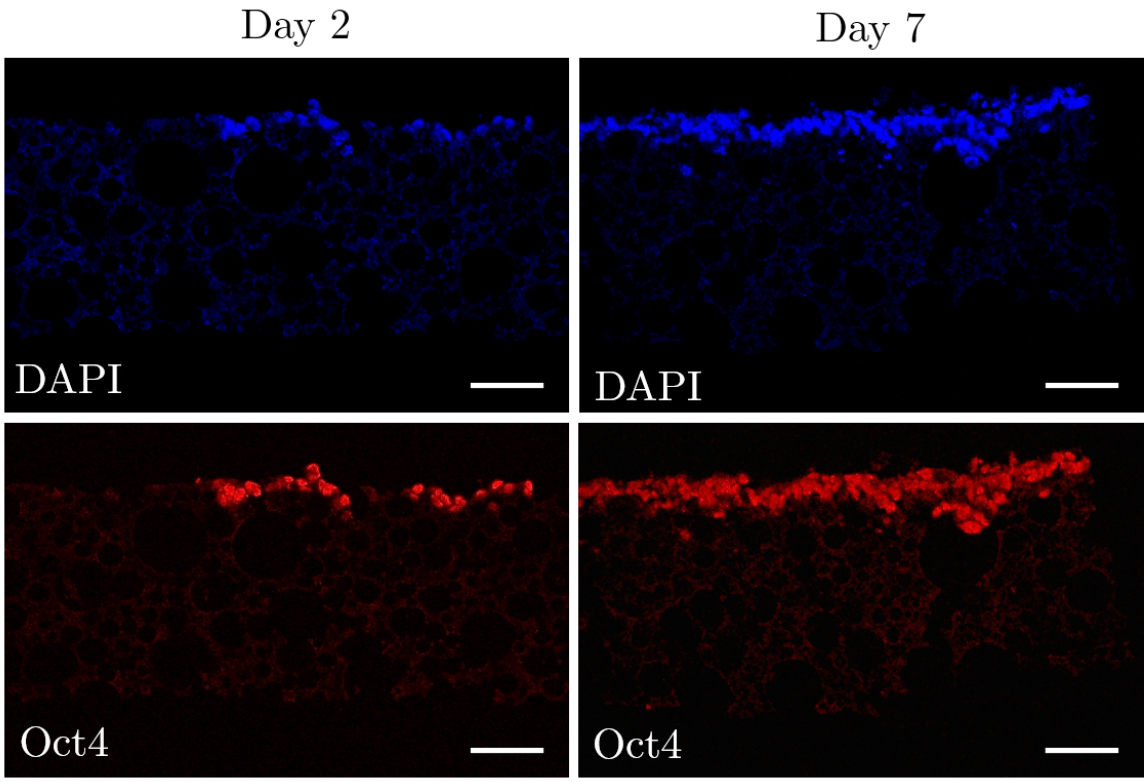

Figure 4.9: *Immunostained sections showing stem cell proliferation after 2 and 7 days in thiol-acrylate scaffolds with sulfo-SANPAH functionalisation and Geltrex® coating. Cell nuclei were stained with DAPI and are shown in blue. Cells expressing Oct4 are shown in red. Scale bar = 100 μm.*

4.3.3.3 Effect of Seeding Density on Cell Proliferation

Initial seeding density affects the viability and fate of stem cells in both 2D [26, 27] and 3D [28, 29] culture formats. More cells should be seeded onto the 3D polyHIPE scaffold than for an equivalent 2D diameter due to increased surface area. However, the cells do not have access to all surface area immediately and they must infiltrate the material *via* interconnects between the voids. The appropriate cell seeding density can not be calculated by seeding at the same cells/cm^2 used for 2D culture. Therefore, attachment and infiltration of cells at different densities was investigated to inform future protocols. The recommended cell seeding density for Alvetex® polystyrene polyHIPE scaffolds in a 12 well plate is 0.25 - 1 $\times$ 10^6 per scaffold [30]. H9 stem cells are small and contact

dependent, so concentrations of 0.5 - 2 $\times$ 10^6 cells per scaffold were trialled.

As shown in Figure 4.10, 0.5 million cells resulted in very low cell numbers in the Geltrex®-coated thiol-acrylate polyHIPE scaffolds. This was likely due to low attachment efficiency, as the same seeding density produces good cell proliferation in Alvetex®. Increasing the seeded cells to 1 million per scaffold appeared to allow enough attachment to achieve a consistent culture across the thiol-acrylate scaffold. Increasing to 1.5 or 2 million cells had minimal effect on final cell density on thiol-acrylate scaffolds. A seeding density of 2 million cells/scaffold appeared to result in reduced cell density at day 7 on Alvetex® scaffolds. Seeding 1 million cells gave good attachment, and there appeared to be no advantage to adding more cells. Therefore, 1 million cells per scaffold were seeded for subsequent experiments.

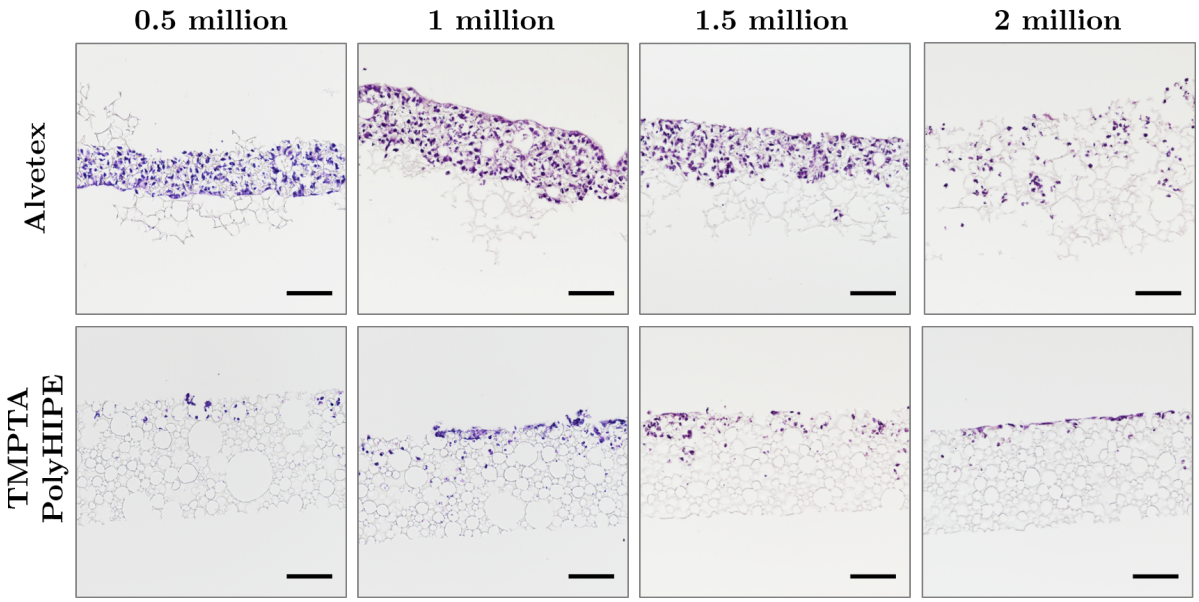

Figure 4.10: *H9 stem cell proliferation after 7 days in Geltrex®-coated Alvetex® or Geltrex®-coated thiol-acrylate polyHIPE scaffolds seeded with 0.5, 1, 1.5 or 2 million cells. H&E stain, scale bar = 100 μm.*

4.3.3.4 Effect of Attachment Time on Stem Cell Proliferation

H9 stem cells were seeded onto functionalised thiol-acrylate polyHIPE scaffolds in a concentrated droplet and allowed to attach for 1 hour before further media was added.

This concentrated method has been shown to result in the highest overall cell density in Alvetex® polyHIPE scaffolds. However, due to variability in final cell numbers found in thiol-acrylate polyHIPEs, it was hypothesised that cells required a longer period to attach to the thiol-acrylate material before media was added or they may risk being washed off the scaffold. Cells were seeded onto sulfo-SANPAH functionalised scaffolds with Geltrex® coatings. Cultures were incubated for 1 or 3 hours before cell metabolism was analysed by PrestoBlue® assay. Figure 4.11a shows cell metabolism as measured by metabolic assay. One hour of attachment time results in the highest average measured metabolism. However, the difference between average metabolism at 1 hour and 3 hours was not found to be statistically significant by 1-way ANOVA analysis. As no significant difference was found between the two incubation times, 1 hour was utilised for further studies for the sake of efficiency.

This result is not entirely unexpected, as H9 stem cells are prone to apoptosis after dissociation and need to be handled carefully. The increased attachment time may have resulted in the small drop of media drying out, further stressing cells and negating any increase in cell number that may have adhered given time. It is however important to investigate attachment time when optimising protocols on 3D porous polymer scaffolds as attachment time varies by cell line.

Stem cells allowed to attach for one or three hours were cultured in polyHIPE scaffolds for seven days. Micrographs of H&E stained sections from these cultures are shown in Figure 4.11 b&c. The number of cells does not vary greatly between conditions. The difference in measured cell metabolism may therefore be due to the health of the cells attached, rather than the number of cells. Alternatively, if fewer cells attach under one condition, other factors in culture may lead to a difference in proliferation rate that results in similar cell numbers at seven days.

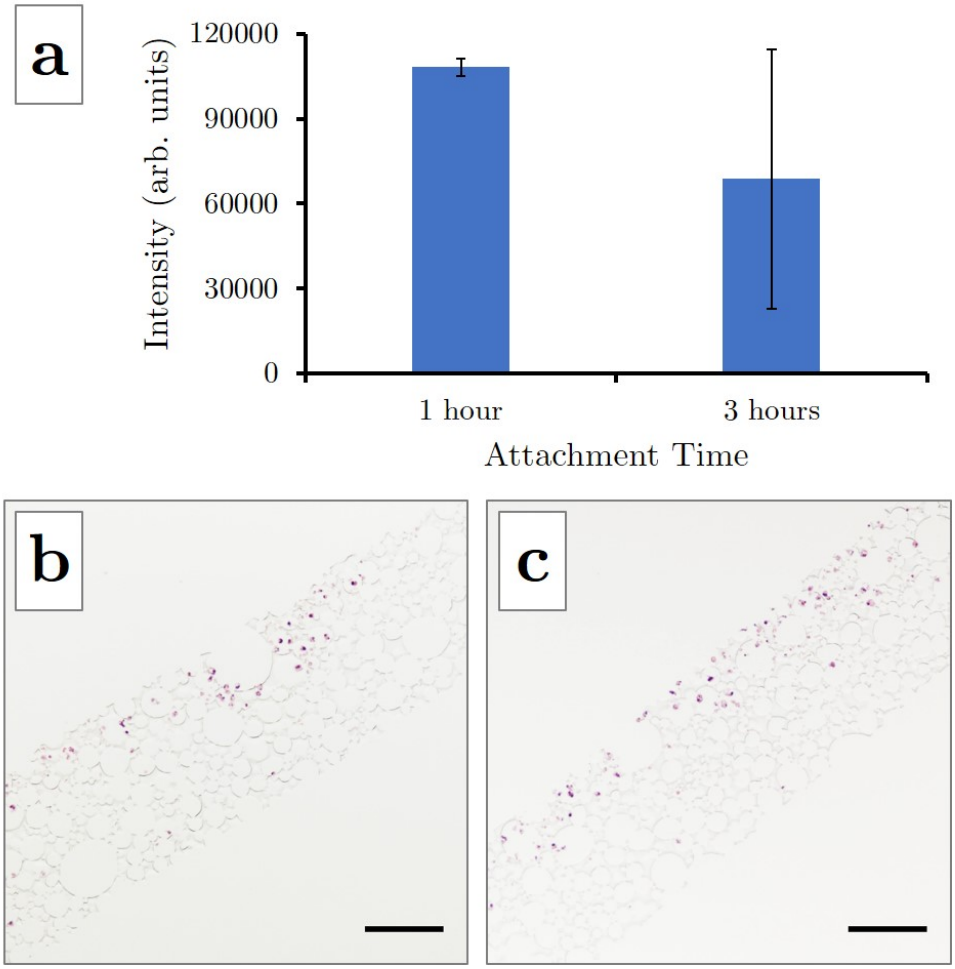

Figure 4.11: *Effect of seeding time on H9 stem in thiol-acrylate scaffolds with sulfo-SANPAH functionalisation and Geltrex® coatings. 1 million cells were seeded per scaffold. a) Metabolic activity of cells after 1 or 3 hour(s) of post-seeding attachment time, as measured by PrestoBlue® assay. Error bars show standard deviation b) H&E stained sections of cells cultured for 7 days after after 1 hour attachment time and c) 3 hours attachment time. Scale bars = 100 μm*

4.3.3.5 Effect of Seeded Cell Format on Cell Proliferation

H9 pluripotent stem cells are attachment dependent. Poor viability after single-cell dissociation is observed in 2D culture of stem cells. This is noted both within our laboratory and in the literature [31]. Dissociating into single cells may increase the chance of karyotypic abnormality and reduce cell viability [29, 32, 33]. Therefore H9 stem cells were typically passaged in small clumps. Clumped cell passaging was achieved by using EDTA as a non-enzymatic dissociation agent. EDTA is a chelator of divalent ions. It causes cell dissociation by sequestering Ca^{2+} ions and disrupting cell adhesion.

Despite their preference for attachment, stem cell cultures must be routinely dissociated to single cells for analyses such as cell counting and fluorescence activated cell sorting (FACS). Single cell seeding is desirable for culture in 3D polyHIPE scaffolds as the ability to seed a precise, counted cell aliquot would reduce variability in seeding and ideally make future experimental results clearer. In addition, single cells may be better able to rapidly penetrate the porous structure of the polyHIPE scaffold, as they do not have existing attachments.

Accutase® is a commercially available solution of proteolytic enzymes that can be used to dissociate H9 stem cells to a single cell suspension. It is used for the dissociation of stem cells in place of trypsin as it is considered less toxic to sensitive cells. Accutase® enzymes are marine-derived, and the solution does not contain mammalian- or bacterially-derived components [34]. This reduces contamination risk.

Figure 4.12 shows growth of H9 stem cells dissociated using Accutase® and seeded as a single cell suspension. It can be seen that single cells attach and survive effectively on Geltrex®-coated surfaces. The change in seeding format did not have a substantial effect on cell adhesion onto thiol-acrylate polyHIPEs. This indicates that a single cell seeding method could be used in future experiments, allowing a specific number of cells to be added to the scaffold.

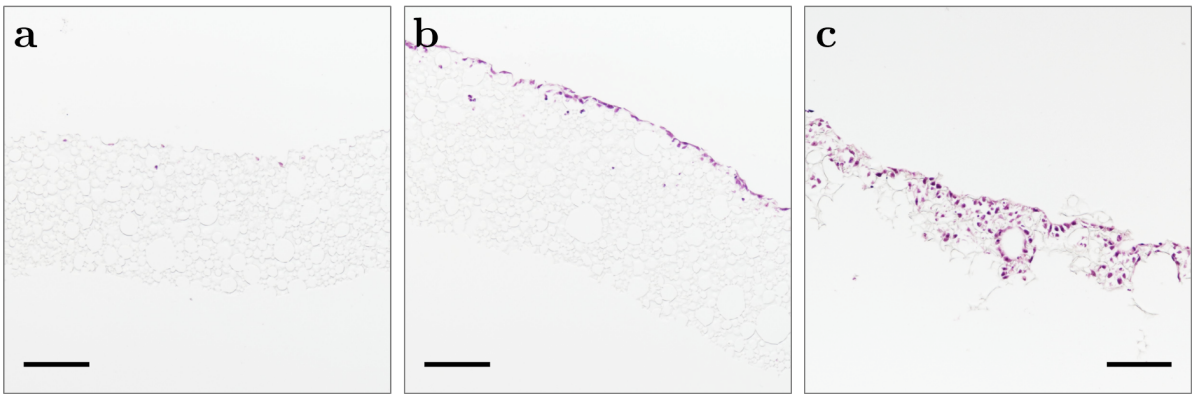

Figure 4.12: *Infiltration of H9 stem cells seeded as single cells onto a) as-synthesised thiol-acrylate polyHIPE b) thiol-acrylate polyHIPE with Geltrex® coating c) Alvetex® with Geltrex® coating. Scale bar = 100μm.*

4.3.4 Cyclic-RGDfK-Maleimide Functionalised Thiol-Acrylate PolyHIPEs as Defined Cell Scaffolds

Cyclic-RGDfK-maleimide (cRGD-mal) was attached to thiol-acrylate polyHIPE scaffolds using the Michael addition protocol optimised in Chapter 3. Figure 4.13 shows this functionalisation diagramatically.

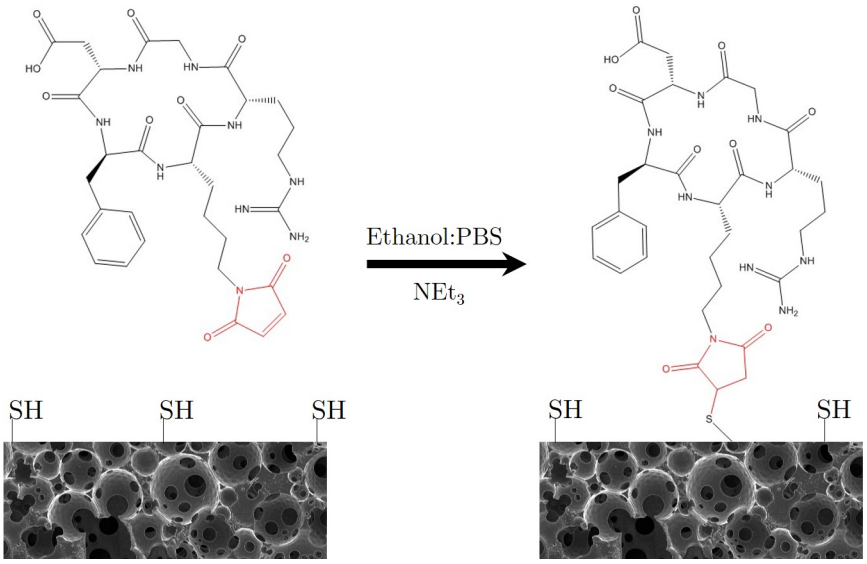

Figure 4.13: *Attachment of cyclic-RGD-maleimide to residual thiol groups on thiol-acrylate polyHIPE scaffolds.*

4.3.4.1 H9 Stem Cell Culture on Thiol-Acrylate Scaffolds with Varied cRGD Functionalisation

The concentration of cRGD-mal added to the scaffold was based on a reported minimum linear RGD peptide density of 10 fmol/cm^2 [10]. Cyclic-RGD promotes cell adhesion more effectively than its linear counterpart, so this minimum was considered suitable to apply to the cRGD functionalisation in this chapter. The surface area of the polyHIPE scaffolds was determined using gas adsorption and BET theory. The minimum linear RGD density equated 2.73×10^{-6} mg per scaffold disk (0.34 μg/mg). Functionalisation reactions were conducted with 1×, 1,000× and 100,000× this minimum density added to the reaction solutions.

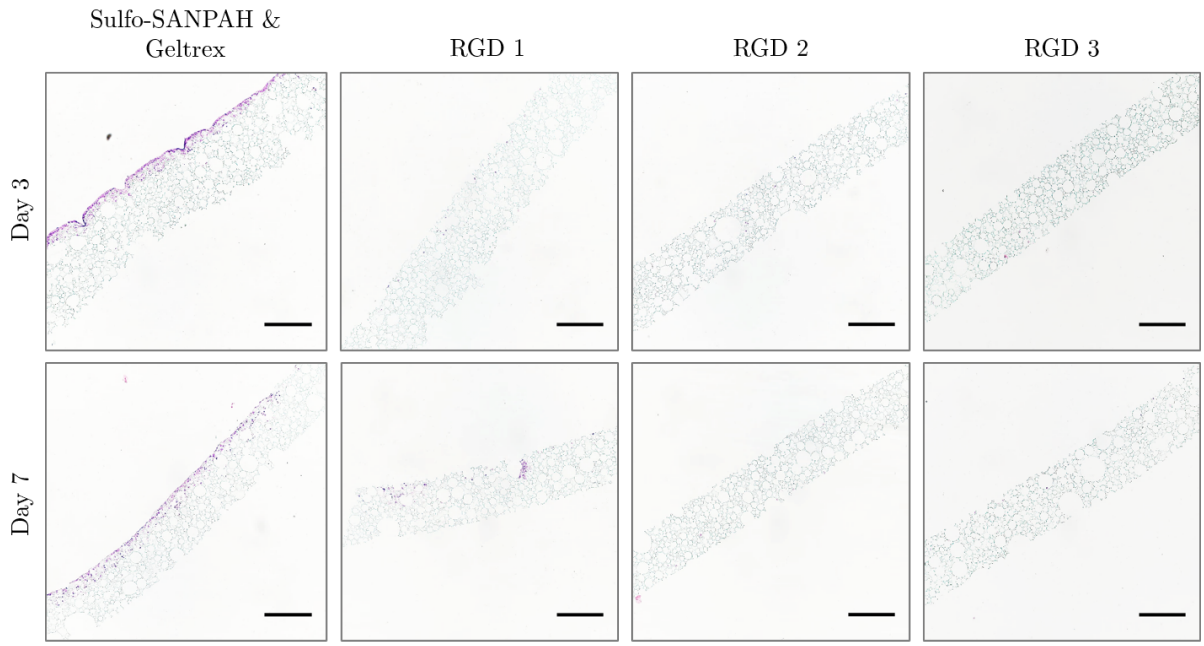

Figure 4.14: *H9 embryonic stem cells cultured on thiol-acrylate polyHIPEs functionalised with varying amounts of cRGD. Cyclic-RGD-maleimide concentrations used were 0.34 µg/mg (RGD1), 0.34 mg/mg (RGD2), and 34.0 mg/mg (RGD3). Stain H&E, scale bar = 200µm*

Figure 4.14 shows very low cell numbers on cRGD functionalised materials. This makes it difficult to assess the relative performance of different cRGD functionalisation concentrations. Possible reasons for this include:

- Failure of cRGD-maleimide to attach to residual thiol groups
- Errors during seeding or staining, resulting in lost cells
- Other culture conditions leading poor attachment or proliferation
- Cyclic-RGD is unsuitable for culture of H9 stem cells on this material

XPS analysis shown in Figure 3.14 in Chapter 3 confirmed that the optimised Michael results in cRGD functionalised scaffolds. Therefore it is unlikely that scaffolds functionalised using the same reaction conditions did not have cRGD on the surface.

As mentioned previously, incomplete mixing of cell suspensions may alter the number of cells seeded onto the scaffold. However, cell suspensions were agitated regularly during culture setup. Overly aggressive handling during the fixation or staining process may remove surface cells, lowering overall cell count. Care was taken to add all reagents carefully down the side of supporting frames so as not to disturb the culture surface, so should not have dislodged cells. The H&E staining process was automated, so conditions would not have varied from those used to successfully visualise cells in other samples such as those shown in Figure 4.12. Other culture conditions were kept consistent and so should not have resulted in low stem cell numbers in cRGD-functionalised scaffolds.

Cyclic-RGD has previously been used to support the H9 embryonic stem cell line under defined conditions, and is therefore considered suitable for this application. However, the shift to a 3D format, change in surface chemistry, and altered mechanical properties may also affect stem cell adhesion and proliferation. Further investigation was therefore required to confirm the effect of cRGD on pluripotent stem cells in thiol-acrylate 3D scaffolds.

4.3.4.2 Effect of Attachment Time on Stem Cell Proliferation

Cell attachment time was also assessed in cRGD-mal functionalised scaffolds. The trend was similar to sulfo-SANPAH functionalised, Geltrex®-coated scaffolds. These results are shown in Figure 4.15. Interestingly, the cell proliferation on the cRGD-functionalised scaffolds shown in figure 4.15 b&c is greater than that on the equivalent 34.0 mg/mg scaffolds shown in Figure 4.14. This indicates that cells can adhere to the peptide-functionalised thiol-acrylate polyHIPEs.

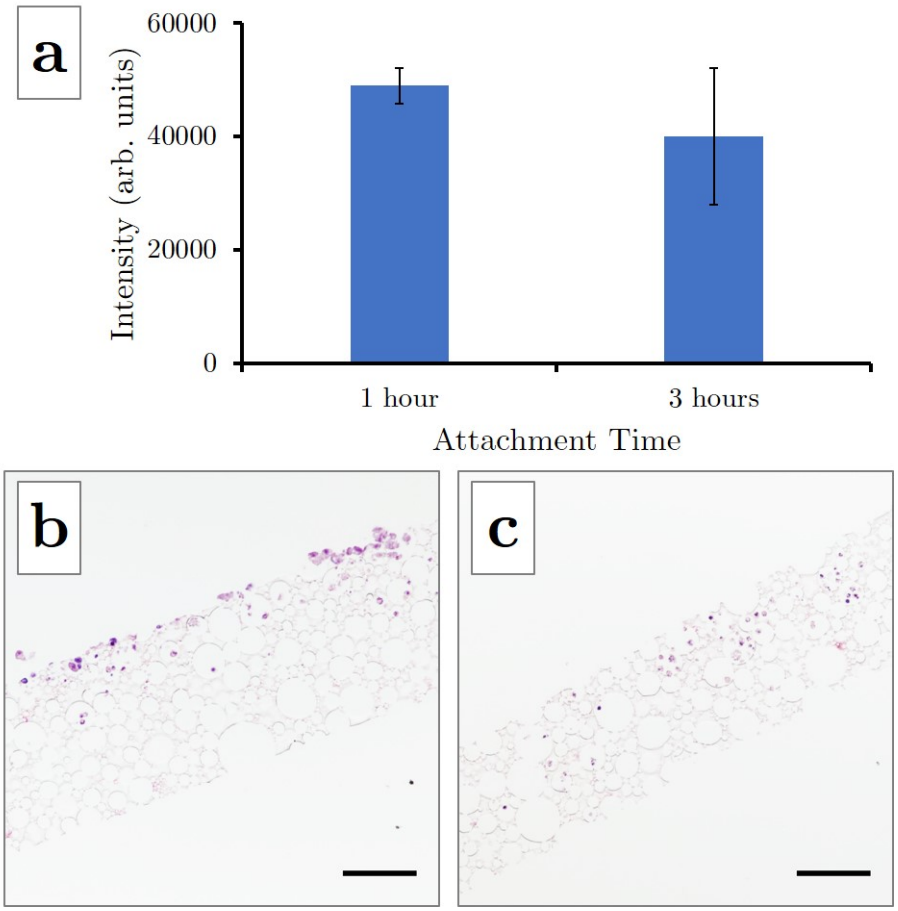

Figure 4.15: *a) Metabolic activity of cells after 1 or 3 hour(s) of post-seeding attachment time, as measured by PrestoBlue® assay. Scaffolds were functionalised with 34.0 mg/mg cRGD-maleimide. 1 million cells were seeded per scaffold. Error bars show standard deviation b) H&E stained H9 stem cells cultured for 7 days in thiol-acrylate scaffolds with cRGD-maleimide functionalisation after 1 hour attachment time and c) 3 hours attachment time. Scale bars = 100 μm*

4.3.5 Scaffold Coating Affects Cell Adhesion Proliferation & Pluripotency

A wide variety of chemistries have been used to synthesise polyHIPE scaffolds for cell culture applications. They may be used to support 3D cell culture in their as-synthesised state, or require further functionalisation or coating to adapt them to specific lines. Polymer materials that do not have added biofunctionality may still support cell adhesion through adsorbed serum proteins and other mechanisms. As-synthesised polyHIPE scaffolds have been used to culture a wide range of cells including human keratinocytes (HaCaT) [13], mouse fibroblasts (L929) [14], osteoblastic cells (MG63) [35], hepatocytic cells (HepG2) [36] and human mesenchymal stem cells (hMSC) [37]. These cultures all used serum containing media, meaning that they were feeder free, but neither xeno-free nor chemically defined.

Chemically defined xeno-free culture media, such as the E8 medium used in this project, do not contain serum [38]. Serum is a mixture of proteins and other nutrients typically of bovine origin and is used routinely in cell culture. Fetal bovine serum (FBS) contains a mixture of cell supporting molecules including growth factors, amino acids, sugars, lipids, and hormones [39]. Components of this serum mixture can adsorb onto the surface of materials that otherwise lack bioactivity, allowing cell adhesion and proliferation. When no serum is used, cells must rely on the specific functionality provided by the substrate. This can be an advantage in fundamental investigations as cell interactions and behaviours are due to specifically supplied chemistries, rather than an undefined and uncontrolled surface fouling effect.

A thiol-acrylate polyHIPE scaffold synthesised from TMPTMP and dipentaerythritol penta/hexa-acrylate (DPEHA) supported keratinocytic (HaCaT) cell culture for 11 days without further functionalisation [13]. As this material has similar chemistry to the TMPTMP/TMPTA thiol-acrylate scaffold presented in this thesis, it might be expected that human pluripotent stem cells would also adhere to the 3D thiol-acrylate scaffold.

However, this chapter has shown that this is not the case. This result may be due to the combined effects of using chemically defined media, and cell line choice.

Polystyrene polyHIPEs can also support some cell lines as-synthesised, while other lines require the surface to be modified. Poly-L-lysine and laminin were added to polystyrene polyHIPE scaffolds to support neural cell cultures [16]. Laminin is also added to polyethylene glycol diacrylate (PEGDA)-based polyHIPE scaffolds to allow culture of sensitive neural precursor cells [3]. Surface functionalisation with galactose allowed improved hepatocyte adhesion to polystyrene scaffolds [40]. Human pluripotent stem cells are known to be technically difficult to culture due to their sensitivity to stress and the instability of the pluripotent state [41]. In addition, they require culture conditions which not only support proliferation and adhesion, but which also control cell fate. Therefore maintaining pluripotent stem cells typically requires functionalisation or coating of the underlying substrate unless that substrate has inherent bioactivity.

The thiol-acrylate polyHIPE scaffolds presented in this chapter do not inherently promote human embryonic stem cell adhesion, and must be coated or functionalised to allow 3D stem cell culture. It was hypothesised that adding the Geltrex® coating used in routine 2D culture to the scaffold would allow embryonic stem cell attachment. This hypothesis was correct, however applying the Geltrex® layer to thiol-acrylate scaffolds was not as simple as for the commercially available Alvetex®. It was determined that Geltrex® did not effectively coat as-synthesised thiol-acrylate polyHIPE scaffolds. The fact that the Geltrex® coating does not adhere suggests that proteins do not adsorb efficiently to the thiol-acrylate materials. This leads to a lack of attachment on as-synthesised thiol-acrylate scaffolds. However, low protein adhesion would result in low surface fouling, reducing the confounding effects of adsorbed components when investigating specific surface functionalisation.

Covalently attaching Geltrex® *via* a sulfo-SANPAH crosslinker allowed the cells to adhere and proliferate throughout the material. This suggests that the coating did not obstruct interconnects between voids and interfere with cell migration. It also indicates that the

material structure is suitable for cell culture.

The Geltrex® coating contains a lot-variable, undefined mixture of proteins derived from a mouse sarcoma. To overcome the problems associated with such coatings, functionalisation methods developed in Chapter 3 were used to attach a cRGD peptide to the scaffold. The attachment was confirmed *via* XPS in Chapter 3. Against expectations, low cell attachment was found on all cRGD concentrations used. No specific cause for this outcome was identified. Cyclic-RGD has previously been found to be effective in promoting cell adhesion. Further cultures were therefore conducted on the highest concentration (34 mg/mg) cRGD-functionalised scaffold, which resulted in some cell attachment after 7 days. This scaffold was therefore selected for optimisation.

4.3.6 Optimising Scaffold Morphology for Increased Stem Cell Infiltration

4.3.6.1 Preparation & Characterisation of Scaffolds with Increased Void & Interconnect Diameters

Stem cell adhesion and proliferation in 3D scaffolds could be promoted by functionalisation and coating of the thiol-acrylate polyHIPE. However, cell cultures did not populate the entire scaffold. The structure of the scaffold was modified with the aim of promoting better stem cell infiltration. The void and interconnect diameters of polyHIPE materials can be modified by changing shear rate, temperature, monomers, surfactant and other additives [42, 43]. These factors affect the droplet diameter of the HIPE template, which in turn controls void and interconnect diameter. Figure 4.16 a-c shows typical morphology of 80 % porous thiol-acrylate polyHIPEs resulting from emulsions produced at different shear rates. As human embryonic cells did not populate the entire scaffold produced at 350 rpm, the stir speed was lowered. This increases the size of water droplets in the HIPE, and thus the diameter of voids in the material. The void diameter distribution of

the scaffolds was calculated by analysing SEM images of these materials, and is shown in Figure 4.17a.

Mercury intrusion porosimetry was used to characterise the porosity of the materials. This method has the added advantage of giving a measure of interconnect diameter, which is not easily determined *via* SEM. It was hypothesised that larger interconnects would allow cells to move through the scaffold more easily, resulting in a 3D culture that uses all available scaffold area. Figure 4.17b gives the mercury intrusion plot for thiol-acrylate polyHIPEs synthesised at 300 rpm. Table 4.1 shows the void and interconnect diameters for each material.

Table 4.1: *Void and interconnect diameters of polyHIPEs synthesised using different stir speeds.*

Stir Speed (rpm)	250	300	350
Void Diameter (μm)	62.1 ± 58	51.3 ± 33	38.8 ± 22
Interconnect Diameter (μm)	N/A[1]	15.3	7.98

The nominal porosity was also increased to 90 % in an attempt to produce a more open polyHIPE structure. Figure 4.16d shows the morphology of 90 % porous thiol-acrylate polyHIPE scaffolds. It had the same interconnected void structure as scaffolds with 80 % nominal porosity. Void diameter measurements are shown in Figure 4.17a, and the differential intrusion plot in Figure 4.17c. The average void diameter of 90 % porous scaffolds was 39.5 ± 20 μm, which was smaller than the 51.3 ± 33 μm found in 80 % porous materials produced at 300 rpm. The interconnect diameter was similar at 13.6 μm for 90 % porous materials, and 15.3μm for 300 rpm 80 % porous. The porosity of polyHIPEs with 90 % aqueous phase content was confirmed to be 88.7 % using mercury intrusion porosimitry. It appeared that the stirrer speed had a greater influence on void and interconnect diameters than the nominal porosity.

[1]Intrusion porosimetry was not conducted on materials synthesised at 250 rpm.

Figure 4.16d shows the macro structure of thiol-acrylate polyHIPEs produced at 250 rpm. The voids in this material were often very large, making it unsuitable as a cell culture scaffold. The 80 % porous material produced at 300 rpm was selected as the appropriate stem cell scaffolds it had increased void diameter without these large holes.

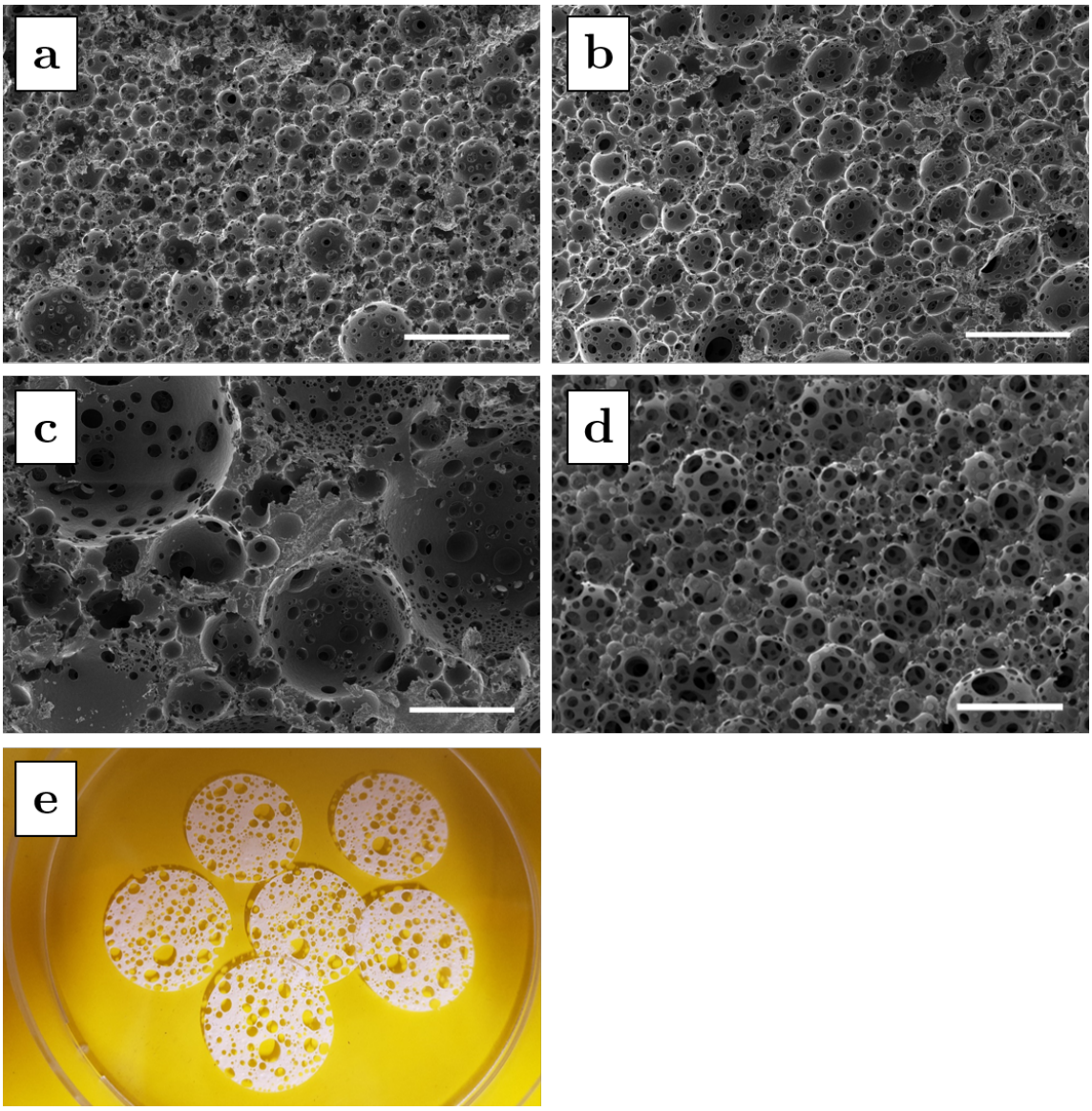

Figure 4.16: *SEM micrographs showing the morphology of 80 % porous thiol-acrylate polyHIPEs produced at a) 350 rpm b) 300 rpm c) and 250 rpm and d) 90 % porous polyHIPE produced at 350 rpm. Scale bars = 100 μm e) Shows the macro structure of the 250 rpm polyHIPE.*

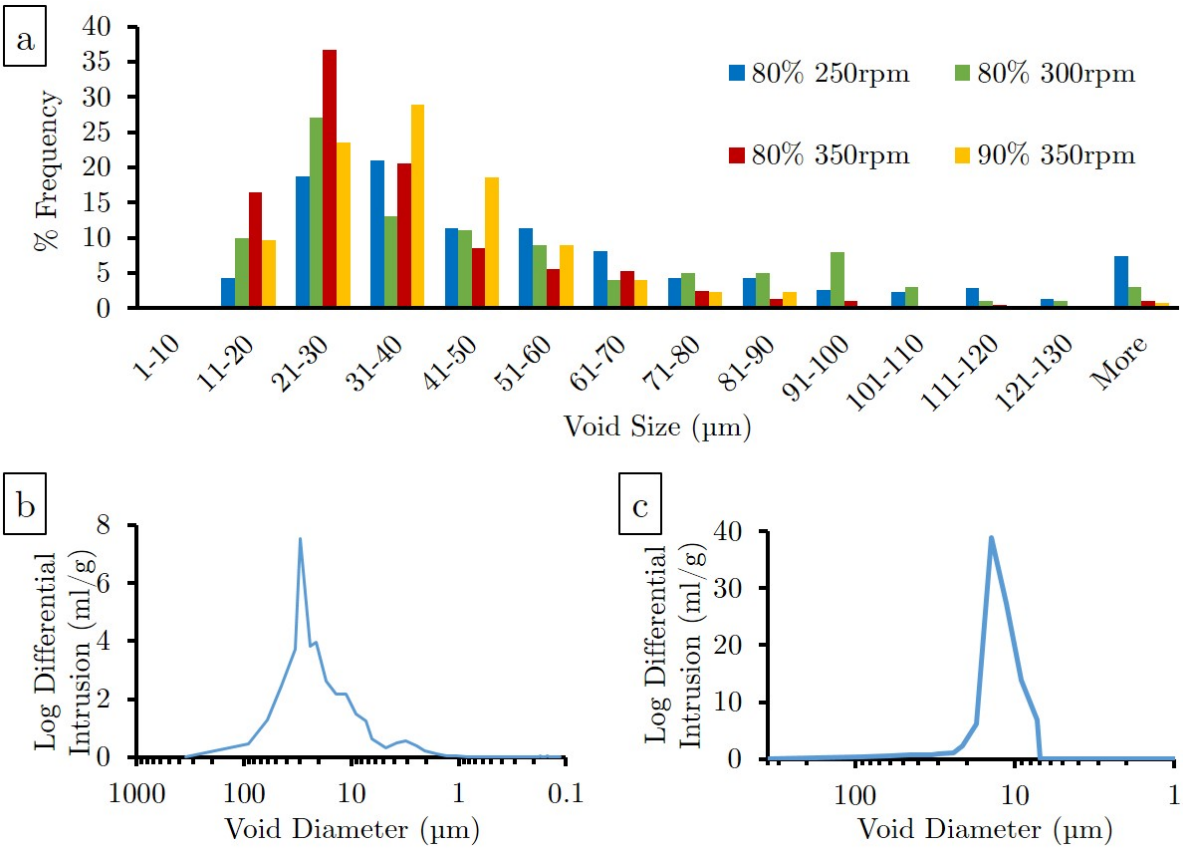

Figure 4.17: *a) Distribution of void diameters in polyHIPE scaffolds produced with stirrer speeds of 250, 300, and 350 rpm. Nominal porosity was 80 or 90 %. b) Log differential intrusion plot of thiol-acrylate polyHIPE with 80 % nominal porosity, produced with a stir speed of 300 rpm. c) Log differential intrusion plot for a 90 % porous polyHIPE material produced at 350 rpm, as analysed by mercury porosimetry.*

4.3.6.2 Stem Cell Infiltration in Materials with Increased Void & Interconnect Diameters

PolyHIPE scaffolds produced with a stir speed of 300 rpm were compared to the previous 350 rpm material to determine the effect of increased void and interconnect diameter on embryonic stem cell infiltration. Figure 4.19 shows the infiltration of H9 stem cells in scaffolds synthesised at 350 rpm and 300 rpm over 14 days. Figure 4.18 shows typical cell proliferation from the same experiment after 14 days at higher magnification. After 3 or 7 days in culture, cells proliferate through all the scaffolds at similar rates. However, it appears that cells typically reach their maximum distance through the 350 rpm material after 7 days, both with Geltrex® coating and with cRGD functionalisation. The larger void and interconnect diameters of the 300 rpm material appear to allow increased migration, and by day 14 the cells populate the entire scaffold.

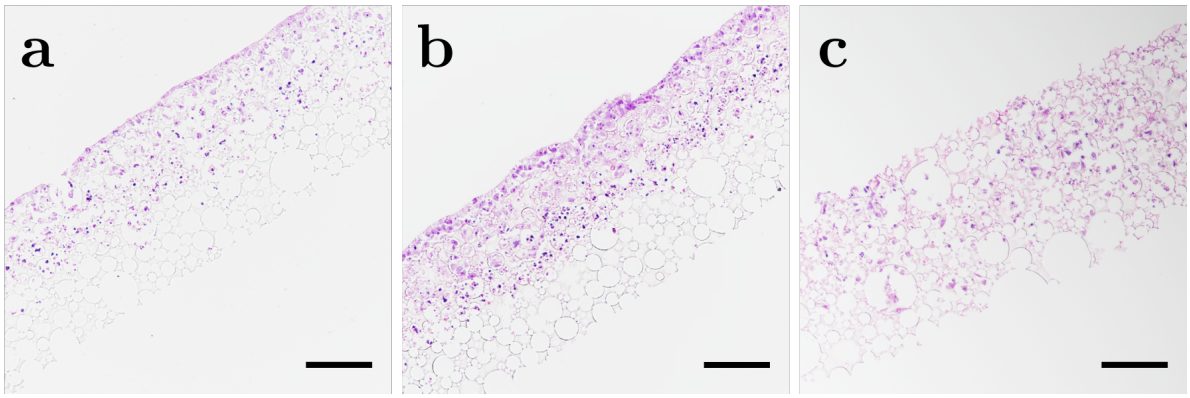

Figure 4.18: *H9 stem cells cultured for 14 days in thiol-acrylate polyHIPE produced at 350 rpm with a) sulfo-SANPAH functionalisation & Geltrex® coating or b) cRGD functionalisation, and on c) polyHIPE produced at 300 rpm with cRGD functionalisation. Stain H&E, scale bars = 100 μm, 20× magnification.*

The average infiltration depth is shown in Figure 4.20. It can be seen that the cell depth is increased in the 300 rpm scaffold. The high standard deviation may be in part due to the analysis method. Infiltration depth was measured on H&E stained images by drawing three equally spaced lines at 90°to the scaffold surface and measuring the depth of the last cell intercepted. This approach is shown schematically in Figure 4.21.

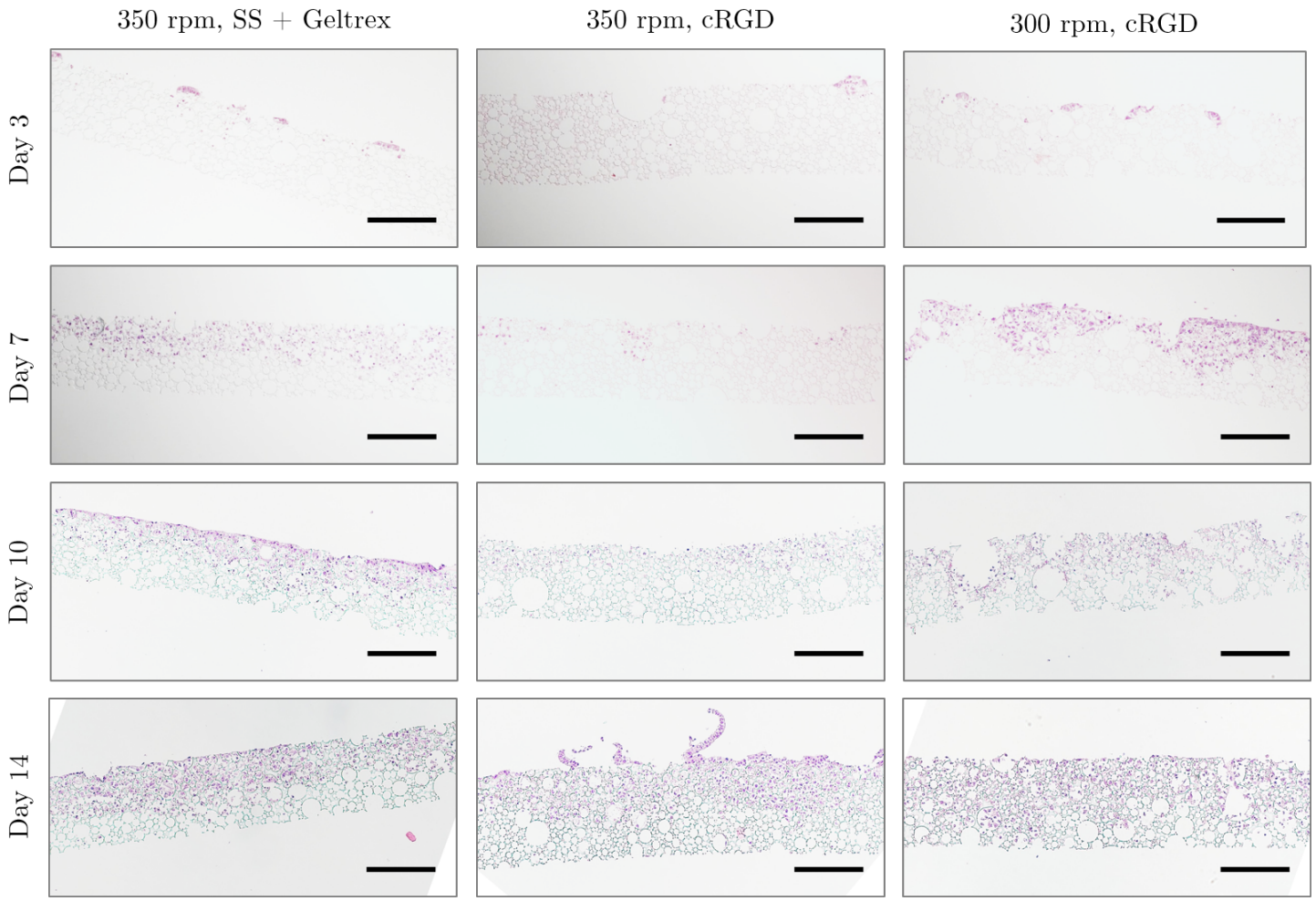

Figure 4.19: *Micrographs of H9 stem cells cultured in thiol-acrylate polyHIPE scaffolds produced at 350 rpm with Sulfo-SANPAH (SS) functionalisation & Geltrex® coating or cRGD functionalisation, and on polyHIPE produced at 300 rpm with cRGD functionalisation. Cultures were imaged at 3,7, 10, and 14 days. Stain H&E, scale bars = 200 μm.*

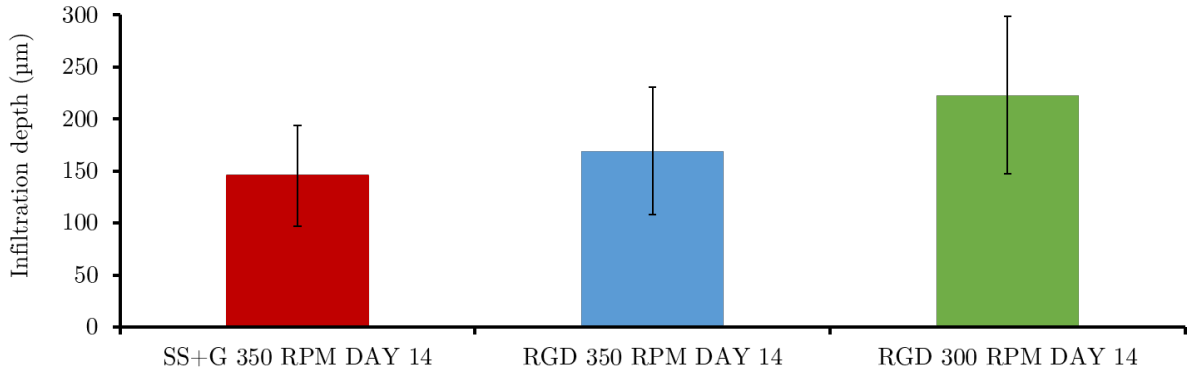

Figure 4.20: *Average H9 stem cell infiltration depth after 14 days culture in different scaffold types. Scaffolds were polyHIPE materials produced at 350 rpm with sulfo-SANPAH functionalisation & Geltrex® coating (SS+G 350) or cRGD functionalisation (RGD350), and polyHIPE produced at 300 rpm with cRGD functionalisation (RGD300).*

This method was designed to give a snapshot of typical cell infiltration depth. It removed human bias by pre-defining the points to be measured on each image. This method assumes a fairly uniform cell front in the material. In samples with low cell density, cells may not be hit by the designated measurement lines, causing the apparent cell infiltration to be null. In cultures with high cell density but highly variable cell infiltration, measuring three points per image, repeated over several images, typically accounted for this. However, abrupt changes in cell infiltration depth, such as those caused by an unusually large void in the material, may not be accurately represented in the cell infiltration measurements. These issues were offset by including representative images, such as those shown in Figures 4.19 and 4.18, and observations of cell distribution to qualitatively show cell behaviour in addition to depth measurements.

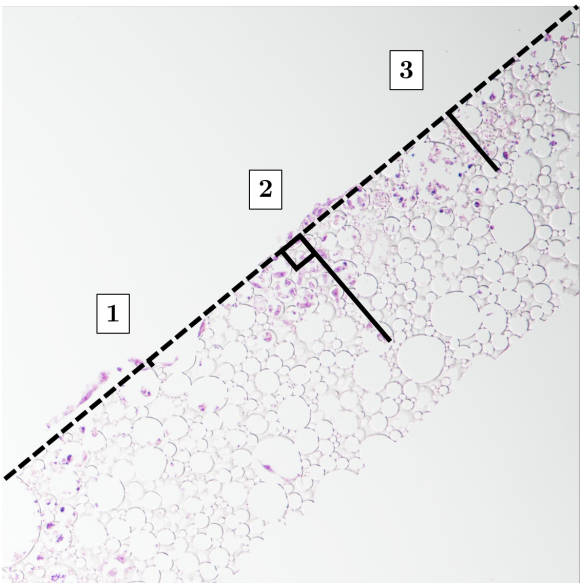

Figure 4.21: *Schematic showing measurement of cell infiltration into scaffolds.*

Another contributor to the spread of cell depths is heterogeneous cell growth. The cells do not populate the entire width of the scaffold at the same rate. As shown in the day 3 images in Figure 4.19, cells do not adhere in an even layer across the scaffold after initial seeding. Sporadic larger voids also accelerate migration at certain points.

Figure 4.22 shows the Oct4 expression in embryonic stem cells cultured in the two scaffolds with different void diameters. Cells in scaffolds produced at 350 rpm typically lost Oct4 expression towards the middle of the scaffold, which usually coincided with the cell front. Thus while cells were able to migrate to the centre of these scaffolds, those that made it that far appear to start differentiating. Cultures in the 300 rpm material had a more even distribution of Oct4 positive cells. Cells in these cultures also had lowered expression by day 14, but this loss did not appear to be correlated with location in the scaffold.

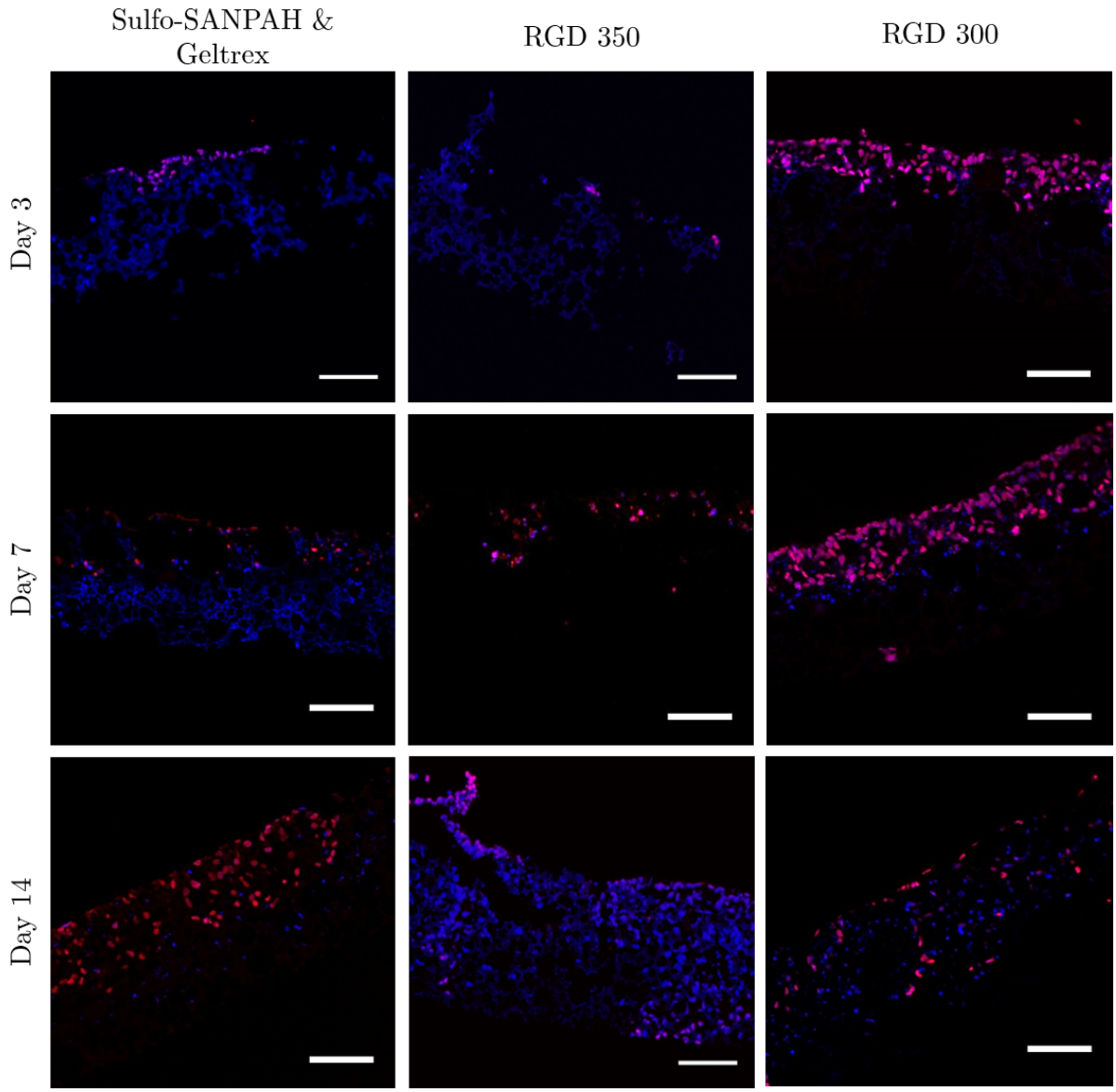

Figure 4.22: *Immunostained H9 stem cells cultured in polyHIPE scaffolds produced at different stir speeds. The three scaffold conditions were 350 rpm with sulfo-SANPAH functionalisation and Geltrex® coating (SS+G 350), 350 rpm with cRGD functionalisation (RGD350), and 300 rpm with cRGD functionalisation (RGD300). Cultures were analysed at day 3,7, and 14. Red indicates Oct4+ cells, DAPI highlights cell nuclei in blue. Scale bar = 100 μm.*

Figure 4.23 shows the relative Oct4 expression of cells cultured in 3D scaffolds for up to 14 days. If the results were to mirror typical 2D trends, then Oct4 expression would be expected to decrease over time. However, Oct4 expression appeared low in the early samples. This result may be due to low cell numbers and high autofluorescence in these samples, which made quantification difficult and may have amplified the effect of potential counting errors.

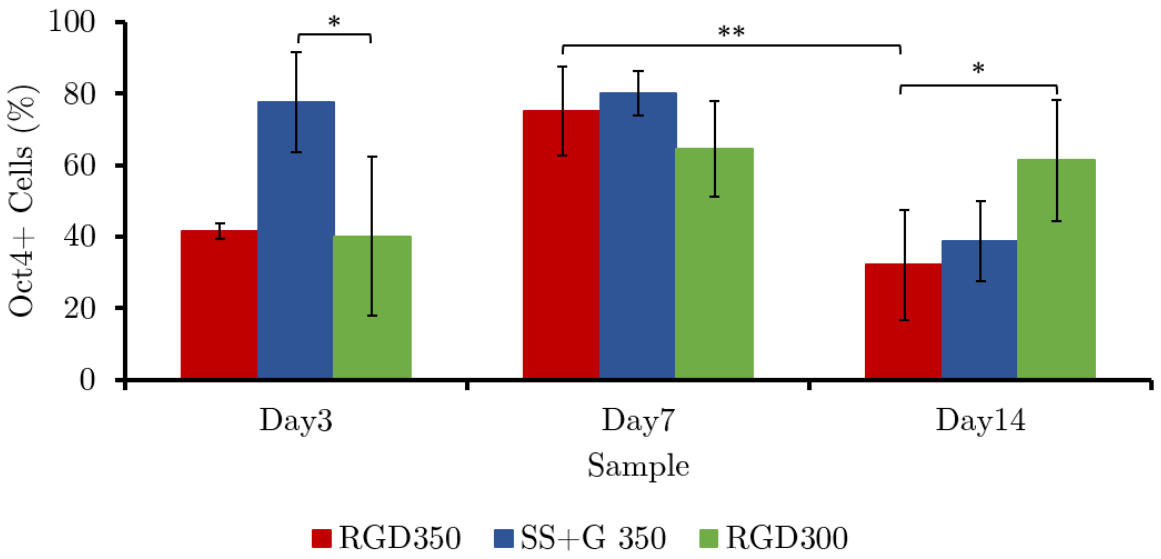

Figure 4.23: *Quantification of relative Oct4 expression of H9 stem cells via image analysis. The number of Oct4+ cells (stained pink) is expressed as a percentage of the total cell count as determined by DAPI (blue) staining. The three scaffold conditions were 350 rpm with sulfo-SANPAH functionalisation and Geltrex® coating (SS+G 350), 350 rpm with cRGD functionalisation (RGD350), and 300 rpm with cRGD functionalisation (RGD300). Cultures were analysed at days 3, 7, and 14.* $* = p \leq 0.05$, $** = p \leq 0.01$

Expression of pluripotency markers such as Oct4 and Nanog decreases as pluripotent stem cells differentiate. If the stem cell populations in the scaffolds were differentiating, the Oct4 expression in Figure 4.23 would be expected to decrease at each time point. If the cells were remaining in the same pluripotent state, Oct4 expression would remain stable. The increase in Oct4 expression from day 3 to day 7 in the RGD350 and RGD300 samples is therefore unexpected. All conditions show a decrease in Oct4 expression from

day 7 to day 14, and all retain Oct4 expression for the duration of the culture.

Interestingly, while fewer Oct4 positive cells were counted in the RGD300 scaffold after 14 days compared to the two scaffolds produced at 350rpm, RGD300 cultures had the highest fraction of Oct4 positive cells. This result may indicate that a lower cell density is beneficial when working towards a completely pluripotent cell population. The culture in the RGD300 scaffolds has a significantly higher fraction of Oct4 positive cells than those in the RGD350 scaffolds. This suggests that the larger void diameters may be beneficial for maintaining stem cell pluripotency in cRGD functionalised scaffolds. Figures 4.22 and 4.23 together indicate that H9 stem cells were capable of maintaining Oct4 expression for 14 days when cultured in thiol-acrylate polyHIPE scaffolds under defined conditions.

4.3.6.3 Cell Infiltration Depth Reflects Scaffold Void Diameter

Void diameter is a key parameter in 3D scaffolds. PolyHIPEs are highly tunable, and void diameters can be synthesised from 1 μm in diameter to greater than 100 μm [44]. The void and interconnect diameter in polyHIPE scaffolds has been shown to affect cell behaviour in culture. For example, large voids of around 100 μm promoted growth of fibroblast cells due to their cells elongated shape [45].

Human embryonic stem cells are relatively small cells with a diameter of approximately 13 μm and nuclei diameter of 5 μm [46, 47]. In this chapter, H9 embryonic stem cells proliferated on thiol-acrylate polyHIPEs synthesised at 350 rpm (void diameter 38.8 $\pm$ 22, see Table 4.1). However, as shown in Figures 4.18 and 4.21, cells do not populate the full scaffold. This is likely due to the average interconnect diameter, which is 7.98 μm as measured by mercury porosimetry. Cells were able to deform and migrate through these smaller interconnects, but migration is slow and appears to cease at around day 10 in culture. Decreasing the stir speed to 300 rpm creates larger droplets in the template HIPE, and results in a material with a void diameter of 51.3 $\pm$ 33 μm. A key feature of these 300 rpm thiol-acrylate polyHIPEs is that the average interconnect diameter

is increased to 15.3 μm. These materials allowed cells to populate the entire scaffold, likely due to the ease of movement through the scaffold. Larger voids and interconnects may also improve nutrient exchange in the centre of the scaffold. As the thiol-acrylate scaffolds do not degrade significantly over the timescale of cell culture, all routes through the material need to be produced during synthesis. Therefore optimisation of not only void diameter, but also interconnect diameter is crucial.

To provide a 3D environment to cells, voids cannot be too large. Very large voids are sensed as curved 2D substrates, rather than as a true 3D environment. Therefore, the distribution of void diameters should be relatively narrow to ensure all cells in the population are exposed to the appropriate environment. While the average void diameter of materials presented in this chapter has been shown to be suitable for the maintenance of H9 stem cells, the distribution of diameters results in some voids that are larger than ideal. Figure 4.16 shows the void morphology of the polyHIPE scaffolds. Figure 4.17 shows the void diameter distribution of these materials. The void diameter distribution is generally quite narrow, however there are some very large 'outlier' voids particularly in the materials produced at slower stirrer speeds. The effect of very large voids is shown in Figure 4.24. The H9 stem cells that migrated to these oversized voids were arranged in a single-layer structure similar to 2D cells, and may not have achieved the 3D interactions found elsewhere in the scaffold. Such "pseudo-3D" culture conditions can be referred to as 2.5-dimensional (2.5D) culture [48]. While the definition of 2.5D culture is somewhat nebulous [49], it typically involves alteration of the texture, coating, or layout of 2D surfaces to give a more physiologically relevant environment. Culturing cells on top of a thick layer of ECM coating is a typical example [50, 51, 52]. Stacked "sandwich" culture is another [49]. As the curved, functionalised or coated surface found in large voids presents neither a flat nor fully 3D environment to the cells, it can also be considered to fit the 2.5D definition. Cells cultured under 2.5D conditions have been shown to display morphology with features from both 2D and 3D cultures [53].

While these effectively 2D areas did not occur frequently, they may still affect the homo-

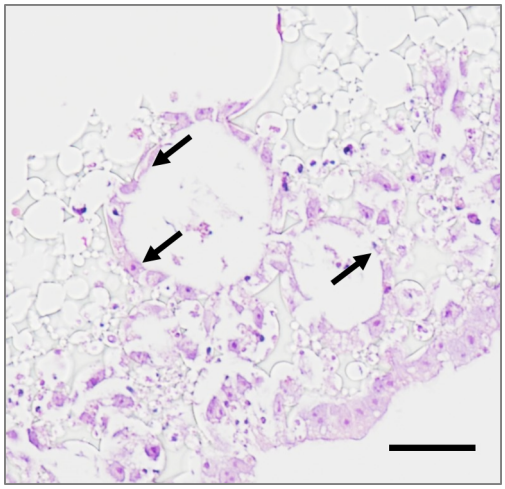

Figure 4.24: *Effective 2D-like or "2.5D" environment in a large void within the 3D polyHIPE scaffold. Arrows indicate cells that appear to be experiencing a curved 2D environment due to large outlier voids. Scale bar = 100 mum.*

geneity of the stem cell culture. Future development might therefore involve calculation of the transition threshold for 3D to 2D behaviours, and tightening of synthesis parameters to maintain 3D cell growth. The distribution of voids in the thiol-acrylate polyHIPEs presented herein could be better controlled *via* several modifications to the synthesis method. For example, a pump could replace the dropping funnel when adding water for a more precise droplet addition rate. Further potential optimisation approaches are discussed in Chapter 6.

4.4 Conclusions

In this chapter, H9 pluripotent stem cell culture on 3D thiol-acrylate polyHIPE scaffolds was investigated. The scaffolds were used in conjunction with the basement membrane coating Geltrex® to support human embryonic stem cell pluripotency for up to 14 days. This coating promoted adhesion and proliferation of H9 stem cells. Culture conditions were also assessed, allowing seeding density, cell format and attachment time to be tailored for the H9 stem cell line on these materials.

The Geltrex® coating is animal derived and un-defined. Functionalisation methods optimised in Chapter 3 allowed the Geltrex® coating to be replaced with cyclic-RGD, an adhesion peptide previously shown to promote stem cell pluripotency in defined 2D conditions. This peptide functionalisation successfully supported pluripotent stem cells in defined media.

However, stem cells were unable to populate the entire scaffold. To further improve cell growth and take advantage of the increased surface area provided by 3D scaffolds, void and interconnect diameters were modified to enhance cell migration. Increasing the diameter of interconnects by modifying the shear applied during emulsion synthesis allowed cells to populate the entirety of the scaffold.

A chemically-defined, and animal component free 3D scaffold was developed and optimised to promote the proliferation and infiltration of human embryonic stem cells. This scaffold could be used in conjunction with E8 media to produce a cell culture system that contained a synthetic polymer scaffold, a specific attached peptide sequence, and media that contains eight known components. H9 human embryonic stem cells could be cultured for 14 days in this culture system, and retained Oct4 expression suggesting they remained pluripotent. While other examples of defined culture formats exist [38, 54], these materials are not always translated to 3D. Defined 3D culture supports for pluripotent stem cells have been reported [55, 56] though they do not always utilise defined, xeno-free media [57]. This makes the cRGD functionalised polyHIPE scaffold presented in this chapter one of the few well-defined 3D polymer scaffolds for pluripotent stem cell culture under fully defined conditions.

References

[1] Amsbio, *Ready-To-Use Feeder Cells FAQ* http://www.amsbio.com/human–and–mouse–feeder–cells.aspx, Accessed 17–08–2018.

[2] Neofytou, E. A.; Chang, E.; Patlola, B.; Joubert, L.-m.; Rajadas, J.; Gambhir, S. S.; Cheng, Z.; Robbins, R. C.; Beygui, R. E. *J. Biomed. Mater. Res. A* **2011**, *98A*, 383–393.

[3] Murphy, A. R.; Laslett, A.; O'Brien, C. M.; Cameron, N. R. *Acta Biomater.* **2017**, *54*, 1–20.

[4] Knight, E.; Murray, B.; Carnachan, R.; Przyborski, S. In *3D Cell Culture: Methods and Protocols*; Haycock, J., Ed.; Methods Mol. Biol.; Humana Press Inc, 2011; Vol. 695; pp 323–340.

[5] Lee, A.; Langford, C. R.; Rodriguez-Lorenzo, L. M.; Thissen, H.; Cameron, N. R. *Biomater. Sci.* **2017**, *5*, 2035–2047.

[6] Yang, Y.; Liu, X.; Yu, W.; Zhou, H.; Li, X.; Ma, X. *Carbohydr. Polym.* **2010**, *80*, 733–739.

[7] Zustiak, S. P.; Wei, Y.; Leach, J. B. *Tissue Eng Part B Rev.* **2013**, *19*, 160–171.

[8] Walters, N. J.; Gentleman, E. *Acta Biomater.* **2015**, *11*, 3–16.

[9] de Mel, A.; Jell, G.; Stevens, M. M.; Seifalian, A. M. *Biomacromolecules* **2008**, *9*, 2969–2979.

[10] Kolhar, P.; Kotamraju, V. R.; Hikita, S. T.; Clegg, D. O.; Ruoslahti, E.; Ramana, V.; Hikita, S. T.; Clegg, D. O.; Ruoslahti, E. *J. Biotechnol.* **2010**, *146*, 143–146.

[11] Lambshead, J. W.; Meagher, L.; Goodwin, J.; Labonne, T.; Ng, E.; Elefanty, A.; Stanley, E.; O'Brien, C. M.; Laslett, A. L. *Sci. Rep.* **2018**, *8*, 701.

[12] Desai, N.; Rambhia, P.; Gishto, A. *Reprod. Biol. Endocrinol.* **2015**, *13*, 9.

[13] Caldwell, S.; Johnson, D. W.; Didsbury, M. P.; Murray, B. A.; Wu, J. J.; Przyborski, S. A.; Cameron, N. R. *Soft Matter* **2012**, *8*, 10344.

[14] Johnson, D. W.; Langford, C. R.; Didsbury, M. P.; Lipp, B.; Przyborski, S. A.; Cameron, N. R. *Polym. Chem.* **2015**, *6*, 7256–7263.

[15] Ugbode, C. I.; Hirst, W. D.; Rattray, M. *Neurochem. Res.* **2016**, *41*, 1857–1867.

[16] Hayman, M.; Smith, K.; Cameron, N.; Przyborski, S. *J. Biochem. Biophys. Methods* **2005**, *62*, 231–240.

[17] ReproCELL, *Alvetex FAQ* **2018**, http://reinnervate.com/alvetex/about–alvetex/frequently–asked–questions/, Accessed 23–11–2017.

[18] Browne, M.; Lubarsky, G.; Davidson, M.; Bradley, R. *Surf. Sci.* **2004**, *553*, 155–167.

[19] Zhang, Z.; Orski, S.; Woys, A. M.; Yuan, G.; Zarraga, I. E.; Wagner, N. J.; Liu, Y. *Colloids. Surf. B Biointerfaces* **2018**, *168*, 94–102.

[20] Addesso, A.; Lund, D. B. *J. Food Process. Preserv.* **1997**, *21*, 319–333.

[21] Poellmann, M. J.; Wagoner Johnson, A. J. *Cell. Mol. Bioeng.* **2013**, *6*, 299–309.

[22] Li, Y. J.; Chung, E. H.; Rodriguez, R. T.; Firpo, M. T.; Healy, K. E. *J. Biomed. Mater. Res. A* **2006**, *79A*, 1–5.

[23] Connelly, J.; Petrie, T.; García, A.; Levenston, M. *Eur. Cell. Mater.* **2011**, *22*, 168–177.

[24] Chung, T.-W.; Lu, Y.-F.; Wang, H.-Y.; Chen, W.-P.; Wang, S.-S.; Lin, Y.-S.; Chu, S.-H. *Artif. Organs* **2003**, *27*, 155–161.

[25] Lin, Y.-S.; Wang, S.-S.; Chung, T.-W.; Wang, Y.-H.; Chiou, S.-H.; Hsu, J.-J.; Chou, N.-K.; Hsieh, K.-H.; Chu, S.-H. *Artif. Organs* **2001**, *25*, 617–621.

[26] Jacobs, K.; Zambelli, F.; Mertzanidou, A.; Smolders, I.; Geens, M.; Nguyen, H. T.; Barbé, L.; Sermon, K.; Spits, C. *Stem Cell Reports* **2016**, *6*, 330–341.

[27] Singh, S. J.; Turner, W.; Glaser, D. E.; McCloskey, K. E.; Filipp, F. V. *Cell Commun. Signal.* **2017**, *15*, 44.

[28] Meng, G.; Liu, S.; Poon, A.; Rancourt, D. E. *Stem Cells Dev.* **2017**, *26*, 1804–1817.

[29] Chen, V. C.; Couture, S. M.; Ye, J.; Lin, Z.; Hua, G.; Huang, H.-I. P.; Wu, J.; Hsu, D.; Carpenter, M. K.; Couture, L. A. *Stem Cell Res.* **2012**, *8*, 388–402.

[30] ReproCELL, *Alvetex® Scaffold Quick Start Protocol* **2015**, http://reinnervate.com/alvetex/alvetex–documentation/protocols/, Accessed 04–02–2016.

[31] Lei, Y.; Schaffer, D. V. *Proc. Natl. Acad. Sci. U.S.A.* **2013**, *110*, 5039–5048.

[32] Garitaonandia, I. et al. *PLoS One* **2015**, *10*, e0118307.

[33] Bai, Q.; Ramirez, J.-M.; Becker, F.; Pantesco, V.; Lavabre-Bertrand, T.; Hovatta, O.; Lemaître, J.-M.; Pellestor, F.; De Vos, J. *Stem Cells Dev.* **2015**, *24*, 653–662.

[34] Corning, *Accutase Cell Detatchment Solution Product Information* **2015**, https://www.corning.com/catalog/cls/documents/sell–sheets, Accessed 25–10–2018.

[35] Bokhari, M.; Carnachan, R. J.; Przyborski, S. A.; Cameron, N. R. *J. Mater. Chem.* **2007**, *17*, 4088.

[36] Bokhari, M.; Carnachan, R. J.; Cameron, N. R.; Przyborski, S. A. *J. Anat.* **2007**, *44*, 567–576.

[37] Whitely, M. E.; Robinson, J. L.; Stuebben, M. C.; Pearce, H. A.; McEnery, M. A.; Cosgriff-Hernandez, E. *ACS Biomater. Sci. Eng.* **2017**, *3*, 409–419.

[38] Chen, G.; Gulbranson, D. R.; Hou, Z.; Bolin, J. M.; Ruotti, V.; Probasco, M. D.; Smuga-Otto, K.; Howden, S. E.; Diol, N. R.; Propson, N. E.; Wagner, R.; Lee, G. O.; Antosiewicz-Bourget, J.; Teng, J. M.; Thomson, J. A. *Nat. Methods* **2011**, *8*, 424–429.

[39] Johnson, M. *Materials & Methods: Fetal Bovine Serum* **2012**, *2*, http://www.labome.com/method/Fetal–Bovine–Serum.html.

[40] Hayward, A. S.; Eissa, A. M.; Maltman, D. J.; Sano, N.; Przyborski, S. A.; Cameron, N. R. *Biomacromolecules* **2013**, *14*, 4271–4277.

[41] Konagaya, S.; Ando, T.; Yamauchi, T.; Suemori, H.; Iwata, H. *Sci. Rep.* **2015**, *5*, 16647.

[42] Carnachan, R. J.; Bokhari, M.; Przyborski, S. A.; Cameron, N. R. *Soft Matter* **2006**, *2*, 608.

[43] Langford, C. R.; Johnson, D. W.; Cameron, N. R. *Macromol. Rapid. Commun.* **2015**, *36*, 834–839.

[44] Cameron, N. R. *Polymer* **2005**, *46*, 1439–1449.

[45] Langford, C. R. *Emulsion Templated Porous Polymers as Scaffolds for Anterior Cruciate Ligament Tissue Engineering*. Ph.D. thesis, Monash University, 2018.

[46] Butler, J. T.; Hall, L. L.; Smith, K. P.; Lawrence, J. B. *J. Cell. Biochem.* **2009**, *107*, 609–621.

[47] Invitrogen, *HES Cell Data Sheet* **2018**, http://www.thermofisher.com/content/dam/LifeTech/migration/en/filelibrary/cell–tissue–analysis/pdfs.par.49756.file.dat/co13964–stem–cell–data–sheet–hesc.pdf, Accessed 28–10–2018.

[48] Li, Y.; Kilian, K. A. *Adv. Healthc. Mater.* **2015**, *4*, 2780–2796.

[49] Sundarakrishnan, A.; Chen, Y.; Black, L. D.; Aldridge, B. B.; Kaplan, D. L. *Adv. Drug Deliv. Rev.* **2018**, *129*, 78–94.

[50] Kopanska, K.; Bussonnier, M.; Geraldo, S.; Simon, A.; Vignjevic, D.; Betz, T. In *Biophysical Methods in Cell Biology*; Paluch, E., Ed.; Academic Press, 2015; p 370.

[51] Shamir, E. R.; Ewald, A. J. *Nat. Rev. Mol. Cell Biol.* **2014**, *15*, 647–664.

[52] Langhans, S. A. *Front. Pharmacol.* **2018**, *9*, 1–14.

[53] Offenbach, E. K. *Influence of the extracellular matrix on cellular behaviour: Development and application of a bioengineered 3D cell culture system for cancer research and high resolution microscopy*. Ph.D. thesis, Technischen Universität Darmstadt, 2014.

[54] Meng, G.; Liu, S.; Rancourt, D. E. *Stem Cells Dev.* **2012**, *21*, 2036–2048.

[55] Zujur, D.; Kanke, K.; Lichtler, A. C.; Hojo, H.; Chung, U.-i.; Ohba, S. *Sci. Adv.* **2017**, *3*, e1602875.

[56] Heng, B. C.; Li, J.; Chen, A. K.-l.; Reuveny, S.; Cool, S. M.; Birch, W. R.; Oh, S. K.-w. *Stem Cells Dev.* **2012**, *21*, 1701–1715.

[57] Caiazzo, M.; Okawa, Y.; Ranga, A.; Piersigilli, A.; Tabata, Y.; Lutolf, M. P. *Nat. Mater.* **2016**, *15*, 344–352.

Chapter 5

Analysis of 3D Cultured Stem Cells

5.1 Introduction

In Chapter 4, porous polyHIPE scaffolds were surface functionalised to promote attachment and proliferation of H9 human embryonic stem cells. By conjugating a cRGD moiety to residual thiol groups in the scaffold, a chemically defined and bioactive scaffold was produced. This porous, interconnected thiol-acrylate polyHIPE scaffold was able to support H9 stem cell culture and the maintenance of Oct4 expression for up to 14 days. Oct4 expression infers that the 3D cultured stem cells maintained pluripotency in the defined 3D environment. Further analysis of the cells is required to confirm their pluripotency. In this chapter further analysis of the 3D culture system is presented. Additionally, the differentiation capacity of stem cells cultured in the cRGD-functionalised thiol-acrylate system is assessed. Through these investigations this chapter demonstrates the effectiveness of the developed cRGD-functionalised scaffold as a system for maintaining human pluripotent stem cells *in vitro*.

5.1.1 Cell Binding Specificity of Peptide-Functionalised Culture Substrates

The arginine-glycine-aspartate (RGD) peptide is one of the most commonly used peptide sequence in biomaterials design. It was originally derived from fibronectin, but can also

be found in a number of proteins including vitronectin, laminin, bone sialoprotein, and osteopontin [1]. RGD is a common cell adhesion sequence that has affinity for a range of ligands, including several integrins expressed by hESCs [2]. Human embryonic stem cells can be maintained in an undifferentiated state *via* ligand binding to RGD. In addition, cyclic-RGD has been shown to promote the maintenance of stem cell pluripotency under defined conditions [3, 4]. While the adhesive properties of RGD are well known, it is not the only route to achieving cell adhesion to biomaterial substrates. Cells are often able to adhere to and proliferate on synthetic surfaces with no inherent biofunctionality due to protein adsorption from the surrounding environment. Adsorbed proteins essentially form an undefined layer on the surface of biomaterials due to a range of interactions, including hydrophobic interactions, hydrogen bonding, and ionic interactions. When undesired, this adsorption is also known as protein fouling. Investigations into the adsorption of Geltrex® in Chapter 4 suggest that the thiol-acrylate surface is resistant to non-specific protein adsorption. However, change in surface properties due to cRGD-maleimide functionalisation may have altered this property. It is important to determine if the H9 stem cells were adhering specifically to the cRGD surface functionality, or if they were undergoing non-specific interaction due to the presence of peptides.

One method to determine the specificity of cell binding to the cRGD peptide is to functionalise the scaffold with an inactive peptide analogue. Analogues are artificial peptides that have minor sequence changes which cause them to maintain similar properties to the original sequence, but prevent them from expressing the same specific bioactivity. Typical alterations used to generate analogues include exchanging an amino acid for one with similar properties (eg alanine and glycine) or 'scrambling' the original sequence. For example, rearranging the RGD peptide sequence to produce RDG results in similar biophysical properties to RGD, but without cell binding activity [5]. This chapter describes the comparison of cRGD functionalised thiol-acrylate scaffolds to cRAD-functionalised analogues in order to investigate whether stem cell adhesion and maintenance is cRGD specific.

5.1.2 Retrieval of Pluripotent Stem Cells from 3D Scaffolds

Pluripotent stem cells embedded within the porous polyHIPE scaffold have potential applications in areas such as tissue modeling and drug testing. However, common analysis techniques such as FACS and teratoma assays require single cell suspensions. Retrieval of cells is also required for the passaging of cells. Therefore removing cells from the 3D scaffold will increase the versatility of this defined 3D culture platform.

In vitro 3D cell cultures have successfully been extracted from the commercial polyHIPE scaffold Alvetex®. Cell retrieval was achieved using trypsinisation and agitation to dissociate cells, and showed a cell retrieval efficiency of around 60 % [6]. Consequently enzymatic dissociation is the first stem cell retrieval method presented in this chapter.

Explant culture is a method that can be used to temporarily maintain tissue *in vitro*, or to obtain primary cells that migrate out of their native ECM and onto an appropriate substrate. This method does not require the use of enzymatic dissociation to retrieve cells from their surrounding support. This is an advantage as enzymatic dissociation can result in decreased pluripotent cell viability. Explant culture is the basis for the second cell retrieval method presented in this chapter.

5.1.3 Assessment of Stem Cell Pluripotency

Pluripotent stem cells cultured *in vivo* ideally have the same properties and potential as those found in the developing embryo. However, the exact 'fingerprint' of a pluripotent cell as determined by laboratory tests is still debated. Analysing cells *via* immunohistochemistry to show endogenous expression of proteins such as Oct4 and Nanog gives good evidence that a cell is pluripotent [7]. In Chapter 4, human embryonic stem cells were found to infiltrate porous polymer scaffolds, and to express OCT4 for 14 days in culture. In this chapter, qPCR is used to determine gene expression profiles of cells and give further evidence of a naive cell population. However, even if cells express the specified

proteins and genes this only points to the potential to form different cell types from all three germ layers. These methods do not directly determine the functionality of stem cells.

To determine a cell population's capacity for differentiation, a teratoma assay can be conducted. In this assay, suspected pluripotent stem cells are injected into immunocompromised mice. If the cells are pluripotent, then they will form a solid tumour containing cell types derived from each germ layer known as a teratoma. This process is summarised in Figure 5.1. Teratoma assays are currently considered the gold standard when determining the pluripotency of stem cells [8]. The ability to form teratomas can be considered part of the functional definition of embryonic stem cells [9] as cells which form teratomas demonstrate the ability to produce cell types from all three germ layers. This chapter further assesses the behaviour of H9 stem cells cultured in the thiol-acrylate scaffolds, including determination of pluripotency *via* teratoma assay.

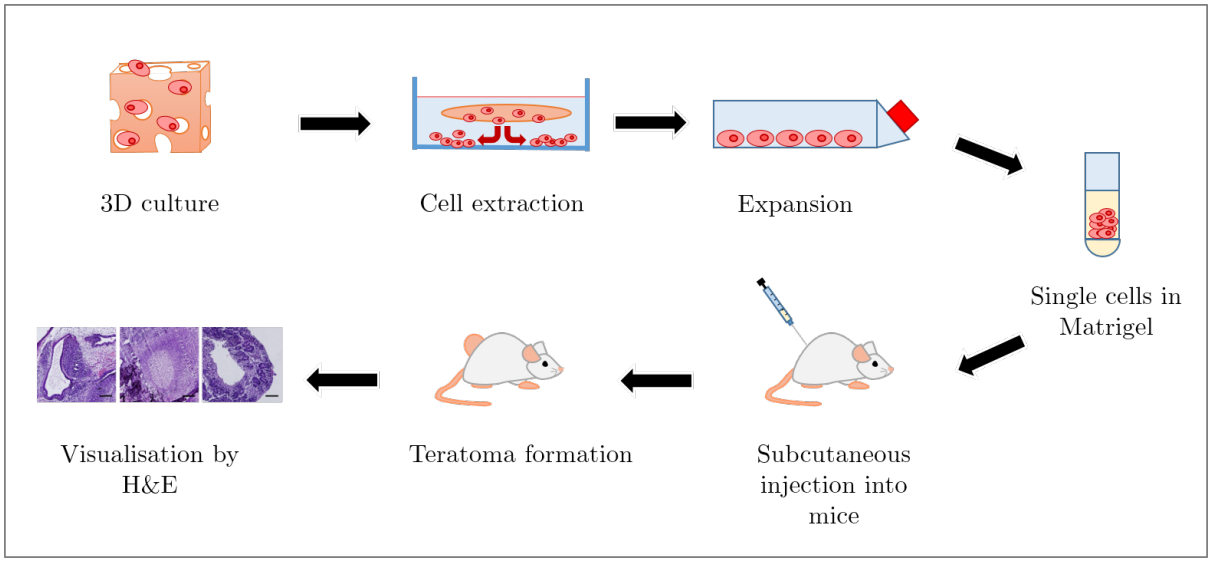

Figure 5.1: *Schematic showing the procedure for teratoma assays.*

5.2 Aims of Chapter

The first aim of this chapter was to determine whether cyclic-RGD functionalisation has an advantage over an inactive peptide sequence. Chapter 4 showed that H9 pluripotent

stem cells grew and proliferated on cRGD-maleimide functionalised scaffolds with similar efficiency to those with a covalently attached, ECM-derived Geltrex® coating. In this chapter, cRGD-maleimide is compared to cRAD-maleimide to determine whether the cRGD sequence is specifically supporting stem cell attachment and growth.

The second aim was to investigate the pluripotency of cells cultured in the 3D thiol-acrylate polyHIPEs scaffold environment. The current gold standard in determining cell pluripotency is the teratoma assay. This was used in addition to immunohistochemistry and qPCR analyses to probe the differentiation potential of the cells. This approach required the development of methods to remove cells from the 3D scaffold.

5.3 Results & Discussion

5.3.1 Determination of Cell Binding Specificity in cRGD Functionalised Scaffolds

Functionalising thiol-acrylate polyHIPE scaffolds with cyclic-RGDfK-maleimide (cRGD) was shown to promote H9 human embryonic stem cell growth in the scaffold in Chapter 4. This was a significant improvement over the as-synthesised scaffold, indicating that functionalisation was necessary. However, it was not clear whether the increase in cell viability was due cRGD attachment specifically, or if any peptide present on the material would produce a similar result due to non-specific interactions. Therefore the scaffold was functionalised with another cyclic peptide, cyclic-RADfK-maleimide (cRAD). Arginine-alanine-aspartate (RAD) is an inactive analogue peptide used as a negative control for RGD. It has a similar amino acid sequence with the glycine exchanged for an alanine, but does not bind specifically to the integrins known to interact with RGD.

The metabolism of H9 stem cells cultured in cRGD- and cRAD-functionalised scaffolds was monitored over 14 days using a PrestoBlue® assay to determine cell activity. Figure

5.2 shows the measured metabolism. Stem cell cultures in cRGD-functionalised scaffolds had much higher metabolism than those in cRAD-functionalised scaffolds. Metabolism in cRGD-functionalised scaffolds increased from day 3 to day 10, likely due to increased cell number (as shown in Figure 5.3). There was a significant decrease in metabolism measured at day 14, despite the expected increase in cell number. Pluripotent stem cells are rapidly proliferating cells with high energy requirements [10]. Metabolism changes as stem cells spontaneously differentiate to less proliferative progeny. Immunostaining previous cultures on cRGD-functionalised scaffolds showed that the proportion of cells expressing Oct4 in each population decreases after 14 days in culture, indicating that the cells are beginning to differentiate. The decrease in metabolism at day 14 in Figure 5.2 may be due to this differentiation. It was expected that cultures in polyHIPE scaffolds functionalised with cRGD would have high metabolism as cells have already been shown to adhere to and proliferate in this material. Metabolic activity measured in the cRAD-functionalised scaffolds was much lower than cRGD at all time points. The low measured metabolism in cRAD-functionalised scaffolds suggested that cells were not able adhere to thiol-acrylate polyHIPE scaffolds *via* non-specific mechanisms, and that cRGD-functionalisation is required.

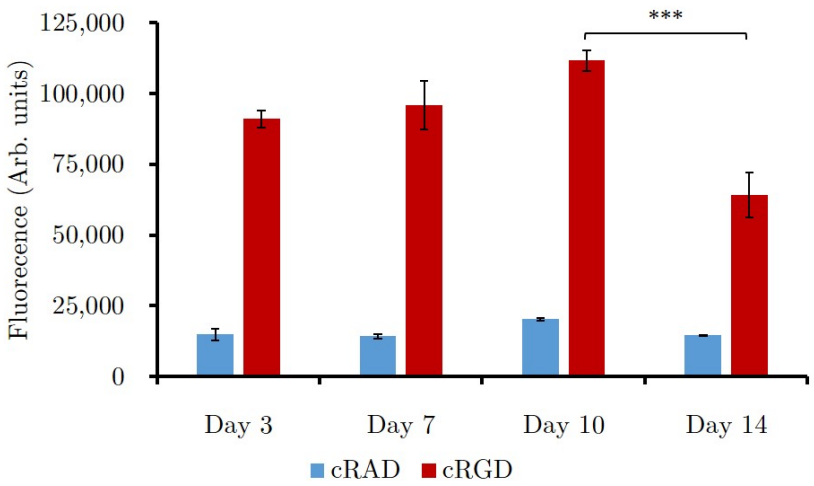

Figure 5.2: *Cellular metabolism of H9 stem cells cultured on cRGD- and cRAD-functionalised thiol-acrylate polyHIPE scaffolds for up to 14 days. Measured using a PrestoBlue® assay. Error bars indicate standard deviation.* $*** = p \leq 0.001$

The metabolic assay results in Figure 5.2 correlate with the very low cell numbers seen on H&E stained sections of cRAD-functionalised thiol-acrylate scaffolds, as shown in Figure 5.3. H9 pluripotent stem cells seeded onto cRAD functionalised materials do not adhere well if at all, and thus very few cells are present even after 14 days in culture. It is possible that the morphology of the scaffold, rather than cell adhesion to peptides, is holding the occasional cells found in the stained cRAD scaffolds in place. RAD and other analogues of functional peptides are widely known to be non-binding and are used as negative controls. Therefore, this result is not unexpected.

As expected, H9 cell adhesion to cRGD-functionalised scaffolds is robust and cells proliferate through the material over the 14 day culture (Figure 5.3). Together, the metabolic assay and imaging results indicate that cell adhesion in thiol-acrylate polyHIPE scaffolds is due to specific interactions with conjugated cRGD.

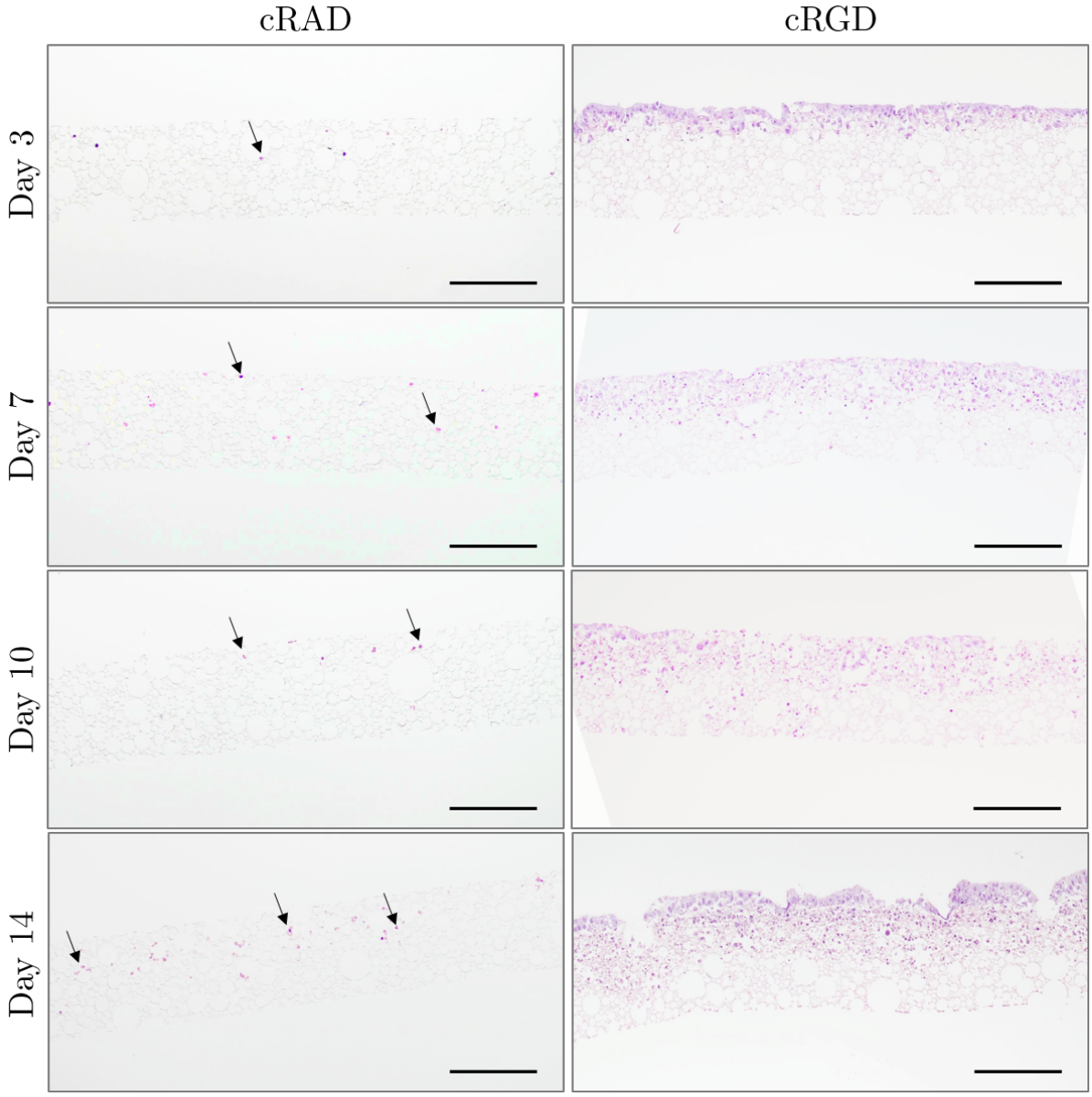

Figure 5.3: *Micrographs of H9 stem cells cultured for up to 14 days in cRGD- and cRAD-functionalised thiol-acrylate polyHIPE scaffolds. Arrows highlight scattered cells in the cRAD-functionalised scaffolds. H&E stain, scale bar = 200 μm.*

5.3.2 Effect of PrestoBlue® Assays on 3D Cultured Stem Cells

One of the aims of this chapter was to assess the differentiation capacity of 3D cultured stem cells. This required the development of retrieval protocols to remove stem cells from the 3D thiol-acrylate scaffold. When retrieving cells from 3D scaffolds, the number of cells remaining in the material after dissociation was of interest. This could be measured visually using H&E stained sections, or by analysing the metabolism of cells remaining in the scaffolds.

Metabolism was monitored using a resazurin-based assay reagent known as PrestoBlue® cell viability reagent. PrestoBlue® does not require cell lysis and leaves cells alive at the completion of the metabolic assay. To streamline the work flow of culture analysis during enzymatic dissociation, it was practical to fix and stain the same scaffold samples used in metabolic assays. It was hypothesised that due to the gentle nature of the PrestoBlue® assay, there would be no difference in cell number or distribution between samples subjected to metabolic assay and those left untreated. To determine if cells were removed from the scaffolds during metabolic assay step, samples were fixed and stained using H&E before and after treatments. Figure 5.4 shows the H9 cells present in sulfo-SANPAH functionalised, Geltrex®-coated thiol-acrylate polyHIPE scaffolds before (control) and after enzymatic dissociation, and the results when PrestoBlue® was applied to these conditions. Figure 5.5 shows the same analysis applied to cells cultured in cRGD functionalised scaffolds.

Figures 5.4 and 5.5 suggest that the manipulation and washing required for metabolic assays removed some of the surface cells from the control cultures in both cRGD-functionalised scaffolds, and those with sulfo-SANPAH and Geltrex®. This is particularly evident when comparing Figure 5.5a, which shows as-cultured cells with no enzymatic treatment, and Figure and 5.5b, which shows as-cultured cells after a metabolic assay. Assuming that the cultures shown in the post-metabolic assay sample had the same cell buildup on the surface as the untreated sample, then significant cell removal has occurred due to the

assay. It should be noted that while there was often a surface layer of cells on the 3D scaffolds, the thickness shown in Figure 5.5a is greater than typical.

This surface effect was less pronounced on enzymatically dissociated samples, as seen when comparing in Figures 5.4c and 5.4d. The dissociation process removed far more cells than the metabolic assay, and so measuring the metabolism of enzymatically treated stem cells does not have an affect on the number of cells remaining in the material. This effect was also seen on cRGD-functionalised scaffolds, as shown in Figure 5.5 c&d.

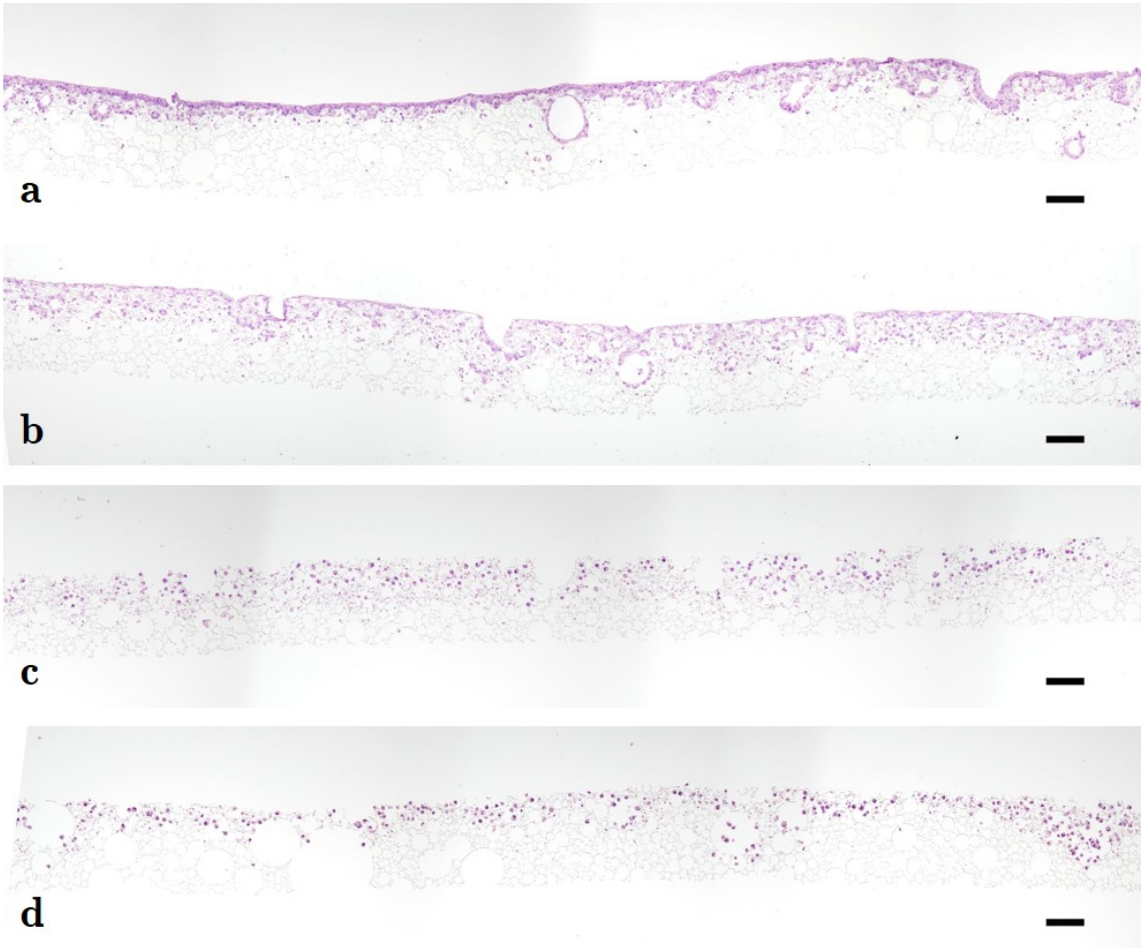

Figure 5.4: *Micrographs of H&E stained stem cell cultures on thiol acrylate polyHIPE scaffolds functionalised with sulfo-SANPAH and coated with Geltrex©. a) Cells present on the untreated condition b) Cells on the untreated condition after a PrestoBlue® metabolic assay c) Remaining cells after attempted extraction with Accutase d) Remaining cells after attempted extraction with Accutase followed by a PrestoBlue® metabolic assay. Scale bars = 100 μm*

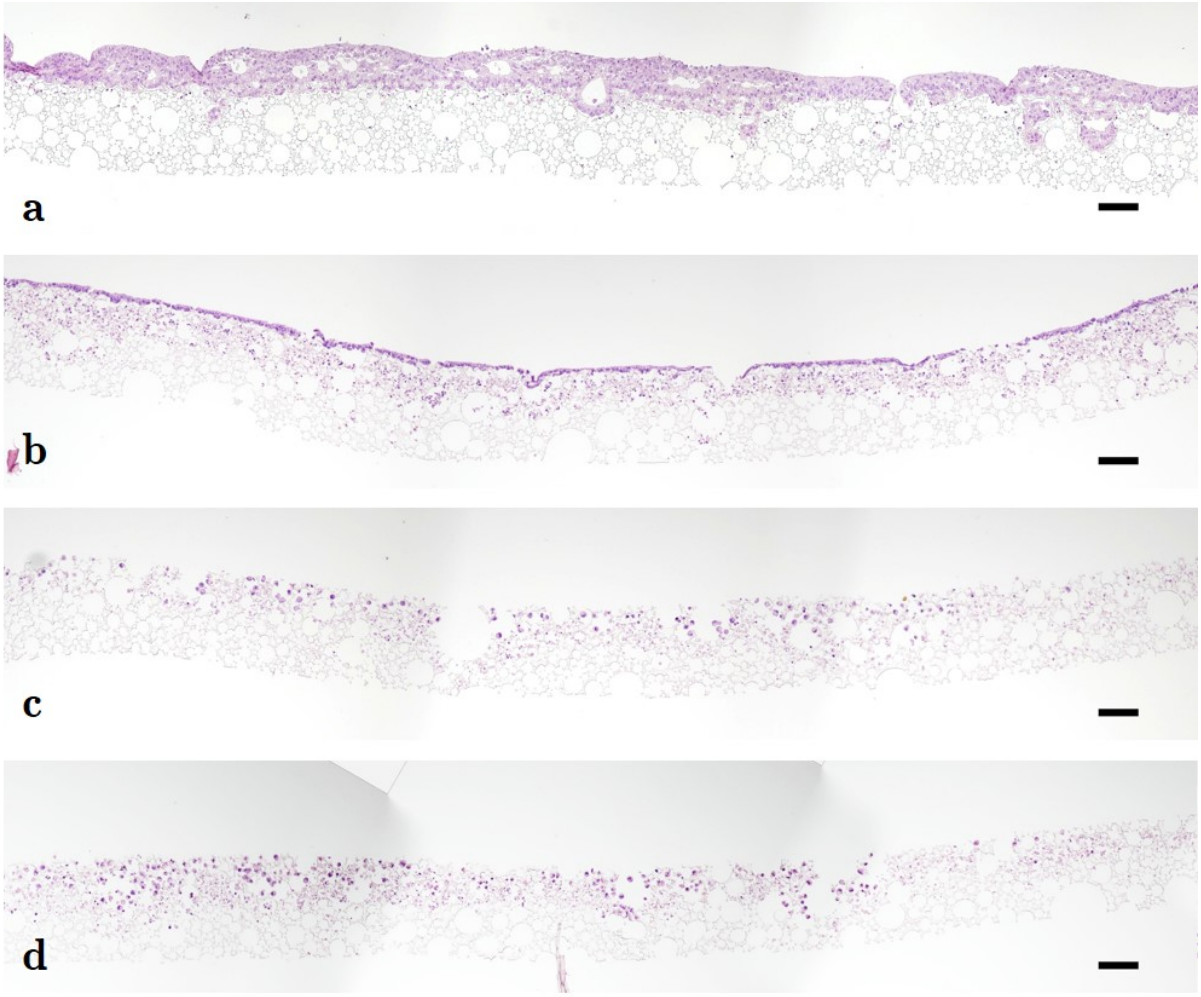

Figure 5.5: *Micrographs of H&E stained stem cell cultures in thiol-acrylate polyHIPE scaffolds functionalised with cRGD. a) Cells present on the untreated condition b) Cells on the untreated condition after a PrestoBlue® metabolic assay c) Remaining cells after attempted extraction with Accutase d) Remaining cells after attempted extraction with Accutase followed by a PrestoBlue® metabolic assay. Scale bars = 100 μm*

5.3.2.1 Media Analysis

While conducting metabolic assays on scaffolds suspended in frames, it became apparent that the metabolites of the reaction were not evenly distributed within the culture well. PrestoBlue® is a colourimetric assay with a distinct blue to pink shift. Over the course of the 1.5 hour reaction, the media inside the frame became noticeably more pink than than that on the outside. To quantify this observation, the solutions from each position were analysed separately instead of being combined to produce an overall measure of culture metabolism. The results of this analysis are presented in Figure 5.6. The measured metabolism was different at each position for stem cell cultures in both cRGD-functionalised scaffolds (Figure 5.6a) and sulfo-SANPAH-functionalised, Geltrex®-coated scaffolds (Figure 5.6b). These metabolic measurements indicate that the PrestoBlue® reagent is not able to diffuse evenly around the scaffold over the time allowed. This may suggest that other components in the cell media are also slow to diffuse, however whether this diffusion rate adversely affects stem cell behaviour is unclear.

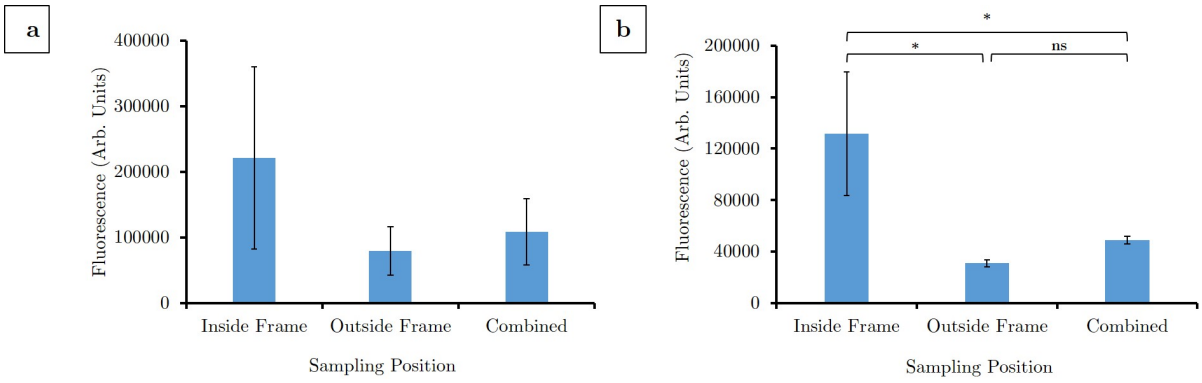

Figure 5.6: *Metabolic activity of cultures on scaffolds functionalised with a) cRGD and b) sulfo-SANPAH with Geltrex® coating. Measurements were taken inside and outside supporting frames.* $* = p \leq 0.05$

The pH of the culture media was also analysed. Figure 5.7 shows a statistically insignificant difference in pH between the inside and outside frame positions. This difference was not found to be significant by one way ANOVA. All media in culture is more acidic on average than fresh media, which is expected. The difference in pH between the cRGD-

functionalised and sulfo-SANPAH-functionalised, Geltrex®-coated samples is most likely due to differing cell metabolism on the scaffolds.

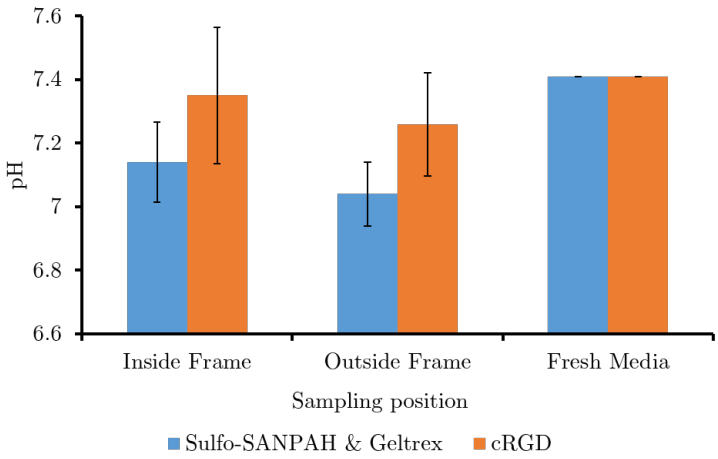

Figure 5.7: *Measurements of media pH inside and outside of the supporting frame. Error bars indicate standard deviation*

These results may indicate a need for further optimisation of the culture system. The pH of the surrounding media can affect pluripotent cell fate [11, 12]. Therefore, it should be controlled and homogeneous. The uneven pH would likely be solved by a shift to dynamic culture, either by agitating the plate containing the current scaffold and frame configuration, or by incorporating thiol-acrylate polyHIPEs into a bioreactor. While such development is beyond the scope of this thesis, potential directions are discussed in Chapter 6.

5.3.3 Extraction of H9 Stem Cells from Porous 3D Scaffolds

5.3.3.1 Extraction *via* Enzymatic Dissociation

As outlined in the introduction to this chapter, stem cell cultures embedded in 3D scaffolds have several applications. However, the ability to remove cells from the scaffold for passaging and downstream applications greatly improves flexibility of the system and opens up far more potential applications. It was therefore beneficial to extract H9 stem

cells from the thiol-acrylate scaffold. The first approach used was enzymatic dissociation. Trialled conditions are listed in Table 5.1.

Figure 5.8 shows the number of cells extracted from scaffolds by ezymatic dissociation as a percentage of the cells initially seeded. It can be seen that most dissociation conditions resulted in few cells being extracted from the scaffold. Condition 3 is the exception, with about 200 % total cell retrieval. However, over half of the cells retrieved were dead, and when plated onto Geltrex®-coated TCPS the cells did not adhere. This failure to adhere when re-plated was seen in all conditions that retrieved appreciable numbers of live cells (conditions 1, 2, 3, 4 and 6). This suggests that live cells extracted from the 3D cultures were not healthy.

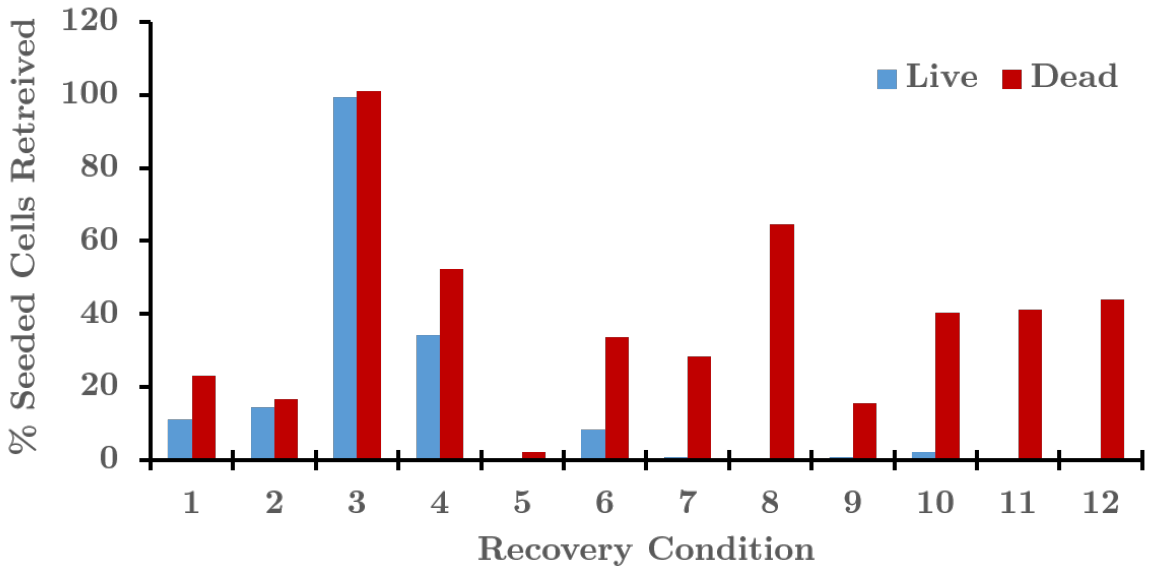

Figure 5.8: *Average numbers of live/dead H9 stem cells retrieved from thiol-acrylate scaffolds using enzymatic dissociation as a percentage of the seeded cell number. Recovery conditions are defined in 5.1.*

Scaffolds were analysed post-dissociation to give insight into the reason for the low stem cell extraction efficiency. Figure 5.9 shows the metabolic activity of H9 stem cells remaining in the scaffolds after enzymatic dissociation, as measured by PrestoBlue® assay. There appeared to be an approximately inverse relationship between the number of live cells removed from the material, and the measured metabolic activity remaining post-

Table 5.1: *Dissociation conditions trialled for retrieval of H9 pluripotent stem cells from porous 3D scaffold cultures. 'SS' refers to sulfo-SANPAH functionalisation.*

No.	Scaffold Type	Dissociation Agent	Incubation Time (min)	Incubation Temp (°C)	Sectioning	ROCKi
1	SS + Geltrex	Accutase	10	37	Quarters	No
2	cRGD	Accutase	10	37	Quarters	No
3	SS + Geltrex	Accutase	5	37	Quarters	No
4	SS + Geltrex	TrypLE	5	37	Quarters	No
5	SS + Geltrex	TrypLE	5	37	Halves	2 hours
6	SS + Geltrex	Accutase	5	37	Halves	No
7	SS + Geltrex	Accutase	5	37	Halves	23 hours
8	SS + Geltrex	Accutase	5	37	No	2 hours

continued on next page

9	SS + Geltrex	Accutase	5	37	No	23 hours
10	SS + Geltrex	TrypLE	5	37	No	No
11	SS + Geltrex	Accutase	20	0	No	24 hours
12	SS + Geltrex[1]	TrypLE	20	0	No	24 hours

[1]Scaffold was also centrifuged during cell collection.

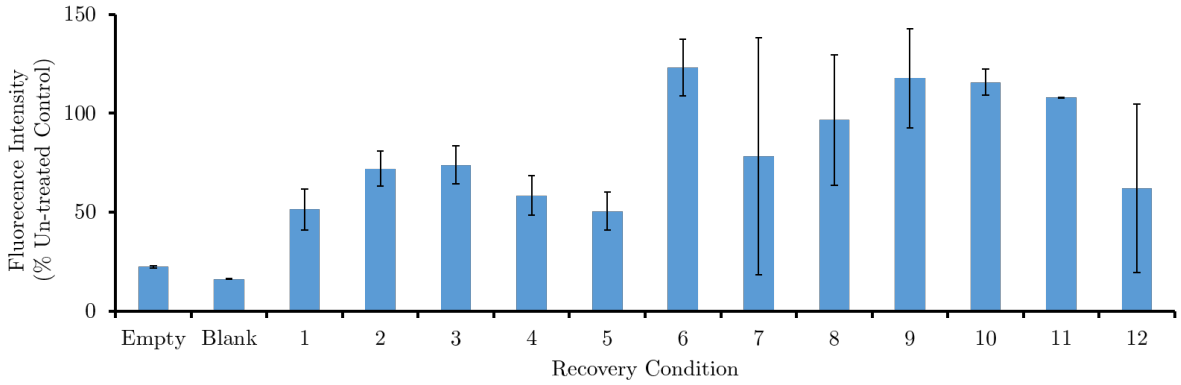

Figure 5.9: *Average metabolic activity of stem cells remaining in scaffolds after being exposed to different dissociation conditions. Values are relative to untreated 3D control cultures. Error bars indicate standard deviation. Recovery conditions are defined in 5.1.*

treatment. This indicated that a large proportion of the original cell culture remains in the scaffold. Some enzymatically treated samples showed greater metabolism than the untreated control condition. This may be due to the stress experienced by the remaining cells, which can increase metabolism. Proliferation can also vary between scaffolds despite consistent experimental conditions, and so it is possible that the control samples had fewer cells than the pre-treatment experimental samples. Metabolic measurements for the untreated control condition were taken from separate scaffolds seeded at the same time as the experimental samples, not from the same scaffolds prior to treatment. Potential variation in proliferation between the scaffolds may also explain the large standard deviation in conditions 7 and 12. These high deviation samples were also exposed to protocols with high mechanical stress or extended processing time.

ROCK inhibitor (ROCKi) inhibits Rho-associated coiled-coil containing protein kinase (ROCK). Addition of ROCKi is used to promote survival of dissociated hPSCs [13]. Addition of ROCKi in dissociation conditions 5, 7-9, 11 and 12 did not improve the live cell count as expected. The majority of cells dissociated from samples treated with this inhibitor were dead. Interestingly, post-treatment metabolism measurements on scaffolds treated with ROCKi were high. This suggests that ROCKi had the intended effect of promoting cell survival, but this did not assist dissociation.

Conducting dissociation on ice was trialled to allow increased time for the cells to move out of the material without causing major enzymatic damage. A modest amount of dead cells was retrieved using this method, as shown by conditions 11 and 12 in Figure 5.8. The post-treatment metabolism in these samples was high (Figure 5.9, conditions 11 & 12). This suggested that while the aim of reduced cell damage was achieved, the ice prevented efficient dissociation. As remaining cell metabolism was good, the dissociation time could potentially be extended to better remove cells.

None of the dissociation treatments trialled resulted in more live cells than dead. This could have occurred because these methods were too harsh for the cell line used. H9 stem cells are adhesion dependent, and their recovery after passaging depends heavily on the restoration of cell-cell and cell-matrix contacts. For this reason, cells are not typically dissociated to single cells during routine passaging. Cells may be damaged by excessive enzyme exposure. However, similar exposure times were used successfully to dissociate 2D H9 stem cell cultures when single cell populations were required.

Cells have previously been removed from polyHIPE scaffolds using the enzyme trypsin combined with agitation. This protocol was developed for use with polystyrene scaffolds, and reported to be effective for hepatic (HepG2) and epithelial (A549) cells. However, the use of this protocol in conjunction with human stem cells is unexplored. Trypsin is often avoided when passaging human embryonic stem cells (hESCs) as it reduces viability of the cells [14]. Trypsin was therefore replaced with dissociation agents known to be compatible with H9 embryonic stem cells, namely TripLExpress (TripLE) and Accutase. TripLE is a solution of recombinant cell-dissociation enzymes that is sold as a replacement for porcine or bovine trypsin. TripLE can typically be used as a direct replacement for trypsin [15]. It is suitable when a dissociation agent free from animal-derived components is required. Accutase is a also a solution of enzymes that is suitable for stem cell dissociation. It does not contain animal- or bacteria-derived proteins, which reduces contamination risk.

Another mechanism of cell damage could be agitation and mechanical damage. The edges of the voids found in polyHIPEs are thin and the polymer is reasonably stiff compared

to a cell, so the cells may have been exposed to mechanical stress. The cell lines successfully extracted from polyHIPEs in the commercial protocol are robust lines. Previous experiments with a variety of cell lines have also shown low cell retrieval from polyHIPE scaffolds with different chemistries [16].

Alternately, it is possible that the dissociation conditions used were most effective at removing weakly attached or dead cells. If this was the case, then the healthy cells should have remained in the scaffold. H&E staining was used to investigate remaining cells further. Figure 5.10 shows the cells remaining in the thiol-acrylate polyHIPE scaffolds after dissociation. Enzymatically treated samples typically had many cells remaining in the scaffolds. This correlates with presence of cell metabolism in treated samples as shown previously (Figure 5.9). Notably, surface cell layers had been removed. This makes sense, as the path cells would need to take to be removed from the scaffold becomes more tortuous as they migrate towards the centre. Such cells would require longer treatment times to retrieve, which may adversely affect cells closer to the scaffold surface. Future optimisation of cell retrieval from these scaffolds may benefit from refinement of scaffold thickness or configuration.

Some scaffolds were cut prior to enzymatic treatment as suggested by the established protocol for polystyrene polyHIPEs. Cutting scaffolds requires extra manipulation, and while care was taken to cut cleanly and quickly, tearing or stretching of scaffolds could occur. Condition 12, which also had very high standard deviation, involved spinning the scaffolds themselves rather than only the dissociation solution and cells. This was intended to pull cells out of the material, but possibly damaged cells instead.

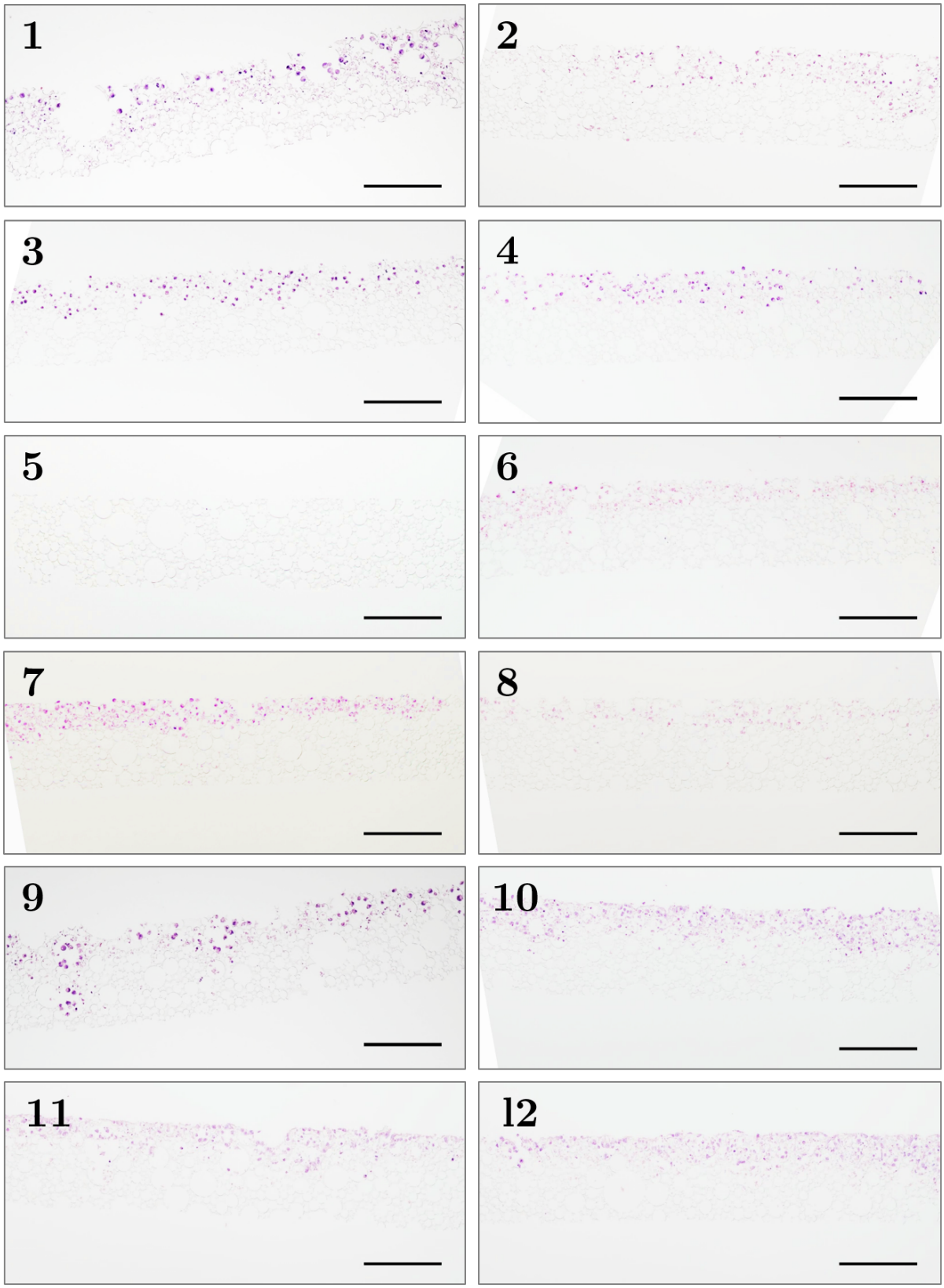

Figure 5.10: *H&E stained sections post enzymatic dissociation for each condition. Scale bar = 200 μm. Image numbers indicate the enzymatic dissociation treatment condition, as listed in table 5.1*

.

Upon analysing H&E stained sections, it was noted that different scaffold pieces from the same condition number occasionally had different amounts of cells remaining in the scaffold after dissociation. In some areas, cells appeared to be retrieved effectively, while other parts of the scaffold had large numbers of cells remaining. This effect is shown in Figure 5.11. All micrographs were taken across the same same edge-to-centre or edge-to-edge ranges. The difference in cells visualised post-dissociation could have been due to natural variation in cell density across the scaffold prior to dissociation. It may also indicate inhomogeneous exposure to the dissociating enzymes. The cut pieces of scaffold may have attached to each other or to the walls of the Falcon tube, limiting the flow of dissociation solution. This could have resulted in some sections of the scaffold being affected differently by enzymatic treatment. Possible solutions to this include separate dissociation solutions for each piece of each scaffold. This would require a large quantity of enzyme solution and more handling, so the effect on cells would need to be monitored. Another option is to change the shape of the dissociation vessel and the agitation method. A well plate may promote separation of the scaffold pieces more effectively than a tube. Inversion or a rocking platform may promote better agitation than a shaker platform.

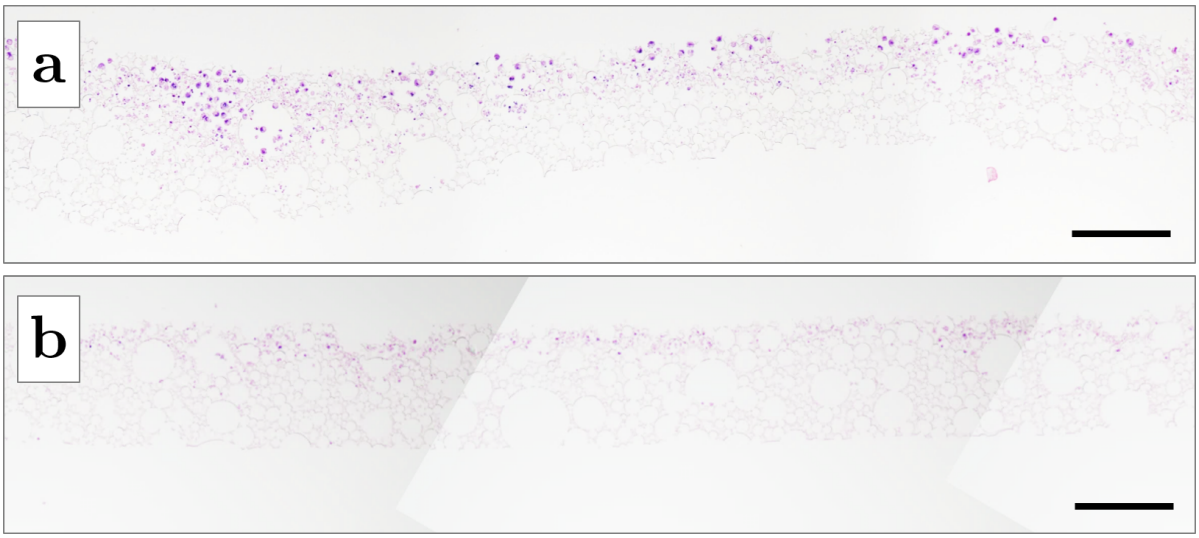

Figure 5.11: *Micrographs of two pieces of scaffold from the same experiment after dissociation with Accutase (Condition 2) showing a) high and b) low remaining cell populations. Scale bar = 200 μm.*

5.3.3.2 Explant-Inspired Passive Stem Cell Extraction

It was apparent that enzymatic treatments used to remove other cell lines from polyHIPE scaffolds were not effective for retrieving H9 pluripotent stem cells from the 3D thiol-acrylate polyHIPE environment. An alternative approach was to allow cells to migrate out of the scaffold over longer periods of time. By culturing H9 stem cells for 7 days on scaffolds and then placing them on typical 2D substrates seeded-side down, it was expected that cells would move out of the 3D structure similar to cells migrating out of tissue in explant culture.

Figure 5.12 shows H9 stem cell colonies that have migrated from the 3D scaffold onto Geltrex®-coated TCPS using this explant-inspired extraction. This method could be used to retrieve H9 stem cells from both sulfo-SANPAH functionalised scaffolds with Geltrex® coating, and from cRGD-functionalised scaffolds. The majority of cells in Figure 5.12 showed typical embryonic stem cell morphology. Figure 5.13 shows the cells remaining in the scaffold after passive extraction. It can be seen that not all cells migrate out of the material.

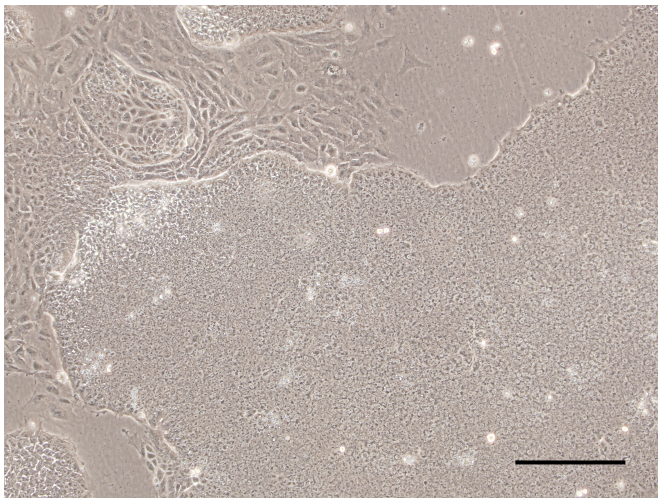

Figure 5.12: *Morphology of H9 embryonic stem cells obtained from sulfo-SANPAH functionalised, Geltrex®-coated polyHIPE scaffolds via explant-inspired passive extraction. Scale bar = 300 μm.*

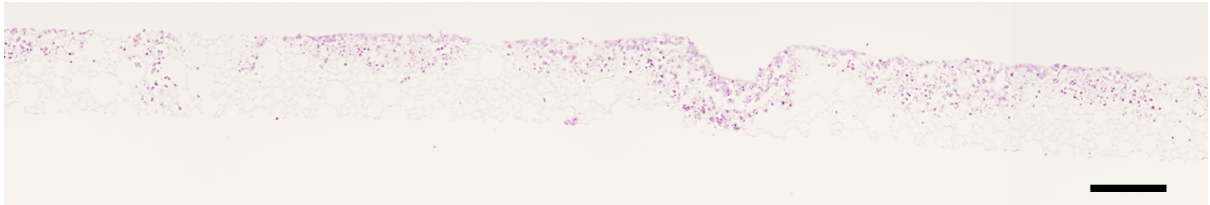

Figure 5.13: *H9 embryonic stem cells remaining in sulfo-SANPAH functionalised, Geltrex®-coated polyHIPE scaffolds after explant-inspired retrieval. Scale bar = 200 μm.*

5.3.4 Analysis of 3D Cultured Stem Cell Properties

5.3.4.1 Karyotype of H9 Cells Extracted from Porous PolyHIPE Scaffolds

Karyotyping is routinely conducted on H9 stem cells during *in vitro* culture to ensure their genetic stability. There are several ways to assess karyotype. Conventional banding techniques, such as the G-banding method used in this work, allow an overview of the karyotype of the cells. Banding techniques are useful for routine assessment of genetic stability. They can typically detect anueploides (incorrect chromosome numbers), mosaicism, large deletions, translocations, or insertions.

Cells that migrated out of sulfo-SANPAH functionalised, Geltrex®-coated scaffolds were found to have a normal karyotype. Figure 5.14 shows the karyotype of cells from cRGD-functionalised scaffolds. Analysis of these cells found that 4 of the 20 cells examined exhibited trisomy 12. This suggested that the culture may be abnormal.

Pluripotent stem cells are known to spontaneously acquire karyotypic abnormalities in culture. Long term culture of hESCs commonly results in chromosomal abnormalities such as trisomy of chromosomes 17q or 12 [17]. Trisomy 12 is the most common genomic aberration acquired by stem cells in culture [18]. Aberrations acquired in culture may affect tumorigenicity and differentiation capacity. Stem cells are also prone to sub-chromosomal abnormalities that are not detectable by karyotyping [19].

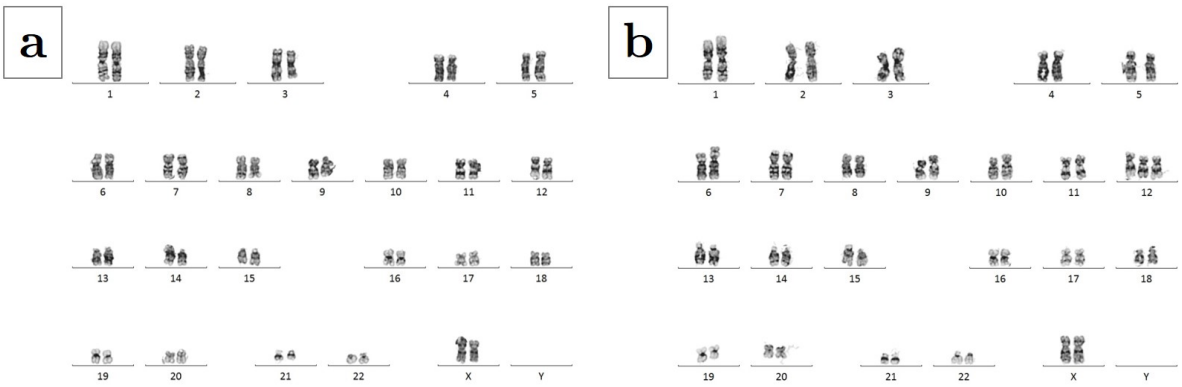

Figure 5.14: *Karyotype of human embryonic stem cells extracted from cRGD-functionalised polyHIPE scaffolds. a) Normal karyotype, found in 16/20 cells b) Karyotype showing trisomy 12, found in 4/20 cells.*

It is uncertain what caused the incidence of trisomy 12 in some stem cells retrieved from the cRGD-functionalised 3D culture. While karyotypes of ongoing 2D H9 stem cell cultures were conducted regularly and found to be normal, the precise passage seeded onto the cRGD functionalised polyHIPE scaffolds was not analysed. Thus, the trisomy may have already been present in the culture prior to seeding. The trisomy may also be a product of culture on the cRGD scaffold. As the abnormality did not occur on Geltrex®-coated scaffolds, it may be that a mixture of extracellular matrix proteins is required, and that cRGD alone cannot maintain genetic stability in H9 stem cells in these defined, 3D culture conditions. Other handling, such as the multi-day extraction protocol, may have also caused the acquisition of trisomy 12 in some cells.

Due to these additional factors, aquisition of trisomy 12 can not be attributed directly to a specific aspect of the culture. In addition, only one sample of cells retrieved from cRGD scaffolds was analysed to determine the karyotype. It is therefore unclear whether all cell populations cultured in this material possessed cells with genetic abnormality. Further analysis is required to assess whether chromosomal abnormality is typical of 3D cultures in cRGD-functionalised polyHIPE scaffolds, and if it is, to determine its origin.

5.3.4.2 Confirmation of the Differentiation Capacity of 3D Cultured H9 Human Embryonic Stem Cells

Thiol-acrylate polyHIPE scaffolds have already been assessed for their ability to support H9 stem cell proliferation and Oct4 expression in Chapter 4. As the cell populations retain Oct4 expression in 3D culture, they are presumed to be pluripotent. In order to confirm this, further analysis was conducted.

QPCR uses targeted probes to measure the amount of RNA associated with specific genes in a cell population. To assess the state of H9 stem cells in 3D culture, a panel of probes was selected to include both genes indicative of pluripotency (Oct4 and Nanog) and genes from each germ layer. This gives a general idea of the fate of the cell population at each timepoint. Figure 5.15 shows the relative expression of mRNA associated with specific genetic markers in H9 stem cells cultured in cRGD functionalised polyHIPE scaffolds for up to 14 days. It can be seen that cells cultured for 14 days in thiol-acrylate 3D scaffolds retain Oct4 and Nanog expression, suggesting the presence of pluripotent cells. The increase in Sox 1 and Pax 6 (ectodermal), T and Runx 1 (mesodermal), and Gata-4 (endodermal) markers indicates that the cell population is beginning to differentiate over the duration of culture. This is expected as stem cells differentiate spontaneously over time. Runx1 and Gata-4 in particular show a clear upward trend. This suggests that after extended time in the 3D scaffold, H9 stem cells differentiate towards cell types from different germ lines.

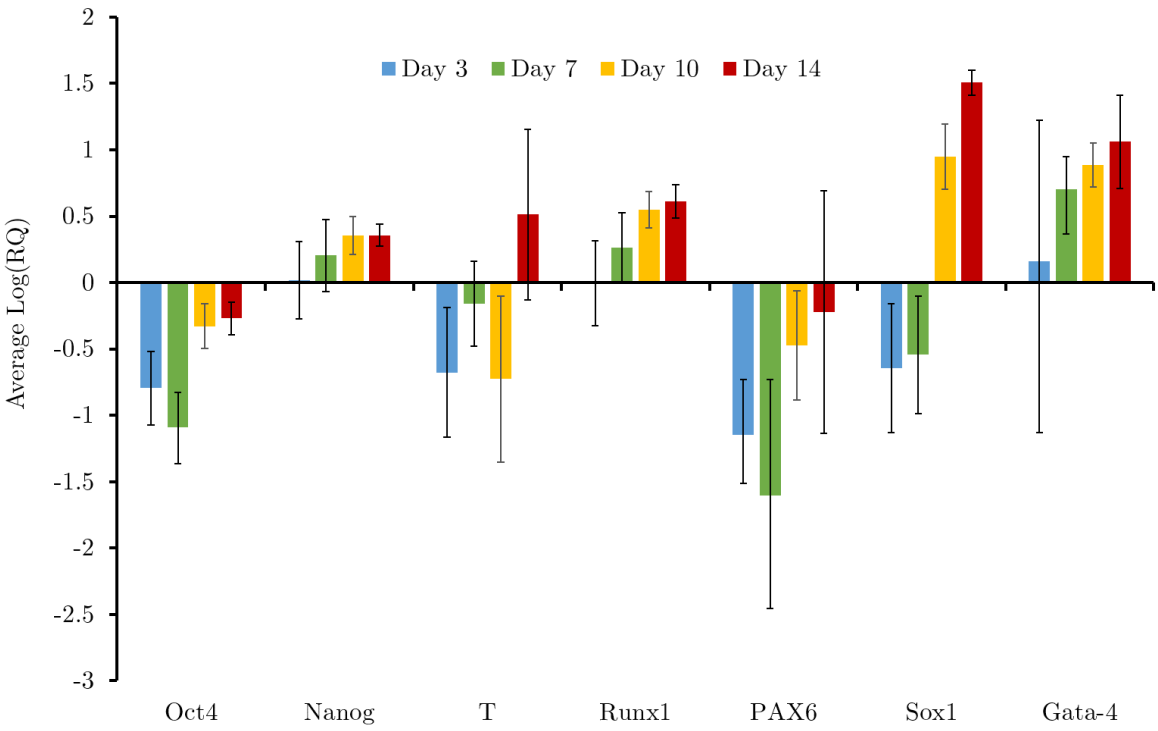

Figure 5.15: *qPCR analysis of H9 stem cells cultured on defined scaffolds for up to 14 days.*

To test the differentiation capacity of the 3D cultured cells and confirm their pluripotency, cells retrieved from 3D cultures using the synthetic explant method were assessed *via* teratoma assay. Cells were retrieved from cRGD functionalised scaffolds, sulfo-SANPAH functionalised scaffolds with Geltrex® coating, or from 2D culture on Geltrex® for analysis. H&E stained sections of the teratomas formed by these cells are shown in Figure 5.16. All conditions produced teratomas containing cells from all three germ layers, confirming that the 3D-cultured embryonic stem cells were pluripotent. All injections formed teratomas, except those in one mouse that became ill and was euthanised before teratomas formed. This suggests that the cells could form teratomas effectively, however more assays would be required to measure formation efficiency.

PCR and teratoma assays are used in combination to determine whether a cell population is pluripotent. The two techniques assess different components of the cells, and so give complementary information. In this case, the longer PCR time-points indicate that markers for the three germ lines are increasing, suggesting that the cells are differentiating

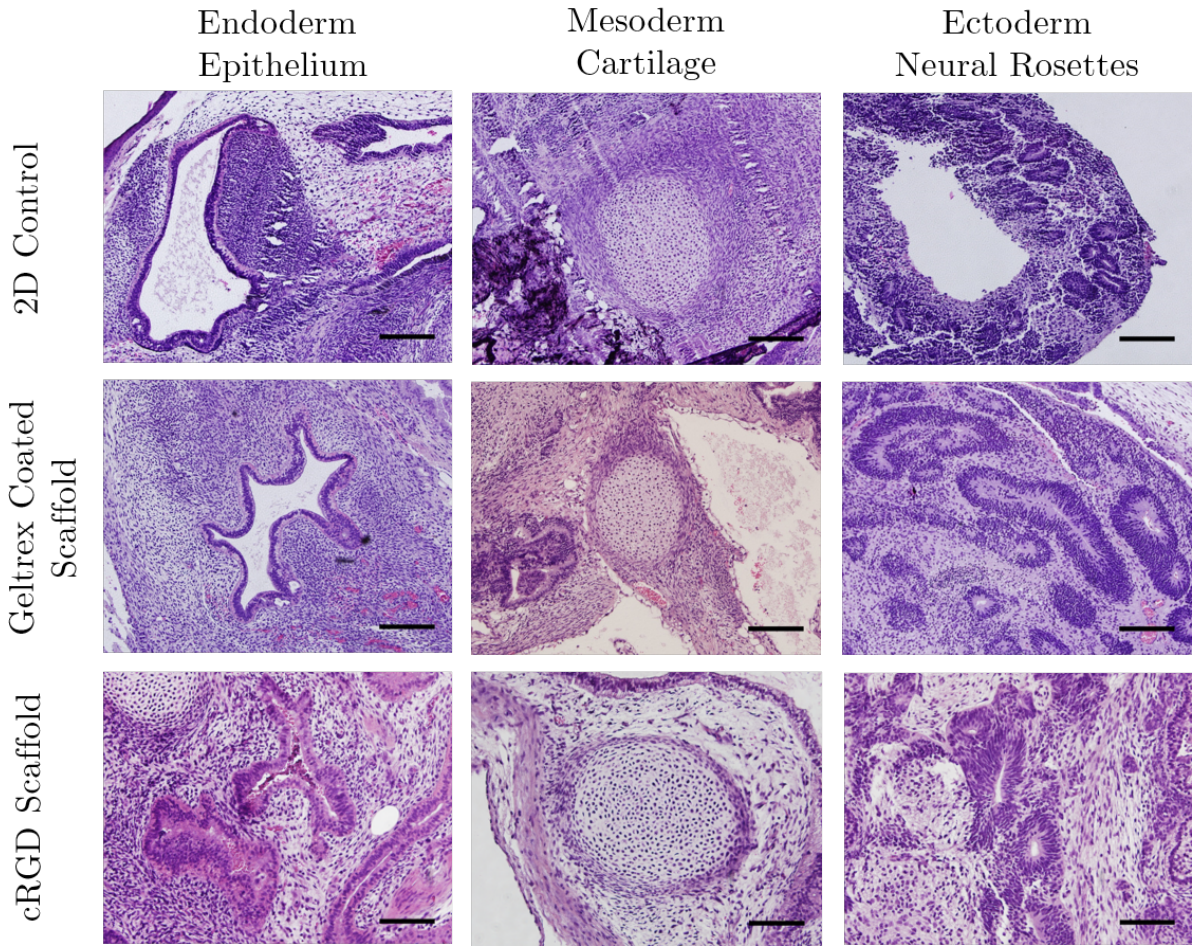

Figure 5.16: *Cultures of H9 stem cells extracted from 3D scaffolds via the synthetic explant method develop teratomas after transplantation into mice. Scaffolds trialled were thiol-acrylate polyHIPEs with either sulfo-SANPAH functionalisation and Geltrex® coating, or cRGD functionalisation. Cells cultured in routine 2D conditions were used as a control. Representative H&E histology analysis of teratomas showing human tissues derived from the different germ layers are shown (ectoderm, mesoderm, and endoderm). Scale bars = 200 μm*

along all three lines. The teratoma assay then shows the final fate of the cells, showing that they have indeed formed a range of cell types.

Limitations include the time-point captured by each technique. PCR measures copies of specific RNA markers within the cells. These markers are assumed to indicate the cells are in a certain state or heading towards a certain fate. Oct4 and Nanog markers are found in pluripotent cells. In addition, if markers for all three germ lines increase over time it suggests that the cells are differentiating into different cell types from all layers. This capacity is unique to pluripotent cells. However, these markers can be detected well before a cell is committed to a certain fate. Teratomas show a later time-point, and indicate that certain cell types did indeed form. As the ability to form cell types from all three germ layers is characteristic of pluripotent stem cells, the presence the different cell types in a teratoma is taken to indicate that in the past, the cells were pluripotent. The two techniques are therefore not directly comparable, but together they show a more complete story and confirm the pluripotency of the cultured cell population.

5.4 Conclusions

In this chapter, the capability of cyclic-RGDfK (cRGD) functionalised scaffolds to specifically support maintenance of pluripotency in H9 human embryonic stem cells was assessed. By comparing to an inactive analogue peptide motif, cyclic-RADfK, cRGD was found to have specific function in the adhesion and proliferation of H9 human embryonic stem cells in porous thiol-acrylate scaffolds. It was therefore shown that the adhesion peptide cRGD, but not an inactive peptide analogue, could be used to replace the undefined Geltrex® coating previously used to support pluripotent stem cells on this scaffold.

Protocols for retrieving stem cells from the 3D scaffolds were developed. Enzymatic dissociation was found to be ineffective in combination with the thiol-acrylate culture scaffold, and did not result in viable cell populations. An alternative method modelled on explant culture was found to be effective.

After removal from the thiol-acrylate polyHIPE scaffold, the differentiation capacity of H9 stem cells was determined. Teratomas were formed which contained cell types derived from each germ layer, demonstrating that the injected stem cell populations were pluripotent. This was supported by the qPCR analyses, which indicated that cells within the scaffold maintained Oct4 and Nanog expression over the 14 day culture period. These analyses also reinforced the cell's differentiation capacity, as an increase in markers from different germ layers was detected over time. Thus, this chapter confirmed that H9 human pluripotent stem cells could be maintained in 3D in cRGD-functionalised, thiol-acrylate polyHIPE scaffolds under fully defined conditions, and that these cells retained their capacity to differentiate into cell types from each germ layer.

References

[1] Walters, N. J.; Gentleman, E. *Acta Biomater.* **2015**, *11*, 3–16.

[2] Kolhar, P.; Kotamraju, V. R.; Hikita, S. T.; Clegg, D. O.; Ruoslahti, E.; Ramana, V.; Hikita, S. T.; Clegg, D. O.; Ruoslahti, E. *J. Biotechnol.* **2010**, *146*, 143–146.

[3] Fadeev, A. G.; Melkoumian, Z. In *Embryonic Stem Cells - Basic Biology to Bioengineering*; Kallos, M., Ed.; InTech, 2011; Chapter 6, pp 89–104.

[4] Lambshead, J. W.; Meagher, L.; Goodwin, J.; Labonne, T.; Ng, E.; Elefanty, A.; Stanley, E.; O'Brien, C. M.; Laslett, A. L. *Sci. Rep.* **2018**, *8*, 701.

[5] Park, Y. D.; Tirelli, N.; Hubbell, J. A. *Biomaterials* **2003**, *24*, 203–210.

[6] ReproCELL, *Retrieval of Cells from Alvetex® Scaffold* **2016**, http://reinnervate.com/alvetex/alvetex–documentation/protocols/, Accessed 23–11–2017.

[7] Stadtfeld, M.; Hochedlinger, K. *Genes Dev.* **2010**, 2239–2263.

[8] Müller, F. J.; Goldmann, J.; Löser, P.; Loring, J. F. *Cell Stem Cell* **2010**, *6*, 412–414.

[9] Desai, N.; Rambhia, P.; Gishto, A. *Reprod. Biol. Endocrinol.* **2015**, *13*, 9.

[10] Dahan, P.; Lu, V.; Nguyen, R. M.; Kennedy, S. A.; Teitell, M. A. *J. Biol. Chem.* **2018**, jbc.TM117.000832.

[11] Gupta, P.; Hourigan, K.; Jadhav, S.; Bellare, J.; Verma, P. *Biochem. Eng. J.* **2017**, *118*, 25–33.

[12] Wilmes, A.; Rauch, C.; Carta, G.; Kern, G.; Meier, F.; Posch, W.; Wilflingseder, D.; Armstrong, L.; Lako, M.; Beilmann, M.; Gstraunthaler, G.; Jennings, P. *Toxicol. In Vitro* **2017**, *45*, 445–454.

[13] Watanabe, K.; Ueno, M.; Kamiya, D.; Nishiyama, A.; Matsumura, M.; Wataya, T.; Takahashi, J. B.; Nishikawa, S.; Nishikawa, S.-i.; Muguruma, K.; Sasai, Y. *Nat. Biotechnol.* **2007**, *25*, 681–686.

[14] Rizzino, A. *Regen. Med.* **2010**, *5*, 799–807.

[15] Invitrogen, *HES Cell Data Sheet* **2018**, http://www.thermofisher.com/content/dam/LifeTech/migration/en/filelibrary/cell–tissue–analysis/pdfs.par.49756.file.dat/co13964–stem–cell–data–sheet–hesc.pdf, Accessed 28–10–2018.

[16] Carthew, J. *Personal Communication* **2017**,

[17] Nie, Y.; Bergendahl, V.; Hei, D. J.; Jones, J. M.; Palecek, S. P. *Biotechnol. Prog.* **2009**, *25*, 20–31.

[18] Ben-David, U.; Arad, G.; Weissbein, U.; Mandefro, B.; Maimon, A.; Golan-Lev, T.; Narwani, K.; Clark, A. T.; Andrews, P. W.; Benvenisty, N.; Carlos Biancotti, J. *Nat. Commun.* **2014**, *5*, 4825.

[19] Garitaonandia, I. et al. *PLoS One* **2015**, *10*, e0118307.

Chapter 6

Conclusions & Future Work

6.1 Conclusions

This thesis presented a porous polymer scaffold that could be peptide-functionalised to provide a chemically-defined culture system for the maintenance of human pluripotent stem cells. The scaffold was composed of a UV-cured, thiol-acrylate, polymerised high internal phase emulsion (polyHIPE) which had both suitable interconnected morphology, and residual thiol groups that allowed surface functionalisation. These materials were coated with the commercially available ECM-derived coating Geltrex®. This provided a scaffold that could support human pluripotent stem cells, however this approach did not create a chemically defined system. In order to achieve defined culture conditions, a protocol to functionalise the residual thiols found in the scaffold was developed. Michael addition was successfully used to conjugate maleimide to the surface. As benign reaction conditions were used, this protocol could then be used to conjugate the maleimide-containing adhesion cyclic-RGDfK-maleimide (cRGD-mal) to the polyHIPE material. The cRGD sequence was capable of promoting H9 embryonic stem cell adhesion in place of Geltrex®. After further modification of the material, these stem cells were able to proliferate throughout the scaffold while retaining their pluripotency.

The key conclusions that can be drawn from the development and analysis of this material are:

- Michael addition can be used to functionalise thiol-acrylate polyHIPE scaffolds with maleimide containing moieties under benign conditions.
- Addition of a crosslinker enables the scaffold to be coated with ECM protein mixtures such as Geltrex®, which promotes stem cell attachment and proliferation.
- Functionalising thiol-acrylate polyHIPEs with cyclic-RGD supports cell proliferation and expression of the pluripotency marker Oct4.
- Cells can be effectively extracted from 3D cultures using an explant-like protocol.
- Cells cultured in 3D under defined conditions retain their capacity for differentiation to all three germ layers, and are thus pluripotent.

6.2 Future Directions

The development of a 3D culture system that effectively maintains pluripotent stem cells in an animal component-free, chemically defined environment has the potential to impact a wide range of applications from drug discovery to cell therapy. Defined 3D culture may be used to overcome bottlenecks in cell supply, to provide better *in vitro* models, and to improve the clinical relevance of pluripotent stem cells. The cRGD-functionalised, thiol-acrylate, porous polymer scaffold presented in this thesis provides many of the features required for these new systems. There are several areas that could could be investigated to further optimise the material and to provide more insight into stem cell response to 3D polyHIPE-based scaffolds. An overview of some areas that may be of interest is provided in this section

6.2.1 Extension of Analyses Presented in this Thesis

A key advantage of synthetic scaffolds over naturally derived materials is their reproducibility. In Chapter 4, the void diameters of the synthesised thiol-acrylate polyHIPE scaffolds were measured. The average void diameter was reproducible, but all synthesis conditions lead to a distribution of void sizes (see Figure 4.17a). As discussed in Chapter 4, a wide void size distribution can affect the environment experienced by cells and impact culture homogeneity. Void diameter should therefore be kept within an acceptable range. Future development of this material might consider tighter control of production parameters in an attempt to narrow void size distribution. This could include using a peristaltic pump, rather than a dropping funnel, to add the aqueous phase to the template emulsion as this has been shown to have a positive influence on the reproducibility of void diameters in polyHIPEs [1]. Temperature also affects the structure of polyHIPEs. While temperature was kept relatively stable during production of the materials in this thesis, deliberate control of ambient and water temperatures could also be used to refine void diameter.

Another modification that could improve the growth and maintenance of pluripotent stem cells in the polyHIPE scaffolds is optimisation of the material's biofunctionality. Cyclic-RGD was used in this thesis as it promotes adhesion more strongly than it's linear equivalent, and has been shown to promote maintenance of pluripotency under defined conditions. The effectiveness of the cRGD motif may be improved by optimising ligand density, grouping, or by adding a spacer. Ligand density is important to the signals received by cells. Surface concentration of an RGD-containing peptide derived from bone sialoprotein has been found to correlate with human embryonic cell number in defined culture [2], indicating that concentration is an important factor to consider. Low ligand density may not maximise cell density within the material. Conversely, while RGD is known to promote adhesion, epitope crowding can reduce its effectiveness [3]. Using excess peptide is not cost effective and may inhibit wider adoption of the culture system. Between these extremes, fate determination of pluripotent stem cells may be sensitive not

only to ligands present, but also to their relative density. Spacing or grouping of functional groups may also impact stem cell behaviour. In a study using human embryonic stem cell-derived mesenchymal progenitor cells, polyHIPEs with adhesive patches that had similar spacing to that found in native ECM produced the greatest cell spreading [4]. This surface patterning could also alter pluripotent stem cell response to the cRGD functionalisation on polyHIPEs in this work. Addition of a spacer such as poly(ethylene oxide) (PEO) or polyethylene glycol (PEG) may benefit cell adhesion and response by reducing steric hinderance. For ligands bound to surfaces to be accessible to cells, they must be a suitable distance from the surface and can't be buried by proteins adsorbed from culture [5]. The protocol for addition of maleimide functionalised molecules *via* Michael addition outlined in Chapter 3 could also be used to attach other biofunctional groups to the scaffold. These could be trialled either in conjunction with cRGD or separately. Some potential functional sequences are discussed in Chapter 1, and include proteins such as fibronectin and laminin, or short peptides.

The 3D scaffolds used in this work were suspended in either commercial or custom 3D printed frames (see Figure 2.1). The frame design, production and optimisation are outside the scope of this thesis, but Chapter 5 briefly examines the exchange of media around the scaffold. The media was found to differ inside and outside the frame. This may be remedied in part by optimising or re-designing the frame. Reducing the bulk of the frame and adding more cutouts may allow better media flow. These requirements were key constraints in the original design, but were at odds with the desire for robustness and ease of handling. The abilities of the Flashforge 3D printer also had to be considered. Further development may involve continued use of 3D printing, either for rapid protoyping or final production. Alternatively, moulding could be used. This would remove the capacity for rapid prototyping, but would expand the available materials and change geometric constraints.

H9 human embryonic stem cells were used to investigate the response of pluripotent stem cells to the 3D scaffold in Chapter 5. These model stem cells were shown to maintain

their differentiation capacity when cultured for up to 14 days under defined conditions. Culturing a range of pluripotent stem cell lines, including induced pluripotent stem cells, would be useful to determine the broader practicality of this culture format.

6.2.2 Further Investigation & Potential Applications

Beyond the potential improvements to the 3D culture scaffold already suggested, there are several areas and applications that could be investigated in the future as the system is refined. PolyHIPE scaffolds can easily be synthesised in a range of shapes. The UV-curing system used in this thesis allows production of monoliths up to 35 mm thick [6], and provides very rapid curing. This flexibility could be used to create shapes that more effectively support large scale expansion of pluripotent stem cells, such as microcarriers. PolyHIPE microcarriers would have the advantage of presenting a specific surface to cells and providing a large surface to which the cells can adhere, while allowing large scale cell expansion in bioreactors. Media analyses in Chapter 5 indicated that diffusion around the supporting frame in static culture may be limited. This issue may be ameliorated by agitated culture formats such as bioreactors.

The rapid curing of polyHIPEs might also be used in conjunction with 3D printing to synthesise scaffolds that not only have the interconnected microstructure typical of polyHIPEs, but that also have channels, pillars, or other layered 3D geometries suited for particular tissue constructs. Such structures may be useful for modelling multi-layer tissue structures, and for the directed differentiation of pluripotent stem cells.

Directed differentiation within the polyHIPE scaffold would be useful in creating tissue-like structures for drug modelling, developmental studies, and eventually transplantation. PolyHIPEs scaffolds have previously been successfully used as scaffolds for the growth of several cell types. If the thiol-acrylate scaffolds outlined in this thesis can be modified to facilitate both the proliferation of pluripotent stem cells and their subsequent differentiation into specific lineages, the versatility of the system would be greatly increased.

The induction of pluripotency has been shown to be enhanced in 3D environments [7]. It may therefore be productive to trial reprogramming of somatic cells to pluripotent stem cells in the thiol-acrylate scaffolds developed in this thesis. In addition to their 3D structure and ability to support pluripotent stem cells, these scaffolds are chemically defined. Producing cell lines on chemically-defined substrates would reduce the chance of contamination and improve the cell line's relevancy in potential clinical applications.

Another possible application of these scaffolds could be the determination of pluripotency. In Chapter 5, stem cells cultured in cRGD-functionalised polyHIPE scaffolds were shown to be capable of spontaneous differentiation *in vivo*. In addition, qPCR analysis suggested that cells started to undergo spontaneous differentiation while still in the scaffold. This may be useful in determining the differentiation capacity of cell populations. A more tissue-like, 3D structure may be capable of allowing pluripotent stem cells to form teratoma-like structures *in vitro*. Despite the development of genome analysis techniques, teratomas are still the gold standard assay for pluripotency. An efficient *in vitro* version of this assay would simplify the routine analysis of pluripotency, both in terms of laboratory protocols and ethics.

PolyHIPE scaffolds may also be used to improve the cryopreservation of pluripotent stem cells. Cryopreservation is important to keep stocks of low passage cells, optimise utilisation of limited cell types, and to allow easy transport between institutions. Preserving cells on Matrigel-coated Cytodex 3 microcarriers has been shown to promote better recovery than typical suspension cryopreservation [8]. Thus, preserving cells in the polyHIPE construct may have applications in this area.

Another area of investigation that may be of interest is the effect of the 3D environment on human pluripotent stem cells. While a 3D format is believed to be beneficial to pluripotent cell culture due to several factors, including the increase in cell interactions and the efficient use of laboratory space, fundamental understanding could still be improved. A study comparing a 3D environment to an equivalent format has been conducted on porous atellocollagen [9], but has not been investigated using a synthetic

polyHIPE structure. Comparing stem cell behaviour in 3D thiol-acrylate materials to that on equivalent 2D membranes may provide further insight into the effects of 3D *in vitro* environments.

With these and many other potential applications, 3D, peptide-functionalised, thiol-acrylate polyHIPE scaffolds show promise as multi-purpose system for the culture and maintenance of human pluripotent stem cells under chemically-defined, xeno-free conditions.

References

[1] Bokhari, M.; Carnachan, R. J.; Przyborski, S. A.; Cameron, N. R. *J. Mater. Chem.* **2007**, *17*, 4088.

[2] Melkoumian, Z. et al. *Nat. Biotechnol.* **2010**, *28*, 606–610.

[3] Gouveia, R. M.; Castelletto, V.; Alcock, S. G.; Hamley, I. W.; Connon, C. J. *J. Mater. Chem. B* **2013**, *1*, 6157.

[4] Viswanathan, P.; Ondeck, M. G.; Chirasatitsin, S.; Ngamkham, K.; Reilly, G. C.; Engler, A. J.; Battaglia, G. *Biomaterials* **2015**, *52*, 140–147.

[5] Hollinger, J. O., Ed. *An Introduction to Biomaterials*, 2nd ed.; CRC Press, 2012.

[6] Kimmins, S. D.; Wyman, P.; Cameron, N. R. *React. Funct. Polym.* **2012**, *72*, 947–954.

[7] Caiazzo, M.; Okawa, Y.; Ranga, A.; Piersigilli, A.; Tabata, Y.; Lutolf, M. P. *Nat. Mater.* **2016**, *15*, 344–352.

[8] Nie, Y.; Bergendahl, V.; Hei, D. J.; Jones, J. M.; Palecek, S. P. *Biotechnol. Prog.* **2009**, *25*, 20–31.

[9] Zujur, D.; Kanke, K.; Lichtler, A. C.; Hojo, H.; Chung, U.-i.; Ohba, S. *Sci. Adv.* **2017**, *3*, e1602875.